HARVARD UNIVERSITY
Graduate School of Arts and Sciences



DISSERTATION ACCEPTANCE CERTIFICATE

The undersigned, appointed by the

Division of Medical Sciences

in the subject of Biological and Biomedical Sciences

have examined a dissertation entitled

The road from thought to action: a brain-wide atlas of spinal projecting neurons

presented by Carla C. Winter

candidate for the degree of Doctor of Philosophy and hereby certify that it is worthy of acceptance.

Signature: Constance L. Cepko
Constance L. Cepko (Sep 2, 2023 20:41 EDT)

Typed Name: Dr. Constance Cepko

Signature:

Typed Name: Dr. Lisa Goodrich

Signature: Maria Lehtinen
Maria Lehtinen (Sep 1, 2023 15:56 EDT)

Typed Name: Dr. Maria Lehtinen

Signature: Ariel Levine
Ariel Levine (Sep 5, 2023 13:26 EDT)

Typed Name: Dr. Ariel Levine

Date: June 13, 2023

The road from thought to action: a brain-wide atlas of spinal projecting neurons

A DISSERTATION PRESENTED

BY

CARLA C. WINTER

TO

THE DIVISION OF MEDICAL SCIENCES

IN PARTIAL FULFILLMENT OF THE REQUIREMENTS

FOR THE DEGREE OF

DOCTOR OF PHILOSOPHY

IN THE SUBJECT OF

DEVELOPMENTAL AND REGENERATIVE BIOLOGY

HARVARD UNIVERSITY

CAMBRIDGE, MASSACHUSETTS

JUNE 2023

© 2023 – Carla C. Winter

ALL RIGHTS RESERVED.

Dissertation advisor: Professor Zhigang He Carla C. Winter

The road from thought to action: a brain-wide atlas of spinal projecting neurons

ABSTRACT

The brain executes control of nearly all bodily functions via spinal projecting neurons (SPNs) that carry command signals from numerous supraspinal regions to the spinal cord. Despite significant progress in identifying the major anatomical tracts and their functions, the molecular and cellular mechanisms underlying SPN connectivity and function remain unknown. In this dissertation, using retrograde labeling, whole-brain imaging, and high-throughput transcriptional profiling, I generated a unified brain-wide anatomic and transcriptomic atlas of adult mouse SPNs at single-cell resolution. This atlas revealed important insights for understanding the anatomic (**Chapter 1**), transcriptomic (**Chapter 2**), and electrophysiologic (**Chapter** 3) features of these neurons:

Chapter 1 provides insights into the anatomical distribution of cervical- and lumbar-projecting SPNs via serial two-photon tomography and registration to the Allen Mouse Common Coordinate Framework. This work comprehensively mapped the distribution of SPNs, confirming concentrations in the cortex, hypothalamus, midbrain, cerebellum, pons, and medulla.

Chapter 2 showcases a multi-level transcriptomic taxonomy developed using single-nucleus transcriptomic profiling of 65,002 SPNs. This taxonomy revealed a three-component organization of SPNs: (1) molecularly homogeneous excitatory SPNs in the cortex, red nucleus, and cerebellum with somatotopic spinal terminations suitable for point-to-point communication; (2) highly heterogeneous excitatory and inhibitory populations in the reticular formation with broad spinal termination patterns,

suitable for relaying commands to the entire spinal cord; and (3) modulatory neurons expressing slow-acting neurotransmitters and/or neuropeptides in the hypothalamus, midbrain, and reticular formation for gain control of brain-spinal signals.

Chapter 3 focuses on the electrophysiological properties of SPNs. Cell-attached and whole-cell recordings of retrogradely labeled SPNs revealed electrophysiological features of a subset of SPNs that highly express transcriptional signatures correlating with fast-firing properties (namely, Pvalb/Kcng4/Spp1). These results show that Spp1+ SPNs are defined by fast-conducting properties, suggesting the presence of different cable lines (i.e., "fast and slow") transmitting brain signals to the spinal cord.

This body of work is the first to systematically describe brain-wide spinal projecting neurons by integrating their anatomic, transcriptomic, and electrophysiologic features, promising to deepen our understanding of how the brain controls the body, and may contribute to the development of new therapeutic approaches for disorders affecting descending pathways.

Contents

Title page.……..…..…….……..i
Copyright.
Abstract.
Contents.
Software, resources, and funding.
Dedication.
Acknowledgements.

0 INTRODUCTION…….1
0.1 Turning thought into action.
0.2 Descending pathways: from anatomy to function.
0.3 Not "just" a motor highway.
0.4 A molecular perspective.
0.5 A new era: single-cell resolution tracing, imaging, and genomics.
0.6 Dissertation overview.
0.7 References.

1 AN ANATOMICAL ATLAS OF CERVICAL- AND LUMBAR- PROJECTING SPINAL PROJECTING NEURONS……...46
1.1 Abstract.
1.2 Introduction.
1.3 Results.
1.3.1 Optimization of retrograde labeling in spinal projecting neurons.
1.3.2 Brain-wide distribution of spinal projecting neurons.
1.3.3 Projection target specificity of anatomical subpopulations.
1.4 Discussion.
1.4.1 Labeling strategy.
1.4.2 Brain-wide distribution.
1.4.3 Topographic innervation patterns.
1.4.4 Future directions.
1.5 Acknowledgements.
1.6 Video Legend.
1.7 Materials and Methods.
1.8 References.

2 A MOLECULAR TAXONOMY OF TRANSCRIPTOMIC CELL TYPES REVEALS ORGANIZATIONAL AND FUNCTIONAL PRINCIPLES OF BRAIN-WIDE SPINAL PROJECTING NEURONS……...87
2.1 Abstract.
2.2 Introduction.
2.3 Results.
2.3.1 Generation of an anatomically informed transcriptomic atlas of spinal projecting neurons.
2.3.2 Detection of first and second order labeled cells.
2.3.3 Overview of the spinal projecting neuron transcriptomic taxonomy.
2.3.4 Integration of spinal projecting neuron and whole brain taxonomies.
2.3.5 Transcriptomic landscape of spinal projecting neurons.
2.3.6 LIM Homeodomain transcription factors parcellate adult pontomedullary spinal projecting neurons.
2.3.7 Molecular specification of spinal projection targets.
2.4 Discussion.
2.4.1 Technical limitations and solutions.
2.4.2 A three-component organization of SPN projections.
2.4.3 Molecular insights into reticular formation SPNs.
2.5 Acknowledgements.
2.6 Table Legends.
2.7 Materials and Methods.
2.8 References.

3 TRANSCRIPTIONAL AND MORPHOLOGICAL CHARACTERISTICS OF FAST-CONDUCTING SPINAL PROJECTING NEURONS…….161
3.1 Abstract.
3.2 Introduction.
3.3 Results.
3.3.1 Anatomical distribution of rubrospinal transcriptomic types.
3.3.2 Morphological and electrophysiological characteristics of rubrospinal transcriptomic types.
3.3.3 Soma size and Spp1 status across spinal projecting neuron populations.
3.4 Discussion.
3.5 Acknowledgements.
3.6 Table Legends.
3.7 Materials and Methods.
3.8 References.

4 CONCLUDING REMARKS……..182
4.1 Summary of this work.

4.2 The continuing effort to build a "parts list" of the brain.
4.3 Hypothesis generation vs. data generation.
4.4 To my fellow trainees.
4.5 References.

APPENDIX……190
A.1 Review article – Axon Regeneration: A Subcellular Extension in Multiple Dimensions.
A.2 Review article – Viral vectors for neuronal cell type-specific visualization and manipulations.

Software, Resources, and Funding:

Software: I used R to perform the single-nucleus RNAseq data analyses presented in this work. Below are the main software packages used. This list is not exhaustive, please refer to Methods sections of each Chapter for further details.

- RStudio: an integrated development environment for R.
- Seurat: R package for QC, analysis, and exploration of single-cell RNA-seq data.
- Tidyverse: collection of R packages design for data science.
- scrattch.bigcat: scalable single cell RNAseq clustering pipeline developed by the Allen Institute for Brain Science

Formatting and Resources:

- This thesis was written in Microsoft Word.
- The formatting of this thesis was inspired by a LaTeX template that can be found online at https://github.com/suchow/Dissertate or from its author, Jordan Suchow, at suchow@post.harvard.edu.
- References were managed by Mendeley.
- Per contemporary use guidelines (https://tinyurl.com/WinterSupplement): during the preparation of this dissertation I used ChatGPT-3.5 (a language model developed by Open AI) as an interactive tool to brainstorm thesis titles and improve readability and language of my original writing and ideas. After using this tool, I carefully reviewed and edited the output and take full responsibility for the content of this thesis. Of note, ChatGPT was *not* used to generate new ideas nor to analyze and draw insights from the data; it was also *not* used in sections published or submitted for publication due to uncertain / emerging guidelines on the use of generative AI in scientific publishing.

Funding: This work was supported by the National Institutes of Health (grant numbers F30AG074598-01 to C.C.W., U19MH114830 to H.Z., 1356 R01NS109947 and R01AT010779 to Z.H.), Allen Institute for Brain Science (to H.Z., B.T., K.A.S, 1357 and Z.Y.), Wings for Life Spinal Cord Research Foundation (to C.C.W. and Z.Z.), Department of Public Health of Massachusetts (to Z.H.), and Dr. Miriam and Sheldon G. Adelson Medical Research Foundation (to Z.H.).

TO THE PATIENTS WHO WILL BENEFIT FROM THIS WORK.

Acknowledgements

The work presented in this dissertation would not have been possible without the support, guidance, and collaboration of numerous individuals for whom I am immensely grateful.

First, thank you to my thesis advisor, Professor Zhigang He. Throughout my training, Zhigang frequently prompted me with the question, "What do you think?", when we were facing a challenge – a reflection of his belief in my abilities and a genuine desire to understand my perspectives. This act of asking rather than telling enriched my growth as a researcher. He also provided a perfect balance of freedom and support: he allowed me to navigate the vastness of this field, yet he remained immediately available whenever I needed help. His responsiveness was nothing short of remarkable. Emails were returned impossibly fast, and written work was always reviewed within 24 hours (even the 3 of the 5 thesis chapters sent to him days before the deadline). His collaborative nature enabled me to undertake a thesis project that would have otherwise not been possible without guidance from the Allen Institute. His exceptional work ethic, passion for science, and belief in my capabilities have shaped not only this dissertation but also the neuroscientist I am today. Zhigang, thank you for your mentorship, patience, and endless support.

I am also grateful to Yuanyuan (Kevin) Liu, the post-doc who first welcomed me into the He Lab. Even years after leaving our lab to start his own at the NIH, Kevin has continued to stay involved with my work, attending bi-weekly meetings amongst collaborators, and even traveling to Boston for my defense day. Following Kevin's departure, I was fortunate to find an exceptional postdoctoral mentor in Anne Jacobi. Her rigorous intellect, light-hearted nature with laughter that often filled the lab, particularly on quiet Friday mornings when she listened to her "weekly German podcast", have made the daily challenges not only bearable but enjoyable. Anne displayed an unwavering commitment to my well-being, always providing support when the pressures of personal life heightened the

challenges of academia. Our countless hours brainstorming together, troubleshooting protocols, and painstakingly generating our final 10x dataset have been some of my favorite moments of the PhD. Despite relocating across the Atlantic, her engagement in our shared work has remained steadfast, and having co-authored two papers with her remains the highlights of my PhD. Anne's mentorship embodies the intersection of curiosity, rigor, and camaraderie that makes science worthwhile – I am so happy to have found not only a mentor but a friend in Anne.

My gratitude also extends to several additional He Lab members. First, an enormous thank you to post-doc Junfeng Su, who's exceptional work ethic and impressive experimental acumen significantly enriched our co-authored manuscript. Leeyup Chung, my bay mate and staff scientist with a quiet humor, didn't hesitate to step in and elevate our manuscript with his electrophysiological expertise. Sara Conti, a post-doc and a friend: our frequent mid-day coffee chats and after-work escapades acted as a much-needed respite from the rigors of research. Makenzie Tomihiro, who transitioned from an undergrad to a dedicated research technician upon graduating from Tufts, has been a joy to mentor. My gratitude additionally extends to fellow grad students Dan Hathaway, Eugene Kegeles, Sophie Eckl, and Xinyi Cai. Despite my initial solitude as the only grad student in the He Lab when I joined, their joining significantly improved the student experience. Lastly, the contributions of all the He Lab members, too numerous to list here, were invaluable.

I have been fortunate to work closely with the cell atlasing team at the Allen Institute for Brain Science (AIBS). Foremost among them is Hongkui Zeng, director of the AIBS and a pioneering force. Her scientific rigor, dedication, and generosity of her incredibly in-demand time are awe-inspiring. It has been an honor to collaborate with such an exceptional researcher, who continues to set a lofty standard that I aspire to emulate. Bosiljka Tasic, a group leader and collaborator at the AIBS, has an exceptional talent for reframing scientific challenges and transforming potential setbacks into

opportunities. The contributions from the AIBS team of incredible computational biologists – Cindy van Velthoven, Zizhen Yao, and Changkyu Lee – cannot be overstated.

I extend thanks to my Dissertation Advisory Committee: Connie Cepko, Fei Chen, Clifford Saper, and Veronique VanderHorst. I handpicked these scientists at the start of my PhD based on the alignment of their expertise with my research plans. Over time, I've come to appreciate the full depth of their heroic contributions to their respective fields. I also thank my thesis examiners for their time and effort: Connie Cepko, Lisa Goodrich (who also graciously served on my qualifying exam), Maria Lehtinen, and Ariel Levine.

I am additionally filled with gratitude for the mentors who guided me before my PhD. First, to Kacy Cullen, my undergraduate PI at UPenn: you exemplify the spirit of mentorship by welcoming undergraduates, like me at the time, who are eager to learn but with little to offer in return. Thank you to Jennifer Dulin, a post-doc at UCSD and now PI herself: your energetic welcoming me to the field of SCI has left a lasting impact on my career. Finally, working with Anne Engmann and Jeff Macklis as an HST research assistant in the Macklis Lab during my first two years of medical school laid a solid foundation for me in neurobiology and was instrumental to my progress in my PhD.

Thanks to the HST MD, MD-PhD, and BBS PhD programs. I am grateful for Drs. Rick Mitchell and Matthew Frosch – two of the most passionate educators whom I have ever crossed paths with. Dr. Mitchell offered me support during some of the most trying times of the MDPhD, and Dr. Frosch, whose passion for teaching and the human brain is unrivaled, has demonstrated a much appreciated a personal interest in all HST students' development. I am thankful for the MD-PhD program director Dr. Loren Walensky and extraordinary staff: Amy Cohen, Johnathan Cheng, and Liz Barks. And lastly, to the BBS PhD program, I extend my thanks to Anne O'Shea and Danny Gonzalez.

I would not have been able to complete this journey without the support of my friends near and far. Miri Zawadzki, your shared interest in neuroscience and our cathartic coffee chats at Nero

have been invaluable. Kristin Tsuo, you're the best friend the PhD has afforded me, and for that I am grateful beyond words. Adam Berger, Preston Ge, and Tong Xu, our weekend bike rides provided much-needed breaks. Daniel Palmieri and Shannon Kelsh, our escapades to places like Hawaii were welcomed reprieves. Ashwin Kumar and Kevin Procopio, who provided immense support to both Rahul and me during some of the most stressful periods. Hannah Cabot and Sarah Garvey, your friendship made Boston feel like home when I first moved here. Sarah Robinson, your move to Boston brought a piece of home with you. Jaya Sondhi, Katelynn Mudgett, and Shriya Joshi, your patience during times when my work was too much to handle have been truly appreciated. Darcy Best, Kristie Garrell, and Sara Prizzi, thank you for being the silliest most lighthearted sources of happiness during my PhD. Finally, to Megan Sidwa, Cassandra Ship, Pranali Sanghvi, and Veronica An, your support from afar was essential.

To my parents, Julie and Carl: thank you for your endless support. While the MD-PhD timeline is admittedly complex (enough so that I've lost track of the number of times I've had to remind you which phase I'm currently in 😜), I'm thrilled to say that, yes, we've finally reached the end of the PhD. And to my brother, Ryan: while I appreciate your commitment to supporting my research interests in neural injury and rehabilitation, it was quite unnecessary to personally experience a TBI just a month before my PhD defense! Jokes aside, I am so grateful that you are alive, recovering brilliantly, and adding an extra dimension of personal understanding to my work.

Finally, to my life partner, Rahul: I am profoundly grateful for your love, support, and opportunity to walk alongside you on this arduous yet gratifying journey. We began our journey together over 7 years ago at Penn and, somehow, found ourselves at Harvard pursuing the same career path together. Your ability to think deeply and creatively about complex problems in pretty much any field, coupled with your drive to uncover the answers with a tenacity I've witnessed in none other, is truly inspirational. I not-so-secretly hope that I might convince you to return to neuroscience someday,

and if I'm lucky, maybe even run a lab together. I'm so grateful for the joy, balance, and stability you've brought to my life. Simply put, I could not have gotten through the PhD without you. Also, thank you for welcoming our cat, Sammie (who is the sweetest of potatoes and deserves acknowledgement in her own right), into our home ☺.

0

Introduction

Publication: This chapter was written for this thesis and was not adapted from a publication.

Author contributions: This chapter was written by Carla C. Winter.

0.1 TURNING THOUGHT INTO ACTION.

Descending pathways, consisting of neurons that project directly from numerous supraspinal regions to the spinal cord, govern not only voluntary movements but also pain modulation, posture, and autonomic functions such as blood pressure, heart rate, and fear response. Dysfunction of these descending pathways contributes to several disorders, including developmental pathologies (e.g., hereditary spastic paraplegia, HSP), degenerative diseases (e.g., amyotrophic lateral sclerosis, ALS), and trauma (e.g., spinal cord injury, SCI). Considerable progress has been made in identifying the major descending anatomical tracts and functions – for example, decades of work have established the textbook view that the corticospinal tract (CST) extends from the cortex to the spinal cord to govern voluntary fine motor control. However, major gaps in our knowledge remain, particularly regarding their molecular and cellular composition. Through my dissertation, I have worked toward filling these gaps by elucidating the transcriptomic profiles of spinal projecting neurons (SPNs) and aligning them with their precise anatomical locations and spinal terminations to uncover novel organizational and functional principles. I begin the dissertation here with an introductory chapter that provides the necessary context for studying descending pathways, delving into their anatomy and functions, known molecular features, and new technologies that have enabled this body of work.

0.2 DESCENDING PATHWAYS: FROM ANATOMY TO FUNCTION.

Descending pathways are critical for the execution of somatic and autonomic motor commands that originate from the brain. Considerable progress has been made in identifying major anatomical tracts and their functions, largely based on early work that detailed the anatomy of these pathways, including the location and morphology of their soma, trajectories of their fibers, and locations of cells on which they terminate. In 1981, Hans Kuypers posited that descending pathways can be organized based on their terminations in the spinal cord and belong to three main groups: the first group includes cortical

pathways, such as the corticospinal and corticobulbar tracts, and the second and third groups are Group A and Group B brainstem pathways (H. G. J. M. Kuypers, 1981)[*]. In this section I will review these systems initially described by Kuypers as well as subsequent extensions of this work to other aspects of bodily control.

0.2.1 CORTICAL PATHWAYS: Descending cortical pathways originate in a highly organized fashion from distinct areas in cortical layer 5. The largest concentrations of corticospinal pathways arise from the primary motor cortex (precentral cortex / Brodmann Area 4 in primates), which have relatively thick fibers and a high degree of topographical organization. Corticospinal pathways also arise in the primary somatosensory cortex (postcentral gyrus / Brodmann Areas 1, 2, and 3 in primates) which have relatively thin fibers and terminate primarily in the spinal dorsal horn. Despite Kuypers' focus on the motor output of descending pathways, the differential termination of primary motor and primary somatosensory fibers in the spinal gray matter suggests these pathways are not exclusively motor relays. Corticospinal pathways also originate in other cortical locations, including in the medial hemisphere (e.g., the cingulate sulcus), supplementary motor cortex, secondary somatosensory cortex, and supplementary sensory area in primates. It is notable that despite Kuypers' focus on the motor output of descending pathways, the differential termination of primary motor and primary somatosensory fibers in the spinal gray matter suggests these pathways are not exclusively motor relays.

From these points of origin, cortical fibers primarily descend ipsilaterally via the internal capsule and cross to the contralateral CNS at the pyramidal decussation in the caudal brainstem. It is important to note, however, that the trajectory and termination of these pathways are varied across

[*] The below sections entitled "CORTICAL PATHWAYS", "GROUP A 'MEDIAL' PATHWAYS", and "GROUP B 'LATERAL' PATHWAYS" reference this work.

species, and the degree of cortical control over lower motoneurons appears to correlate with evolutionary sophistication. In relatively "primitive" species (e.g., edentates, elephants, marsupials, and lagomorphs), cortical pathways only extend to the lower brainstem and cervicothoracic spinal cord. In these organisms, the terminal distribution is primarily in the spinal dorsal horn, suggesting these cortical pathways play more of a role in sensory processing than motor output. In more evolved species (e.g., bats, rodents, carnivores), cortical pathways extend axons throughout the whole length of the spinal cord and primarily synapse in the IMZ in a somatotopically organized fashion. In the most evolved species (i.e., primates), a subset of corticospinal neurons (CSNs) in primates form direct, somatotopic motoneuronal synapses of distal extremity muscles (as well as proximal muscles in chimp and human). Corticobulbar neurons and CSNs collateralize to a small extent throughout their trajectory, though direct corticomotoneuronal fibers show little branching. Kuypers' suggested that the highly organized origin and somatotopic termination of descending cortical pathways imply they are a highly differentiated system that allows for highly fractionated movements, particularly of distal extremities, and are particularly important in primates.

0.2.2 GROUP A 'MEDIAL' PATHWAYS: Kuypers classified descending brainstem pathways according to the locations of their spinal terminations. Medially-projecting Group A pathways originate in centrally located brainstem structures such as the medial tegmental fields, vestibular complex, mesencephalic reticular formation, interstitial nucleus of Cajal, and superior colliculus. They descend bilaterally and terminate in the ventromedial IMZ (laminae VII and VIII), giving off a significant number of axon collaterals along their trajectory. Group A pathways have little somatotopic organization but contain some monosynaptic connections with motor neurons, primarily for axial and proximal limb muscles. Their extensive collateralization and termination on long propriospinal neurons in the ventromedial IMZ suggest they are well suited for synergistic activation of many

muscles; therefore, Kuypers concluded these pathways are the basic system by which the brain controls synergistic actions such as posture, whole limb movements, and integrated body and limb actions.

0.2.3 GROUP B 'LATERAL' PATHWAYS: These pathways primarily originate in the midbrain red nucleus and to a small extent in the ventrolateral pontine tegmentum. They descend contralaterally to terminate in the dorsolateral IMZ (laminae V-VII). Like corticospinal pathways, rubrospinal neurons (RuSNs) from the red nucleus are somatotopically organized; however, they have few axon collaterals which are restricted to neighboring spinal segments. Direct motoneuronal connections are rare, though some exist for distal extremity motor neurons in rhesus. Kuypers concluded that these laterally-projecting pathways supplement the medially-projecting pathways and provide the capacity for independent, flexion-biased, movements of the extremities and shoulder.

0.2.4 EXTENDING KUYPERS' THEORY – THE EMOTIONAL MOTOR SYSTEM: Kuypers' theory of the motor system organization explains most voluntary motor output: through these systems, we can sit upright in our chairs, type on our keyboard, walk, and run. Other "involuntary" motor activities, such as smiling, crying, laughing, and responding to fear-inducing stimuli, however, are not readily explained by Kuypers' initial theory. Several years later in 1987, Kuypers' and colleague Gert Holstege revisited this theory to incorporate new studies that identified descending pathways from supraspinal regions not evidently involved in motor control such as the hypothalamus, locus coeruleus, caudal raphe, and dorsal column nuclei (G. Holstege, 1991; G. Holstege et al., 1996; J. C. Holstege & Kuypers, 1987)†.

† This section entitled "EXTENDING KUYPERS' THEORY – THE EMOTIONAL MOTOR SYSTEM" references these works.

Follow up studies of descending pathways from these additional supraspinal regions revealed characteristics that distinguished them from the group A and B brainstem pathways. First, in contrast to earlier studies that indicated group A brainstem projections terminate only in the IMZ, updated anterograde tracing experiments from the locus coeruleus, subcoeruleus, and caudal raphe nuclei showed extensive terminations onto all parts of the spinal gray matter. Second, retrograde labeling studies demonstrated coeruleo- and raphe-spinal pathways extensively collateralize at all levels of the spinal cord, indicating a diffuse projection pattern. Third, histofluorescent studies showed that spinal projections from the locus coeruleus and raphe nuclei were noradrenergic and serotonergic, respectively, and that peptides such as thyrotropin releasing hormone (TRH), Substance P, cholecystokinin (CCK), and enkephalin co-exist with serotonin in the soma and terminals in the spinal ventral horn. Finally, functional studies demonstrated that noradrenaline and serotonin (as well as TRH and Substance P) enhanced the excitability of motor neurons and that electrical stimulation of the locus coeruleus or raphe nuclei have a faciliatory effect on motor neurons. Together, these features of noradrenergic and serotonergic descending pathways supported a new hypothesis presented by Holstege and Kuypers that they act as a gain-setting system to enhance overall responsiveness of somatic and autonomic motor neurons throughout the spinal cord. Examining the termination patterns of coeruleo- and raphe-spinal fibers underscores the utility of such a gain-setting system: neurons from the raphe pallidus and obscurus were shown to project to and have a facilitatory effect on the ventral horn, and the raphe magnus was shown to project to the dorsal horn and have an inhibitory influence on pain transmission. Similarly, the locus coeruleus descending pathways was shown to have a facilitatory effect on motor neurons and inhibitory effect on pain transmission in the dorsal horn. Thus, simultaneous action of these dorsal and ventral horn projections would lead to a state of "fight or flight": enhanced responsiveness of the motor system accompanied by decreased pain transmission.

In addition to their spinal terminations, the upstream afferent inputs into the coeruleo- and raphe-spinal systems provide further insights into their role in the broader network of spinal cord control. Specifically, studies showed that these systems receive inputs from limbic structures such as the hypothalamus, bed nucleus of the stria terminalis, amygdala, and periaqueductal gray, indicating that the limbic system, via these spinal projections, may influence whole-spinal cord physiology. These findings set the stage for Holstege's "emotional motor system": a set of motor pathways parallel to Kuypers' "voluntary somatic motor system" that govern somatic, autonomic, and endocrine motor responses (**Figure 0-1**). This parallel motor system provides a framework for involuntary motor activities and may account for clinical conditions in which involuntary somatic motor responses such as laughing are preserved in the setting of absent voluntary motor responses (**Figure 0-2**).

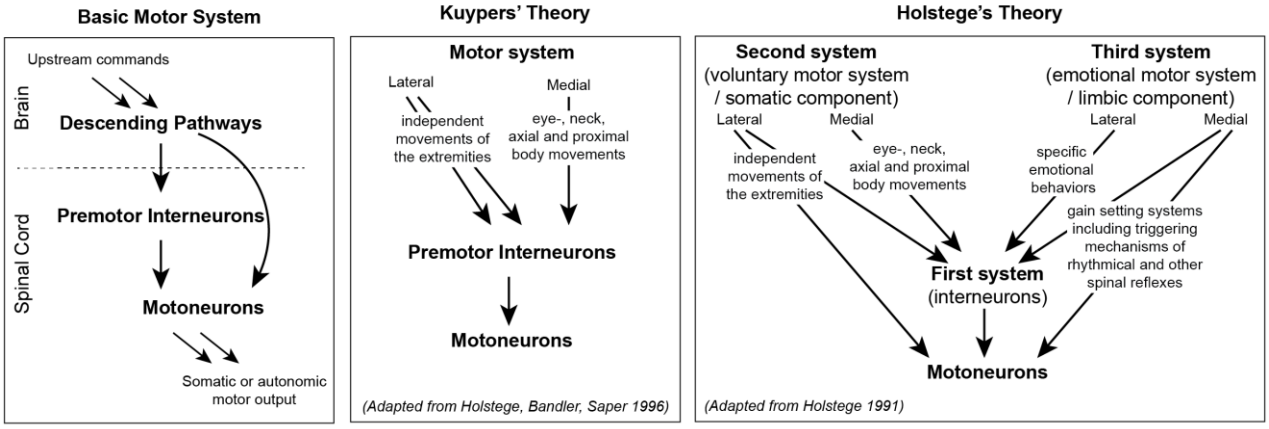


Figure 0-1. Schematic of the theories of motor systems. (Left) Basic theory of the motor system in which upstream brain commands are relayed to descending pathways which then transmit information to motoneurons via premotor interneurons or direct motoneuronal connections. These signals then effect somatic or autonomic output. (Middle) Kuypers posited that descending brainstem pathways are organized into lateral and medial, governing movements of the extremities and axial musculature, respectively. Schematic adapted from (G. Holstege et al., 1996). (Right) Kuypers' and colleague Gert Holstege revisited Kuypers; theory to incorporate studies that identified descending pathways from supraspinal regions not evidently involved in motor control such as the hypothalamus, locus coeruleus, caudal raphe, and dorsal column nuclei. Schematic adapted from (G. Holstege, 1991).



(From Holstege, Bandler, Saper 1996)

Figure 0-2. Clinical evidence of voluntary and emotional motor systems. A patient with an infarct interrupting the corticobulbar fibers. On the left, the patient shows her teeth upon request (demonstrating the voluntary motor system). On the right, she reacts to a joke (demonstrating the emotional motor system). Adapted from (G. Holstege et al., 1996).

0.2.5 A HIGHER-RESOLUTION UNDERSTANDING: As demonstrated above, extensive early work using anterograde and retrograde degeneration labeling, transport labeling (e.g., radiolabeling and fluorescent tracers), and orthodromic and antidromic electrical stimulation has provided a solid foundation to understand the anatomy and function of descending pathways. The foundational work summarized by Kuypers' and Holstege's theories of motor system organization established that descending pathways are widely conserved across mammals and arise in numerous supraspinal locations, with the most numerous populations in the cerebral cortex, red nucleus, brainstem reticular formation, vestibular system, paraventricular nucleus, and the deep cerebellar nuclei (J. C. Holstege & Kuypers, 1987; H. G. J. M. Kuypers, 1981). Though this foundational work was largely definitive, conclusions about the overall anatomical organization of descending pathways were made based on piecemeal descriptions of supraspinal regions across studies and species.

To overcome this challenge, Liang, Paxinos, and Watson established the first comprehensive, brain-wide description of descending pathways in the mouse using FluoroGold- and horseradish peroxidase-based retrograde labeling (Liang et al., 2011). This anatomical atlas of descending pathways provided an invaluable resource to the descending pathways research community, as it unified disparate findings across early works and provided a comprehensive baseline for future studies in

physiological and pathological settings. The supraspinal origins of descending pathways were further clarified by the Blackmore group in 2018 with the use of highly efficient viral-mediated retrograde labeling and 3D imaging, providing qualitative characterizations of descending pathways and placing these neurons into their three-dimensional spatial context.

0.2.6 FUNCTIONAL IMPLICATIONS: Efforts to detail the anatomy of descending pathways have set the stage for functional dissection of supraspinal regions in control of spinal cord motor circuits. Several methods have been employed over the decades and are detailed in this section, using skilled forelimb movement to illustrate each. Initially, function was deduced from anatomy. For example, direct connections between the primary motor cortex and motor neurons in the cervical spinal cord implied corticospinal projections govern forelimb movement. More specifically, it was thought that corticospinal projections were responsible for highly fractionated movements in distal extremities based on the observation that the number of monosynaptic connections between corticospinal pathways and motor neurons increase alongside increased acquisition of skilled forelimb movements from rodents to humans (H. Kuypers, 1964; H. G. J. M. Kuypers, 1981). Electrophysiological recordings supported this notion, but also revealed contributions from other supraspinal regions such as the red nucleus in skilled forelimb tasks (Jarratt & Hyland, 1999). Surgical lesioning experiments have yielded additional functional insights. For example, selective ablation of the CST via pyramidotomy has been extensively used to illustrate its role in skilled forelimb tasks including reach-grasp behavior (Whishaw et al., 1993), and rubrospinal tract lesions were shown to lead to defects in the arpeggio phase of reach-grasp (Morris et al., 2011), underscoring that activity in multiple supraspinal populations may coordinate the same motor output. The utility of surgical lesioning experiments is limited, however, because of the difficulty associated with specifically ablating a descending tract. The CST is uniquely tractable for surgical lesioning experiments because its passage

through the pyramid allows lesioning via pyramidotomy, yet even these relatively simple lesioning experiments are not absolute as they may disrupt neighboring medullary regions. More selective ablation of neuronal populations can be achieved by direct injection of a toxin; for example, injection of Cre-dependent diphtheria toxin receptor demonstrated glutamatergic medullary reticular formation neurons mediate skilled forelimb tasks (Esposito et al., 2014). However, direct toxin injection is also limited because it may affect neighboring off-target cells and is not specific for descending pathways. Intersectional genetic approaches, where injection of a retrograde Cre recombinase is injected into the spinal cord and a Cre-dependent construct is delivered to the soma via injection in supraspinal regions, offers a more targeted approach. Intersectional genetics has been employed to show various descending pathways contribute to skilled forelimb tasks (Sathyamurthy et al., 2020; X. Wang et al., 2017; Z. Wang et al., 2018).

In sum, from anatomical connections to electrophysiological recordings, surgical lesioning experiments, and more targeted intersectional genetic approaches, these methods have provided a more nuanced understanding of the coordinated activity of supraspinal regions in spinal cord motor circuits. The convergence of several different supraspinal regions on a single motor output (e.g., skilled forelimb movement) highlights the complexity of descending pathways and underscores the need for continued research to fully understand their organization and function. Further, as the above sections highlight, much of our understanding of descending pathways stems from conclusions pieced together from disparate studies; future efforts should seek to study descending systems as a unified system coordinating a diverse array of functions.

0.3 NOT "JUST" A MOTOR HIGHWAY.

Although descending pathways have been traditionally viewed as relays for motor output, early work showed that these fibers terminate in all parts of the spinal gray including the dorsal horn. For example,

the aforementioned corticospinal fibers in relatively "primitive" animals only extend to the cervicothoracic spinal cord and primarily terminate in the dorsal horn (H. G. J. M. Kuypers, 1981), and brainstem pathways such as the coeruleo-spinal projections were shown to make direct projections to the dorsal horn (Nygren & Olson, 1977). These projections to the spinal dorsal horn imply that these pathways may play additional important roles in sensory processing rather than "just" serving as motor relays.

Indeed, multiple supraspinal regions have been shown to have a descending inhibitory influence on spinal somatosensory circuits. Stemming from observations of direct coeruleo-spinal projections to the dorsal horn, early studies demonstrated that projections from the locus coeruleus as well as the raphe magnus mediate control of spinal nociceptive transmission (Jones & Gebhart, 1986; Mokha et al., 1985, 1986). More recently, corticospinal pathways were shown to modulate tactile allodynia as well as normal touch, suggesting direct cortical modulation of spinal sensory processing (Y. Liu et al., 2018). Thus, in addition to commanding motor neurons, corticospinal pathways may relay cortical control of spinal sensory circuits. The mostly likely mechanism for this "sensory gating" (i.e., inhibition of sensory information) is via presynaptic inhibition (Fink et al., 2014) of spinal interneurons by corticospinal axons (Abraira et al., 2017; Moreno-Lopez et al., 2021). Taken together, these findings emphasize the need to consider the role of descending pathways beyond "just" motor control.

0.4 A MOLECULAR PERSPECTIVE.

0.4.1 INSIGHTS FROM A MOLECULAR CATALOGUE: Generating a molecular catalogue of descending pathways promises to deepen our understanding of how the brain controls the body. Below I highlight examples of key insights that can be gleaned from detailing their molecular identities.

0.4.1.1 Intercellular communication: Information flows through the nervous system via intercellular communication between neurons. Generally, this information is transmitted via the release of chemical transmitters such as canonical fast-acting transmitters (e.g., GABA, glutamate), slow-acting transmitters (e.g., dopamine, norepinephrine, serotonin), neuropeptides (e.g., cholecystokinin, oxytocin, vasopressin), gaseous signaling molecules (e.g., nitric oxide), and lipophilic molecules (e.g., prostaglandins). Classically, neurons are defined by one fast-acting neurotransmitter, but are known to co-release neuropeptides (Hökfelt et al., 2018; Nusbaum et al., 2017), slow-acting neurotransmitters (Trudeau, 2004), and/or even a second fast-acting neurotransmitter (Granger et al., 2017). These chemical transmitters may have an excitatory, inhibitory, or modulatory effect on downstream targets, and different chemical transmitters released from the same neuronal subtype may produce distinct behaviors (Pomrenze et al., 2019). Thus, understanding the complete neurotransmitter signature of each neuronal subtype, which may be accomplished via investigation of its molecular identity, is critical to understanding its function and integration within a circuit.

0.4.1.2 Evo-Devo Principles: Unraveling the molecular signatures that define descending pathways promises critical insights into their organization, development, and evolution. Descending pathways have the extraordinary task of extending exceptionally long axons to precise spinal locations during development; investigating their molecular repertoire and its developmental changes should yield insights into axon pathfinding (McCormick & Gupton, 2020), midline crossing (Flanagan & Van Vactor, 1998), and developmental pruning (Low et al., 2008). Additionally, extending molecular studies to other species has the potential to yield insights into the evolution of neuronal subtypes and their common vs. species-specific functions. Comparative studies across species have revealed a fascinating correlation between the presence of descending pathways and specific functions. For

instance, relatively primitive sea animals like lamprey and shark, which employ undulating movements via axial musculature for locomotion, contain reticulospinal neurons (ReSNs). In contrast, rays and land animals that also use limbs for movement have additionally developed rubrospinal pathways, and those with fine limb function have developed corticospinal pathways (**Figure 0-3**) (Olivares-Moreno et al., 2021; ten Donkelaar, 2009). Interestingly, mammalian development mirrors this evolution of descending pathways. The phylogenetically oldest reticulospinal pathways are the first to reach the spinal cord (Auclair et al., 1999), followed by the rubrospinal tract which supports early forelimb control before the corticospinal pathways reach their targets (Bertucco & Dayanidhi, 2015; Williams et al., 2014). While the dictum "ontogeny recapitulates phylogeny" may not be entirely accurate, the evolutionary and developmental acquisition of limb and skilled motor control alongside acquisition of additional descending pathways provides further evidence of their functional roles. Analyzing the molecular and cellular mechanisms underlying these phylogenetic and developmental changes will yield important insights, including conservation of developmental, evolutionary, and functional programs. Additionally, this knowledge may guide the selection of animal models with conserved programs for studying human disease.

0.4.1.3 Selective targeting: To fully elucidate a neuronal subtype's development and function, more selective targeting tools are required. A catalogue of genetically defined neuronal populations would enable visualization, manipulation, or treatment of specific cell types (Y. Liu et al., 2020). As aforementioned, intersectional genetic approaches have been employed to study descending pathways in specific tasks (Sathyamurthy et al., 2020; X. Wang et al., 2017; Z. Wang et al., 2018); however, these studies are limited because they do not consider the diversity of neuronal types comprising an anatomically defined tract. Instead, genetic targeting methods in which a subtype marker gene is used

to drive one (or multiple) DNA recombinase(s) (e.g., Cre, Flp, Dre) could be used to more specifically target molecularly defined subtypes.

0.4.1.4 Disease and regeneration: It is a well-known but poorly understood phenomenon that neurons exhibit a heterogeneous response to injury and disease (Fu et al., 2018). For example, although huntingtin (*HTT*) is expressed in all neurons, an *HTT* mutation preferentially affects striatal GABAergic neurons and leads to Huntington's disease phenotype. Additionally, distinct retinal ganglion cell (RGC) subtypes have also been shown to undergo spontaneous axon regeneration following injury (Campbell et al., 1999; Duan et al., 2015) and exhibit differential response to treatments (Norsworthy et al., 2017). Descending pathways also offer salient examples of heterogeneous injury response and recovery; for instance, unlike the classically regrowth-refractory CSNs, subsets of ReSNs demonstrate appreciable regrowth and plasticity which is thought to contribute to spontaneous locomotor recovery following SCI and stroke (S. Baker, 2011; S. N. Baker & Perez, 2017; Ballermann & Fouad, 2006; Filli et al., 2014; Filli & Schwab, 2015; Zaaimi et al., 2012, 2018; Zörner et al., 2014). Interestingly, descending pathways' plasticity following injury appears to parallel their evolutionary history, with ReSNs being the most primitive pathways and most appreciated for their capacity for plasticity following injury (Z. Zhang et al., 2012). Despite extensive reports across neuronal populations, the mechanisms underlying selective neuronal vulnerability have remained elusive; identifying the molecular identities of these selectively vulnerable neurons may provide critical insights into the mechanisms underlying cell type-specific responses and lead to more effective treatments for regeneration[‡] and functional recovery.

[‡] For a detailed review of axon regeneration (Winter et al., 2022), refer to **Appendix A.1**.

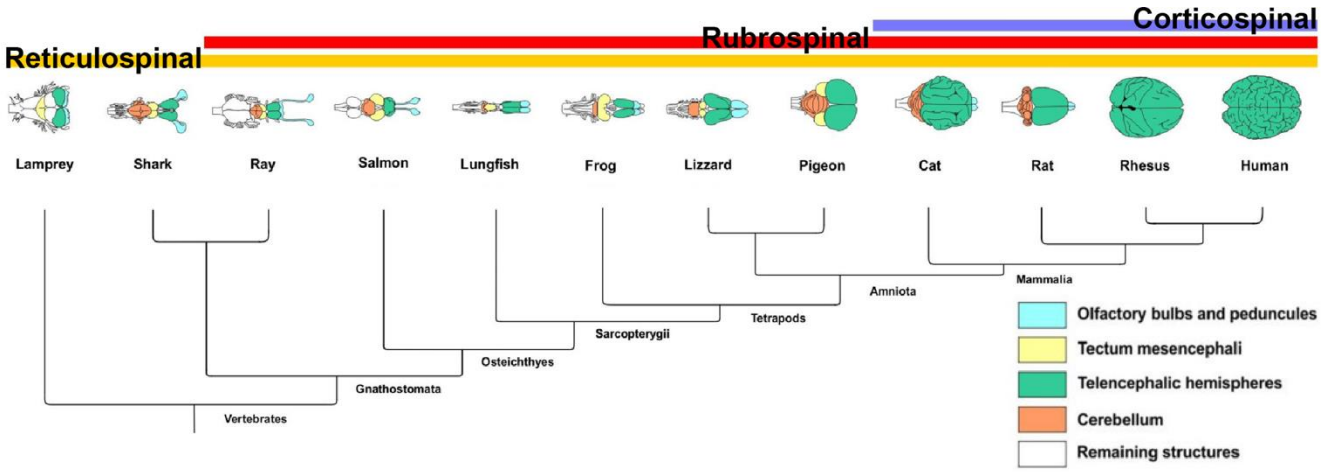


Figure 0-3: Relationship of corticospinal, rubrospinal, and reticulospinal tracts across phylogenetically distinct vertebrates. Adapted from (Olivares-Moreno et al., 2021).

0.4.2 KNOWN MOLECULAR PROFILES OF DESCENDING PATHWAYS: Though knowledge of the molecular identities of descending pathways lags behind anatomical insights, a preliminary foundation has been laid using immunohistochemical and expression studies.

0.4.2.1 Neurotransmitters: The first molecular insights within descending pathways were gained from immunohistochemical studies which revealed various neurotransmitters and neuromodulators. Early studies combining retrograde tracing and immunohistochemistry established CSNs as glutamatergic (Giuffrida & Rustioni, 1989; Valtschanoff et al., 1993), and follow up studies showed corticospinal axons are immunoreactive for vesicular glutamate transporter 1 (VGLUT1) but not VGLUT2 (Persson et al., 2006). RuSNs were also shown to be glutamatergic with immunoreactivity for glutamate and not glutamic acid decarboxylase (GAD), GABA, or glycine (Antal et al., 1992; Beitz & Ecklund, 1988). The red nucleus is immunoreactive for VGLUT2 instead of VGLUT1 (Fremeau et al., 2001). Forebrain hypothalamospinal neurons are neurochemically complex, including populations reactive for arginine vasopressin (paraventricular hypothalamus), α-melanocyte stimulating hormone

(lateral hypothalamic area, retrochiasmatic area), atrial natriuretic peptide (perifornical hypothalamic area), tyrosine hydroxylase (dorsal hypothalamic area), among other neuropeptides (Cechetto & Saper, 1988). Vestibulospinal neurons have been shown to have GAD and glutamate immunoreactive populations (Cai et al., 2008; Valla et al., 2003), though follow-up studies have indicated vestibulospinal neurons are purely excitatory (Du Beau et al., 2012). ReSNs, the most anatomically complex descending population, were also determined to have complex neurotransmitter profiles, including glutamatergic (VGLUT2) (Du Beau et al., 2012), GABAergic (G. Holstege, 1991), glycinergic (J. C. Holstege & Bongers, 1991), noradrenergic (Vanderhorst & Ulfhake, 2006), serotonergic (Bowker et al., 1981), and various neuropeptidergic populations (Bowker & Abbott, 1990; J. C. Holstege & Kuypers, 1987). Though these immunohistochemical studies have laid a foundation for the overall neurotransmitter landscape of descending pathways (i.e., majority glutamatergic with heterogeneous subcortical populations), many questions remain. Beyond the canonical neurotransmitters, what other chemical messengers do these populations contain? Do these populations act via co-transmission (Hossaini et al., 2012)? What are the precise anatomical locations of the heterogeneous reticulospinal populations? Further systematic and comprehensive molecular exploration is crucial to unveil the diverse neurotransmitter signatures of brain-wide descending pathways.

0.4.2.2 Beyond neurotransmission: Beyond clarifying their mechanisms of intercellular communication, elucidating the complete molecular identities of descending pathways promises insights into their development, organization, regulatory mechanisms, diverse functional roles, disease processes, and therapeutic targets.

Molecularly, CSNs are the most studied descending pathway, likely owing to their functional importance in skilled forelimb control, relevance to human disease (e.g., ALS), and perhaps anatomical accessibility relative to subcortical pathways. Early histochemical studies gave insights into singular

markers specifying CSNs during development (Hevner et al., 2003; Weimann et al., 1999), but the advent of large-scale expression studies (e.g., microarray and bulk RNA sequencing) has given more comprehensive insights into molecular drivers of their development (Arlotta et al., 2005; Lodato et al., 2014; Molyneaux et al., 2005, 2015), axon targeting (Sahni, Itoh, et al., 2021; Sahni, Shnider, et al., 2021), and injury (Poplawski et al., 2020).

The investigation by Arlotta et al provided a pivotal technological and conceptual framework for detailing the molecular profiles of neuronal subtypes (Arlotta et al., 2005). The authors used fluorescent retro-beads to retrogradely labeled CSNs from the pons (at E18 and P3) and cervical spinal cord (at P6). They then used fluorescence activated cell sorting (FACS) to enrich for CSNs and subsequently profiled them with cDNA microarray across developmental stages (E18, P3, P6, and P14). They used a similar strategy to label and profile corticotectal and interhemispheric callosal neurons to provide insights into genes that are CSN-specific among the same layer 5 (i.e., CSN vs. callosal) and other sub-cerebral projection types (i.e., CSN vs. corticotectal). Comparing "pure" populations of CSNs across time points and to callosal/corticotectal neurons, the authors found that Diap3, Igfbp4, Crim1 distinguished CSNs from other sub-cerebral projection neurons, and Ctip2, Fezf2, and Crym (among others) are expressed in CSNs as well as a broader set of sub-cerebral projection neurons. Though this study provided an important foundation for investigating subtype- and stage-specific genes controlling development of SPNs, the use of microarray technology precluded genome-wide coverage. To address this limitation, the group conducted a follow up study where they purified and profiled sub-cerebral, corticothalamic, and callosal projection neurons using antibodies and FACS enrichment for CTIP2, TLE4, and SATB2, respectively, followed by bulk RNA-sequencing (Molyneaux et al., 2015). This study thus enabled both high-throughput isolation of projection neuron subtypes and genome-wide assessment of their transcriptome.

Despite these influential contributions, a comprehensive transcriptomic atlas of CSNs is still lacking because of three key limitations in these studies. First, the design of both studies did not ensure pure corticospinal populations. In Arlotta et al, the pontine injections used to label CSNs at E18 and P3 would also label corticopontine neurons that will not extend their axons to the spinal cord (though this is a natural limitation, as corticospinal axons have not reached their spinal targets at E18 and P3). In Molyneaux et al, the authors relied on neuronal enrichment via antibodies for marker genes rather than retrograde labeling; the chosen gene for CSNs, CTIP2, also labels non-spinal projecting sub-cerebral projection neurons (as discussed above). Thus, conclusions on marker genes for CSNs may be confounded by impure populations. Second, both studies defined neuronal "subtype" by their anatomical features (i.e., projection target) without considering within-tract heterogeneity. Considering the CST as a singular, homogeneous unit fails to account for its functional, and likely molecular and cellular, diversity. Additionally, pooling impure corticospinal populations for bulk cDNA microarray and RNA-seq may further cofound identification of marker genes. Third, both studies focused on sub-cerebral projection neurons during development, leaving the adult transcriptome unmapped. Both studies demonstrated that CSN gene expression changes throughout development, underscoring the need to additionally assess the transcriptome during adulthood, particularly for insights into adult-onset disease and injury.

A similar subtype-specific, genome-wide study has not been conducted in subcortical populations. Like early corticospinal studies, our molecular understanding of subcortical descending pathways comes from experiments detailing a handful of neurotransmitters (see above) and select marker genes. For example, Liang, Paxinos, and Watson followed up their systematic anatomic assessment of descending pathways with a more targeted investigation of rubrospinal projections (Liang et al., 2012). The authors characterized RuSNs based on their morphology (Nissl staining), protein content (immunofluorescence), and gene expression (in situ hybridization, ISH) in

combination with retrograde (fluoro-gold, FG) labeling. Nissl staining showed that the rostral red nucleus contains both large and small neurons, whereas the caudal portion is primarily magnocellular. Immunofluorescence using an SMI-32 antibody (non-phosphorylated neurofilament H) on retrogradely labeled tissue showed that a large proportion SMI-32 neurons are rubrospinal (50% and 80% of SMI-32+ neurons in rostral and caudal red nucleus, respectively). ISH data from the Allen In Situ Atlas showed that C1ql2 is a marker for the red nucleus, and that the rostral and caudal portions of the red nucleus containing RuSNs express Vglut2 (Slc17a6) but not Gad (Gad1). This study represents an important contribution, being among the first to unify morphological and molecular features of adult descending pathways. This approach is limited, however, for several reasons. First, the motivation for selecting and functional significance of the studied marker genes is unclear, though neurofilament's known relation to axon caliber suggests that rubrospinal axons are large in diameter. Further, the ISH data from non-retrogradely labeled tissue only allows the authors to conclude that C1ql2 and Slc17a6 positive neurons are present in the same regions as RuSNs but may not be RuSNs themselves; indeed, the authors acknowledged that the location of some C1ql2 positive neurons are not in regions containing RuSNs. Therefore, the need for a rubrospinal-specific marker remains. Finally, the study was limited to three molecular markers (SMI-32, C1ql2, Slc17a6), leaving the full molecular profile of RuSNs to be determined.

Our molecular understanding of other subcortical descending pathways is similarly limited. ReSNs represent the most complex population of descending pathways in terms of both their anatomy and function, yet investigation of their neuronal subtypes currently relies on only a few available molecular handles. Insights into reticulospinal molecular identity were first gained when Cepeda-Nieto and colleagues investigated the role of LIM homeodomain genes in reticulospinal development (Cepeda-Nieto et al., 2005). Various LIM homeodomain genes were already known to govern diversification of motor neuron pools in the spinal cord and brainstem (Briscoe et al., 2000; Pfaff et

al., 1996; Sharma et al., 1998; Tsuchida et al., 1994; Varela-Echavarría et al., 1996), so the authors set out to investigate if the same factors controlled reticulospinal development. The authors employed retrograde labeling and immunostaining for LIM homeodomain genes Lhx1, Lhx5, Lhx3, Lhx4, and homeobox gene Chx10 in chick and mouse embryos. They found three molecularly defined populations during development (Lhx1/5^{+}, Lhx3/4^{+}, and Lhx1/5^{-}–Lhx3/4^{-}) and showed that Chx10 is expressed in a dynamic pattern within the Lhx3/4^{+} population. Initially, these neurons have only Lhx3/4 expression, followed by co-expression with Chx10, and eventual loss of Lhx3/4 in some Chx10^{+} populations. By HH-stage 22 in chicks, Lhx3/4^{+}, Lhx1/5^{+}, and Lhx1/5^{-}–Lhx3/4^{-} populations comprised 13%, 18%, and 69% of ipsilaterally projecting ReSNs. Contralaterally projecting ReSNs were comprised of 31% Lhx1/5^{+} and 69% Lhx1/5^{-}–Lhx3/4^{-} populations. The authors used over-expression, morpholino knock-down, and ectopic expression experiments to demonstrate these factors have a functional role in determination of ReSNs. Importantly, this study demonstrated that anatomically defined (i.e., originating in the reticular formation) ReSNs can be partitioned into unique molecular subpopulations.

Since this early investigation of homeobox genes in reticulospinal development, the existence of Lhx3/Lhx4/ Chx10^{+} populations were confirmed in adulthood (Bretzner & Brownstone, 2013) and functional studies have relied on Chx10 as a genetic marker of ReSNs. Strikingly, Chx10^{+} populations are involved in numerous motor activities, including locomotion (Bretzner & Brownstone, 2013), swimming (Kimura et al., 2013), breathing (W. C. Li & Soffe, 2019), movement halting (Bouvier et al., 2015; W. C. Li & Soffe, 2019), and left-right turning (Cregg et al., 2020). Their role in multiple distinct motor activities suggests the Chx10^{+} class is likely comprised of numerous subpopulations, underscoring a major limitation of using Chx10 molecular handle for functional dissection. Unlike SPNs arising from well-defined anatomical nuclei, like the cortex and red nucleus, ReSNs arise across numerous nuclei largely without well-delineated anatomical borders (Liang et al.,

2011; Perreault & Giorgi, 2019). Given their overlapping spatial distributions, the use of a broad molecular marker like Chx10 is not sufficient for characterize different aspect of their functional repertoire and may yield confounding results. Ultimately, comprehensively profiling ReSNs is needed for finer molecular classifications and to answer remaining numerous questions. What sub-populations exist within the $Chx10^{+}$ class? Are there markers specific to ReSNs, among local interneurons (Chopek et al., 2021)? Do $Lhx1/5^{+}$ neurons exist during adulthood? What subpopulations and molecular identities exist in the $Lhx1/5^{-}$–$Lhx3/4^{-}$ class? How do mesencephalic, pontine, and medullary ReSNs differ?

Though corticospinal, rubrospinal, and reticulospinal neurons comprise most of the descending pathway literature, molecular insight into other descending pathways is equally critical yet similarly sparse. Vestibulospinal neurons from the brainstem vestibular nucleus have been transcriptionally characterized with bulk RNA-sequencing (Lunde et al., 2019), but like Arlotta et al, these efforts were focused on development and did not consider within-tract heterogeneity. Other major descending systems such as cerebellospinal and hypothalamospinal neurons have not been molecularly investigated or examined only in relation to their neuromodulator profiles (Cechetto & Saper, 1988).

0.5 A NEW ERA: SINGLE-CELL RESOLUTION TRACING, IMAGING, AND GENOMICS.

There is a clear and urgent need for a comprehensive, brain-wide molecular investigation of descending pathways. Molecular studies to date are largely incomplete: most investigate populations during development and not adulthood, consider only a few marker genes, and do not consider possible within-tract heterogeneity. Further, each study has investigated only a single anatomical population, precluding assessment of molecular profiles in the context of the global descending

network. Like Liang and colleagues' contribution to our anatomical understanding (Liang et al., 2011), a molecular atlas of descending pathways should present a unified view of all descending pathways together. To generate a molecular atlas unified with anatomical, six technological criteria must be met: (1) high labeling efficiency across anatomic populations, (2) high-throughput neuron isolation, (3) ability to profile both developing and adult populations, (4) consideration of within-tract heterogeneity, (5) genome-wide coverage, and (6) unification of anatomic and molecular features. Recent technological advancements in separate fields in have made these criteria achievable, opening the door for my thesis work.

0.5.1 TECHNOLOGICAL ADVANCEMENTS:

0.5.1.1 Viral tracing:[§] Efforts to characterize descending pathways have relied on a variety of anatomical tracing methods, including silver degeneration, radiolabeling, and fluorescent dyes and beads (Lemon, 2008). Newer recombinant viral technology offers a more powerful and versatile toolbox for targeted, high-efficiency transgene expression in specific neuronal populations. Specifically, recombinant viruses capable of infecting neurons from their axon terminals can be used to target cells with distinct projection targets through retrograde viral infection. Many types of viral vectors have axonal tropism, three of which are reviewed here.

First, recombinant rabies viruses have been developed for efficient retrograde neuronal labeling. Rabies viruses infect neurons from axon terminals (Kelly & Strick, 2000), but the use of rabies viruses for labeling specific populations is limited because they are neurotoxic and uncontrollably propagate between hierarchically connected neurons. Within the five genes of rabies viral genome,

[§] This section is adapted from a review published in Current Opinion in Neurobiology (Y. Liu et al., 2020). For the full review on viral vectors for cell type specific visualization and manipulation, refer to **Appendix A.2.**

only *G* encodes the glycoprotein to mediate retrogradely trans-synaptic viral transmission. Thus, replacing the rabies envelope glycoprotein (RG) with fluorescent proteins (e.g., GFP) allows non-transsynaptic retrograde neuronal labeling (Wickersham et al., 2006). Further, double deletion (L and G proteins) reduces neurotoxicity and enables long-term anatomical or physiological study. The recombinant rabies viruses SADB19-base vectors (Wickersham et al., 2007) and less toxic CVS-N2c strain (Reardon et al., 2016) may be used for monosynaptic tracing of neuronal connections (Callaway & Luo, 2015; Luo et al., 2018). Several studies have combined cell type-specific viral vectors with these transsynaptic vectors to dissect input-output circuits (Schwarz et al., 2015).

Second, retrograde lentiviruses have been developed to address the issue of neurotoxicity presented by rabies viruses. Lentiviruses are single stranded RNA viruses that stably integrate into the host genome of both pre- and post-mitotic cells (Nassi et al., 2015). Based on the discovery that the RG mediates axonal retrograde transport, the Kobayashi group packaged lentiviruses with a fusion envelope composed of the extracellular domain of RG and the transmembrane and intracellular domain of the vesicular stomatitis virus (VSV) glycoprotein (HiRet-LV, also called RG-LV). These retrograde lentiviral vectors are highly effective in infecting axon terminals of long-distance projection neurons in both rodent and nonhuman primate (Kato et al., 2011, 2019; Kobayashi et al., 2017). Retrograde lentiviruses have since been successfully used for axonal projection-dependent labeling and manipulation of neuronal cell types (Y. Liu et al., 2018; Nelson et al., 2013; Stanek et al., 2016; X. Wang et al., 2017).

Third, recombinant AAV2-retro (rAAV2-retro) exhibits high efficiency in retrograde labeling of long-projecting neurons such as CSNs (Tervo et al., 2016). rAAV2-retro is versatile with limited toxicity and can drive high-level gene expression like other AAVs. Compared to HiRet-LV, rAAV2-retro is easier to produce, has higher expression levels, and is quicker to transfect neuronal cell bodies.

rAAV2-retro has broad but not pan-neuronal tropism for retrograde infection, however, so its tropism for desired neurons must be tested before use.

Recombinant viruses may be preferred over fluorescent dye based retrograde labeling due to their high-efficiency and versatility. These viral vectors with cross-species targeting and minimal cytotoxic effects offer unprecedented delivery systems to selectively express different desired transgenes in specific neuronal populations. In addition to the natural tropisms of individual viral types (Nassi et al., 2015; Schön et al., 2015), their transduction specificity can, in principle, be refined by altering their capsid or envelope proteins (to dictate which cells to bind and enter) and/or the promoter/enhancer in the viral genome (to determine whether or when to express the target gene). Combining these techniques to alter viral tropism with various delivery methods would allow recombinant viral vectors to serve as a collection of region-selective, neuron type-specific, and activity-dependent tools that can be readily used in multiple species.

0.5.1.2 Whole-brain imaging: Development of modern imaging techniques such as light sheet fluorescence microscopy (LSFM) and serial two-photon tomography (STPT) have enabled researchers to image at single-cell resolution across a whole-brain. Like any imaging modality, LSFM and STPT each have strengths and limitations, which are reviewed below.

LSFM is performed by first removing light-scattering components (e.g., lipids) via tissue clearing followed by imaging with a thin sheet of light to excite fluorescent markers within a tissue (Stelzer et al., 2021). This allows acquisition of three-dimensional data with high spatial resolution and relatively fast imaging speeds. Though tissue clearing is required to allow light sheet penetration, clearing techniques may introduce artifacts thereby affecting the accuracy of acquired images and subsequent registration and/or segmentation. Further, the light sheet laser has limited penetration –

while LSFM enables high-resolution imaging of thin tissue slices, optical clarity diminishes with increased tissue depth, resulting in reduced image quality for deeper brain regions.

In STPT, a specialized two-photon microscope captures block-face images of the tissue surface after each section is removed via automated sectioning (Ragan et al., 2012). This process enables precise block-face imaging with minimal sectioning artifact, resulting in consecutive image stacks that, when combined, comprise a three-dimensional representation of the entire brain. This offers a distinct advantage over LSFM as it does not require tissue clearing but compared to LSFM, has relatively slow acquisition time.

Following the acquisition of whole-brain imaging data, computational methods are used to segment structures of interest (e.g., neuronal soma, axons, and/or dendrites) and register them to a common atlas such as the Allen Institute's Common Coordinate Framework (Q. Wang et al., 2020). Several computational approaches, such as commercially available "NeuroInfo" or open source "brainreg" (Tappan et al., 2019; Tyson et al., 2022), have been developed to automate segmentation and registration.

0.5.1.3 Single-cell expression profiling: Gene expression profiling is essential for identifying molecular pathways underlying both health and disease. Historically, researchers have used methods such as in situ hybridization (ISH) and cDNA microarray to determine gene expression patterns across tissue types. While these approaches have provided invaluable insights, they are limited in their ability to assess genome-wide expression profiles. To address this limitation, next generation sequencing (NGS) and subsequently bulk RNA sequencing were developed to enable high-throughput, whole-genome coverage. However, a major limitation of these methods is their inability to consider cell-to-cell heterogeneity across a tissue. This limitation is amplified in a tissue like the brain, which, more so than

other tissues in the body, is thought to be comprised of an exceptionally diverse set of cell types (Zeng, 2022).

Single-cell genomics, in particular single-cell RNA sequencing (scRNAseq), has emerged as a breakthrough technology over the past several years, allowing genome-wide assessment at single-cell resolution. scRNAseq was first performed in a mouse blastomere in 2009 (Tang et al., 2009) and has become widely available with the development of plate- and droplet-based methods. Plate-based methods, such as SMART-seq (Picelli et al., 2014), allow high sensitivity and full-length mRNA sequencing at the expense of relative low throughput. Droplet-based methods, such as Drop-seq (Macosko et al., 2015) and the commercially available 10x Genomics platform, however, allow high-throughput analysis of single cells by encapsulating individual cells in nanoliter-sized droplets with barcoded beads containing unique molecular identifiers. This approach has revolutionized scRNAseq by dramatically increasing throughput while reducing cost per cell. The use of plate- vs. droplet-based methods depends on the specific research question at hand and available resources (e.g., financial, equipment).

A major drawback of single-cell analyses is that harsh isolation, sorting, and other processing steps may not be feasible for certain cell types. For example, particularly fragile populations like projection neurons may not survive dissociation procedures. To address this, single nucleus RNA sequencing (snRNAseq) was developed: by isolating and sequencing the RNA from the *nuclei* of individual cells, snRNAseq precludes the need for viable cells while preserving high information content of RNA for characterization of cellular diversity (Bakken et al., 2018).

0.5.1.4 Spatially resolved expression profiling: While single-cell genomics has provided invaluable insights into cellular diversity, these techniques remove cells from their spatial context. To address this limitation, spatial transcriptomics approaches, such as Visium and MERFISH (Chen et al., 2015),

were developed (Moses & Pachter, 2022). Unlike scRNAseq, these approaches allow for assessment of genome-wide expression while preserving the spatial relationships between cells. Further, integration techniques have been developed to allow mapping of scRNAseq profiles back into their anatomical context. Visium and MERFISH, among other spatial transcriptomics methods, have benefits and limitations in their detection efficiency, spatial resolution, and genome-wide coverage (Moses & Pachter, 2022). Detection efficiency (i.e., ability to detect RNA molecules within a sample) tends to be higher in highly multiplexed single molecule FISH (smFISH) techniques like MERFISH, whereas NGS barcoding techniques like Visium have lower efficiency. Further, smFISH techniques have superior spatial resolution – i.e., single molecule, by definition – whereas NGS techniques like Visium tend to have reduced spatial resolution (e.g., 55μm for Visium). NGS techniques, on the other hand, have superior coverage as they enable genome-wide expression profiling whereas smFISH based techniques are limited to a panel of predefined genes.

0.5.2 CELL-TYPE CLASSIFICATION:

Neurons exhibit tremendous diversity in their morphology, molecular makeup, and electrophysiological properties, highlighting the need for precise classification to identify their distinct roles in circuits and behaviors. The technological advancements detailed above have revolutionized the field by allowing insights into the molecular and spatial organization of neuronal "cell types" that comprise the brain. Here, we will explore this concept of "cell type", examine specific examples of classification of molecularly-defined cell types throughout the CNS, and explore a conceptual framework to organize the explosion of cell type classification data rapidly being generated.

0.5.2.1 What is a cell type?: While the field has not yet precisely defined what a "cell type" means, researchers have identified five key properties that are commonly considered when classifying cell

types: anatomy, morphology, molecular identity, physiology, and cell state (Zeng, 2022; Zeng & Sanes, 2017). (1) Anatomy: a cell type's anatomical origin is fundamental to defining the features and behaviors the cell may govern. (2) Morphology: a cell type's structural characteristics such as dendrites and axonal projection caliber and length provides additional functional insights. (3) Molecular identity: gene expression profiles likely underly functional features, and molecular markers are crucial for distinguishing different cell types. (4) Physiology: electrophysiology yields insights about the intrinsic features and circuit-level functions of cell types. (5) Cell state: a cell type may exist as various "states" across time, such as during development, adulthood, and aging.

0.5.2.2 Transcriptional profiling of the adult CNS: Cell type classification has seen an explosion of progress over the past several years across the CNS. One of the first studies to characterize the transcriptional diversity of the adult mouse brain constructed a cellular taxonomy of the primary visual cortex (VISp) (Tasic et al., 2016). To access both rare and abundant cell types within VISp, the authors used a set of transgenic (Cre, Dre, and/or Flp) recombinase lines crossed with reporter lines (*Ai14*, *Ai65*, or *Ai66*) to label neuronal subpopulations. They then performed precise layer-enriching dissections across the VISp and developed a protocol for isolating live adult cells from the dissections followed by FACS-enrichment and deep scRNAseq. They established robust quality-control metrics and developed a classification approach to define cell types and their marker genes. From this, they identified 49 cell types across the VISp: 23 GABAergic, 19 glutamatergic, and 7 non-neuronal types. They then assigned location of cell types via dissection information and expression patterns of marker genes within the Allen In Situ Atlas. Finally, they further characterized select molecularly defined subtypes via assessment of axonal projections and electrophysiological properties. This groundbreaking study established a robust framework for discovering and classifying cell types in the

adult mouse, setting the stage for comprehensive exploration of cellular diversity across the entire CNS.

Following this pioneering work, numerous studies employed this framework of targeted dissection, single-cell isolation, scRNAseq, and validation to generate cell type taxonomies across various regions of adult mouse CNS. The same research group extended their study to another cortical area, the anterior lateral motor cortex (Tasic et al., 2018), while other groups investigated the architecture of other brain regions such as the thalamic reticular nucleus (Y. Li et al., 2020), hippocampal formation (Yao, van Velthoven, et al., 2021), and the deep cerebellar nuclei (Kebschull et al., 2020). Critically, as the brain is not the sole component of the CNS, other groups have extended this framework to the retina (Rheaume et al., 2018; Tran et al., 2019) and spinal cord (Alkaslasi et al., 2021; Blum et al., 2021; Russ et al., 2021; Sathyamurthy et al., 2018) to begin to generate a "parts list" of the entire adult mouse CNS. Most recently and most relevant for this body of work, there has been an increasing interest to follow up early molecular studies of SPNs described above (Arlotta et al., 2005; Lodato et al., 2014; Molyneaux et al., 2005, 2015) using modern scRNAseq technologies (Beine et al., 2022; Golan, 2022; Golan & Cafferty, 2021)[**].

0.5.2.3 BRAIN Initiative Cell Census Network (BICCN): Developing a cell atlas of the entire brain is inconceivably complex. To systematize and accelerate this task, the BICCN (Brain Research through Advancing Innovative Neurotechnologies (BRAIN) Initiative - Cell Census Network) was established with the overarching goal of creating a detailed inventory of cell types in the mouse brain through comprehensive analysis of single-cell transcriptomics, epigenetics, neuronal morphology, connectivity,

[**]At the same time the work in this dissertation was being conducted, the Blackmore and Cafferty groups were also working towards profiling SPNs using scRNAseq technologies. Golan's PhD dissertation focusing specifically on CSNs, published in 2022, is referenced above and beautifully outlines the state scRNAseq in neuroscience at the time, like the overview presented here. The strengths and limitations of these works are further touched upon in **Chapter 2.**

and electrophysiology across diverse brain regions. In 2021, the BICCN published a set of companion papers focusing on the cortex, offering a comprehensive and in-depth exploration of its cellular composition (BICCN, 2021). These landmark studies encompassed multiple cortical areas and layers, providing a wealth of information about the diverse cell types present in the cortex. Specifically, they leveraged scRNAseq (Di Bella et al., 2021; Kozareva et al., 2021; Yao, Liu, et al., 2021), epigenomics (Y. E. Li et al., 2021; H. Liu et al., 2021; Yao, Liu, et al., 2021; Z. Zhang et al., 2021), spatial transcriptomics (M. Zhang et al., 2021), morphological and electrophysiological studies (Muñoz-Castañeda et al., 2021; Scala et al., 2020), transgenic lines (Matho et al., 2021), circuit tracing (Foster et al., 2021), isoform investigation (Booeshaghi et al., 2021), and comparative species analyses (Bakken et al., 2021; Berg et al., 2021; Bhaduri et al., 2021; Ziffra et al., 2021).

The integration of these multimodal datasets shed light on the remarkable heterogeneity and organization of cortical cells. These companion papers not only served as a valuable resource for understanding the cortex but paved the way for efforts currently underway seeking to generate a comprehensive whole-brain atlas of transcriptomic cell types in the mouse. The work presented in this dissertation is a component of this greater effort to profile the whole mouse brain and will be included in the BICCN Whole-Brain Taxonomy.

0.6 DISSERTATION OVERVIEW.

As described above, our knowledge of the molecular and cellular diversity of brain-wide descending pathways is limited. This is largely due to the lack of adequate tools to profile their complex anatomy, morphology, and molecular identity at sufficient resolution. Recent technological advances coupled with newly established paradigms for cell-type classification, however, have positioned me to develop this body of work and fill these critical gaps. In this dissertation, I present a brain-wide atlas

of spinal projecting neurons (SPNs), through the investigation and integration of their complex anatomy (**Chapter 1**), molecular identities (**Chapter 2**), and physiological properties (**Chapter 3**).

Using viral-mediated retrograde labeling, whole-brain imaging, and high-throughput transcriptional profiling, I generated a unified brain-wide anatomic and transcriptomic atlas of adult mouse SPNs at single-cell resolution. In **Chapter 1**, I established the brain-wide anatomical distribution of cervical- and lumbar-projecting SPNs via serial two-photon tomography and registration to the Allen Mouse Common Coordinate Framework so that the molecular atlas could be unified with precise anatomical features. In **Chapter 2**, I transcriptionally profiled 65,002 SPNs and employed a multi-level iterative clustering approach to generate a hierarchically organized transcriptomic taxonomy of SPNs organized into 3 divisions, 13 subclasses, and 76 types. The divisions revealed a three-component organization of SPNs: (1) molecularly homogeneous excitatory SPNs in the cortex, red nucleus, and cerebellum with somatotopic spinal terminations suitable for point-to-point communication; (2) highly heterogeneous excitatory and inhibitory populations in the reticular formation with broad spinal termination patterns, suitable for relaying commands related to activities of the entire spinal cord; and (3) modulatory neurons expressing slow-acting neurotransmitters and/or neuropeptides in the hypothalamus, midbrain, and reticular formation for gain control of brain-spinal signals. I mapped the 76 SPN transcriptomic types to their precise anatomical locations via integration with a companion whole mouse brain MERFISH dataset generated by the Allen Institute for Brain Science and BICCN (Yao et al., 2023). Further, I discovered a LIM homeobox transcription factor code that parcellates the most transcriptionally complex population, pontomedullary ReSNs comprised of 53 transcriptomic subtypes, into five LIM-defined and spatially segregated populations. In **Chapter 3**, I leverage insights gained from the molecular atlas to dissect physiological properties of SPNs. By performing cell-attached and whole-cell recordings of retrogradely labeled SPNs, I investigated the electrophysiological features of a subset of SPNs that

highly express transcriptional signatures correlating with fast-firing properties (namely, Pvalb/Kcng4/Spp1). I find that Spp1+ SPNs are defined by fast-conducting properties, suggesting the presence of different cable lines (i.e., fast and slow) transmitting brain signals to the spinal cord.

This is the first study to systematically describe brain-wide SPNs by integrating their anatomical, molecular, and physiological features, providing an important foundation for understanding organizational principles of SPNs. Ultimately, this work may contribute to the development of new therapeutic approaches for disorders affecting descending pathways and promises to deepen our understanding of how the brain controls the body.

0.7 REFERENCES

Abraira, V. E., Kuehn, E. D., Chirila, A. M., Springel, M. W., Toliver, A. A., Zimmerman, A. L., Orefice, L. L., Boyle, K., Bai, L., Song, B. J., Bashista, K. A., O'Neill, T. G., Zhuo, J., Tsan, C., Hoynoski, J., Rutlin, M., Kus, L., Niederkofler, V., Watanabe, M., … Ginty, D. D. (2017). The Cellular and Synaptic Architecture of the Mechanosensory Dorsal Horn. *Cell*, *168*(1–2), 295. https://doi.org/10.1016/J.CELL.2016.12.010

Alkaslasi, M. R., Piccus, Z. E., Hareendran, S., Silberberg, H., Chen, L., Zhang, Y., Petros, T. J., & Le Pichon, C. E. (2021). Single nucleus RNA-sequencing defines unexpected diversity of cholinergic neuron types in the adult mouse spinal cord. *Nature Communications 2021 12:1*, *12*(1), 1–14. https://doi.org/10.1038/s41467-021-22691-2

Antal, M., Sholomenko, G. N., Moschovakis, A. K., Storm-Mathisen, J., Heizmann, C. W., & Hunziker, W. (1992). The termination pattern and postsynaptic targets of rubrospinal fibers in the rat spinal cord: A light and electron microscopic study. *Journal of Comparative Neurology*, *325*(1), 22–37. https://doi.org/10.1002/CNE.903250103

Arlotta, P., Molyneaux, B. J., Chen, J., Inoue, J., Kominami, R., & MacKlis, J. D. (2005). Neuronal Subtype-Specific Genes that Control Corticospinal Motor Neuron Development In Vivo. *Neuron*, *45*(2), 207–221. https://doi.org/10.1016/J.NEURON.2004.12.036

Auclair, F. O., Marchand, R., & Glover, J. C. (1999). Regional Patterning of Reticulospinal and Vestibulospinal Neurons in the Hindbrain of Mouse and Rat Embryos. *J. Comp. Neurol*, *411*, 288–300. https://doi.org/10.1002/(SICI)1096-9861(19990823)411:2

Baker, S. (2011). The primate reticulospinal tract, hand function and functional recovery. *The Journal of Physiology*, *589*(23), 5603–5612. https://doi.org/10.1113/JPHYSIOL.2011.215160

Baker, S. N., & Perez, M. A. (2017). Reticulospinal Contributions to Gross Hand Function after Human Spinal Cord Injury. *Journal of Neuroscience*, *37*(40), 9778–9784. https://doi.org/10.1523/JNEUROSCI.3368-16.2017

Bakken, T. E., Hodge, R. D., Miller, J. A., Yao, Z., Nguyen, T. N., Aevermann, B., Barkan, E., Bertagnolli, D., Casper, T., Dee, N., Garren, E., Goldy, J., Graybuck, L. T., Kroll, M., Lasken, R. S., Lathia, K., Parry, S., Rimorin, C., Scheuermann, R. H., … Tasic, B. (2018). Single-nucleus and single-cell transcriptomes compared in matched cortical cell types. *PLoS ONE*, *13*(12), 1–24. https://doi.org/10.1371/journal.pone.0209648

Bakken, T. E., Jorstad, N. L., Hu, Q., Lake, B. B., Tian, W., Kalmbach, B. E., Crow, M., Hodge, R. D., Krienen, F. M., Sorensen, S. A., Eggermont, J., Yao, Z., Aevermann, B. D., Aldridge, A. I., Bartlett, A., Bertagnolli, D., Casper, T., Castanon, R. G., Crichton, K., … Lein, E. S. (2021). Comparative cellular analysis of motor cortex in human, marmoset and mouse. *Nature 2021 598:7879*, *598*(7879), 111–119. https://doi.org/10.1038/s41586-021-03465-8

Ballermann, M., & Fouad, K. (2006). Spontaneous locomotor recovery in spinal cord injured rats is accompanied by anatomical plasticity of reticulospinal fibers. *The European Journal of Neuroscience*, *23*(8), 1988–1996. https://doi.org/10.1111/J.1460-9568.2006.04726.X

Beine, Z., Wang, Z., Tsoulfas, P., & Blackmore, M. G. (2022). Single Nuclei Analyses Reveal Transcriptional Profiles and Marker Genes for Diverse Supraspinal Populations. *Journal of Neuroscience*, *42*(47), 8780–8794. https://doi.org/10.1523/JNEUROSCI.1197-22.2022

Beitz, A. J., & Ecklund, L. J. (1988). Colocalization of fixative-modified glutamate and glutaminase but not GAD in rubrospinal neurons. *Journal of Comparative Neurology*, *274*(2), 265–279. https://doi.org/10.1002/CNE.902740210

Berg, J., Sorensen, S. A., Ting, J. T., Miller, J. A., Chartrand, T., Buchin, A., Bakken, T. E., Budzillo, A., Dee, N., Ding, S. L., Gouwens, N. W., Hodge, R. D., Kalmbach, B., Lee, C., Lee, B. R., Alfiler, L., Baker, K., Barkan, E., Beller, A., … Lein, E. S. (2021). Human neocortical expansion

involves glutamatergic neuron diversification. *Nature 2021 598:7879*, *598*(7879), 151–158. https://doi.org/10.1038/s41586-021-03813-8

Bertucco, M., & Dayanidhi, S. (2015). Can the period of postnatal codevelopment of the rubrospinal and corticospinal systems provide new insights into refinement of limb movement? *Journal of Neurophysiology*, *113*(3), 681–683. https://doi.org/10.1152/JN.00442.2014/ASSET/IMAGES/LARGE/Z9K0021526090001.JPEG

Bhaduri, A., Sandoval-Espinosa, C., Otero-Garcia, M., Oh, I., Yin, R., Eze, U. C., Nowakowski, T. J., & Kriegstein, A. R. (2021). An atlas of cortical arealization identifies dynamic molecular signatures. *Nature 2021 598:7879*, *598*(7879), 200–204. https://doi.org/10.1038/s41586-021-03910-8

BICCN. (2021). A multimodal cell census and atlas of the mammalian primary motor cortex. *Nature 2021 598:7879*, *598*(7879), 86–102. https://doi.org/10.1038/s41586-021-03950-0

Blum, J. A., Klemm, S., Shadrach, J. L., Guttenplan, K. A., Nakayama, L., Kathiria, A., Hoang, P. T., Gautier, O., Kaltschmidt, J. A., Greenleaf, W. J., & Gitler, A. D. (2021). Single-cell transcriptomic analysis of the adult mouse spinal cord reveals molecular diversity of autonomic and skeletal motor neurons. *Nature Neuroscience 2021 24:4*, *24*(4), 572–583. https://doi.org/10.1038/s41593-020-00795-0

Booeshaghi, A. S., Yao, Z., van Velthoven, C., Smith, K., Tasic, B., Zeng, H., & Pachter, L. (2021). Isoform cell-type specificity in the mouse primary motor cortex. *Nature 2021 598:7879*, *598*(7879), 195–199. https://doi.org/10.1038/s41586-021-03969-3

Bouvier, J., Caggiano, V., Leiras, R., Balueva, K., Fuchs, A., & Correspondence, O. K. (2015). Descending Command Neurons in the Brainstem that Halt Locomotion. *Cell*, *163*. https://doi.org/10.1016/j.cell.2015.10.074

Bowker, R. M., & Abbott, L. C. (1990). Quantitative re-evaluation of descending serotonergic and non-serotonergic projections from the medulla of the rodent: evidence for extensive co-existence of serotonin and peptides in the same spinally projecting neurons, but not from the nucleus raphe magnus. *Brain Research*, *512*(1), 15–25. https://doi.org/10.1016/0006-8993(90)91164-C

Bowker, R. M., Westlund, K. N., & Coulter, J. D. (1981). Origins of serotonergic projections to the spinal cord in rat: an immunocytochemical-retrograde transport study. *Brain Research*, *226*(1–2), 187–199. https://doi.org/10.1016/0006-8993(81)91092-1

Bretzner, F., & Brownstone, R. M. (2013). Lhx3-Chx10 Reticulospinal Neurons in Locomotor Circuits. *The Journal of Neuroscience*, *33*(37), 14681. https://doi.org/10.1523/JNEUROSCI.5231-12.2013

Briscoe, J., Pierani, A., Jessell, T. M., & Ericson, J. (2000). A homeodomain protein code specifies progenitor cell identity and neuronal fate in the ventral neural tube. *Cell*, *101*(4), 435–445. https://doi.org/10.1016/S0092-8674(00)80853-3

Cai, Y. L., Ma, W. L., Wang, J. Q., Li, Y. Q., & Li, M. (2008). Excitatory pathways from the vestibular nuclei to the NTS and the PBN and indirect vestibulo-cardiovascular pathway from the vestibular nuclei to the RVLM relayed by the NTS. *Brain Research*, *1240*, 96–104. https://doi.org/10.1016/J.BRAINRES.2008.08.093

Callaway, E. M., & Luo, L. (2015). Monosynaptic Circuit Tracing with Glycoprotein-Deleted Rabies Viruses. *Journal of Neuroscience*, *35*(24), 8979–8985. https://doi.org/10.1523/JNEUROSCI.0409-15.2015

Campbell, G., Holt, J. K. L., Shotton, H. R., Anderson, P. N., Bavetta, S., & Lieberman, A. R. (1999). Spontaneous axonal regeneration after optic nerve injury in adult rat. *NeuroReport*, *10*(18), 3955–3960. https://doi.org/10.1097/00001756-199912160-00042

Cechetto, D. F., & Saper, C. B. (1988). Neurochemical organization of the hypothalamic projection to the spinal cord in the rat. *Journal of Comparative Neurology*, *272*(4), 579–604. https://doi.org/10.1002/CNE.902720410

Cepeda-Nieto, A. C., Pfaff, S. L., & Varela-Echavarría, A. (2005). Homeodomain transcription factors in the development of subsets of hindbrain reticulospinal neurons. *Molecular and Cellular Neuroscience*, *28*(1), 30–41. https://doi.org/10.1016/J.MCN.2004.06.016

Chen, K. H., Boettiger, A. N., Moffitt, J. R., Wang, S., & Zhuang, X. (2015). Spatially resolved, highly multiplexed RNA profiling in single cells. *Science*, *348*(6233). https://doi.org/10.1126/SCIENCE.AAA6090/SUPPL_FILE/CHEN-SM.PDF

Chopek, J. W., Zhang, Y., & Brownstone, R. M. (2021). Intrinsic brainstem circuits comprised of Chx10-expressing neurons contribute to reticulospinal output in mice. *Journal of Neurophysiology*, *126*(6), 1978–1990. https://doi.org/10.1152/JN.00322.2021/ASSET/IMAGES/LARGE/JN.00322.2021_F006.JPEG

Cregg, J. M., Leiras, R., Montalant, A., Wanken, P., Wickersham, I. R., & Kiehn, O. (2020). Brainstem neurons that command mammalian locomotor asymmetries. *Nature Neuroscience 2020 23:6*, *23*(6), 730–740. https://doi.org/10.1038/s41593-020-0633-7

Di Bella, D. J., Habibi, E., Stickels, R. R., Scalia, G., Brown, J., Yadollahpour, P., Yang, S. M., Abbate, C., Biancalani, T., Macosko, E. Z., Chen, F., Regev, A., & Arlotta, P. (2021). Molecular logic of cellular diversification in the mouse cerebral cortex. *Nature 2021 595:7868*, *595*(7868), 554–559. https://doi.org/10.1038/s41586-021-03670-5

Du Beau, A., Shakya Shrestha, S., Bannatyne, B. A., Jalicy, S. M., Linnen, S., & Maxwell, D. J. (2012). Neurotransmitter phenotypes of descending systems in the rat lumbar spinal cord. *Neuroscience*, *227*, 67–79. https://doi.org/10.1016/J.NEUROSCIENCE.2012.09.037

Duan, X., Qiao, M., Bei, F., Kim, I. J., He, Z., & Sanes, J. R. (2015). Subtype-Specific Regeneration of Retinal Ganglion Cells following Axotomy: Effects of Osteopontin and mTOR Signaling. *Neuron*, *85*(6), 1244–1256. https://doi.org/10.1016/J.NEURON.2015.02.017

Esposito, M. S., Capelli, P., & Arber, S. (2014). Brainstem nucleus MdV mediates skilled forelimb motor tasks. *Nature 2014 508:7496*, *508*(7496), 351–356. https://doi.org/10.1038/nature13023

Filli, L., Engmann, A. K., Zörner, B., Weinmann, O., Moraitis, T., Gullo, M., Kasper, H., Schneider, R., & Schwab, M. E. (2014). Bridging the Gap: A Reticulo-Propriospinal Detour Bypassing an Incomplete Spinal Cord Injury. *Journal of Neuroscience*, *34*(40), 13399–13410. https://doi.org/10.1523/JNEUROSCI.0701-14.2014

Filli, L., & Schwab, M. E. (2015). Structural and functional reorganization of propriospinal connections promotes functional recovery after spinal cord injury. *Neural Regeneration Research*, *10*(4), 509. https://doi.org/10.4103/1673-5374.155425

Fink, A. J. P., Croce, K. R., Huang, Z. J., Abbott, L. F., Jessell, T. M., & Azim, E. (2014). Presynaptic inhibition of spinal sensory feedback ensures smooth movement. *Nature 2014 509:7498*, *509*(7498), 43–48. https://doi.org/10.1038/nature13276

Flanagan, J. G., & Van Vactor, D. (1998). Through the Looking Glass: Axon Guidance at the Midline Choice Point. *Cell*, *92*(4), 429–432. https://doi.org/10.1016/S0092-8674(00)80935-6

Foster, N. N., Barry, J., Korobkova, L., Garcia, L., Gao, L., Becerra, M., Sherafat, Y., Peng, B., Li, X., Choi, J. H., Gou, L., Zingg, B., Azam, S., Lo, D., Khanjani, N., Zhang, B., Stanis, J., Bowman, I., Cotter, K., … Dong, H. W. (2021). The mouse cortico–basal ganglia–thalamic network. *Nature 2021 598:7879*, *598*(7879), 188–194. https://doi.org/10.1038/s41586-021-03993-3

Fremeau, R. T., Troyer, M. D., Pahner, I., Nygaard, G. O., Tran, C. H., Reimer, R. J., Bellocchio, E. E., Fortin, D., Storm-Mathisen, J., & Edwards, R. H. (2001). The Expression of Vesicular

Glutamate Transporters Defines Two Classes of Excitatory Synapse. *Neuron*, *31*(2), 247–260. https://doi.org/10.1016/S0896-6273(01)00344-0

Fu, H., Hardy, J., & Duff, K. E. (2018). Selective vulnerability in neurodegenerative diseases. *Nature Neuroscience 2018 21:10*, *21*(10), 1350–1358. https://doi.org/10.1038/S41593-018-0221-2

Giuffrida, R., & Rustioni, A. (1989). Glutamate and aspartate immunoreactivity in corticospinal neurons of rats. *Journal of Comparative Neurology*, *288*(1), 154–164. https://doi.org/10.1002/CNE.902880112

Golan, N. (2022). Molecular Profiling of the Adult Corticospinal Tract Reveals Transcriptional, Anatomical, and Reactive Heterogeneity. *Yale Graduate School of Arts and Sciences Dissertations*. https://elischolar.library.yale.edu/gsas_dissertations

Golan, N., & Cafferty, W. B. (2021). Dissociation of intact adult mouse cortical projection neurons for single-cell RNA-seq. *STAR Protocols*, *2*(4). https://doi.org/10.1016/J.XPRO.2021.100941

Granger, A. J., Wallace, M. L., & Sabatini, B. L. (2017). Multi-transmitter neurons in the mammalian central nervous system. *Current Opinion in Neurobiology*, *45*, 85–91. https://doi.org/10.1016/j.conb.2017.04.007

Hevner, R. F., Daza, R. A. M., Rubenstein, J. L. R., Stunnenberg, H., Olavarria, J. F., & Englund, C. (2003). Beyond Laminar Fate: Toward a Molecular Classification of Cortical Projection/Pyramidal Neurons. *Developmental Neuroscience*, *25*(2–4), 139–151. https://doi.org/10.1159/000072263

Hökfelt, T., Barde, S., Xu, Z. Q. D., Kuteeva, E., Rüegg, J., Le Maitre, E., Risling, M., Kehr, J., Ihnatko, R., Theodorsson, E., Palkovits, M., Deakin, W., Bagdy, G., Juhasz, G., Prud'homme, H. J., Mechawar, N., Diaz-Heijtz, R., & Ögren, S. O. (2018). Neuropeptide and small transmitter coexistence: Fundamental studies and relevance to mental illness. *Frontiers in Neural Circuits*, *12*. https://doi.org/10.3389/FNCIR.2018.00106/FULL

Holstege, G. (1991). *Descending motor pathways and the spinal motor system. Limbic and non-limbic components. september*.

Holstege, G., Bandler, R., & Saper, C. B. (1996). The emotional motor system. *Progress in Brain Research*, *107*.

Holstege, J. C., & Bongers, C. M. H. (1991). A glycinergic projection from the ventromedial lower brainstem to spinal motoneurons. An ultrastructural double labeling study in rat. *Brain Research*, *566*(1–2), 308–315. https://doi.org/10.1016/0006-8993(91)91715-D

Holstege, J. C., & Kuypers, H. G. J. M. (1987). Brainstem projections to spinal motoneurons: An update. *Neuroscience*, *23*(3), 809–821. https://doi.org/10.1016/0306-4522(87)90160-6

Hossaini, M., Goos, J. A. C., Kohli, S. K., & Holstege, J. C. (2012). Distribution of Glycine/GABA Neurons in the Ventromedial Medulla with Descending Spinal Projections and Evidence for an Ascending Glycine/GABA Projection. *PLOS ONE*, *7*(4), e35293. https://doi.org/10.1371/JOURNAL.PONE.0035293

Jarratt, H., & Hyland, B. (1999). Neuronal activity in rat red nucleus during forelimb reach-to-grasp movements. *Neuroscience*, *88*(2), 629–642. https://doi.org/10.1016/S0306-4522(98)00227-9

Jones, S. L., & Gebhart, G. F. (1986). Quantitative characterization of ceruleospinal inhibition of nociceptive transmission in the rat. *Journal of Neurophysiology*, *56*(5), 1397–1410. https://doi.org/10.1152/JN.1986.56.5.1397

Kato, S., Kobayashi, K., Inoue, K. I., Kuramochi, M., Okada, T., Yaginuma, H., Morimoto, K., Shimada, T., Takada, M., & Kobayashi, K. (2011). A lentiviral strategy for highly efficient retrograde gene transfer by pseudotyping with fusion envelope glycoprotein. *Human Gene Therapy*, *22*(2), 197–206. https://doi.org/10.1089/HUM.2009.179/ASSET/IMAGES/LARGE/FIGURE6.JPEG

Kato, S., Sugawara, M., Kobayashi, K., Kimura, K., Inoue, K. ichi, Takada, M., & Kobayashi, K. (2019). Enhancement of the transduction efficiency of a lentiviral vector for neuron-specific retrograde gene delivery through the point mutation of fusion glycoprotein type E. *Journal of Neuroscience Methods*, *311*, 147–155. https://doi.org/10.1016/J.JNEUMETH.2018.10.023

Kebschull, J. M., Richman, E. B., Ringach, N., Friedmann, D., Albarran, E., Kolluru, S. S., Jones, R. C., Allen, W. E., Wang, Y., Cho, S. W., Zhou, H., Ding, J. B., Chang, H. Y., Deisseroth, K., Quake, S. R., & Luo, L. (2020). Cerebellar nuclei evolved by repeatedly duplicating a conserved cell-type set. *Science*, *370*(6523). https://doi.org/10.1126/SCIENCE.ABD5059/SUPPL_FILE/ABD5059_TABLE_S5.XLS

Kelly, R. M., & Strick, P. L. (2000). Rabies as a transneuronal tracer of circuits in the central nervous system. *Journal of Neuroscience Methods*, *103*(1), 63–71. https://doi.org/10.1016/S0165-0270(00)00296-X

Kimura, Y., Satou, C., Fujioka, S., Shoji, W., Umeda, K., Ishizuka, T., Yawo, H., & Higashijima, S. I. (2013). Hindbrain V2a Neurons in the Excitation of Spinal Locomotor Circuits during Zebrafish Swimming. *Current Biology*, *23*(10), 843–849. https://doi.org/10.1016/J.CUB.2013.03.066

Kobayashi, K., Inoue, K. I., Tanabe, S., Kato, S., Takada, M., & Kobayashi, K. (2017). Pseudotyped lentiviral vectors for retrograde gene delivery into target brain regions. *Frontiers in Neuroanatomy*, *11*, 65. https://doi.org/10.3389/FNANA.2017.00065/BIBTEX

Kozareva, V., Martin, C., Osorno, T., Rudolph, S., Guo, C., Vanderburg, C., Nadaf, N., Regev, A., Regehr, W. G., & Macosko, E. (2021). A transcriptomic atlas of mouse cerebellar cortex comprehensively defines cell types. *Nature 2021 598:7879*, *598*(7879), 214–219. https://doi.org/10.1038/s41586-021-03220-z

Kuypers, H. (1964). The Descending Pathways to the Spinal Cord, their Anatomy and Function. *Progress in Brain Research*, *11*, 178–202.

Kuypers, H. G. J. M. (1981). Anatomy of the Descending Pathways. *Comprehensive Physiology*, 597–666. https://doi.org/10.1002/cphy.cp010213

Lemon, R. N. (2008). Descending Pathways in Motor Control. *Https://Doi.Org/10.1146/Annurev.Neuro.31.060407.125547*, *31*, 195–218. https://doi.org/10.1146/ANNUREV.NEURO.31.060407.125547

Li, W. C., & Soffe, S. R. (2019). Stimulation of single, possible CHX10 hindbrain neurons turns swimming on and off in young Xenopus tadpoles. *Frontiers in Cellular Neuroscience*, *13*, 47. https://doi.org/10.3389/FNCEL.2019.00047/BIBTEX

Li, Y. E., Preissl, S., Hou, X., Zhang, Z., Zhang, K., Qiu, Y., Poirion, O. B., Li, B., Chiou, J., Liu, H., Pinto-Duarte, A., Kubo, N., Yang, X., Fang, R., Wang, X., Han, J. Y., Lucero, J., Yan, Y., Miller, M., … Ren, B. (2021). An atlas of gene regulatory elements in adult mouse cerebrum. *Nature 2021 598:7879*, *598*(7879), 129–136. https://doi.org/10.1038/s41586-021-03604-1

Li, Y., Lopez-Huerta, V. G., Adiconis, X., Levandowski, K., Choi, S., Simmons, S. K., Arias-Garcia, M. A., Guo, B., Yao, A. Y., Blosser, T. R., Wimmer, R. D., Aida, T., Atamian, A., Naik, T., Sun, X., Bi, D., Malhotra, D., Hession, C. C., Shema, R., … Feng, G. (2020). Distinct subnetworks of the thalamic reticular nucleus. *Nature 2020 583:7818*, *583*(7818), 819–824. https://doi.org/10.1038/s41586-020-2504-5

Liang, H., Paxinos, G., & Watson, C. (2011). Projections from the brain to the spinal cord in the mouse. *Brain Structure and Function 2010 215:3*, *215*(3), 159–186. https://doi.org/10.1007/S00429-010-0281-X

Liang, H., Paxinos, G., & Watson, C. (2012). The red nucleus and the rubrospinal projection in the mouse. *Brain Structure and Function*, *217*(2), 221–232. https://doi.org/10.1007/S00429-011-0348-3/FIGURES/7

Liu, H., Zhou, J., Tian, W., Luo, C., Bartlett, A., Aldridge, A., Lucero, J., Osteen, J. K., Nery, J. R., Chen, H., Rivkin, A., Castanon, R. G., Clock, B., Li, Y. E., Hou, X., Poirion, O. B., Preissl, S., Pinto-Duarte, A., O'Connor, C., … Ecker, J. R. (2021). DNA methylation atlas of the mouse brain at single-cell resolution. *Nature 2021 598:7879*, *598*(7879), 120–128. https://doi.org/10.1038/s41586-020-03182-8

Liu, Y., Hegarty, S., Winter, C., Wang, F., & He, Z. (2020). Viral vectors for neuronal cell type-specific visualization and manipulations. *Current Opinion in Neurobiology*, *2020*, 67–76. https://doi.org/10.1016/j.conb.2020.03.011

Liu, Y., Latremoliere, A., Li, X., Zhang, Z., Chen, M., Wang, X., Fang, C., Zhu, J., Alexandre, C., Gao, Z., Chen, B., Ding, X., Zhou, J. Y., Zhang, Y., Chen, C., Wang, K. H., Woolf, C. J., & He, Z. (2018). Touch and tactile neuropathic pain sensitivity are set by corticospinal projections. *Nature 2018 561:7724*, *561*(7724), 547–550. https://doi.org/10.1038/s41586-018-0515-2

Lodato, S., Molyneaux, B. J., Zuccaro, E., Goff, L. A., Chen, H. H., Yuan, W., Meleski, A., Takahashi, E., Mahony, S., Rinn, J. L., Gifford, D. K., & Arlotta, P. (2014). Gene co-regulation by Fezf2 selects neurotransmitter identity and connectivity of corticospinal neurons. *Nature Neuroscience 2014 17:8*, *17*(8), 1046–1054. https://doi.org/10.1038/NN.3757

Low, L. K., Liu, X. B., Faulkner, R. L., Coble, J., & Cheng, H. J. (2008). Plexin signaling selectively regulates the stereotyped pruning of corticospinal axons from visual cortex. *Proceedings of the National Academy of Sciences of the United States of America*, *105*(23), 8136–8141. https://doi.org/10.1073/PNAS.0803849105/SUPPL_FILE/0803849105SI.PDF

Lunde, A., Okaty, B. W., Dymecki, S. M., & Glover, J. C. (2019). Molecular Profiling Defines Evolutionarily Conserved Transcription Factor Signatures of Major Vestibulospinal Neuron Groups. *ENeuro*, *6*(1). https://doi.org/10.1523/ENEURO.0475-18.2019

Luo, L., Callaway, E. M., & Svoboda, K. (2018). Genetic Dissection of Neural Circuits: A Decade of Progress. *Neuron*, *98*(2), 256–281. https://doi.org/10.1016/J.NEURON.2018.03.040

Macosko, E. Z., Basu, A., Satija, R., Nemesh, J., Shekhar, K., Goldman, M., Tirosh, I., Bialas, A. R., Kamitaki, N., Martersteck, E. M., Trombetta, J. J., Weitz, D. A., Sanes, J. R., Shalek, A. K., Regev, A., & McCarroll, S. A. (2015). Highly parallel genome-wide expression profiling of individual cells using nanoliter droplets. *Cell*, *161*(5), 1202–1214. https://doi.org/10.1016/J.CELL.2015.05.002/ATTACHMENT/4A61AA26-CCB0-48AC-9D09-485C9571EDBD/MMC6.ZIP

Matho, K. S., Huilgol, D., Galbavy, W., He, M., Kim, G., An, X., Lu, J., Wu, P., Di Bella, D. J., Shetty, A. S., Palaniswamy, R., Hatfield, J., Raudales, R., Narasimhan, A., Gamache, E., Levine, J. M., Tucciarone, J., Szelenyi, E., Harris, J. A., … Huang, Z. J. (2021). Genetic dissection of the glutamatergic neuron system in cerebral cortex. *Nature 2021 598:7879*, *598*(7879), 182–187. https://doi.org/10.1038/s41586-021-03955-9

McCormick, L. E., & Gupton, S. L. (2020). Mechanistic Advances in Axon Pathfinding. *Current Opinion in Cell Biology*, *63*, 11. https://doi.org/10.1016/J.CEB.2019.12.003

Mokha, S. S., McMillan, J. A., & Iggo, A. (1985). Descending control of spinal nociceptive transmission. Actions produced on spinal multireceptive neurones from the nuclei locus coeruleus (LC) and raphe magnus (NRM). *Experimental Brain Research*, *58*(2), 213–226. https://doi.org/10.1007/BF00235305/METRICS

Mokha, S. S., McMillan, J. A., & Iggo, A. (1986). Pathways mediating descending control of spinal nociceptive transmission from the nuclei locus coeruleus (LC) and raphe magnus (NRM) in the cat. *Experimental Brain Research*, *61*(3), 597–606. https://doi.org/10.1007/BF00237586/METRICS

Molyneaux, B. J., Arlotta, P., Hirata, T., Hibi, M., & Macklis, J. D. (2005). Fezl Is Required for the Birth and Specification of Corticospinal Motor Neurons. *Neuron*, *47*(6), 817–831. https://doi.org/10.1016/J.NEURON.2005.08.030

Molyneaux, B. J., Goff, L. A., Brettler, A. C., Chen, H. H., Brown, J. R., Hrvatin, S., Rinn, J. L., & Arlotta, P. (2015). DeCoN: Genome-wide Analysis of In Vivo Transcriptional Dynamics during Pyramidal Neuron Fate Selection in Neocortex. *Neuron*, *85*(2), 275–288. https://doi.org/10.1016/J.NEURON.2014.12.024

Moreno-Lopez, Y., Bichara, C., Delbecq, G., Isope, P., & Cordero-Erausquin, M. (2021). The corticospinal tract primarily modulates sensory inputs in the mouse lumbar cord. *ELife*, *10*, 1–19. https://doi.org/10.7554/eLife.65304

Morris, R., Tosolini, A. P., Goldstein, J. D., & Whishaw, I. Q. (2011). Impaired Arpeggio Movement in Skilled Reaching by Rubrospinal Tract Lesions in the Rat: A Behavioral/Anatomical Fractionation. *Https://Home.Liebertpub.Com/Neu*, *28*(12), 2439–2451. https://doi.org/10.1089/NEU.2010.1708

Moses, L., & Pachter, L. (2022). Museum of spatial transcriptomics. *Nature Methods 2022 19:5*, *19*(5), 534–546. https://doi.org/10.1038/s41592-022-01409-2

Muñoz-Castañeda, R., Zingg, B., Matho, K. S., Chen, X., Wang, Q., Foster, N. N., Li, A., Narasimhan, A., Hirokawa, K. E., Huo, B., Bannerjee, S., Korobkova, L., Park, C. S., Park, Y. G., Bienkowski, M. S., Chon, U., Wheeler, D. W., Li, X., Wang, Y., … Dong, H. W. (2021). Cellular anatomy of the mouse primary motor cortex. *Nature 2021 598:7879*, *598*(7879), 159–166. https://doi.org/10.1038/s41586-021-03970-w

Nassi, J. J., Cepko, C. L., Born, R. T., & Beier, K. T. (2015). Neuroanatomy goes viral! *Frontiers in Neuroanatomy*, *9*(July), 80. https://doi.org/10.3389/FNANA.2015.00080/BIBTEX

Nelson, A., Schneider, D. M., Takatoh, J., Sakurai, K., Wang, F., & Mooney, R. (2013). A Circuit for Motor Cortical Modulation of Auditory Cortical Activity. *Journal of Neuroscience*, *33*(36), 14342–14353. https://doi.org/10.1523/JNEUROSCI.2275-13.2013

Norsworthy, M. W., Bei, F., Kawaguchi, R., Wang, Q., Tran, N. M., Li, Y., Brommer, B., Zhang, Y., Wang, C., Sanes, J. R., Coppola, G., & He, Z. (2017). Sox11 Expression Promotes Regeneration of Some Retinal Ganglion Cell Types but Kills Others. *Neuron*, *94*(6), 1112-1120.e4. https://doi.org/10.1016/J.NEURON.2017.05.035

Nusbaum, M. P., Blitz, D. M., & Marder, E. (2017). Functional consequences of neuropeptide and small-molecule co-transmission. *Nature Reviews Neuroscience 2017 18:7*, *18*(7), 389–403. https://doi.org/10.1038/nrn.2017.56

Nygren, L.-G., & Olson, L. (1977). A New Major Projection From Locus Coeruleus: The Main Source of Noradrenergic Nerve Terminals in the Ventral and Dorsal Columns of the Spinal Cord. *Brain Research*, *132*, 85.

Olivares-Moreno, R., Rodriguez-Moreno, P., Lopez-Virgen, V., Macías, M., Altamira-Camacho, M., & Rojas-Piloni, G. (2021). Corticospinal vs Rubrospinal Revisited: An Evolutionary Perspective for Sensorimotor Integration. *Frontiers in Neuroscience*, *15*, 680. https://doi.org/10.3389/FNINS.2021.686481/BIBTEX

Perreault, M. C., & Giorgi, A. (2019). Diversity of reticulospinal systems in mammals. *Current Opinion in Physiology*, *8*, 161. https://doi.org/10.1016/J.COPHYS.2019.03.001

Persson, S., Boulland, J. L., Aspling, M., Larsson, M., Fremeau, R. T., Edwards, R. H., Storm-Mathisen, J., Chaudhry, F. A., & Broman, J. (2006). Distribution of vesicular glutamate transporters 1 and 2 in the rat spinal cord, with a note on the spinocervical tract. *The Journal of Comparative Neurology*, *497*(5), 683–701. https://doi.org/10.1002/CNE.20987

Pfaff, S. L., Mendelsohn, M., Stewart, C. L., Edlund, T., & Jessell, T. M. (1996). Requirement for LIM Homeobox Gene Isl1 in Motor Neuron Generation Reveals a Motor Neuron– Dependent Step

in Interneuron Differentiation. *Cell*, *84*(2), 309–320. https://doi.org/10.1016/S0092-8674(00)80985-X

Picelli, S., Faridani, O. R., Björklund, Å. K., Winberg, G., Sagasser, S., & Sandberg, R. (2014). Full-length RNA-seq from single cells using Smart-seq2. *Nature Protocols 2013 9:1*, *9*(1), 171–181. https://doi.org/10.1038/nprot.2014.006

Pomrenze, M. B., Giovanetti, S. M., Maiya, R., Gordon, A. G., Kreeger, L. J., & Messing, R. O. (2019). Dissecting the Roles of GABA and Neuropeptides from Rat Central Amygdala CRF Neurons in Anxiety and Fear Learning. *Cell Reports*, *29*(1), 13-21.e4. https://doi.org/10.1016/J.CELREP.2019.08.083/ATTACHMENT/EF7EA191-740A-4579-AF86-A38E099D0B6C/MMC1.PDF

Poplawski, G. H. D., Kawaguchi, R., Van Niekerk, E., Lu, P., Mehta, N., Canete, P., Lie, R., Dragatsis, I., Meves, J. M., Zheng, B., Coppola, G., & Tuszynski, M. H. (2020). Injured adult neurons regress to an embryonic transcriptional growth state. *Nature 2020 581:7806*, *581*(7806), 77–82. https://doi.org/10.1038/s41586-020-2200-5

Ragan, T., Kadiri, L. R., Venkataraju, K. U., Bahlmann, K., Sutin, J., Taranda, J., Arganda-Carreras, I., Kim, Y., Seung, H. S., & Osten, P. (2012). Serial two-photon tomography: an automated method for ex-vivo mouse brain imaging. *Nature Methods*, *9*(3), 255. https://doi.org/10.1038/NMETH.1854

Reardon, T. R., Murray, A. J., Turi, G. F., Wirblich, C., Croce, K. R., Schnell, M. J., Jessell, T. M., & Losonczy, A. (2016). Rabies Virus CVS-N2cΔG Strain Enhances Retrograde Synaptic Transfer and Neuronal Viability. *Neuron*, *89*(4), 711–724. https://doi.org/10.1016/J.NEURON.2016.01.004

Rheaume, B. A., Jereen, A., Bolisetty, M., Sajid, M. S., Yang, Y., Renna, K., Sun, L., Robson, P., & Trakhtenberg, E. F. (2018). Single cell transcriptome profiling of retinal ganglion cells identifies cellular subtypes. *Nature Communications 2018 9:1*, *9*(1), 1–17. https://doi.org/10.1038/s41467-018-05134-3

Russ, D. E., Cross, R. B. P., Li, L., Koch, S. C., Matson, K. J. E., Yadav, A., Alkaslasi, M. R., Lee, D. I., Le Pichon, C. E., Menon, V., & Levine, A. J. (2021). A harmonized atlas of mouse spinal cord cell types and their spatial organization. *Nature Communications 2021 12:1*, *12*(1), 1–20. https://doi.org/10.1038/s41467-021-25125-1

Sahni, V., Itoh, Y., Shnider, S. J., & Macklis, J. D. (2021). Crim1 and Kelch-like 14 exert complementary dual-directional developmental control over segmentally specific corticospinal axon projection targeting. *Cell Reports*, *37*(3), 109842. https://doi.org/10.1016/J.CELREP.2021.109842

Sahni, V., Shnider, S. J., Jabaudon, D., Song, J. H. T., Itoh, Y., Greig, L. C., & Macklis, J. D. (2021). Corticospinal neuron subpopulation-specific developmental genes prospectively indicate mature segmentally specific axon projection targeting. *Cell Reports*, *37*(3), 109843. https://doi.org/10.1016/J.CELREP.2021.109843

Sathyamurthy, A., Barik, A., Dobrott, C. I., Matson, K. J. E., Stoica, S., Pursley, R., Chesler, A. T., & Levine, A. J. (2020). Cerebellospinal Neurons Regulate Motor Performance and Motor Learning. *Cell Reports*, *31*(6), 107595. https://doi.org/10.1016/J.CELREP.2020.107595

Sathyamurthy, A., Johnson, K. R., Matson, K. J. E., Dobrott, C. I., Li, L., Ryba, A. R., Bergman, T. B., Kelly, M. C., Kelley, M. W., & Levine, A. J. (2018). Massively Parallel Single Nucleus Transcriptional Profiling Defines Spinal Cord Neurons and Their Activity during Behavior. *Cell Reports*, *22*(8), 2216–2225. https://doi.org/10.1016/J.CELREP.2018.02.003

Scala, F., Kobak, D., Bernabucci, M., Bernaerts, Y., Cadwell, C. R., Castro, J. R., Hartmanis, L., Jiang, X., Laturnus, S., Miranda, E., Mulherkar, S., Tan, Z. H., Yao, Z., Zeng, H., Sandberg, R., Berens, P., & Tolias, A. S. (2020). Phenotypic variation of transcriptomic cell types in mouse motor

cortex. *Nature 2020 598:7879*, *598*(7879), 144–150. https://doi.org/10.1038/s41586-020-2907-3

Schön, C., Biel, M., & Michalakis, S. (2015). Retinal gene delivery by adeno-associated virus (AAV) vectors: Strategies and applications. *European Journal of Pharmaceutics and Biopharmaceutics*, *95*, 343–352. https://doi.org/10.1016/J.EJPB.2015.01.009

Schwarz, L. A., Miyamichi, K., Gao, X. J., Beier, K. T., Weissbourd, B., Deloach, K. E., Ren, J., Ibanes, S., Malenka, R. C., Kremer, E. J., & Luo, L. (2015). Viral-genetic tracing of the input–output organization of a central noradrenaline circuit. *Nature 2015 524:7563*, *524*(7563), 88–92. https://doi.org/10.1038/nature14600

Sharma, K., Sheng, H. Z., Lettieri, K., Li, H., Karavanov, A., Potter, S., Westphal, H., & Pfaff, S. L. (1998). LIM Homeodomain Factors Lhx3 and Lhx4 Assign Subtype Identities for Motor Neurons. *Cell*, *95*(6), 817–828. https://doi.org/10.1016/S0092-8674(00)81704-3

Stanek, E., Rodriguez, E., Zhao, S., Han, B. X., & Wang, F. (2016). Supratrigeminal Bilaterally Projecting Neurons Maintain Basal Tone and Enable Bilateral Phasic Activation of Jaw-Closing Muscles. *Journal of Neuroscience*, *36*(29), 7663–7675. https://doi.org/10.1523/JNEUROSCI.0839-16.2016

Stelzer, E. H. K., Strobl, F., Chang, B. J., Preusser, F., Preibisch, S., McDole, K., & Fiolka, R. (2021). Light sheet fluorescence microscopy. *Nature Reviews Methods Primers 2021 1:1*, *1*(1), 1–25. https://doi.org/10.1038/s43586-021-00069-4

Tang, F., Barbacioru, C., Wang, Y., Nordman, E., Lee, C., Xu, N., Wang, X., Bodeau, J., Tuch, B. B., Siddiqui, A., Lao, K., & Surani, M. A. (2009). mRNA-Seq whole-transcriptome analysis of a single cell. *Nature Methods 2009 6:5*, *6*(5), 377–382. https://doi.org/10.1038/nmeth.1315

Tappan, S. J., Eastwood, B. S., O'Connor, N., Wang, Q., Ng, L., Feng, D., Hooks, B. M., Gerfen, C. R., Hof, P. R., Schmitz, C., & Glaser, J. R. (2019). Automatic navigation system for the mouse brain. *Journal of Comparative Neurology*, *527*(13), 2200–2211. https://doi.org/10.1002/CNE.24635

Tasic, B., Menon, V., Nguyen, T. N., Kim, T. K., Jarsky, T., Yao, Z., Levi, B., Gray, L. T., Sorensen, S. A., Dolbeare, T., Bertagnolli, D., Goldy, J., Shapovalova, N., Parry, S., Lee, C., Smith, K., Bernard, A., Madisen, L., Sunkin, S. M., … Zeng, H. (2016). Adult mouse cortical cell taxonomy revealed by single cell transcriptomics. *Nature Neuroscience 2016 19:2*, *19*(2), 335–346. https://doi.org/10.1038/nn.4216

Tasic, B., Yao, Z., Graybuck, L. T., Smith, K. A., Nguyen, T. N., Bertagnolli, D., Goldy, J., Garren, E., Economo, M. N., Viswanathan, S., Penn, O., Bakken, T., Menon, V., Miller, J., Fong, O., Hirokawa, K. E., Lathia, K., Rimorin, C., Tieu, M., … Zeng, H. (2018). Shared and distinct transcriptomic cell types across neocortical areas. *Nature 2018 563:7729*, *563*(7729), 72–78. https://doi.org/10.1038/s41586-018-0654-5

ten Donkelaar, H. J. (2009). Evolution of Motor Systems: Corticospinal, Reticulospinal, Rubrospinal and Vestibulospinal Systems. *Encyclopedia of Neuroscience*, 1248–1254. https://doi.org/10.1007/978-3-540-29678-2_3131

Tervo, D. G. R., Hwang, B. Y., Viswanathan, S., Gaj, T., Lavzin, M., Ritola, K. D., Lindo, S., Michael, S., Kuleshova, E., Ojala, D., Huang, C. C., Gerfen, C. R., Schiller, J., Dudman, J. T., Hantman, A. W., Looger, L. L., Schaffer, D. V., & Karpova, A. Y. (2016). A Designer AAV Variant Permits Efficient Retrograde Access to Projection Neurons. *Neuron*, *92*(2), 372–382. https://doi.org/10.1016/J.NEURON.2016.09.021

Tran, N. M., Shekhar, K., Whitney, I. E., Jacobi, A., Benhar, I., Hong, G., Yan, W., Adiconis, X., Arnold, M. E., Lee, J. M., Levin, J. Z., Lin, D., Wang, C., Lieber, C. M., Regev, A., He, Z., & Sanes, J. R. (2019). Single-Cell Profiles of Retinal Ganglion Cells Differing in Resilience to Injury Reveal Neuroprotective Genes. *Neuron*, *104*(6), 1039-1055.e12. https://doi.org/10.1016/J.NEURON.2019.11.006

Trudeau, L. É. (2004). Glutamate co-transmission as an emerging concept in monoamine neuron function. *Journal of Psychiatry and Neuroscience*, *29*(4), 296. /pmc/articles/PMC446224/

Tsuchida, T., Ensini, M., Morton, S. B., Baldassare, M., Edlund, T., Jessell, T. M., & Pfaff, S. L. (1994). Topographic organization of embryonic motor neurons defined by expression of LIM homeobox genes. *Cell*, *79*(6), 957–970. https://doi.org/10.1016/0092-8674(94)90027-2

Tyson, A. L., Vélez-Fort, M., Rousseau, C. V., Cossell, L., Tsitoura, C., Lenzi, S. C., Obenhaus, H. A., Claudi, F., Branco, T., & Margrie, T. W. (2022). Accurate determination of marker location within whole-brain microscopy images. *Scientific Reports 2022 12:1*, *12*(1), 1–8. https://doi.org/10.1038/s41598-021-04676-9

Valla, J., Delfini, C., Diagne, M., Pinganaud, G., Buisseret, P., & Buisseret-Delmas, C. (2003). Vestibulotrigeminal and vestibulospinal projections in rats: retrograde tracing coupled to glutamic acid decarboxylase immunoreactivity. *Neuroscience Letters*, *340*(3), 225–228. https://doi.org/10.1016/S0304-3940(03)00127-7

Valtschanoff, J. G., Weinberg, R. J., & Rustioni, A. (1993). Amino acid immunoreactivity in corticospinal terminals. *Experimental Brain Research*, *93*(1), 95–103. https://doi.org/10.1007/BF00227784/METRICS

Vanderhorst, V. G. J. M., & Ulfhake, B. (2006). *The organization of the brainstem and spinal cord of the mouse: Relationships between monoaminergic, cholinergic, and spinal projection systems*. https://doi.org/10.1016/j.jchemneu.2005.08.003

Varela-Echavarría, A., Pfaff, S. L., & Guthrie, S. (1996). Differential Expression of LIM Homeobox Genes among Motor Neuron Subpopulations in the Developing Chick Brain Stem. *Molecular and Cellular Neuroscience*, *8*(4), 242–257. https://doi.org/10.1006/MCNE.1996.0061

Wang, Q., Ding, S. L., Li, Y., Royall, J., Feng, D., Lesnar, P., Graddis, N., Naeemi, M., Facer, B., Ho, A., Dolbeare, T., Blanchard, B., Dee, N., Wakeman, W., Hirokawa, K. E., Szafer, A., Sunkin, S. M., Oh, S. W., Bernard, A., … Ng, L. (2020). The Allen Mouse Brain Common Coordinate Framework: A 3D Reference Atlas. *Cell*, *181*(4), 936-953.e20. https://doi.org/10.1016/J.CELL.2020.04.007

Wang, X., Liu, Y., Li, X., Zhang, Z., Yang, H., Zhang, Y., Williams, P. R., Alwahab, N. S. A., Kapur, K., Yu, B., Zhang, Y., Chen, M., Ding, H., Gerfen, C. R., Wang, K. H., & He, Z. (2017). Deconstruction of Corticospinal Circuits for Goal-Directed Motor Skills. *Cell*, *171*(2), 440-455.e14. https://doi.org/10.1016/J.CELL.2017.08.014

Wang, Z., Maunze, B., Wang, Y., Tsoulfas, P., & Blackmore, M. G. (2018). Global Connectivity and Function of Descending Spinal Input Revealed by 3D Microscopy and Retrograde Transduction. *Journal of Neuroscience*, *38*(49), 10566–10581. https://doi.org/10.1523/JNEUROSCI.1196-18.2018

Weimann, J. M., Alex Zhang, Y., Levin, M. E., Patrick Devine, W., Brû let, P., & McConnell, S. K. (1999). Cortical Neurons Require Otx1 for the Refinement of Exuberant Axonal Projections to Subcortical Targets. *Neuron*, *24*, 819–831.

Whishaw, I. Q., Pellis, S. M., Gorny, B., Kolb, B., & Tetzlaff, W. (1993). Proximal and distal impairments in rat forelimb use in reaching follow unilateral pyramidal tract lesions. *Behavioural Brain Research*, *56*(1), 59–76. https://doi.org/10.1016/0166-4328(93)90022-I

Wickersham, I. R., Finke, S., Conzelmann, K. K., & Callaway, E. M. (2006). Retrograde neuronal tracing with a deletion-mutant rabies virus. *Nature Methods 2007 4:1*, *4*(1), 47–49. https://doi.org/10.1038/NMETH999

Wickersham, I. R., Lyon, D. C., Barnard, R. J. O., Mori, T., Finke, S., Conzelmann, K. K., Young, J. A. T., & Callaway, E. M. (2007). Monosynaptic Restriction of Transsynaptic Tracing from Single, Genetically Targeted Neurons. *Neuron*, *53*(5), 639–647. https://doi.org/10.1016/J.NEURON.2007.01.033

Williams, P. T. J. A., Kim, S., & Martin, J. H. (2014). Postnatal Maturation of the Red Nucleus Motor Map Depends on Rubrospinal Connections with Forelimb Motor Pools. *Journal of Neuroscience*, *34*(12), 4432–4441. https://doi.org/10.1523/JNEUROSCI.5332-13.2014

Winter, C. C., He, Z., & Jacobi, A. (2022). Axon Regeneration: A Subcellular Extension in Multiple Dimensions. *Cold Spring Harbor Perspectives in Biology*, *14*(3), 1–20. https://doi.org/10.1101/cshperspect.a040923

Yao, Z., Liu, H., Xie, F., Fischer, S., Adkins, R. S., Aldridge, A. I., Ament, S. A., Bartlett, A., Behrens, M. M., Van den Berge, K., Bertagnolli, D., de Bézieux, H. R., Biancalani, T., Booeshaghi, A. S., Bravo, H. C., Casper, T., Colantuoni, C., Crabtree, J., Creasy, H., … Mukamel, E. A. (2021). A transcriptomic and epigenomic cell atlas of the mouse primary motor cortex. *Nature*, *598*(7879), 103–110. https://doi.org/10.1038/S41586-021-03500-8

Yao, Z., van Velthoven, C. T. J., Nguyen, T. N., Goldy, J., Sedeno-Cortes, A. E., Baftizadeh, F., Bertagnolli, D., Casper, T., Chiang, M., Crichton, K., Ding, S. L., Fong, O., Garren, E., Glandon, A., Gouwens, N. W., Gray, J., Graybuck, L. T., Hawrylycz, M. J., Hirschstein, D., … Zeng, H. (2021). A taxonomy of transcriptomic cell types across the isocortex and hippocampal formation. *Cell*, *184*(12), 3222-3241.e26. https://doi.org/10.1016/J.CELL.2021.04.021

Yao, Z., Velthoven, C. T. J. van, Kunst, M., Zhang, M., McMillen, D., Lee, C., Jung, W., Goldy, J., Abdelhak, A., Baker, P., Barkan, E., Bertagnolli, D., Campos, J., Carey, D., Casper, T., Chakka, A. B., Chakrabarty, R., Chavan, S., Chen, M., … Zeng, H. (2023). A high-resolution transcriptomic and spatial atlas of cell types in the whole mouse brain. *BioRxiv*, 2023.03.06.531121. https://doi.org/10.1101/2023.03.06.531121

Zaaimi, B., Edgley, S. A., Soteropoulos, D. S., & Baker, S. N. (2012). Changes in descending motor pathway connectivity after corticospinal tract lesion in macaque monkey. *Brain*, *135*(7), 2277–2289. https://doi.org/10.1093/BRAIN/AWS115

Zaaimi, B., Soteropoulos, D. S., Fisher, K. M., Riddle, C. N., & Baker, S. N. (2018). Classification of Neurons in the Primate Reticular Formation and Changes after Recovery from Pyramidal Tract Lesion. *Journal of Neuroscience*, *38*(27), 6190–6206. https://doi.org/10.1523/JNEUROSCI.3371-17.2018

Zeng, H. (2022). What is a cell type and how to define it? *Cell*, *185*, 2739–2755. https://doi.org/10.1016/j.cell.2022.06.031

Zeng, H., & Sanes, J. R. (2017). Neuronal cell-type classification: challenges, opportunities and the path forward. *Nature Reviews Neuroscience 2017 18:9*, *18*(9), 530–546. https://doi.org/10.1038/nrn.2017.85

Zhang, M., Eichhorn, S. W., Zingg, B., Yao, Z., Cotter, K., Zeng, H., Dong, H., & Zhuang, X. (2021). Spatially resolved cell atlas of the mouse primary motor cortex by MERFISH. *Nature 2021 598:7879*, *598*(7879), 137–143. https://doi.org/10.1038/s41586-021-03705-x

Zhang, Z., Li, F., & Sun, T. (2012). Does repair of spinal cord injury follow the evolutionary theory? *Neural Regeneration Research*, *7*(11), 849. https://doi.org/10.3969/J.ISSN.1673-5374.2012.11.009

Zhang, Z., Zhou, J., Tan, P., Pang, Y., Rivkin, A. C., Kirchgessner, M. A., Williams, E., Lee, C. T., Liu, H., Franklin, A. D., Miyazaki, P. A., Bartlett, A., Aldridge, A. I., Vu, M., Boggeman, L., Fitzpatrick, C., Nery, J. R., Castanon, R. G., Rashid, M., … Callaway, E. M. (2021). Epigenomic diversity of cortical projection neurons in the mouse brain. *Nature 2021 598:7879*, *598*(7879), 167–173. https://doi.org/10.1038/s41586-021-03223-w

Ziffra, R. S., Kim, C. N., Ross, J. M., Wilfert, A., Turner, T. N., Haeussler, M., Casella, A. M., Przytycki, P. F., Keough, K. C., Shin, D., Bogdanoff, D., Kreimer, A., Pollard, K. S., Ament, S. A., Eichler, E. E., Ahituv, N., & Nowakowski, T. J. (2021). Single-cell epigenomics reveals mechanisms of human cortical development. *Nature 2021 598:7879*, *598*(7879), 205–213. https://doi.org/10.1038/s41586-021-03209-8

Zörner, B., Bachmann, L. C., Filli, L., Kapitza, S., Gullo, M., Bolliger, M., Starkey, M. L., Röthlisberger, M., Gonzenbach, R. R., & Schwab, M. E. (2014). Chasing central nervous system plasticity: the brainstem's contribution to locomotor recovery in rats with spinal cord injury. *Brain*, *137*(6), 1716–1732. https://doi.org/10.1093/BRAIN/AWU078

1

An anatomical atlas of cervical- and lumbar- projecting spinal projecting neurons

Publication: This chapter was adapted from a manuscript under revision at *Nature*, revision submitted in September 2023.

A taxonomy of transcriptomic cell types reveals organizational and functional principles of brain-wide spinal projecting neurons

Carla C. Winter[1,2,3,4,12], Anne Jacobi[1,2,11,12,✉], Junfeng Su[1,2,12], Leeyup Chung[1,2], Cindy T. J. van Velthoven[5], Zizhen Yao[5], Changkyu Lee[5], Zicong Zhang[1,2], Shuguang Yu[1,2], Kun Gao[6,7], Geraldine Duque Salazar[1,2], Evgenii Kegeles[1,2,3], Riki Kawaguchi[6,7], Yu Zhang[1,2], Makenzie C. Tomihiro[1,2], Junjie Zhu[1,2], Jing Tang[1,2], Xuan Song[1,2], Ryan J. Donahue[1,2], Qing Wang[6,7], Delissa McMillen[5], Michael Kunst[5], Kimberly A. Smith[5], Alexandra Krol[8], Guoping Feng[8,9], Yuanyuan Liu[10], Daniel H. Geschwind[6,7], Bosiljka Tasic[5], Hongkui Zeng[5,✉], Zhigang He[1,2,✉]

1. F.M. Kirby Neurobiology Center, Boston Children's Hospital, Boston, MA, USA
2. Departments of Neurology and Ophthalmology, Harvard Medical School, Boston, MA, USA
3. PhD Program in Biological and Biomedical Sciences, Harvard Medical School, Boston, MA, USA
4. Harvard-MIT MD-PhD Program, Harvard Medical School, Boston, MA, USA
5. Allen Institute for Brain Science, Seattle, WA, USA
6. Program in Neurogenetics, Department of Neurology, David Geffen School of Medicine, University of California Los Angeles, Los Angeles, CA, USA
7. Semel Institute for Neuroscience and Human Behavior, David Geffen School of Medicine, University of California Los Angeles, Los Angeles, CA, USA
8. McGovern Institute for Brain Research and the Department of Brain and Cognitive Sciences, Massachusetts Institute of Technology, Cambridge, MA, USA
9. The Stanley Center for Psychiatric Research, Broad Institute of MIT and Harvard, Cambridge, MA, USA
10. Somatosensation and Pain Unit, National Institute of Dental and Craniofacial Research, National Center for Complementary and Integrative Health, National Institutes of Health, Bethesda, MD, USA
11. Present address: F. Hoffman-La Roche, pRED, Basel, Switzerland
12. These authors contributed equally.

✉Correspondence: Zhigang He (zhigang.he@childrens.harvard.edu), Hongkui Zeng (HongkuiZ@alleninstitute.org), and Anne Jacobi (Anne.Jacobi@roche.com)

Author contributions: Conceptualization: C.C.W., A.J., H.Z., Z.H. Manuscript writing: C.C.W. and Z.H. Figure generation: Led by C.C.W, with help from J.S. Manuscript review and editing: contributions from all authors. Data analysis lead and coordination: C.C.W. Retrograde Injections: Led by Z.Z. Histology and analysis: Led by C.C.W., with help from J.S.

1.1 ABSTRACT.

Spinal projecting neurons (SPNs) play critical roles in transmitting command signals from the brain to the spinal cord to control motor, sensory, and autonomic functions, and their comprehensive anatomical mapping can provide crucial insights into how the brain controls the body. In this study, we developed an optimized strategy using AAV2/retro-hSyn-H2B recombinant viral vector for retrograde labeling of cervical- and lumbar- projecting SPNs across the whole mouse brain. This method offered a marked improvement over traditional techniques, providing efficient and robust expression that effectively distinguished neuronal soma from neighboring fibers. Additionally, we devised a pipeline employing serial two-photon tomography for high-resolution whole-brain imaging and subsequent brain-wide automated segmentation and registration to the Allen Common Coordinate Framework. This allowed us to comprehensively map the distribution of SPNs within the brain, confirming concentrations in the cortex, hypothalamus, midbrain, cerebellum, pons, and medulla. By leveraging our anatomical atlas, we explored projection target specificity across distinct SPN populations, revealing differential somatotopic distributions among corticospinal, rubrospinal, and cerebellospinal neurons. This work has set the stage for deeper understanding of brain-spinal cord circuits and holds significant potential for advancing treatments for neurodegenerative diseases and spinal cord injuries.

1.2 INTRODUCTION.

Spinal projecting neurons (SPNs) carry command signals from numerous supraspinal regions to the spinal cord to execute control of nearly all bodily functions. The importance of these descending tracts is illustrated by sensory, motor, and autonomic dysfunction in conditions such as spinal cord injury (SCI) and as amyotrophic lateral sclerosis. Thus, comprehensive characterization of SPNs is essential for decoding brain-body interactions and developing neural repair strategies after injury.

Pioneered by Kuypers (Kuypers, 1981), early efforts aimed to characterize SPNs and their projections with a variety of anatomical tracing methods such as silver degeneration, and retrograde and anterograde labeling using radiolabeling, fluorescent, and other tracers. These and other follow up studies led to the classification of SPNs into different descending tracts (Lemon, 2008). For example, corticospinal neurons (CSNs) in motor and somatosensory cortices and rubrospinal neurons (RuSNs) in the midbrain red nucleus elaborate the densely projecting corticospinal tract (CST) and rubrospinal tract (RuST), respectively. In contrast, the reticulospinal neurons (ReSNs) in the hindbrain reticular formation project their axons diffusely in different parts of the spinal cord, forming the anatomically poorly defined reticulospinal tract (ReST).

Though this foundational work was informative, conclusions about the overall anatomical organization of descending pathways were limited for several reasons. First, early anatomical conclusions relied on fragmented descriptions of supraspinal regions across studies and species. To overcome this challenge, Liang et al. produced the first comprehensive, brain-wide characterization of SPNs in mice using FluoroGold- and horseradish peroxidase-based retrograde labeling (Liang et al., 2011). This anatomical atlas provided an invaluable resource, harmonizing disparate findings from earlier studies and establishing a comprehensive foundation for future investigations in physiological and pathological contexts. However, two additional limitations emerged from this atlas: first, the targeting efficiency and second, the throughput of analytical methods were both limited. The use of dye-based retrograde tracers likely underestimated the number of retrogradely labeled neurons, and manual sectioning and assignment to anatomical atlases is a time-consuming process and demands extensive background knowledge, making data analysis inaccessible for the broader community. Finally, imaging modalities and signal detection have limited our understanding of SPNs. SPNs constitute only a small portion of the resident neurons in individual brain regions and their projections

in the spinal cord are often spatially overlapping with each other, making precise localization of their cell bodies challenging (Steward et al., 2021; Z. Wang et al., 2018).

In this chapter, we address the current limitations by developing a streamlined pipeline for efficient retrograde labeling and high-resolution imaging of SPNs. We leverage recombinant viral technology to achieve highly efficient transduction of SPNs and demonstrate the suitability of serial two-photon tomography (STPT) as an accessible imaging modality for automated whole-brain imaging and registration. These advancements provide a valuable resource for further exploration of the anatomical characteristics of SPNs.

1.3 RESULTS.

1.3.1 OPTIMIZATION OF RETROGRADE LABELING IN SPINAL PROJECTING NEURONS:

Historically, spinal projecting neurons (SPNs) have been characterized using different anatomical tracing techniques such as silver degeneration, radiolabeling, and fluorescent dyes. However, the emergence of recombinant viral technology has revolutionized the field of neuronal tracing by providing a more robust and flexible approach for targeted and efficient transgene expression in specific neuronal populations (Liu et al., 2020; Nassi et al., 2015). Notably, recombinant viruses can transduce neurons starting from their axon terminals, enabling the targeting of cells with specific projection targets through retrograde viral infection. Here, we sought to optimize a retrograde labeling strategy for SPNs using recombinant viral technology.

To label SPNs for whole-brain imaging, we identified several criteria that the chosen recombinant viral vector must meet: the virus must 1) be highly efficient, 2) have limited tropism for neuronal subpopulations (i.e., transfects SPN populations throughout the brain), 3) drive bright fluorophore signal such that it does not need to be amplified with immunohistochemistry (IHC), 4)

allow soma to be distinguished from neighboring neuronal fibers, 5) have limited time between injection and transfection, 6) be relatively easy to produce, 7) have limited cytotoxicity, and 8) have limited transsynaptic labeling. With these criteria in mind, we tested three candidate vectors. AAV2/retro (Tervo et al., 2016), CVS-N2c(ΔG) rabies virus (Reardon et al., 2016), and HiRet-lentivirus (Kato et al., 2011; Kinoshita et al., 2012; Liu et al., 2018; X. Wang et al., 2017) have each been shown to exhibit high efficiency retrograde labeling of long-projecting neurons with limited cytotoxicity. Importantly, deletion of the glycoprotein G gene in the CVS-N2c(ΔG) rabies virus restricts transsynaptic viral transmission typically exhibited by rabies strains.

We retrogradely labeled SPNs via injection of the recombinant viral vectors into the cervical (segments 4-6) and lumbar (segments 2-4) spinal cord of adult C57BL/6J mice. Two to four weeks post injection (wpi), we qualitatively assessed the labeling of SPNs across the whole mouse brain (**Figure 1-1**). At two wpi, we found AAV2/retro had robust expression in SPN populations across the whole mouse brain, including cortex, red nucleus, and medulla. In contrast, CVS-N2c(ΔG) and HiRet-Lenti had minimal or no expression at two wpi (data not shown). At four wpi, CVS-N2c(ΔG) and HiRet-Lenti still exhibited minimal labeling in cortical layer 5, but varying degrees of expression in red nucleus and medulla. Globally, CVS-N2c(ΔG) had more limited expression compared to HiRet-Lenti, and while the HiRet-Lenti vector had robust expression in the medulla, labeling in the red nucleus was limited compared to AAV2/retro. The difference in injection to transfection time across vectors indicates that AAV2/retro may undergo more rapid axonal uptake and retrograde axonal transport than CVS-N2c(ΔG) and HiRet-Lenti. Further, the robust expression in the medulla by HiRet-Lenti but less robust in red nucleus and cortex suggests longer time may be needed for the HiRet-Lenti to reach the more distant soma targets in midbrain and cortex, and/or this vector may exhibit tropism for medullary SPNs.

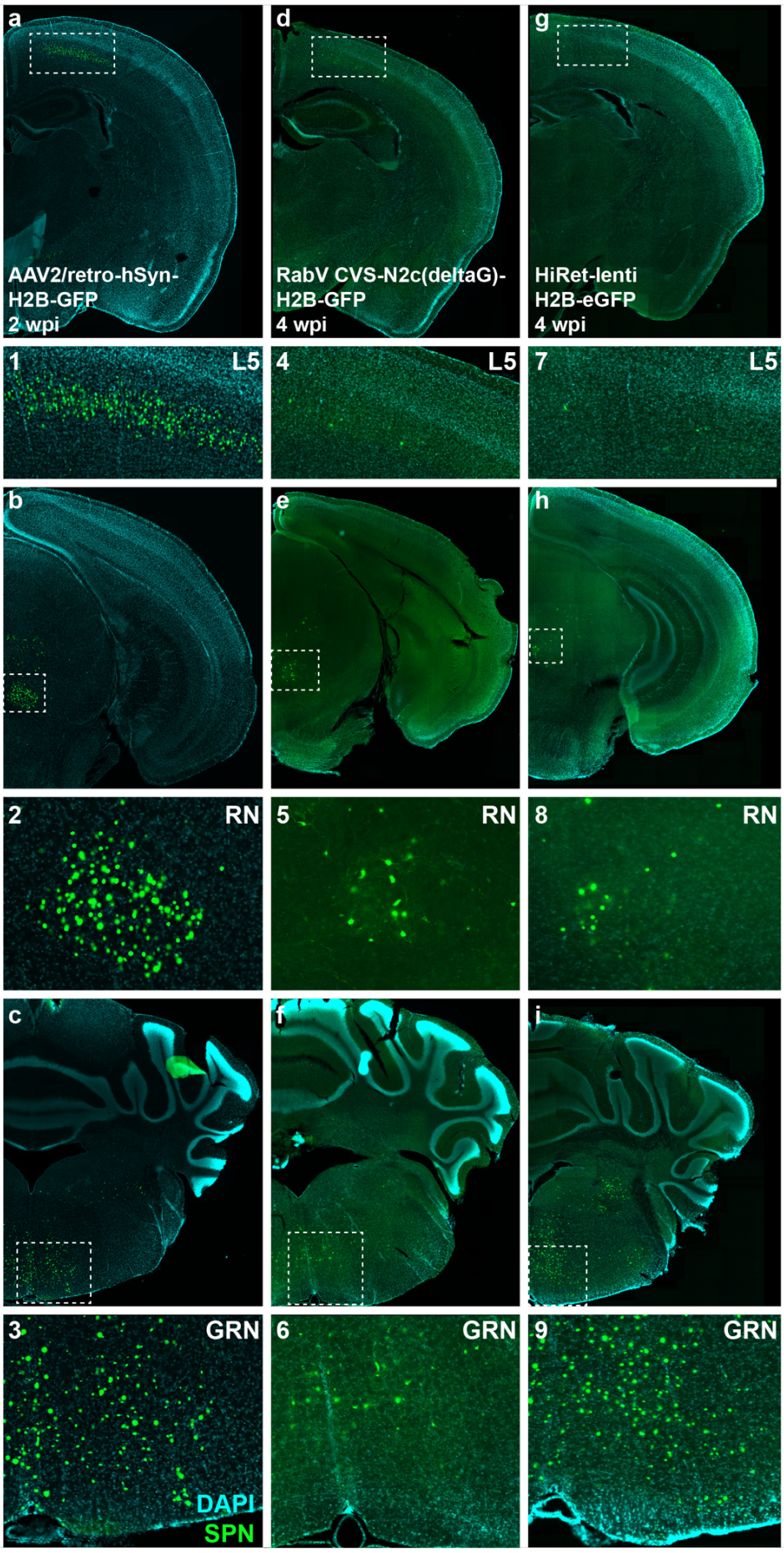

a
AAV2/retro-hSyn-
H2B-GFP
2 wpi
d
RabV CVS-N2c(deltaG)-
H2B-GFP
4 wpi
g
HiRet-lenti
H2B-eGFP
4 wpi
1
L5
4
L5
7
L5
b
e
h
2
RN
5
RN
8
RN
c
f
i
3
GRN
6
GRN
9
GRN
DAPI
SPN

Figure 1-1: Choice of recombinant viral vector for retrograde labeling of spinal projecting neurons. Three recombinant viral vectors were assessed for their capacity to retrogradely label spinal projecting neurons in adult mice. **a-c**, 2 wpi after AAV2/retro-hSyn-H2B-GFP was injected into C4-6 and L2-4 spinal cord in P42 mice. **d-f**, 4 wpi after RabV CVS-N2c(ΔG)-H2B-GFP. Signal not detectable after 2 wpi (data not shown). **g-i**, 4 wpi after HiRet-lenti-H2B-GFP. Signal not detectable after 2 wpi (data not shown). Panels 1-3, 4-6, and 7-9 are insets from boxed regions in panels a-c, d-f, and g-i, respectively. DAPI is depicted in cyan, viral labeling depicted in green. P = post-natal day, L5 = layer 5 cortex, RN = red nucleus, GRN = gigantocellular reticular nucleus, wpi = weeks post injection.

As AAV2/retro outperformed CVS-N2c(ΔG) and HiRet-Lenti in these preliminary labeling studies, we proceeded with AAV2/retro for SPN labeling. In addition to labeling efficiency, detection efficiency is equally important when generating an anatomical atlas. Prior studies using AAV2/retro to retrogradely express fluorescent proteins (FPs) in SPN populations have demonstrated variable fluorescence intensity across populations (Steward et al., 2021), likely due to differing capacities for viral transfection in neuronal subtypes and variable viral particle uptake at axon terminals. Further, AAV2/retro labels neuronal fibers (i.e., dendrites, axons) in addition to soma, which presents a challenge for automated cell segmentation in whole brain imaging data (X. Wang et al., 2017; Z. Wang et al., 2018). To address both challenges, we explored the use of nuclear localization. Specifically, we qualitatively compared AAV2/retro-CAG-FP to two constructs that localize FP expression to the nucleus: AAV2/retro-hSyn-FP-NLS and AAV2/retro-hSyn-H2B-FP (**Figure 1-2**). The NLS construct contains a nuclear localization sequence (NLS) that tags the FP for import into the cell nucleus, and the H2B construct fuses the FP to histone H2B for nuclear localization of fluorescent signal. Of these three constructs, the H2B virus yielded the cleanest nuclear-localized signal. While the NLS construct enabled bright nuclear labeling, labeling in neuronal fibers was much brighter than with the H2B construct, which would complicate automated nuclear segmentation. Further, neuronal fibers labeled by the NLS construct exhibit "beading", a hallmark of degeneration (Datar et al., 2019) and

likely indicator of cytotoxicity, whereas fibers labeled by the H2B construct appear to have healthy morphology (**Figure 1-2g**). Automated cell detection in QuPath demonstrated that nuclei labeled with the H2B construct could be effectively detected and segmented (**Figure 1-2h**).

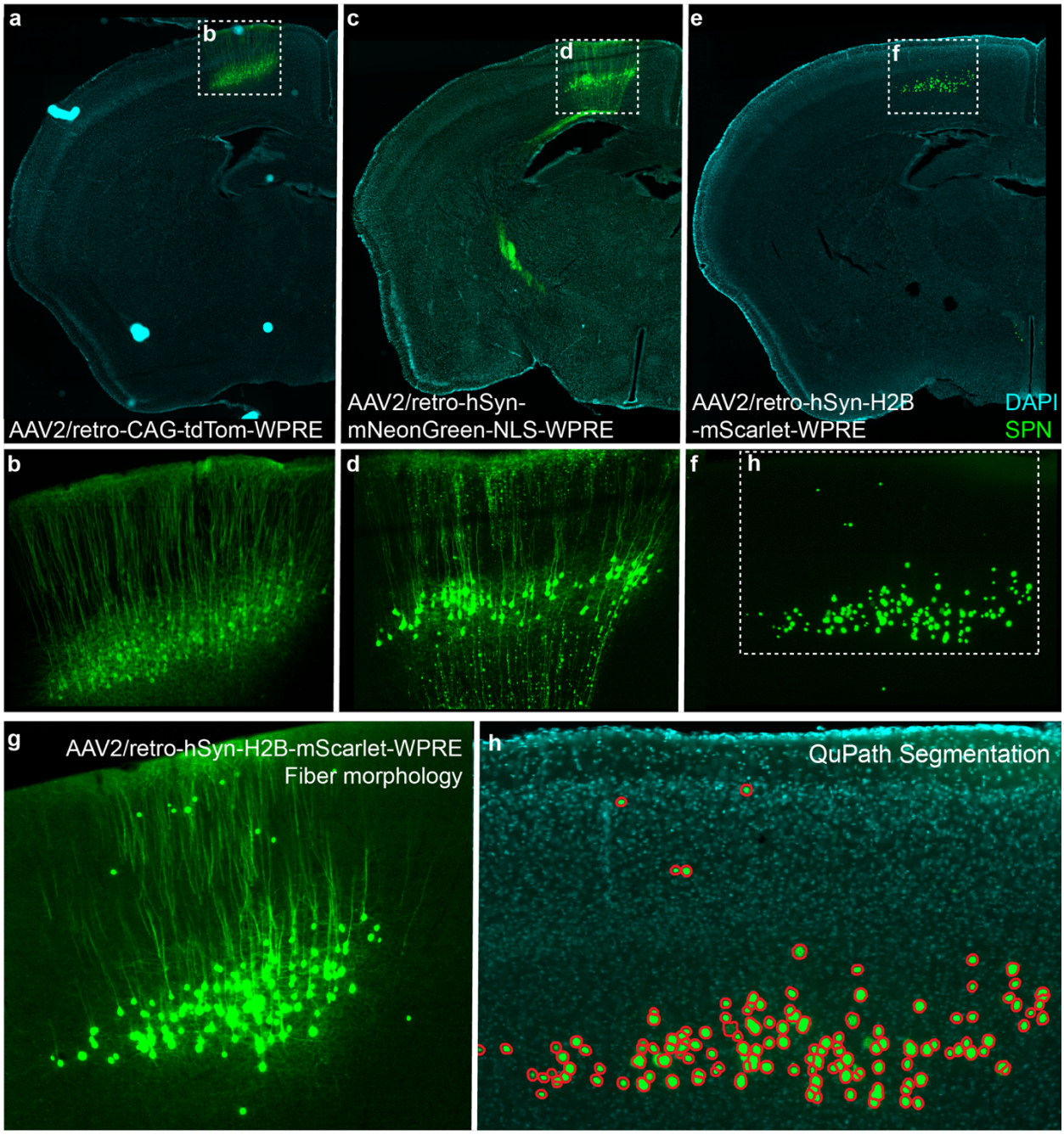


Figure 1-2: Optimization of retrograde adeno-associated viral vectors for retrograde labeling of spinal projecting neurons. Three retrograde AAV vectors were tested to retrogradely label SPNs. Images depict retrograde labeling in CSNs

2 wpi into L2-4. **a-b**, AAV2/retro-CAG-tdTomato-WPRE labels whole cells, including soma, axon, and dendrites. **c-d**, AAV2/retro-hSyn-mNeonGreen-NLS-WPRE labels nuclei with axon and dendritic labeling. Fibers exhibit beading morphology, characteristic of degenerating neurons. **e-f**, AAV2/retro-hSyn-H2B-mScarlet-WPRE labels nuclei only without axon or dendritic labeling. **g**, AAV2/retro-hSyn-H2B-mScarlet-WPRE signal amplified using IHC and slide-scanner signal overexposed to reveal neuronal fibers do not exhibit beading morphology. **h**, Inset from f; automated nucleus segmentation using QuPath depictd as red outlines. DAPI is depicted in cyan, viral labeling depicted in green. SPN = spinal projecting neuron; CSN = corticospinal neuron; L2-4 = lumbar segments 2, 3, and 4.

To further assess this labeling strategy, we evaluated the spinal injection locations and the distribution of labeling across the whole brain using traditional cryo-sectioning and slide-scanning. As expected, spinal injections are centered around the injected cervical and lumbar segments and label all parts of the spinal gray matter, though with some variability (**Figure 1-3**). Importantly, we found AAV2/retro-hSyn-H2B-FP labels the major expected SPN populations across the cortex, hypothalamus, midbrain, pons, medulla, and cerebellum (Liang et al., 2011; Z. Wang et al., 2018) without the need for IHC amplification (**Figure 1-4**). Taken together, these results establish AAV2/retro-hSyn-H2B-FP as an optimized method for labeling brain-wide SPNs that meet the 8 abovementioned recombinant vector criteria.

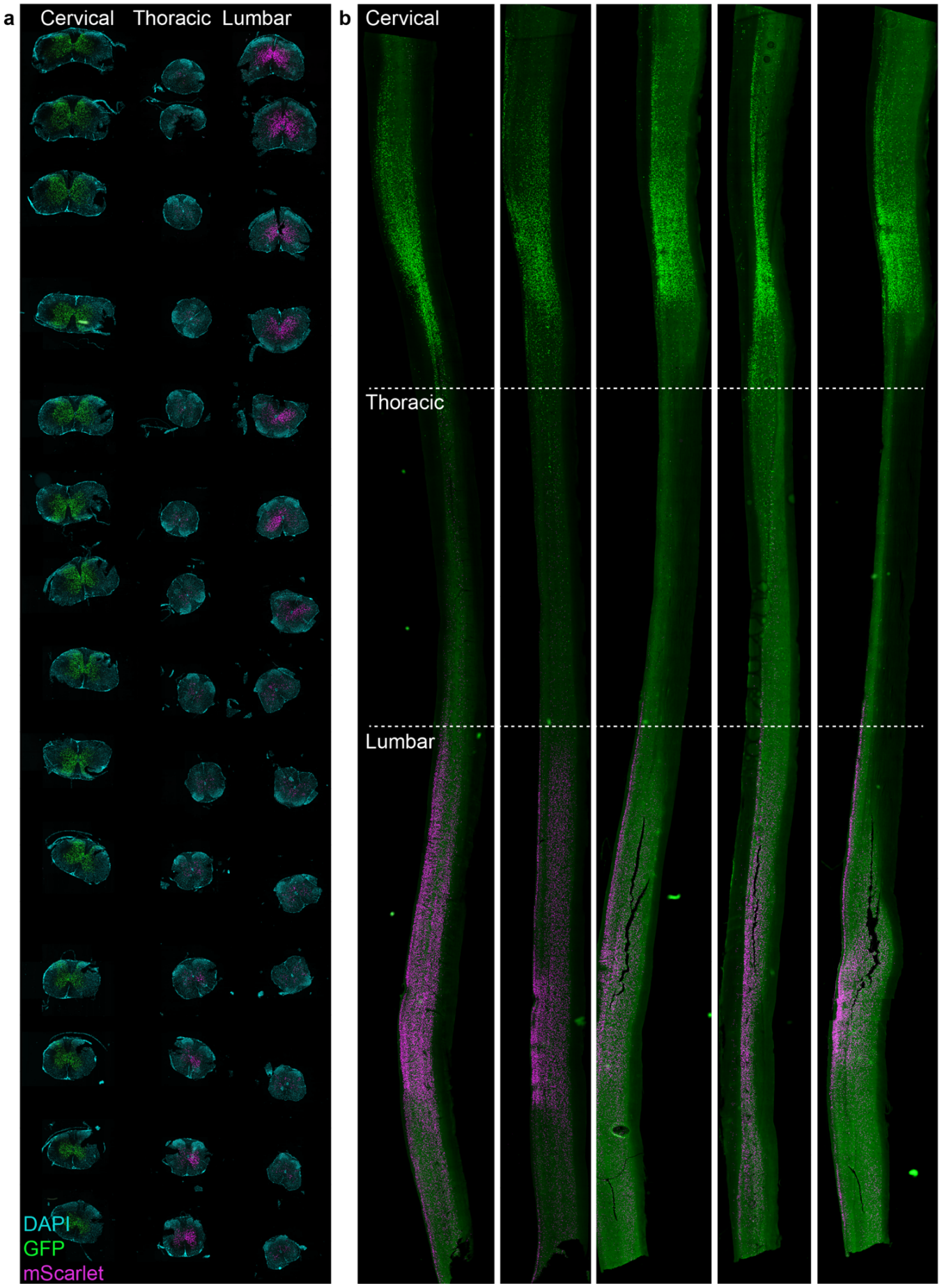

a
Cervical
Thoracic
Lumbar
DAPI
GFP
mScarlet
b
Cervical
Thoracic
Lumbar

Figure 1-3: Representative images of spinal cord injection sites. SPNs are retrogradely labeled via injection of retrograde AAV2/retro-hSyn-H2B-XFP-WPRE into C4-6 (GFP) and L2-4 (mScarlet) at P42. At P56, mice are perfused and histological assessment is performed. **a**, Representative coronal sections from the cervical through sacral spinal cord, 40μm thickness. **b**, Representative sagittal sections through the spinal cord, 40μm thickness. SPNs = spinal projecting neurons; C4-6 = cervical segments 5, 6, and 6; L2-4 = lumbar segments 2, 3, and 4; P = post-natal day.

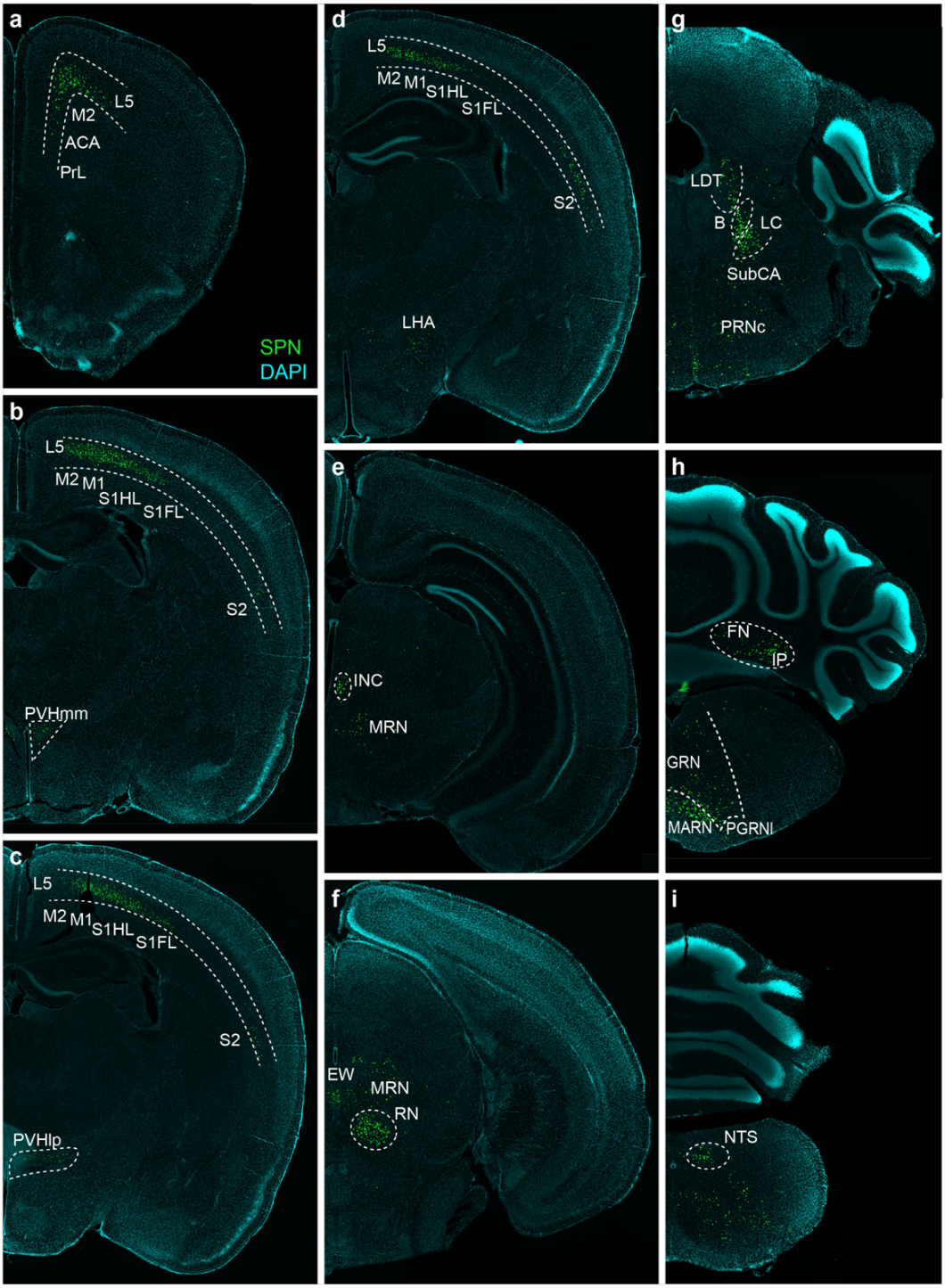


Figure 1-4: Representative images of retrogradely-labeled brain sections. SPNs are retrogradely labeled via injection of retrograde AAV2/retro-hSyn-H2B-XFP-WPRE into C4-6 (GFP) and L2-4 (mScarlet) at P42. At P56, mice are perfused and histological assessment is performed. **a-i**) Representative images of coronal brain slices, generated with cryosectioning and slide-scanner imaging, 50μm thickness. DAPI is depicted in cyan, cervical- and lumbar-projecting SPNs are both depicted in green. L5 = layer 5 cortex, M2 = secondary motor cortex, ACA = anterior cingulate area, PrL = prelimbic cortex (Paxinos nomenclature (Franklin & Paxinos, 2008)), M1 = primary motor cortex, S1HL = primary somatosensory cortex hindlimb region, S1FL = primary somatosensory cortex forelimb region, S2 = secondary somatosensory cortex, PVHmm = paraventricular hypothalamic nucleus medial magnocellular part, PVHlp = paraventricular hypothalamic nucleus lateral parvicellular part, LHA = lateral hypothalamic part, INC = interstitial nucleus of Cajal, MRN = midbrain reticular nucleus, RN = red nucleus, EW = Edinger-Westphal Nucleus, LDT = laterodorsal tegmental nucleus, B = Barrington's nucleus, LC = locus coeruleus, SubCA = subcoeruelus nucleus alpha part (Paxinos), PRNc = pontine reticular nucleus caudal part, FN = fastigial nucleus, IP = interposed nucleus, GRN = gigantocellular reticular nucleus, MARN = magnocellular reticular nucleus, PGRNl = paragigantocellular reticular nucleus lateral part, NTS = nucleus of the solitary tract.

1.3.2 BRAIN-WIDE DISTRIBUTION OF SPINAL PROJECTING NEURONS:

After optimizing retrograde labeling of SPNs, we sought an imaging paradigm that (1) requires limited tissue pre-processing, (2) minimizes artifacts due to sectioning and imaging, (3) places SPNs in their three-dimensional (3D), brain-wide anatomical context, and (4) is systematic, reproducible, and requires limited expertise to interpret. Serial two-photon tomography (STPT) and light sheet fluorescence microscopy (LSFM) offer two imaging solutions. STPT offers a distinct advantage over LSFM because it does not require tissue clearing, which is time-intensive and can introduce distortions and artifacts during the clearing process. We therefore devised a pipeline for assessing their brain-wide anatomical distribution using STPT followed by brain-wide automated segmentation and registration to the Allen Common Coordinate Framework (CCF) (Q. Wang et al., 2020) (**Figure 1-5**).

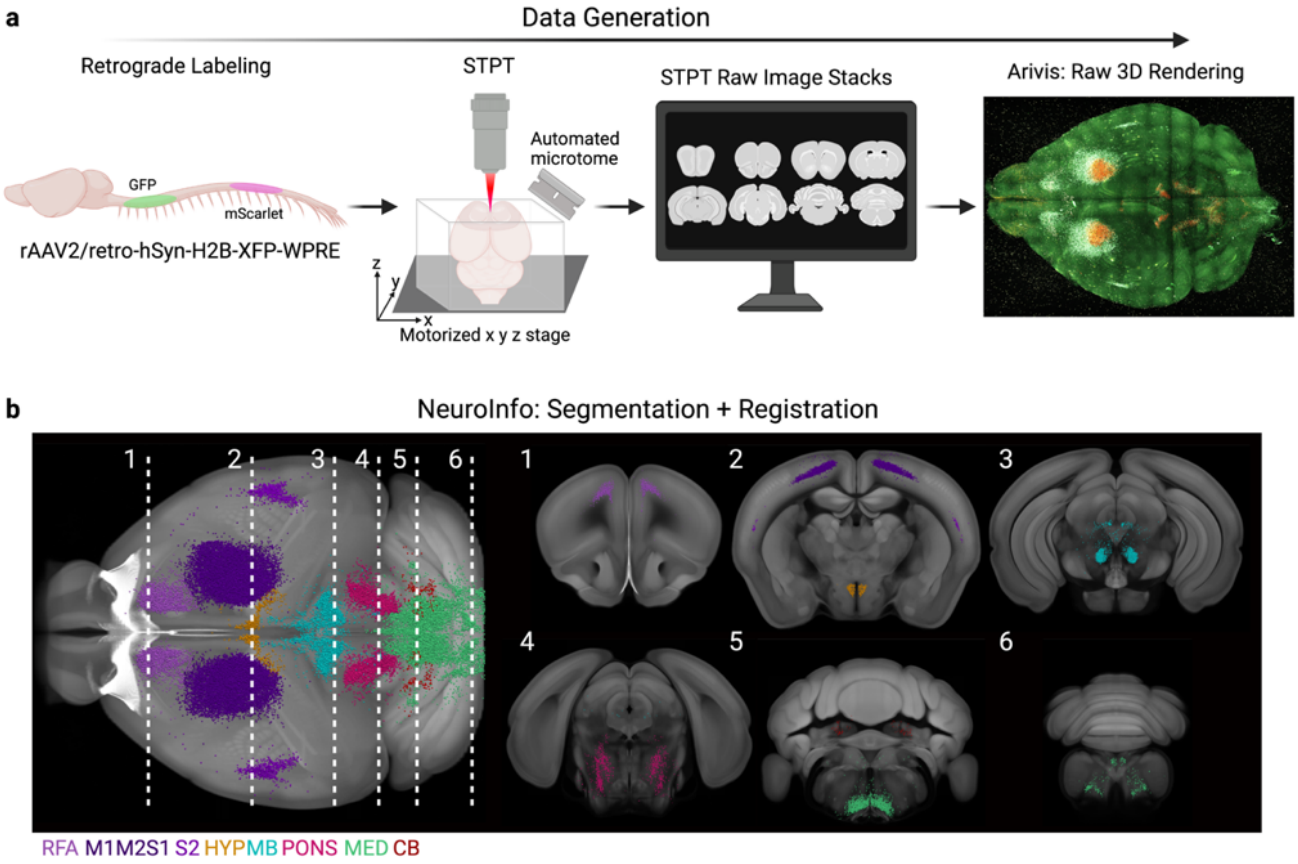


Figure 1-5: Pipeline for labeling and imaging brain-wide spinal projecting neurons. a, Dataset generation. SPNs are retrogradely labeled via injection of retrograde AAV into C4-6 and L2-4 at P42. At P56, mice are perfused, brains are dissected and embedded in agarose, and STPT imaging is performed. Through interleaved steps of imaging and sectioning, STPT generates a series of sequential image stacks. Raw data is viewed and reconstructed in 3D using Arivis software. **b**, Data analysis. Raw image stacks are exported into NeuroInfo software for registration to the Allen Common Coordinate Framework and labeled nuclei are segmented. Colors of segmented nuclei correspond to the 8 major ROIs containing SPNs. SPNs = spinal projecting neurons; C4-6 = cervical segments 5, 6, and 6; L2-4 = lumbar segments 2, 3, and 4; P = post-natal day; STPT = serial two-photon tomography; ROI = region of interest; RFA = rostral forelimb area, M1 = primary motor cortex, M2 = secondary motor cortex, S1 = primary somatosensory cortex, S2 = secondary somatosensory cortex, HY = hypothalamus, MB = midbrain, CB = cerebellum, MED = medulla. Panel (a) created with BioRender.com.

After retrograde labeling and imaging with STPT, image stacks were imported into Arivis for quality control (e.g., fluorescence signal, tissue quality) and subsequently into NeuroInfo for automated segmentation and registration to the Allen CCF (Tappan et al., 2019). As expected, SPNs are widely distributed across the mouse brain but with concentrations in cortex (CTX; 41.77% of all SPNs), hypothalamus (HY; 2.90%), midbrain (MB; 12.88%), cerebellum (CB; 2.18%), pons (PONS; 16.01%), and medulla (MED; 24.26%), consistent with findings from non-viral labeling methods (Liang et al., 2011) (**Figures 1-6**, **1-7**).

NeuroInfo enables detailed visualization of data in coronal reconstructions (**Figure 1-6**, **Video 1-1**) to identify anatomical regions throughout the forebrain, midbrain, and hindbrain. Forebrain SPNs were found to arise from the cortex and hypothalamus (**Figure 1-8**). Most labeled nuclei were in cortical layer 5 (i.e., CSNs). CSNs were distributed in the rostral forelimb area (RFA), primary and secondary motor cortices (M1 and M2, respectively), and primary and secondary somatosensory cortices (S1 and S2, respectively), consistent with previous reports from our lab (X. Wang et al., 2017). SPNs detected in the hypothalamus arose from two main regions: the paraventricular hypothalamic nucleus (PVH) and lateral hypothalamic area (LHA). Within the PVH, nuclei arose from the PVH medial magnocellular (PVHmm) and lateral parvicellular (PVHlp) divisions. In the midbrain, SPNs were detected in the red nucleus (RN), Edinger-Westphal nucleus (EW), Interstitial Nucleus of Cajal (INC), midbrain reticular nucleus (MRN), as well as various populations in periaqueductal gray (PAG) extending from the rostral to caudal midbrain (**Figure 1-9**). The most rostral PAG population is likely the A11 group of neurons (Koblinger et al., 2014; Skagerberg & Lindvall, 1985). In the hindbrain, SPNs were detected throughout the pons and medulla (**Figure 1-10**). The most rostral hindbrain populations arise in the pontine tegmental nuclei. These include paralemniscal nucleus (PL), pedunculopontine nucleus (PPN), pontine reticular nucleus rostral part (PRNr), laterodorsal tegmental nucleus (LDT), locus coeruleus (LC), subcoeruleus nucleus (SubC), and Barrington's nucleus (B). In

the caudal pons and throughout the medulla, nuclei arose in widespread anatomical locations including the pontine reticular nucleus caudal part (PRNc), paragigantocellular reticular nucleus dorsal part (PGRNd), gigantocellular reticular nucleus (GRN), magnocellular reticular nucleus (MARN), and nucleus of the solitary tract (NTS). Nuclei also arose in the ventral raphe nuclei, including nucleus raphe obscurus (RO), nucleus raphe magnus (RM), and nucleus raphe pallidus (RPA). Lastly, nuclei were detected in the fastigial (FN) and interposed (IP) deep cerebellar nuclei.

In sum, this pipeline systematically and reproducibly identified SPNs across the entire adult mouse brain. Notably, the mapping performed here aligns with current knowledge of SPN connectivity (Liang et al., 2011; Z. Wang et al., 2018), while offering a streamlined pipeline and high-resolution assessment of brain wide SPNs in their 3D spatial context.

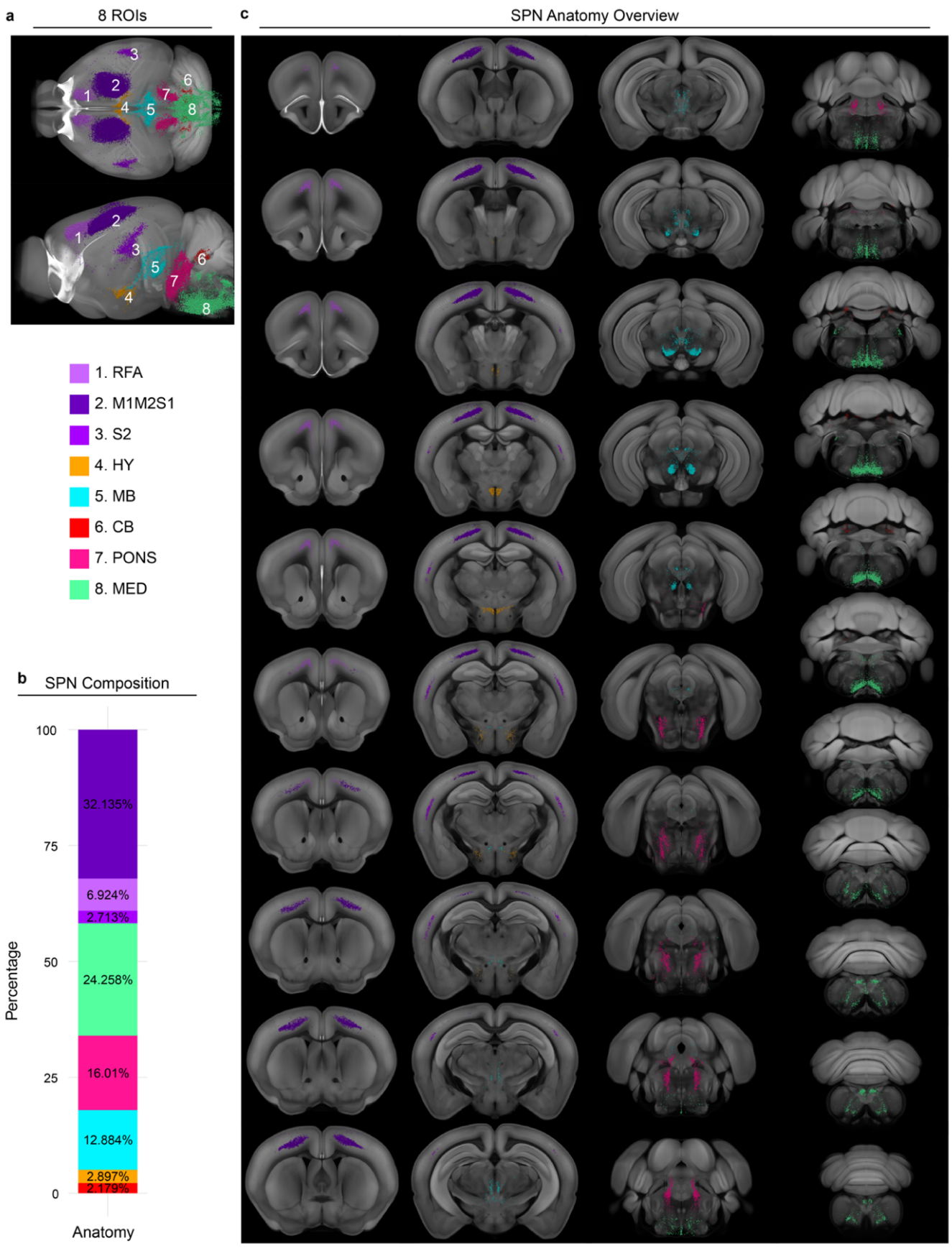

a
8 ROIs
1. RFA
2. M1M2S1
3. S2
4. HY
5. MB
6. CB
7. PONS
8. MED
b
SPN Composition
100
75
50
25
0
Percentage
32.135%
6.924%
2.713%
24.258%
16.01%
12.884%
2.897%
2.179%
Anatomy
c
SPN Anatomy Overview

Figure 1-6: Anatomical overview of spinal projecting neurons. a, Whole brain reconstructions of segmented and registered SPN nuclei imaged with serial two-photon tomography revealed SPNs are present across the cortex (RFA, M1M2S1, and S2), hypothalamus, midbrain, cerebellum, pons, medulla. **b**, Bar plots represent percentages of SPNs profiled from each SPN-containing brain region (slide-scanner imaging, N = 5 mice, mean and standard deviation for number of nuclei in each ROI are as follows, RFA: 5586.40 +/- 425.76, S2: 2188.80 +/- 101.84, M1M2S1: 25925.60 +/- 857.80, HY: 2337.60 +/- 267.77, MB: 10394.40 +/- 654.72, CB: 1757.60 +/- 265.87, PONS: 12916.80 +/- 1124.68, MED: 19570.40 +/- 465.30). **c**, Coronal reconstructions (250 μm thickness) of segmented and registered SPN nuclei imaged with serial two-photon tomography and processed with NeuroInfo software. SPN = spinal projecting neuron, RFA = rostral forelimb area, M1 = primary motor cortex, M2 = secondary motor cortex, S1 = primary somatosensory cortex, S2 = secondary somatosensory cortex, HY = hypothalamus, MB = midbrain, CB = cerebellum, MED = medulla.

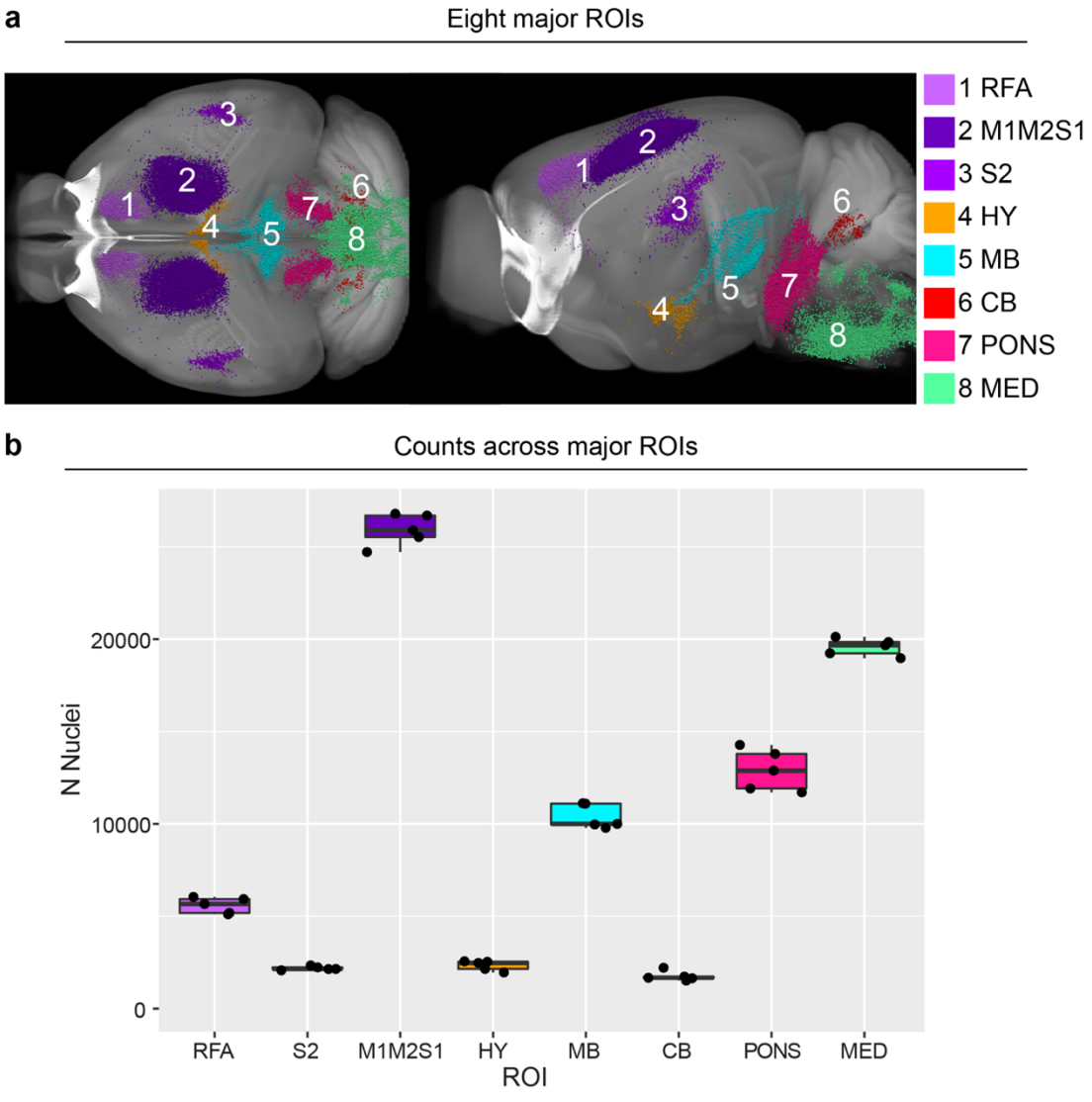


Figure 1-7: Counts across major regions containing spinal projecting neurons. a, Whole brain reconstructions of segmented and registered SPN nuclei imaged with serial two-photon tomography revealed SPNs are present across the cortex (RFA, M1M2S1, and S2), hypothalamus, midbrain, cerebellum, pons, medulla. **b**, Counts of SPNs profiled from each SPN-containing brain region (slide-scanner imaging, N = 5 mice, mean and standard deviation for number of nuclei in each ROI are as follows, RFA: 5586.40 +/- 425.76, S2: 2188.80 +/- 101.84, M1M2S1: 25925.60 +/- 857.80, HY: 2337.60 +/- 267.77, MB: 10394.40 +/- 654.72, CB: 1757.60 +/- 265.87, PONS: 12916.80 +/- 1124.68, MED: 19570.40 +/- 465.30). SPN = spinal projecting neuron, RFA = rostral forelimb area, M1 = primary motor cortex, M2 = secondary motor cortex, S1 = primary somatosensory cortex, S2 = secondary somatosensory cortex, HY = hypothalamus, MB = midbrain, CB = cerebellum, MED = medulla.

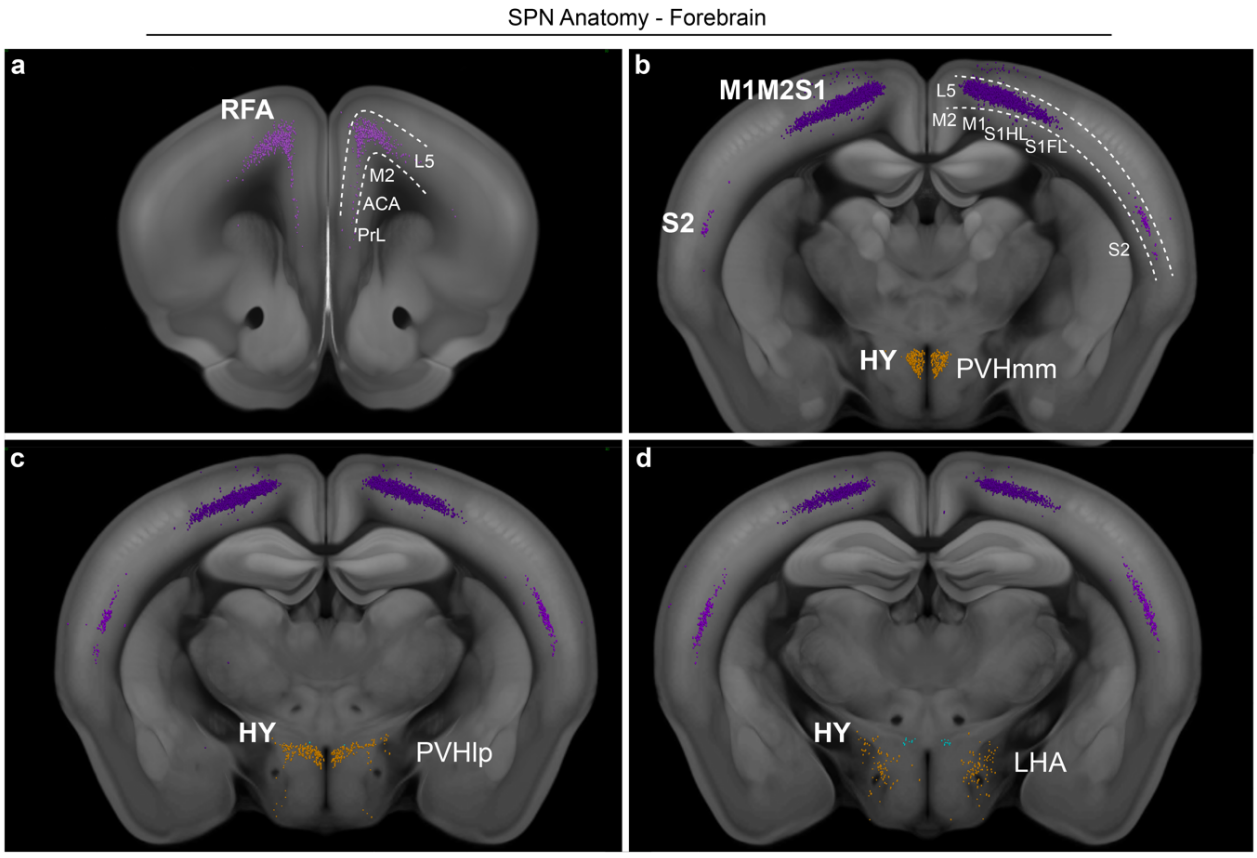


Figure 1-8: Forebrain spinal projecting neurons. Coronal reconstructions (250 μm thickness) of segmented and registered SPN nuclei in the forebrain. Labels in **bold** (left hemisphere) annotate the 8 major brain regions SPNs arise from, labels in right hemisphere annotate more detailed brain regions. Colors of segmented nuclei correspond to the 8 major ROIs containing SPNs. Note: NeuroInfo can overlay the registered Allen CCF; however, annotations were manually drawn for clarity. L5 = layer 5 cortex, M2 = secondary motor cortex, ACA = anterior cingulate area, PrL = prelimbic

cortex (Paxinos nomenclature (Franklin & Paxinos, 2008)), M1 = primary motor cortex, S1HL = primary somatosensory cortex hindlimb region, S1FL = primary somatosensory cortex forelimb region, S2 = secondary somatosensory cortex, PVHmm = paraventricular hypothalamic nucleus medial magnocellular part, PVHlp = paraventricular hypothalamic nucleus lateral parvicellular part, LHA = lateral hypothalamic part, RFA = rostral forelimb area, HY = hypothalamus.

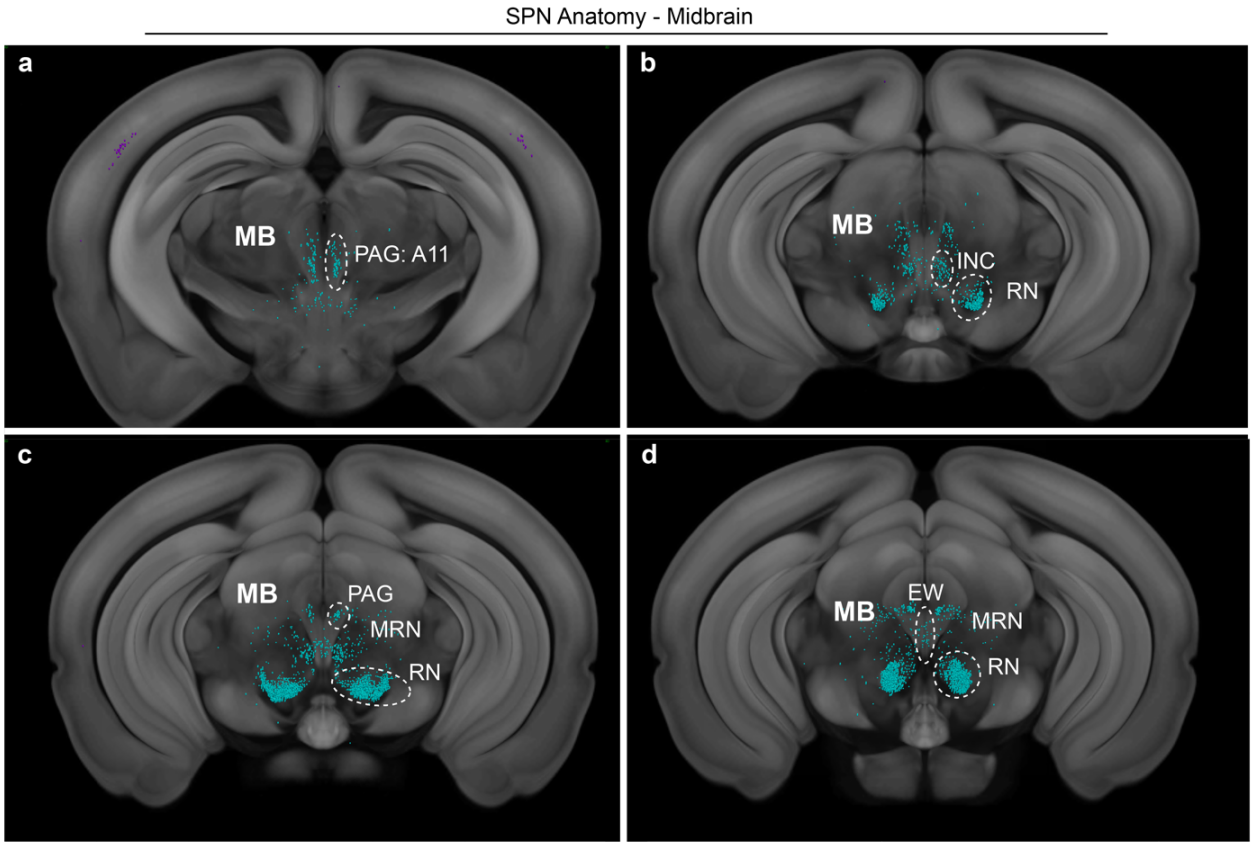


Figure 1-9: Midbrain spinal projecting neurons. Coronal reconstructions (250 μm thickness) of segmented and registered SPN nuclei in the midbrain. Labels in **bold** (left hemisphere) annotate the 8 major brain regions SPNs arise from, labels in right hemisphere annotate more detailed brain regions. Colors of segmented nuclei correspond to the 8 major ROIs containing SPNs. Note: NeuroInfo can overlay the registered Allen CCF; however, annotations were manually drawn for clarity. RN = red nucleus, EW = Edinger-Westphal Nucleus, INC = interstitial nucleus of Cajal, MRN = midbrain reticular nucleus, PAG = periaqueductal gray, A11 = A11 cell group, MB = midbrain.

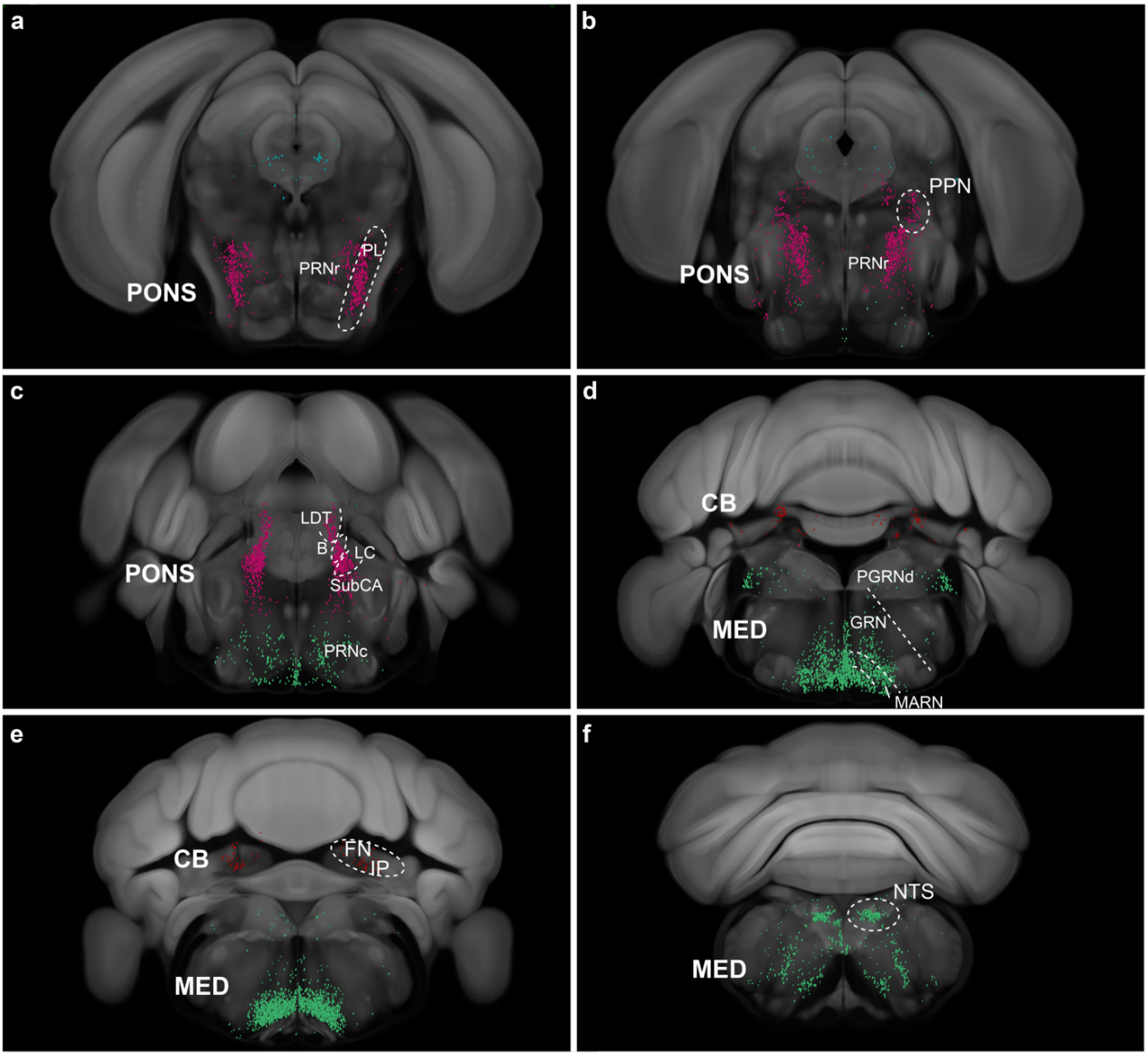


Figure 1-10: Hindbrain spinal projecting neurons. Coronal reconstructions (250 μm thickness) of segmented and registered SPN nuclei in the hindbrain. Labels in **bold** (left hemisphere) annotate the 8 major brain regions SPNs arise from, labels in right hemisphere annotate more detailed brain regions. Colors of segmented nuclei correspond to the 8 major ROIs containing SPNs. Note: NeuroInfo can overlay the registered Allen CCF; however, annotations were manually drawn for clarity. PL = paralemniscal nucleus (Paxinos nomenclature (Franklin & Paxinos, 2008)), PPN = pedunculopontine nucleus, PRNr = pontine reticular nucleus rostral part, LDT = laterodorsal tegmental nucleus, LC = locus coeruleus, SubCA = subcoeruelus nucleus alpha part (Paxinos), B = Barrington's nucleus, PGRNd = paragigantocellular reticular nucleus dorsal part, GRN = gigantocellular reticular nucleus, MARN = magnocellular reticular nucleus, NTS = nucleus of the solitary tract, fastigial nucleus (FN), interposed nucleus (IP). PONS = pons, MED = medulla, CB = cerebellum.

1.3.3 PROJECTION TARGET SPECIFICITY OF ANATOMICAL SUBPOPULATIONS:

In 1937, Penfield and Boldrey presented work showing that electrical stimulation of specific regions in the primary motor cortex (M1) produced movement in distinct body parts in humans (Penfield & Boldrey, 1937). This publication presented the concept of a continuous "homunculus", where body parts from head-to-toe map onto distinct regions of M1. Since then, numerous studies have shown that SPNs within M1 (i.e., CSNs) correspondingly display somatotopic mapping to specific spinal levels in rodents (Akintunde & Buxton, 1992; Li et al., 2009; Miller, 1987; Steward et al., 2021; Ullan & Artieda, 1981; Z. Wang et al., 2018; Wise et al., 1979) and primates (Dawnay & Glees, 1986; He et al., 1993; Morecraft et al., 2013). RuSNs from the midbrain red nucleus have also long been known to exhibit topographic organization corresponding to neurons projecting to the forelimb and hindlimb regions of the spinal cord (Liang et al., 2012; Murray & Gurule, 1979; Shieh et al., 1983), and more recently cerebellospinals (CbSNs) were shown to exhibit a similar forelimb/hindlimb division (Sathyamurthy et al., 2020). While this distinct organization of projection target has important implications for function of these various SPN circuits, the projection target specificity of other SPN populations throughout the brain is less well characterized. We therefore leveraged the SPN anatomical atlas presented above to assess the broad distributions of cervical- and/or lumbar-projecting SPNs across the whole brain.

We injected AAV2/retro-hSyn-H2B-GFP and AAV2/retro-hSyn-H2B-mScarlet into the spinal cord centering cervical (C4-6) and lumbar (L2-4) segments, respectively (**Figure 1-11a**). This injection scheme allows comparison of cervical- and lumbar- projections within the same animal, and identification of "dual" projecting populations that contain collaterals terminating in both spinal targets. Consistent with previous reports, we find CSNs, RuSNs, and CbSNs exhibit distinct somatotopic segregations of cervical- and lumbar- projecting neurons (**Figure 1-11b-f**). The three anatomical concentrations of CSNs (i.e., the rostral "RFA" cluster, the caudal "M1M2S1" cluster, and

the lateral "S2" cluster) regions exhibited distinct spinal projections: the RFA and S2 concentrations were entirely cervical-projecting, whereas the caudal "M1M2S1" cluster is comprised of a lumbar-projecting concentration surrounded by a concentric ring of cervical-projecting CSNs (**Figure 1-11c**). We found that the STPT imaging and registration scheme did not have sufficient resolution to accurately discern co-localization of GFP and mScarlet signal to identify dual populations, but qualitative assessment with confocal imaging demonstrated that the M1M2S1 CSN concentration contains numerous dual projecting neurons, whereas RuSN and CbSN contain few (**Figure 1-11d-f**). In contrast, SPNs arising within anatomical nuclei in other supraspinal locations did not exhibit clear somatotopic segregations between cervical and lumbar projecting areas (**Figure 1-12**). Specific hindbrain anatomical nuclei exhibited bias towards cervical vs. dual/lumbar projections, however. For example, SPNs in the ventrally located MARN in the medulla were primarily dual- and lumbar-projecting, whereas the those arising in the GRN dorsal to MARN were primarily cervical-projecting (**Figure 1-12f**,**g**).

Taken together, 3D imaging and registration complemented by confocal microscopy provides a methodological framework for assessing the topographic innervation patterns of SPNs across the whole brain. These results refine our understanding of populations known to exhibit clear somatotopic distributions: we find that lumbar-projecting CSNs collateralize to the cervical spinal cord, whereas RuSNs and CbSNs are comprised of neurons projecting to either the cervical or lumbar spinal cord. Additionally, we show that subcortical populations generally do not exhibit somatotopic distributions within anatomically defined nuclei, but certain regions show preference for cervical vs. dual/lumbar projections (e.g., the ventrally located MARN shows preference for dual/lumbar projecting neurons, whereas the more dorsal GRN is primarily cervical projecting). These data have important implications for inferring functions of anatomical populations.

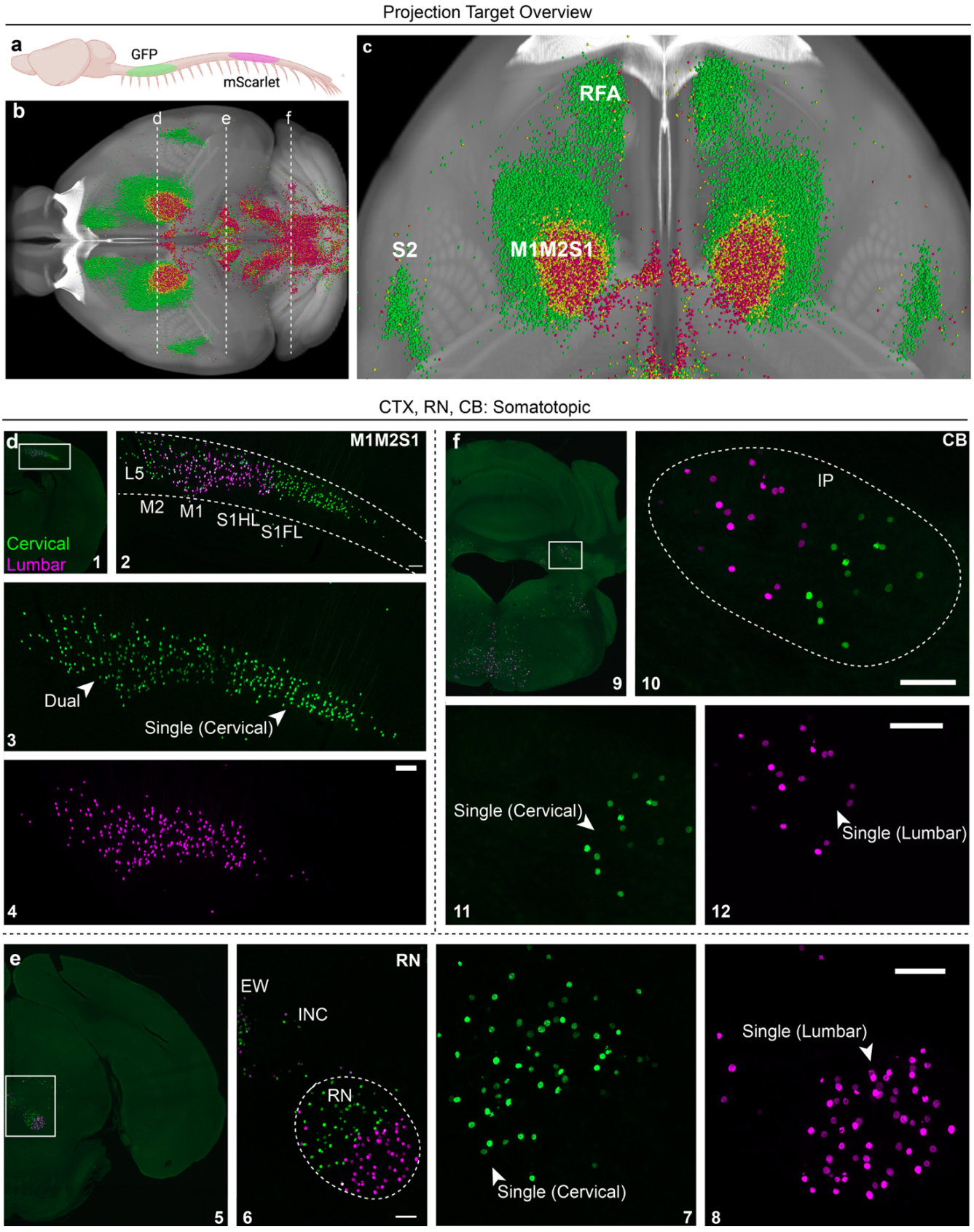

Projection Target Overview
a
GFP
mScarlet
b
d
e
f
c
RFA
S2
M1M2S1
CTX, RN, CB: Somatotopic
d
Cervical
Lumbar
1
M1M2S1
L5
M2
M1
S1HL
S1FL
2
Dual
Single (Cervical)
3
4
f
9
CB
IP
10
Single (Cervical)
11
Single (Lumbar)
12
e
5
RN
EW
INC
RN
6
Single (Cervical)
7
Single (Lumbar)
8

Figure 1-11: Somatotopic segregation in corticospinal, rubrospinal, and cerebellospinal neurons. a, SPNs are retrogradely labeled via injection of retrograde AAV2/retro-H2B-GFP and AAV2/retro-H2B-mScarlet into C4-6 and L2-4, respectively. **b**, Whole brain reconstructions showing distribution of cervical (green), lumbar (magenta), and dual (yellow) projecting SPNs. **c**, CSNs arising from RFA and S2 are entirely cervical projecting, whereas the those arising across M1M2S1 contain a central dual and lumbar projecting population surrounded by cervical projecting. **d-f**, Confocal microscopy images of retrogradely labeled cervical and lumbar projecting SPNs in the M1M2S1 cortex (**d**), red nucleus (**e**), and cerebellum interposed nucleus (**f**). Panels 1-4, 5-8, and 9-12 are insets from boxed regions in panels d, e, and f, respectively. Cervical and lumbar projecting neurons depicted in green and magenta, respectively. Scale bars = 100μm. RFA = rostral forelimb area, M1 = primary motor cortex, M2 = secondary motor cortex, S1 = primary somatosensory cortex, S2 = secondary somatosensory cortex, S1HL = primary somatosensory cortex hindlimb region, S1FL = primary somatosensory cortex forelimb region, L5 = layer 5 cortex, RN = red nucleus, EW = Edinger-Westphal Nucleus, INC = interstitial nucleus of Cajal, CB = cerebellum, IP = interposed nucleus. Panel (a) created with BioRender.com.

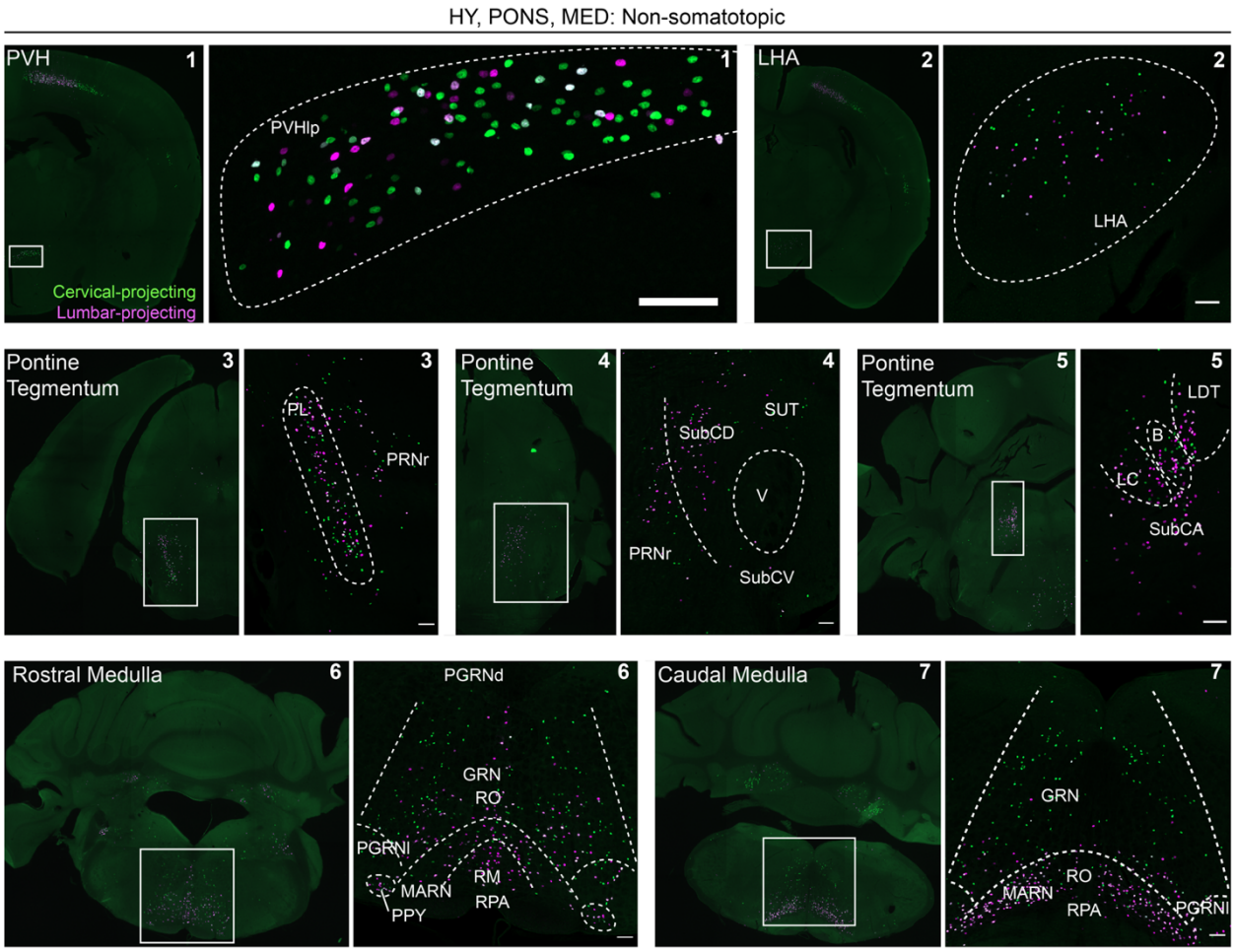


Figure 1-12: Spinal projecting neurons from hypothalamus, pons, and medulla are not somatotopically segregated. Confocal microscopy images of retrogradely labeled cervical- (green) and lumbar- (magenta) projecting SPNs throughout the hypothalamus, pons, and medulla. Scale = 100 μm. PVH = paraventricular hypothalamus, PVHlp = paraventricular hypothalamic nucleus lateral parvicellular part, LHA = lateral hypothalamic area, PL = paralemniscal nucleus (Paxinos nomenclature (Franklin & Paxinos, 2008)), PRNr = pontine reticular nucleus rostral part, SUT = supratrigeminal nucleus, SubCD = subcoeruelus nucleus dorsal part (Paxinos), SubCV = subcoeruelus nucleus ventral part (Paxinos), V = motor trigeminal nucleus, LDT = laterodorsal tegmental nucleus, B = Barrington's nucleus, LC = locus coeruleus, SubCA = subcoeruelus nucleus alpha part (Paxinos), PGRNl = paragigantocellular reticular nucleus lateral part, PGRNd = paragigantocellular reticular nucleus dorsal part, PPY = parapyramidal nucleus, GRN = gigantocellular reticular nucleus, MARN = magnocellular reticular nucleus, RO = nucleus raphe obscurus, RM = nucleus raphe magnus, RPA = nucleus raphe pallidus.

1.4 DISCUSSION.

In this study, we present an optimized pipeline for retrograde labeling and imaging that enables comprehensive characterization of spinal projecting neurons (SPNs) across the whole adult mouse brain. These findings demonstrate that AAV2/retro outperforms recombinant rabies and lentivirus in retrograde labeling of SPNs. Additionally, we establish the suitability of STPT as an accessible imaging modality for automated whole-brain imaging and registration to the Allen CCF without the need for tissue clearing. The mapping conducted in this study is consistent with the current understanding of SPN connectivity (Liang et al., 2010; Z. Wang et al., 2018). Importantly, our streamlined pipeline enables a high-resolution assessment of SPNs in their complex three-dimensional spatial context. Further, these data provide novel insights into the topographic innervation patterns of SPNs, which hold significant functional implications. Overall, these data offer an accessible resource for further investigations into the anatomical features of SPNs.

1.4.1 LABELING STRATEGY:

The AAV2/retro labeling strategy employed in this study enables high-efficiency labeling of SPNs throughout numerous anatomical nuclei in the mouse forebrain, midbrain, and hindbrain. Importantly, the chosen FPs enable detection without the need for IHC amplification, and nuclear localization of FP expression produces high signal-to-noise ratio to reduce interference from nearby labeled neuronal fibers, which poses a challenge in whole-cell labeling strategies (Steward et al., 2021; Z. Wang et al., 2018). Additionally, compared to the HiRet-Lenti and CVS-N2c-(ΔG) constructs, we found AAV2/retro requires less time from injection to signal detection and is simpler to produce.

Despite the successful use of this labeling strategy here, important caveats should be considered. First, despite demonstrating better capacity for SPN labeling compared to HiRet-Lenti and CVS-N2c-(ΔG) (**Figure 1-1**), AAV2/retro has been shown to exhibit unequal tropism for neuronal subpopulations. Specifically, previous studies have shown AAV2/retro has limited capacity for transducing noradrenergic LC (Ganley et al., 2021) and serotonergic raphe (Z. Wang et al., 2018) neurons. However, results here demonstrate labeling in these anatomical regions (**Figures 1-4, 1-10, 1-12**). It is possible that LC and raphe neurons are transduced but with lower efficiency, and nuclear localization enabled signal detection in this study. Further molecular studies are needed, however, to confirm the identity of AAV2/retro-labeled LC and raphe SPNs as noradrenergic and serotonergic, respectively (addressed in **Chapter 2**). Second, the possibility of AAV2/retro uptake by axons of passage, versus by axon terminals, must be considered. This has particularly important implications for interpretation of the results assessing cervical versus lumbar innervation patterns. For example, uptake by passing axons may suggest "dual" projecting CSNs are technical artifact. However, the results showing selective transduction of cervical and lumbar RuSNs and CbSNs with minimal dual transduction suggests AAV2/retro uptake is likely via axon terminals and is consistent with previous studies (Sathyamurthy et al., 2020; Z. Wang et al., 2018). Third, ability to co-localize GFP and mScarlet

signal as well as differences in their signal intensities may bias interpretation of topographic mapping results. In light of these limitations, we provide qualitative assessments of topographic innervation here and leave quantitative assessment for future work. Finally, STPT imaging and automated segmentation may introduce additional bias. For example, though STPT enables isotropic imaging by optimizing optical / physical section size and imaging resolution, NeuroInfo software segments nuclei in two-dimensional (rather than 3D reconstructed) space, leading to double counting of partial nuclei appearing in consecutive image stacks. For this reason, we opted not to quantify the segmentation results using NeuroInfo in the present study. Future studies may seek to quantify the datasets generated in this study using pipelines optimized for STPT such as cellfinder (Tyson et al., 2021).

1.4.2 BRAIN-WIDE DISTRIBUTION:

The identification of numerous SPN populations throughout the forebrain, midbrain, and hindbrain has important implications for the functional organization of SPNs. In the forebrain, we find the majority of SPNs arise from cortical layer 5 (**Figures 1-6**, **1-7**). CSNs arise across the cortex, including both motor and sensory areas (**Figure 1-8**), implying CSNs play roles in not only voluntary motor control but also modulating sensory information from the body. Indeed, corticospinal pathways have been shown to modulate tactile allodynia as well as normal touch, suggesting direct cortical modulation of spinal sensory processing (Liu et al., 2018). The atlas also identifies major populations of SPNs in the hypothalamus, including the PVH and LHA (**Figure 1-8**). The hypothalamus is involved in various homeostatic processes such as thermoregulation, blood pressure, and neuroendocrine functions, thus hypothalamospinal projections provide a direct command pathway from the forebrain to control autonomic functions (Saper et al., 1976). The midbrain houses SPNs arising multiple anatomical nuclei (**Figure 1-9**). RuSNs, the largest midbrain SPN population, project to cervical and lumbar regions of the spinal cord (**Figure 1-11**), likely providing a supplementary, more primitive motor pathway to the

CST for control of forelimb and hindlimb movement (Olivares-Moreno et al., 2021). Additionally, although less well characterized, the centrally projecting part of the EW containing SPNs plays roles in stress response and coordinating energy homeostasis during stress (Cano et al., 2021; Priest et al., 2021). Finally, hindbrain SPNs arising throughout the pons, medulla, and cerebellum (**Figure 1-10**) play numerous and varied functions. Like the forebrain and midbrain, hindbrain SPNs contain machinery for control of autonomic functions such as the Barrington's nucleus that controls micturition (Kawatani et al., 2021) and NTS which participates in visceral reflexes (Kawatani et al., 2021; Mtui et al., 1995). Major regions involved in motor control, such as the GRN (Brownstone & Chopek, 2018) and PGRN lateral (PGRNl) (Capelli et al., 2017), arise throughout the pontomedullary reticular formation. SPNs from deep cerebellar nuclei have also recently been shown to participate in skilled forelimb movement and locomotor learning (Sathyamurthy et al., 2020).

The dataset generated by this study allows brain-wide SPNs to be considered as unified system. Examining their anatomy across the forebrain, midbrain, and hindbrain, in conjunction with known functional roles, reveals important organizational principles of SPNs. Namely, it becomes apparent that subpopulations governing unique functions are distributed throughout the brain, but also the overall SPN system has built-in redundancies and/or complementary components, with each major brain division (i.e., forebrain, midbrain, hindbrain) containing SPNs commanding basic motor, sensory, and autonomic processes. It is intriguing to think of this system as a multi-layered evolutionary outcome, with the phylogenetically newer and newest midbrain and forebrain, respectively, each adding enhanced repertoires for brain control of bodily function.

1.4.3 TOPOGRAPHIC INNVERATION PATTERNS: Beyond characterizing their supraspinal origins, the ability to classify SPNs based on their spinal terminations offers further insights into their functional organization.

Point-to-point communication: The clearest functional consequence of topographic innervation patterns is their ability to govern functions specific to a spinal level. For example, SPNs exhibiting somatotopic patterns in the cortex, red nucleus, and interposed nucleus are uniquely suited for transmitting point-to-point command signals to govern forelimb and hindlimb movements. Indeed, forelimb and hindlimb function are the most well characterized roles of SPNs arising in each of these supraspinal regions (Sathyamurthy et al., 2020; X. Wang et al., 2017; Whishaw et al., 1998). Additionally, the GRN, which we show has cervical-projecting predominance (**Figure 1-12**), has been shown to participate in skilled forelimb tasks (Esposito et al., 2014).

The presence of "dual" projecting neurons with axon collaterals in both the cervical- and lumbar- spinal cord provides further insights into the structure-function relationship of SPNs. Interestingly, we find that CSNs contain numerous dual projecting neurons whereas RuSNs and CbSNs contain few (**Figure 1-11**). Dual projecting CSNs may therefore provide a direct cellular-level system for commanding interlimb coordination. This is corroborated by the presence of "dual" projecting neurons throughout the pons and medulla (**Figure 1-12**), which have long been known to branch extensively throughout the spinal cord to govern synergistic action of multiple muscle groups (Baker, 2011; Matsuyama et al., 1997; Peterson et al., 1975). Further, though the red nucleus has also been shown to play a role in interlimb postural coordination (Zelenin et al., 2010), the mechanism is likely on a circuit, rather than cellular, level.

Fine and gross motor systems: The structure of the caudal M1M2S1 concentration of CSNs bears an intriguing resemblance to the "new" (fine motor) and "old" (gross motor) M1 described in primate literature (**Figure 1-13**). Retrograde tracing in rhesus monkeys demonstrated that the primate M1 is subdivided into an "old" rostral M1 region containing few direct corticomotoneuronal (CM)

connections and a "new" caudal M1 region containing many direct CM connections (Kuypers & Brinkman, 1970; Rathelot & Strick, 2009). It is thought that these direct CM connections are the substrates that enable enhanced manual dexterity in primates. Though mice do not have direct CM connections, the unique structure of "dual" projecting CSNs may enable interlimb coordination, a form of increased "dexterity" like the direct CM connections of "new" M1 enable in primates. In contrast, the portion of the M1M2S1 concentration that does not contain "dual" projecting neurons project only to the cervical spinal cord; this region may effect motor actions to both forelimb and hindlimb regions via intraspinal circuits similar to the "old" M1 in primates.

Additionally, investigations conducted in primates have suggested that limbs are represented in concentric functional zones, where digits (associated with fine motor control) are represented centrally, while shoulders (related to gross motor movements) are represented peripherally (Kwan et al., 1978). Strikingly, the caudal M1M2S1 concentration of CSNs is similarly arranged in concentric zones, with "dual" CSNs enclosed by a ring of cervical-only projecting CSNs.

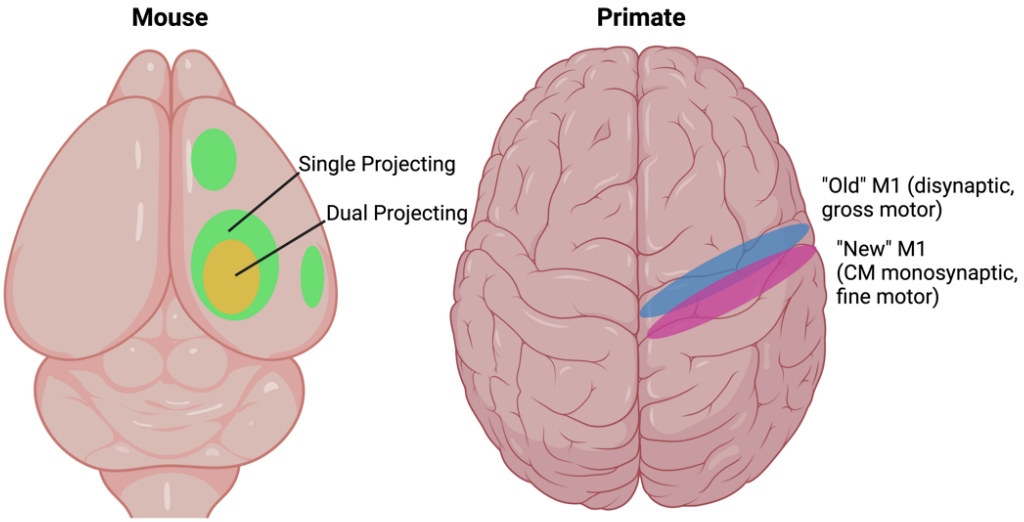


Figure 1-13: Cortical pathways arising from mouse and primate primary motor cortex (M1). (Left) Schematic of adult mouse brain depicting regions of cervical (green) and dual/lumbar (orange) projecting corticospinal neurons. (Right) Schematic of adult human brain depicting "new", fine motor M1 and "old", gross motor M1 (Rathelot & Strick, 2009). Figure created with BioRender.com.

Sensory processing: In his 1981 review of descending pathways, Hans Kuypers noted that in relatively "primitive" species (e.g., edentates, elephants, marsupials, and lagomorphs), corticospinal pathways only extend to the lower brainstem and cervicothoracic spinal cord (Kuypers, 1981). The terminal distribution is primarily in the spinal dorsal horn, suggesting these pathways play more of a role in sensory processing than motor output. In more evolved species (e.g., bats, rodents, carnivores, and primates), corticospinal neurons extend axons throughout the whole length of the spinal cord and primarily synapse in the intermediate zone (IMZ) in a somatotopically organized fashion, consistent with our findings of the caudal M1M2S1 population (**Figure 1-11**). Additionally, however, our topographic mapping results show that the rostral part of the M1M2S1 population, RFA, and S2 each project solely to the cervical spinal cord (**Figure 1-11**), reminiscent of cortical pathways in the aforementioned primitive species. This likeness, coupled with their supraspinal origins in areas relevant for somatosensation (i.e., S1, S2, ACA, PrL), suggest that these corticospinal pathways may primarily play roles in sensory processing (Abraira et al., 2017; Liu et al., 2018).

1.4.4 FUTURE DIRECTIONS:

Overall, these results provide a valuable resource and framework for further investigations into the connectivity of SPNs. Numerous aspects of their anatomy remain uncharted, however, and future efforts will seek to extend this work.

First, additional labeling strategies should be explored to address possible tropism biases and to investigate additional termination features. Specifically, though the CVS-N2c-(ΔG) and rabies constructs remain unoptimized for global SPN labeling in the present study, future work should seek to use retrograde labeled schemes to identify populations that AAV2/retro may lack tropism for. Further, the current study investigates the cervical and lumbar projection features of SPNs throughout the brain; investigating additional spinal levels (i.e., thoracic), termination zones in spinal gray (i.e.,

dorsal horn, IMZ, ventral horn), laterality (i.e., ipsi- or contra- laterally projecting), and presence of direct motoneuronal connections will be important for gaining a more thorough understanding of SPN anatomy. Second, this anatomical atlas provides a comprehensive qualitative overview of SPNs, but future work should seek to quantify the results presented herein. A recent similar study conducted by the Blackmore group leveraged LSFM and automated whole-brain segmentation and registration to quantify SPN populations throughout the brain during baseline physiology and following SCI (Z. Wang et al., 2022)[*]. Future efforts will similarly analyze these data for a (1) quantitative assessment of SPNs throughout anatomically defined nuclei and (2) a more definitive evaluation of dual populations throughout the brain, particularly in the understudied hindbrain populations. Third, the framework and principles applied in the current study can be expediently applied to compare SPNs across various species. Namely, providing a similarly resolved assessment of brain wide SPNs in a primate model will more readily uncover principles relevant to human physiology and disease. Finally, anatomy is just one feature that provides insights into the functional and organizational principles of SPNs; this atlas is leveraged in **Chapters 2** and **3** to probe into their transcriptomic and electrophysiological features, respectively.

1.5 ACKNOWLEDGEMENTS.

We thank Michael Blanchard, Michelle Ocaña, and the Neurobiology Imaging Facility at Harvard Medical School, Boston MA, for imaging samples at the TissueCyte; Yiming Wang and the BCH Viral Core for production of AAV; the Yuanyuan Liu group at the NIDCR/NCCIH (NIH) and Huyan

[*] This publication by the Blackmore group was published during the time the studies presented in this chapter were reaching completion. The results presented in their papers cited above generally align with our findings, as illustrated in the results and discussion sections. Given the Blackmore group's rigorous quantification of a similar whole-brain SPN dataset, we instead decided to focus our efforts on bolstering the molecular (**Chapter 2**) and physiological (**Chapter 3**) studies presented in **Chapters 2** and **3**, respectively. Nonetheless, differences across these datasets likely exist (e.g., due to differences in precise spinal injection levels and LSFM vs. STPT imaging modalities). These data will be made public upon publication of my thesis manuscript for the community to analyze and compare.

Meng (He Lab) for production of HiRet Lenti; the Tasic group at the Allen Institute for Brain Science for the CVS-N2c-(ΔG) virus; and Ashwin Kumar for QuPath guidance.

1.6 VIDEO LEGEND.

Video 1-1: Anatomical overview of spinal projecting neurons. Coronal view panning through segmented and registered SPN nuclei imaged with serial two-photon tomography. Video may be found at: https://tinyurl.com/WinterSupplement.

1.7 MATERIALS AND METHODS.

Animals

All experimental procedures were performed in compliance with animal protocols approved by the Institutional Animal Care and Use Committee at Boston Children's Hospital (Protocol #20-05-4165R). Mice were provided food and water *ad libitum*, housed on a 12-hour light-dark schedule (7am-7pm light period) with no more than 5 mice of the same sex per cage, and allowed to acclimate for 1 week after arrival. C57BL/6J wild-type mice (Jackson Labs, Strain #:000664) were used to generate all retrogradely labeled histological datasets. Equal male and female mice were used.

Virus production and retrograde labeling of adult spinal projecting neurons

AAV2/retro-hSyn-H2B-FP (GFP and mScarlet) constructs were produced by the Boston Children's Hospital Viral Core, RabV CVS-N2c(ΔG)-H2B-GFP was produced by the Tasic group at the Allen Institute for Brian Science, and HiRet-lenti-H2B-GFP was produced by Yuanyuan Liu (NIH) and Huyan Meng (He Lab). To retrogradely label SPNs, viral constructs were injected into the cervical and lumbar spinal cord. Briefly, adult mice (P42) were anesthetized with intraperitoneal injection of

ketamine-xylazine (KX, 100-120 mg/Kg ketamine, 10 mg/Kg xylazine) and placed on a stereotactic frame. For cervical level (C4-6) injection, a dorsal incision was made along the vertebral column at cervical level. The overlying muscle was dissected to expose the cervical vertebral column and a laminectomy was performed at C4-6 to expose the spinal cord. 2.4 μL of the viral construct ($5x10^{12}$ genome copies per mL, gc/mL) were injected at 0.40 mm lateral to midline and 0.60 mm and 1.00 mm depth using a glass micropipette (tipped at 25 μm in diameter). The dorsal muscle layers were sutured, and skin closed with sterile wound clips. For lumbar level (L2-4) injections, this process was repeated with the constructs at 0.35 mm lateral to midline and 0.60 mm and 1.00 mm depth.

Histology and imaging of retrogradely labeled brains

At P56, retrogradely labeled mice were anesthetized with KX and sacrificed by transcardiac perfusion with phosphate buffered saline (PBS) followed by 4% paraformaldehyde (PFA) in PBS. The skull and spinal column were dissected and post-fixed in 4% PFA in PBS for 24 hours. The brain and spinal cord tissue were then microdissected and cryoprotected in 30% sucrose, embedded and frozen in optimal cutting temperature (OCT) medium and processed using a cryostat (50 μm coronal sections; olfactory bulb through caudal medulla; four series). Sections were washed with PBS and then treated with a blocking solution (5% normal donkey serum, 0.5% Triton-X) for 1 hour at room temperature (RT). Floating sections were incubated in primary antibodies (AVES Chicken anti-GFP, Rockland Rabbit-anti-RFP; 1:500 dilution in blocking solution) at 4ºC overnight, washed three times for 10 minutes with PBS, and subsequently incubated with secondary antibodies (Alexa Fluor 488 donkey-anti-chicken, Alexa Fluor 594 donkey-anti-rabbit; 1:500 dilution in PBS) for 2 hours at RT. Finally, sections were washed with PBS, mounted with DAPI Fluoromount-G mounting medium, sealed with clear nail polish, and stored at 4ºC until imaging. Whole sections were imaged on an Olympus VS120

Virtual Slide Microscope at 10x magnification. Higher magnification images were acquired as z-stacks with a 20x objective on a Zeiss LSM 900 Confocal Laser Scanning Microscope.

Quantification of spinal projecting neurons across major brain regions

SPNs were quantified across the eight major brain regions (i.e., RFA, M1M2S1, S2, HY, MB, PONS, MED) using QuPath. Briefly, VS120 slide scanner images of one (of four) IHC processed coronal series were loaded into QuPath as a project. The polygon tool was used to manually annotate ROIs. Classifiers were then created using 'Positive Cell Detection' (for GFP and mScarlet nuclei) and 'Composite Classifier' (for GFP+/mScarlet+ nuclei). 'Annotation results' were saved per ROI, and the number of nuclei quantified per ROI were multiplied by four (as only 1 of 4 coronal series was quantified) to get total brain counts. N = 5 retrogradely labeled brains were quantified to yield total SPN counts across each of the eight ROIs.

Serial two-photon tomography, registration, and nucleus segmentation

Image acquisition: Whole retrogradely labeled brains were imaged using the TissueCyte serial two-photon tomography platform. Briefly, at P56, retrogradely labeled mice were anesthetized with KX and sacrificed by transcardiac perfusion with PBS and 4%PFA/PBS, the skull and spinal column were dissected and post-fixed in 4% PFA in PBS for 24 hours. The brain was then microdissected, rinsed with PBS, and embedded in covalent agarose. Briefly, a 4.5% agarose solution in 10mM NaIO4 was made by gently stirring agarose and NaIO4 with Phosphate Buffer (PB; 0.42g/L monobasic sodium phosphate, 0.92g/L Dibasic sodium phosphate) for 2-3 hours at RT in a hood protected from light and filtered with a 0.2 μm filter. A microwave was then used to bring agarose to a boil, then cooled down to 60-65ºC to embed the brain. The agarose-embedded brain was mounted in the TissueCyte

using Quick Bond adhesive. The sample was immersed in PB during image acquisition. Images were captured at XY resolution of 1.38 μm/pixel with 10 μm stacks and 50 μm vibratome planes. Images were stitched with TissueVision's proprietary stitching algorithm 'Stitcher'.

Quality control: Image stacks were imported into Arivis (Zeiss) and assessed for tissue quality in "2D" and "4D" viewer modes. Specifically, signal intensity was assessed and image stacks were inspected for tears or missing sections.

Registration and segmentation: Labeled nuclei were segmented and reconstructed using NeuroInfo (MBF Bioscience). Briefly, stitched images were first stacked with MicroFile+. Stacked images were then registered to the Allen Mouse Common Coordinate Framework (Allen CFF) with the volume registration function in NeuroInfo. H2B signals in red (mScarlet) or green (GFP) channels were detected and labeled separately. The detected nuclei were manually annotated with different colors based on their mapped regions. Videos and horizontal, coronal, or sagittal projections of the three-dimension reconstructions were output via Neuroinfo's 3D visualization window.

1.8 REFERENCES.

Abraira, V. E., Kuehn, E. D., Chirila, A. M., Springel, M. W., Toliver, A. A., Zimmerman, A. L., Orefice, L. L., Boyle, K., Bai, L., Song, B. J., Bashista, K. A., O'Neill, T. G., Zhuo, J., Tsan, C., Hoynoski, J., Rutlin, M., Kus, L., Niederkofler, V., Watanabe, M., … Ginty, D. D. (2017). The Cellular and Synaptic Architecture of the Mechanosensory Dorsal Horn. *Cell*, *168*(1–2), 295. https://doi.org/10.1016/J.CELL.2016.12.010

Akintunde, A., & Buxton, D. F. (1992). Differential sites of origin and collateralization of corticospinal neurons in the rat: a multiple fluorescent retrograde tracer study. *Brain Research*, *575*, 86–92.

Baker, S. N. (2011). The primate reticulospinal tract, hand function and functional recovery. *The Journal of Physiology*, *589*(Pt 23), 5603. https://doi.org/10.1113/JPHYSIOL.2011.215160

Brownstone, R. M., & Chopek, J. W. (2018). Reticulospinal systems for tuning motor commands. *Frontiers in Neural Circuits*, *12*, 1–10. https://doi.org/10.3389/FNCIR.2018.00030/BIBTEX

Cano, G., Hernan, S. L., & Sved, A. F. (2021). Centrally Projecting Edinger-Westphal Nucleus in the Control of Sympathetic Outflow and Energy Homeostasis. *Brain Sciences*, *11*(8). https://doi.org/10.3390/BRAINSCI11081005

Capelli, P., Pivetta, C., Esposito, M. S., & Arber, S. (2017). Locomotor speed control circuits in the caudal brainstem. *Nature 2017 551:7680*, *551*(7680), 373–377. https://doi.org/10.1038/nature24064

Datar, A., Ameeramja, J., Bhat, A., Srivastava, R., Mishra, A., Bernal, R., Prost, J., Callan-Jones, A., & Pullarkat, P. A. (2019). The Roles of Microtubules and Membrane Tension in Axonal Beading, Retraction, and Atrophy. *Biophysical Journal*, *117*(5), 880. https://doi.org/10.1016/J.BPJ.2019.07.046

Dawnay, N. A. H., & Glees, P. (1986). Somatotopic Analysis of Fibre and Terminal Distribution in the Primate Corticospinal Pathway. *Developmental Brain Research*, *26*, 115–123.

Esposito, M. S., Capelli, P., & Arber, S. (2014). Brainstem nucleus MdV mediates skilled forelimb motor tasks. *Nature 2014 508:7496*, *508*(7496), 351–356. https://doi.org/10.1038/nature13023

Franklin, K., & Paxinos, G. (2008). *The Mouse Brain in Stereotaxic Coordinates* (Third). Elsevier Academic Press. https://scholar.google.com/scholar_lookup?&title=The%20mouse%20brain%20in%20stereotaxic%20coordinates&publication_year=2008&author=Franklin%2CKBJ&author=Paxinos%2CG

Ganley, R. P., Werder, K., Wildner, H., & Zeilhofer, H. U. (2021). Spinally projecting noradrenergic neurons of the locus coeruleus display resistance to AAV2retro-mediated transduction. *Molecular Pain*, *17*. https://doi.org/10.1177/17448069211037887

He, S.-Q., Dum, R. P., & Strick, P. L. (1993). *Topographic Organization of Corticospinal Projections from the Frontal Lobe: Motor Areas on the Lateral Surface of the Hemisphere*.

Kato, S., Kobayashi, K., Inoue, K. I., Kuramochi, M., Okada, T., Yaginuma, H., Morimoto, K., Shimada, T., Takada, M., & Kobayashi, K. (2011). A lentiviral strategy for highly efficient retrograde gene transfer by pseudotyping with fusion envelope glycoprotein. *Human Gene Therapy*, *22*(2), 197–206. https://doi.org/10.1089/HUM.2009.179

Kawatani, M., de Groat, W. C., Itoi, K., Uchida, K., Sakimura, K., Yamanaka, A., Yamashita, T., & Kawatani, M. (2021). Downstream projection of Barrington's nucleus to the spinal cord in mice. *Journal of Neurophysiology*, *126*(6), 1959–1977. https://doi.org/10.1152/JN.00026.2021/ASSET/IMAGES/LARGE/JN.00026.2021_F009.JPEG

Kinoshita, M., Matsui, R., Kato, S., Hasegawa, T., Kasahara, H., Isa, K., Watakabe, A., Yamamori, T., Nishimura, Y., Alstermark, B., Watanabe, D., Kobayashi, K., & Isa, T. (2012). Genetic dissection of the circuit for hand dexterity in primates. *Nature*, *487*(7406), 235–238. https://doi.org/10.1038/NATURE11206

Koblinger, K., Füzesi, T., Ejdrygiewicz, J., Krajacic, A., Bains, J. S., & Whelan, P. J. (2014). Characterization of A11 Neurons Projecting to the Spinal Cord of Mice. *PLoS ONE*, *9*(10), 109636. https://doi.org/10.1371/JOURNAL.PONE.0109636

Kuypers, H. G. J. M. (1981). Anatomy of the Descending Pathways. *Comprehensive Physiology*, 597–666. https://doi.org/10.1002/cphy.cp010213

Kuypers, H. G. J. M., & Brinkman, J. (1970). Precentral projections to different parts of the spinal intermediate zone in the rhesus monkey. *Brain Research*, *24*(1), 29–48. https://doi.org/10.1016/0006-8993(70)90272-6

Kwan, H. C., MacKay, W. A., Murphy, J. T., & Wong, Y. C. (1978). Spatial organization of precentral cortex in awake primates. II. Motor outputs. *Journal of Neurophysiology*, *41*(5), 1120–1131. https://doi.org/10.1152/JN.1978.41.5.1120

Lemon, R. N. (2008). Descending Pathways in Motor Control. *Https://Doi.Org/10.1146/Annurev.Neuro.31.060407.125547*, *31*, 195–218. https://doi.org/10.1146/ANNUREV.NEURO.31.060407.125547

Li, X. G., Florence, S. L., & Kaas, J. H. (2009). Areal Distributions of Cortical Neurons Projecting to Different Levels of the Caudal Brain Stem and Spinal Cord in Rats. *Somatosensory & Motor Research*, *7*(3), 315–335. https://doi.org/10.3109/08990229009144711

Liang, H., Paxinos, G., & Watson, C. (2011). Projections from the brain to the spinal cord in the mouse. *Brain Structure and Function 2010 215:3*, *215*(3), 159–186. https://doi.org/10.1007/S00429-010-0281-X

Liang, H., Paxinos, G., & Watson, C. (2012). The red nucleus and the rubrospinal projection in the mouse. *Brain Structure and Function*, *217*(2), 221–232. https://doi.org/10.1007/S00429-011-0348-3/FIGURES/7

Liu, Y., Hegarty, S., Winter, C., Wang, F., & He, Z. (2020). Viral vectors for neuronal cell type-specific visualization and manipulations. *Current Opinion in Neurobiology*, *2020*, 67–76. https://doi.org/10.1016/j.conb.2020.03.011

Liu, Y., Latremoliere, A., Li, X., Zhang, Z., Chen, M., Wang, X., Fang, C., Zhu, J., Alexandre, C., Gao, Z., Chen, B., Ding, X., Zhou, J. Y., Zhang, Y., Chen, C., Wang, K. H., Woolf, C. J., & He, Z. (2018). Touch and tactile neuropathic pain sensitivity are set by corticospinal projections. *Nature 2018 561:7724*, *561*(7724), 547–550. https://doi.org/10.1038/s41586-018-0515-2

Matsuyama, K., Takakusaki, K., Nakajima, K., & Mori, S. (1997). Multi-Segmental Innervation of Single Pontine Reticulospinal Axons in the Cervico-Thoracic Region of the Cat: Anterograde PHA-L Tracing Study. *Inc. THE JOURNAL OF COMPARATIVE NEUROLOGY*, *377*, 234–250. https://doi.org/10.1002/(SICI)1096-9861(19970113)377:2

Miller, M. W. (1987). The origin of corticospinal projection neurons in rat. *Experimental Brain Research*, *67*(2), 339–351. https://doi.org/10.1007/BF00248554/METRICS

Morecraft, R. J., Ge, J., Stilwell-Morecraft, K. S., Mcneal, D. W., Pizzimenti, M. A., & Darling, W. G. (2013). Terminal distribution of the corticospinal projection from the hand/arm region of the primary motor cortex to the cervical enlargement in rhesus monkey. *Journal of Comparative Neurology*, *521*(18), 4205–4235. https://doi.org/10.1002/CNE.23410

Mtui, E. P., Anwar, M., Reis, D. J., & Ruggiero, D. A. (1995). Medullary visceral reflex circuits: Local afferents to nucleus tractus solitarii synthesize catecholamines and project to thoracic spinal cord. *Journal of Comparative Neurology*, *351*(1), 5–26. https://doi.org/10.1002/CNE.903510103

Murray, H. M., & Gurule, M. E. (1979). Origin of the Rubrospinal Tract if the Rat. *Neuroscience Letters*, *14*, 19–23.

Nassi, J. J., Cepko, C. L., Born, R. T., & Beier, K. T. (2015). Neuroanatomy goes viral! *Frontiers in Neuroanatomy*, *9*(July), 80. https://doi.org/10.3389/FNANA.2015.00080/BIBTEX

Olivares-Moreno, R., Rodriguez-Moreno, P., Lopez-Virgen, V., Macías, M., Altamira-Camacho, M., & Rojas-Piloni, G. (2021). Corticospinal vs Rubrospinal Revisited: An Evolutionary Perspective for Sensorimotor Integration. *Frontiers in Neuroscience*, *15*, 680. https://doi.org/10.3389/FNINS.2021.686481/BIBTEX

Penfield, W., & Boldrey, E. (1937). Somatic motor and sensory representation in the cerebral cortex of man as studied by electrical stimulation. *Brain*, *60*, 389–443. https://academic.oup.com/brain/article/60/4/389/332082

Peterson, B. W., Maunz, R. A., Pitts, N. G., & Mackel, R. G. (1975). Patterns of projection and braching of reticulospinal neurons. *Experimental Brain Research*, *23*(4), 333–351. https://doi.org/10.1007/BF00238019

Priest, M. F., Freda, S. N., Badong, D., Dumrongprechachan, V., & Kozorovitskiy, Y. (2021). Peptidergic modulation of fear responses by the Edinger-Westphal nucleus. *BioRxiv*, 2021.08.05.455317. https://doi.org/10.1101/2021.08.05.455317

Rathelot, J. A., & Strick, P. L. (2009). Subdivisions of primary motor cortex based on cortico-motoneuronal cells. *Proceedings of the National Academy of Sciences of the United States of America*, *106*(3), 918–923. https://doi.org/10.1073/PNAS.0808362106/SUPPL_FILE/0808362106SI.PDF

Reardon, T. R., Murray, A. J., Turi, G. F., Wirblich, C., Croce, K. R., Schnell, M. J., Jessell, T. M., & Losonczy, A. (2016). Rabies Virus CVS-N2cΔG Strain Enhances Retrograde Synaptic Transfer and Neuronal Viability. *Neuron*, *89*(4), 711–724. https://doi.org/10.1016/J.NEURON.2016.01.004

Saper, C. B., Loewy, A. D., Swanson, L. W., & Cowan, W. M. (1976). Direct hypothalamo-autonomic connections. *Brain Research*, *117*, 305.

Sathyamurthy, A., Barik, A., Dobrott, C. I., Matson, K. J. E., Stoica, S., Pursley, R., Chesler, A. T., & Levine, A. J. (2020). Cerebellospinal Neurons Regulate Motor Performance and Motor Learning. *Cell Reports*, *31*(6), 107595. https://doi.org/10.1016/J.CELREP.2020.107595

Shieh, J. Y., Leong, S. K., & Wong, W. C. (1983). Origin of the rubrospinal tract in neonatal, developing, and mature rats. *Journal of Comparative Neurology*, *214*(1), 79–86. https://doi.org/10.1002/CNE.902140108

Skagerberg, G., & Lindvall, O. (1985). Organization of diencephalic dopamine neurones projecting to the spinal cord in the rat. *Brain Research*, *342*(2), 340–351. https://doi.org/10.1016/0006-8993(85)91134-5

Steward, O., Yee, K. M., Metcalfe, M., Willenberg, R., Luo, J., Azevedo, R., Martin-Thompson, J. H., & Gandhi, S. P. (2021). Rostro-Caudal Specificity of Corticospinal Tract Projections in Mice. *Cerebral Cortex*, *31*(5), 2322–2344. https://doi.org/10.1093/CERCOR/BHAA338

Tappan, S. J., Eastwood, B. S., O'Connor, N., Wang, Q., Ng, L., Feng, D., Hooks, B. M., Gerfen, C. R., Hof, P. R., Schmitz, C., & Glaser, J. R. (2019). Automatic navigation system for the mouse brain. *Journal of Comparative Neurology*, *527*(13), 2200–2211. https://doi.org/10.1002/CNE.24635

Tervo, D. G. R., Hwang, B. Y., Viswanathan, S., Gaj, T., Lavzin, M., Ritola, K. D., Lindo, S., Michael, S., Kuleshova, E., Ojala, D., Huang, C. C., Gerfen, C. R., Schiller, J., Dudman, J. T., Hantman, A. W., Looger, L. L., Schaffer, D. V., & Karpova, A. Y. (2016). A Designer AAV Variant Permits Efficient Retrograde Access to Projection Neurons. *Neuron*, *92*(2), 372–382. https://doi.org/10.1016/J.NEURON.2016.09.021

Tyson, A. L., Rousseau, C. V., Niedworok, C. J., Keshavarzi, S., Tsitoura, C., Cossell, L., Strom, M., & Margrie, T. W. (2021). A deep learning algorithm for 3D cell detection in whole mouse brain image datasets. *PLOS Computational Biology*, *17*(5), e1009074. https://doi.org/10.1371/JOURNAL.PCBI.1009074

Ullan, J., & Artieda, J. (1981). Somatotopy of the corticospinal neurons in the rat. *Neuroscience Letters*, *21*, 13–18.

Wang, Q., Ding, S. L., Li, Y., Royall, J., Feng, D., Lesnar, P., Graddis, N., Naeemi, M., Facer, B., Ho, A., Dolbeare, T., Blanchard, B., Dee, N., Wakeman, W., Hirokawa, K. E., Szafer, A., Sunkin, S. M., Oh, S. W., Bernard, A., … Ng, L. (2020). The Allen Mouse Brain Common Coordinate Framework: A 3D Reference Atlas. *Cell*, *181*(4), 936-953.e20. https://doi.org/10.1016/J.CELL.2020.04.007

Wang, X., Liu, Y., Li, X., Zhang, Z., Yang, H., Zhang, Y., Williams, P. R., Alwahab, N. S. A., Kapur, K., Yu, B., Zhang, Y., Chen, M., Ding, H., Gerfen, C. R., Wang, K. H., & He, Z. (2017). Deconstruction of Corticospinal Circuits for Goal-Directed Motor Skills. *Cell*, *171*(2), 440-455.e14. https://doi.org/10.1016/J.CELL.2017.08.014

Wang, Z., Maunze, B., Wang, Y., Tsoulfas, P., & Blackmore, M. G. (2018). Global Connectivity and Function of Descending Spinal Input Revealed by 3D Microscopy and Retrograde Transduction. *Journal of Neuroscience*, *38*(49), 10566–10581. https://doi.org/10.1523/JNEUROSCI.1196-18.2018

Wang, Z., Romanski, A., Mehra, V., Wang, Y., Brannigan, M., Campbell, B. C., Petsko, G. A., Tsoulfas, P., & Blackmore, M. G. (2022). Brain-wide analysis of the supraspinal connectome reveals anatomical correlates to functional recovery after spinal injury. *ELife*, *11*. https://doi.org/10.7554/ELIFE.76254

Whishaw, I. Q., Gorny, B., & Sarna, J. (1998). Paw and limb use in skilled and spontaneous reaching after pyramidal tract, red nucleus and combined lesions in the rat: behavioral and anatomical dissociations. *Behavioural Brain Research*, *93*(1–2), 167–183. https://doi.org/10.1016/S0166-4328(97)00152-6

Wise, S. P., Murray, E. A., & Coulter, J. D. (1979). Somatotopic organization of corticospinal and corticotrigeminal neurons in the rat. *Neuroscience*, *4*, 65–78.

Zelenin, P. V., Beloozerova, I. N., Sirota, M. G., Orlovsky, G. N., & Deliagina, T. G. (2010). Activity of Red Nucleus Neurons in the Cat during Postural Corrections. *Journal of Neuroscience*, *30*(43), 14533–14542. https://doi.org/10.1523/JNEUROSCI.2991-10.2010

2

A molecular taxonomy of transcriptomic cell types reveals organizational and functional principles of brain-wide spinal projecting neurons

Publication: This chapter was adapted from a manuscript under revision at *Nature*, revision submitted in September 2023.

A taxonomy of transcriptomic cell types reveals organizational and functional principles of brain-wide spinal projecting neurons

Carla C. Winter[1,2,3,4,12], Anne Jacobi[1,2,11,12,✉], Junfeng Su[1,2,12], Leeyup Chung[1,2], Cindy T. J. van Velthoven[5], Zizhen Yao[5], Changkyu Lee[5], Zicong Zhang[1,2], Shuguang Yu[1,2], Kun Gao[6,7], Geraldine Duque Salazar[1,2], Evgenii Kegeles[1,2,3], Riki Kawaguchi[6,7], Yu Zhang[1,2], Makenzie C. Tomihiro[1,2], Junjie Zhu[1,2], Jing Tang[1,2], Xuan Song[1,2], Ryan J. Donahue[1,2], Qing Wang[6,7], Delissa McMillen[5], Michael Kunst[5], Kimberly A. Smith[5], Alexandra Krol[8], Guoping Feng[8,9], Yuanyuan Liu[10], Daniel H. Geschwind[6,7], Bosiljka Tasic[5], Hongkui Zeng[5,✉], Zhigang He[1,2,✉]

1. F.M. Kirby Neurobiology Center, Boston Children's Hospital, Boston, MA, USA
2. Departments of Neurology and Ophthalmology, Harvard Medical School, Boston, MA, USA
3. PhD Program in Biological and Biomedical Sciences, Harvard Medical School, Boston, MA, USA
4. Harvard-MIT MD-PhD Program, Harvard Medical School, Boston, MA, USA
5. Allen Institute for Brain Science, Seattle, WA, USA
6. Program in Neurogenetics, Department of Neurology, David Geffen School of Medicine, University of California Los Angeles, Los Angeles, CA, USA
7. Semel Institute for Neuroscience and Human Behavior, David Geffen School of Medicine, University of California Los Angeles, Los Angeles, CA, USA
8. McGovern Institute for Brain Research and the Department of Brain and Cognitive Sciences, Massachusetts Institute of Technology, Cambridge, MA, USA
9. The Stanley Center for Psychiatric Research, Broad Institute of MIT and Harvard, Cambridge, MA, USA
10. Somatosensation and Pain Unit, National Institute of Dental and Craniofacial Research, National Center for Complementary and Integrative Health, National Institutes of Health, Bethesda, MD, USA
11. Present address: F. Hoffman-La Roche, pRED, Basel, Switzerland
12. These authors contributed equally.

✉Correspondence: Zhigang He (zhigang.he@childrens.harvard.edu), Hongkui Zeng (HongkuiZ@alleninstitute.org), and Anne Jacobi (Anne.Jacobi@roche.com)

Author contributions: Conceptualization: C.C.W., A.J., H.Z., Z.H. Manuscript writing: C.C.W. and Z.H. Figure generation: Led by C.C.W, with help from A.J., J.S, C.T.J.vV., Z.Y., C.L., S.Y., K.G., Y.Z., X.S. Manuscript review and editing: contributions from all authors. Data analysis lead and coordination: C.C.W. Retrograde Injections: Led by Z.Z., with help from J.Z. and J.T. snRNAseq data generation: Led by C.C.W., with help from A.J., Z.Z., Q.W., K.A.S. snRNAseq data processing and analysis: Led by C.C.W., with help from A.J., J.S., C.T.J.vV., Z.Y., C.L., S.Y., K.G., Y.Z., X.S., R.K. AIBS WB scRNAseq and MERFISH mapping: Led by C.T.J.vV. and Z.Y., with help from C.L., D.M., M.K.

2.1 ABSTRACT.

The brain executes control of all bodily functions largely via spinal projecting neurons (SPNs) that carry command signals from numerous supraspinal regions to the spinal cord. Despite their physiological and clinical relevance, a comprehensive molecular characterization of SPNs is lacking. Here, we use retrograde labeling, whole-brain imaging, and high-throughput transcriptional profiling to generate a unified brain-wide anatomic and transcriptomic atlas of adult mouse SPNs at single-cell resolution. We transcriptionally profiled a total of 65,002 SPNs and employed a multi-level iterative clustering approach to generate a hierarchically organized transcriptomic taxonomy of SPNs organized into 3 divisions, 13 subclasses, and 76 types. These types were mapped to their spatial locations via integration with a companion atlas of the whole mouse brain generated by the Allen Institute for Brain Science within the BRAIN Initiative Cell Census Network (BICCN) (Yao et al., 2023). This SPN taxonomy reveals a three-component organization: (1) molecularly homogeneous excitatory SPNs from the cortex, red nucleus, and cerebellum with somatotopic spinal terminations suitable for point-to-point communication; (2) highly heterogeneous excitatory and inhibitory populations in the reticular formation with broad spinal termination patterns, thus suitable for relaying commands related to the activities of the entire spinal cord; and (3) modulatory neurons expressing slow-acting neurotransmitters and/or neuropeptides in the hypothalamus, midbrain, and reticular formation for gain control of brain-spinal signals. We discovered a LIM homeobox transcription factor code that parcellates the most transcriptionally complex population, pontomedullary reticulospinal neurons, into five LIM-defined and spatially segregated populations. Lastly, we linked transcriptomic types with their spinal termination levels and identify transcriptomic signatures that correspond to spinal cord projection patterns.

2.2 INTRODUCTION.

The spinal cord is the first center of bodily sensory processing and hosts the final execution machinery for both somatic and autonomic motor programs. Without commands from the brain, however, the spinal cord cannot initiate and execute any meaningful behavior (Ferreira-Pinto et al., 2018; Grillner & Wallén, 1985; Kiehn, 2011). The brain-derived spinal projecting neurons (SPNs), which form different descending projections and terminate in various spinal locations, are essential for the transformation of these brain commands ("thoughts") into the bodily behavioral repertoire ("actions") (Baker et al., 2015; Brownstone & Chopek, 2018; Ferreira-Pinto et al., 2018; Jordan et al., 2008; Lemon, 2008). The importance of these descending tracts is illustrated by sensory, motor, and autonomic dysfunction following spinal cord injury (Courtine & Sofroniew, 2019; Griffin & Bradke, 2020; Tuszynski & Steward, 2012; Zheng & Tuszynski, 2023), stroke (Marin & Carmichael, 2018; Pirondini et al., 2022), and amyotrophic lateral sclerosis (Hardiman et al., 2017; Kim et al., 2020). To understand how SPNs transduce brain commands into diverse actions, and the mechanisms underlying the disruption of these processes during disease and injury, it is essential to comprehensively profile their anatomical structure and corresponding cellular and molecular components.

Significant progress has been made in identifying major anatomical tracts, including cataloguing the location and morphology of their soma, trajectories of their fibers, and locations of cells on which they terminate. Early studies established that descending pathways are widely conserved across mammals and arise in numerous supraspinal locations, with the most abundant populations in the cerebral cortex, red nucleus, and brainstem reticular formation, forming the corticospinal tract (CST), rubrospinal tract (RuST), and reticulospinal tract (ReST), respectively (J. C. Holstege & Kuypers, 1987; Kuypers, 1981; Lemon, 2008). Efforts to develop brain-wide anatomical atlases offered major advances in our understanding of the overall anatomical organization of descending pathways,

as they unified fragmentary findings across early works and provided a comprehensive baseline for future studies (Liang et al., 2011; Z. Wang et al., 2018, 2022) (also detailed in **Chapter 1**).

The functional output of these anatomically defined pathways is, in large part, determined by their cellular and molecular components, yet our knowledge in these domains remains relatively limited. Previous studies have investigated molecular markers for broadly defined anatomical tracts, such as the CST (Arlotta et al., 2005; Molyneaux et al., 2015; Sahni et al., 2021), RuST (Liang et al., 2012), and ReST (Bretzner & Brownstone, 2013; Cepeda-Nieto et al., 2005). These molecular studies are largely incomplete, however: most investigate populations during development and not adulthood, consider only a few marker genes, and/or do not consider within-tract cellular heterogeneity. Thus, no molecular markers are available for many SPN groups and the overall cellular organization of SPNs is unknown.

Efforts to catalogue the extraordinary diversity of cell types throughout the brain have been rapidly accelerated by the advent of high-throughput single-cell genomics technologies. Single-cell RNA sequencing (scRNAseq) has been employed to generate cell type taxonomy across the CNS, including the retina (Rheaume et al., 2018; Tran et al., 2019), brain (BICCN, 2021; Tasic et al., 2016, 2018), and spinal cord (Alkaslasi et al., 2021; Blum et al., 2021; Russ et al., 2021; Sathyamurthy et al., 2018). To systematize and accelerate this task, the BICCN (Brain Research through Advancing Innovative Neurotechnologies (BRAIN) Initiative - Cell Census Network) (Ecker et al., 2017) was established with the goal of building a cell atlas of the entire CNS. As SPNs constitute only a small portion of the resident neurons in individual brain regions, and their extraordinary size underlies selective vulnerability during high-throughput cell isolation procedures, transcriptomic profiling efforts across the whole brain must specifically enrich and optimize for these unique cells.

As part of the BICCN, we sought to create a unified anatomic and transcriptomic atlas of SPNs across the entire mouse brain at single-cell resolution. Here, we used retrograde labeling, whole-

brain imaging, and high-throughput transcriptomics to profile a total of 65,002 SPNs. We employed a multi-level iterative clustering approach to generate a hierarchically organized transcriptomic taxonomy of 76 SPN types. We harmonized these transcriptomic types with their anatomical locations via integration with a multiplexed error-robust fluorescence in situ hybridization (MERFISH) dataset generated by the Allen Institute for Brain Science and BICCN (Yao et al., 2023). We leveraged the taxonomy and spatial mapping to discover a LIM homeobox transcription factor code that parcellates the most transcriptionally complex population, pontomedullary reticulospinal neurons, into five LIM-defined and spatially segregated populations. Finally, we linked transcriptomic types with their spinal termination levels and identify transcriptomic signatures that correspond to spinal cord projection patterns.

2.3 RESULTS.

2.3.1 GENERATION OF AN ANATOMICALLY INFORMED TRANSCRIPTOMIC ATLAS OF SPINAL PROJECTING NEURONS.

Due to their complex anatomical distribution and fragility, spinal projecting neurons (SPNs) have been challenging to characterize at single-cell resolution. To address this challenge, we developed a pipeline to efficiently label, image, and transcriptionally profile SPN nuclei across the entire adult mouse brain (**Figure 2-1a**). First, we retrogradely labeled SPNs via injection of recombinant retrograde adeno associated virus (rAAV2/retro-Syn-H2B-fluorescent protein) (Tervo et al., 2016) into multiple segments centering the cervical (GFP) and lumbar (mScarlet) spinal cord of adult C57BL/6J mice. With serial two-photon tomography (STPT) (**Figure 2-1b**), we assessed the anatomical distribution of SPNs across the whole mouse brain. As expected, SPNs are widely distributed across the mouse brain but with concentrations in cortex (CTX; 41.77% of all SPNs), hypothalamus (HY; 2.90%), midbrain (MB; 12.88%), cerebellum (CB; 2.18%), pons (PONS; 16.01%), and medulla (MED; 24.26%)

(see Chapter 1 **Figure 1-6**), consistent with findings from viral and non-viral labeling methods (Liang et al., 2011; Z. Wang et al., 2018, 2022).

To generate the transcriptomic taxonomy, adult C57BL/6J mice were used for retrograde labeling of SPNs via the injection scheme used for above anatomical analyses. At P56, the mice were sacrificed, and the major regions of interest (ROIs) were microdissected, guided by the STPT anatomical map (**Figure 2-2a-c**). We found that most adult SPNs do not survive harsh cell dissociation and fluorescent activated cell sorting (FACS) protocols traditionally used for single-cell RNA sequencing (scRNAseq), likely due to their exceptionally long axons and large cell volumes that render them highly vulnerable. Thus, we relied on high-throughput fluorescence activated nucleus sorting (FANS) and single nucleus RNA sequencing (snRNAseq). Equal numbers of male and female mice were pooled per ROI to input sufficient nuclei for FANS (**Figure 2-2b**). Each dissection ROI was kept as a separate sample, and SPNs were collected via nucleus isolation and sorting by FANS (**Figure 2-2d**). Nuclei were inspected post-FANS to assess morphology and confirm enrichment of fluorescently labeled populations (**Figure 2-2e**). snRNAseq profiles of all ROIs were generated with the 10x version 3.1 (10x) platform and profiles of targeted regions were generated with SMART-Seq version 4 (SSv4) (**Table 2-1**).

2.3.2 DETECTION OF FIRST AND SECOND ORDER LABELED CELLS.

In addition to their capacity to directly retrogradely label SPNs (termed "first-order"), AAV vectors may also transduce "second-order" cells due to transsynaptic labeling (Zingg et al., 2017) or release of AAV after neuronal death or degeneration. This poses a challenge for any dataset that relies on AAV retrograde labeling to enrich specific neuronal populations as it may produce false positives for the intended population, albeit at low levels. Indeed, in addition to labeling expected SPNs in cortical layer 5 (i.e., corticospinal neurons, CSNs), the retrograde targeting protocol also led to labeling of a small

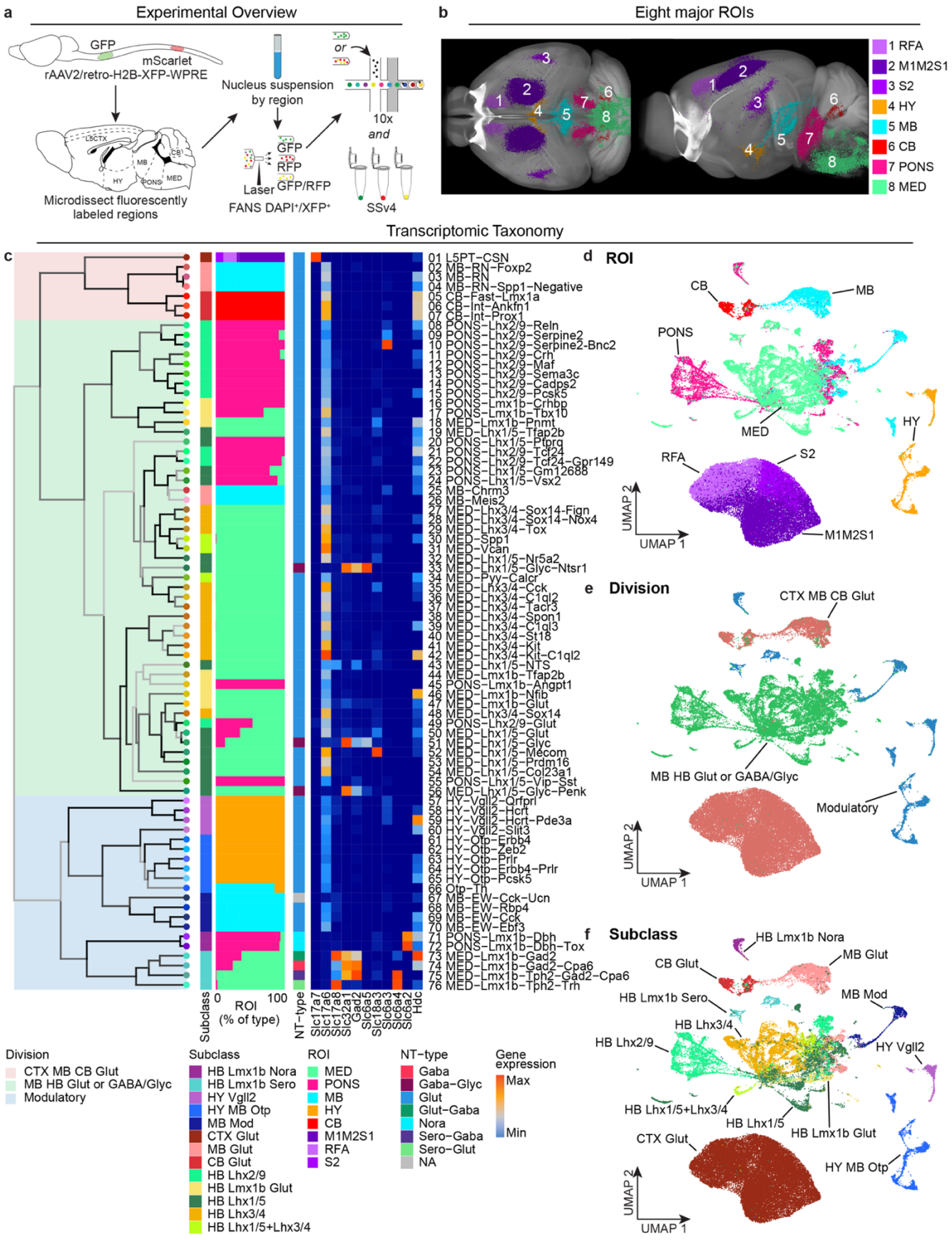

a
Experimental Overview
GFP
mScarlet
rAAV2/retro-H2B-XFP-WPRE
Microdissect fluorescently labeled regions
Nucleus suspension by region
GFP
RFP
Laser
GFP/RFP
FANS DAPI+/XFP+
or
10x
and
SSv4
b
Eight major ROIs
1 RFA
2 M1M2S1
3 S2
4 HY
5 MB
6 CB
7 PONS
8 MED
Transcriptomic Taxonomy
c
01 L5PT-CSN
02 MB-RN-Foxp2
03 MB-RN
04 MB-RN-Spp1-Negative
05 CB-Fast-Lmx1a
06 CB-Int-Ankfn1
07 CB-Int-Prox1
08 PONS-Lhx2/9-Reln
09 PONS-Lhx2/9-Serpine2
10 PONS-Lhx2/9-Serpine2-Bnc2
11 PONS-Lhx2/9-Crh
12 PONS-Lhx2/9-Maf
13 PONS-Lhx2/9-Sema3c
14 PONS-Lhx2/9-Cadps2
15 PONS-Lhx2/9-Pcsk5
16 PONS-Lmx1b-Crhbp
17 PONS-Lmx1b-Tbx10
18 MED-Lmx1b-Pnmt
19 MED-Lhx1/5-Tfap2b
20 PONS-Lhx1/5-Ptprq
21 PONS-Lhx2/9-Tcf24
22 PONS-Lhx2/9-Tcf24-Gpr149
23 PONS-Lhx1/5-Gm12688
24 PONS-Lhx1/5-Vsx2
25 MB-Chrm3
26 MB-Meis2
27 MED-Lhx3/4-Sox14-Fign
28 MED-Lhx3/4-Sox14-Nox4
29 MED-Lhx3/4-Tox
30 MED-Spp1
31 MED-Vcan
32 MED-Lhx1/5-Nr5a2
33 MED-Lhx1/5-Glyc-Ntsr1
34 MED-Pyy-Calcr
35 MED-Lhx3/4-Cck
36 MED-Lhx3/4-C1ql2
37 MED-Lhx3/4-Tacr3
38 MED-Lhx3/4-Spon1
39 MED-Lhx3/4-C1ql3
40 MED-Lhx3/4-St18
41 MED-Lhx3/4-Kit
42 MED-Lhx3/4-Kit-C1ql2
43 MED-Lhx1/5-NTS
44 MED-Lmx1b-Tfap2b
45 PONS-Lmx1b-Angpt1
46 MED-Lmx1b-Nfib
47 MED-Lmx1b-Glut
48 MED-Lhx3/4-Sox14
49 PONS-Lhx2/9-Glut
50 MED-Lhx1/5-Glut
51 MED-Lhx1/5-Glyc
52 MED-Lhx1/5-Mecom
53 MED-Lhx1/5-Prdm16
54 MED-Lhx1/5-Col23a1
55 PONS-Lhx1/5-Vip-Sst
56 MED-Lhx1/5-Glyc-Penk
57 HY-Vgll2-Qrfprl
58 HY-Vgll2-Hcrt
59 HY-Vgll2-Hcrt-Pde3a
60 HY-Vgll2-Slit3
61 HY-Otp-Erbb4
62 HY-Otp-Zeb2
63 HY-Otp-Prlr
64 HY-Otp-Erbb4-Prlr
65 HY-Otp-Pcsk5
66 Otp-Th
67 MB-EW-Cck-Ucn
68 MB-EW-Rbp4
69 MB-EW-Cck
70 MB-EW-Ebf3
71 PONS-Lmx1b-Dbh
72 PONS-Lmx1b-Dbh-Tox
73 MED-Lmx1b-Gad2
74 MED-Lmx1b-Gad2-Cpa6
75 MED-Lmx1b-Tph2-Gad2-Cpa6
76 MED-Lmx1b-Tph2-Trh
Subclass
ROI (% of type)
0
100
NT-type
Slc17a7
Slc17a6
Slc17a8
Slc32a1
Gad2
Slc6a5
Slc18a3
Slc6a3
Slc6a4
Slc6a2
Hdc
d
ROI
CB
MB
PONS
MED
HY
RFA
S2
M1M2S1
UMAP 2
UMAP 1
e
Division
CTX MB CB Glut
MB HB Glut or GABA/Glyc
Modulatory
UMAP 2
UMAP 1
f
Subclass
HB Lmx1b Nora
MB Glut
CB Glut
HB Lmx1b Sero
MB Mod
HB Lhx3/4
HB Lhx2/9
HY Vgll2
HB Lhx1/5+Lhx3/4
HB Lhx1/5
HB Lmx1b Glut
CTX Glut
HY MB Otp
UMAP 2
UMAP 1
Division
CTX MB CB Glut
MB HB Glut or GABA/Glyc
Modulatory
Subclass
HB Lmx1b Nora
HB Lmx1b Sero
HY Vgll2
HY MB Otp
MB Mod
CTX Glut
MB Glut
CB Glut
HB Lhx2/9
HB Lmx1b Glut
HB Lhx1/5
HB Lhx3/4
HB Lhx1/5+Lhx3/4
ROI
MED
PONS
MB
HY
CB
M1M2S1
RFA
S2
NT-type
Gaba
Gaba-Glyc
Glut
Glut-Gaba
Nora
Sero-Gaba
Sero-Glut
NA
Gene expression
Max
Min

Figure 2-1: An anatomically informed transcriptomic atlas of brain-wide spinal projecting neurons. a, SPNs were labeled via spinal cord injections of a retrograde AAV construct that localizes fluorescent protein expression to the nucleus for parallel anatomical and transcriptomic profiling. Sagittal atlas outline from Franklin and Paxinos (Franklin & Paxinos, 2008). **b,** Whole brain reconstructions of segmented and registered SPN nuclei imaged with serial two-photon tomography revealed SPNs are present across the cortex (RFA, M1M2S1, and S2), hypothalamus, midbrain, cerebellum, pons, medulla. **c,** Multi-level iterative clustering revealed 76 SPN transcriptomic 'types' organized into a taxonomy across 13 'subclasses' and 3 'divisions' (N = 61,484 10x; N = 3,518 SSv4). The color blocks shading the taxonomy tree indicate division. The nodes at the end of the dendrogram indicate 'type', with type numbers and names on the far right. From left to right, the bar plots indicate subclass, fractions of nuclei profiled from brain region-enriching dissections, and NT-type across each type. The heatmap shows expression of neurotransmitter marker genes. **d, e, f,** Clustering of SPNs and visualization in UMAP space colored by brain region-enriching dissections (**d**), division (**e**), and subclass (**f**). ROI, Division, and Subclass colors in **c** apply to **d**, **e**, and **f**, respectively. SPN = spinal projecting neuron, ROI = region of interest, L5CTX = cortical layer 5, RFA = rostral forelimb area, M1 = primary motor cortex, M2 = secondary motor cortex, S1 = primary somatosensory cortex, S2 = secondary somatosensory cortex, HY = hypothalamus, MB = midbrain, CB = cerebellum, MED = medulla, NT-type = neurotransmitter type.

proportion of nuclei in other cortical layers (**Figure 2-3a, b**), which are unlikely to be CSNs. We thus attempted to distinguish the directly labeled SPNs (first-order) from these indirectly labeled (second-order) nuclei in the snRNAseq dataset *in silico*. We reasoned that first-order neurons should have higher expression of fluorescent proteins than second-order nuclei because of longer expression duration and higher viral load. Indeed, we found that fluorescent protein level, on average, was higher in nuclei within layer 5 vs. nuclei outside of layer 5 (**Figure 2-3c**). Based on these histological results, we sought to determine if XFP (i.e., GFP and mScarlet) expression was lower in clusters corresponding to second-order nuclei. Because of sequencing dropout in snRNAseq data, we analyzed XFP expression on a cluster, rather than single-nucleus, basis. In the 10x dataset, we found that the proportion of nuclei within a cluster that expressed mRNA for XFP was below 10% in clusters corresponding to known non-SPNs: glia, non-layer 5 cortical neurons, and cerebellar granule cells (**Figure 2-3d**). Thus,

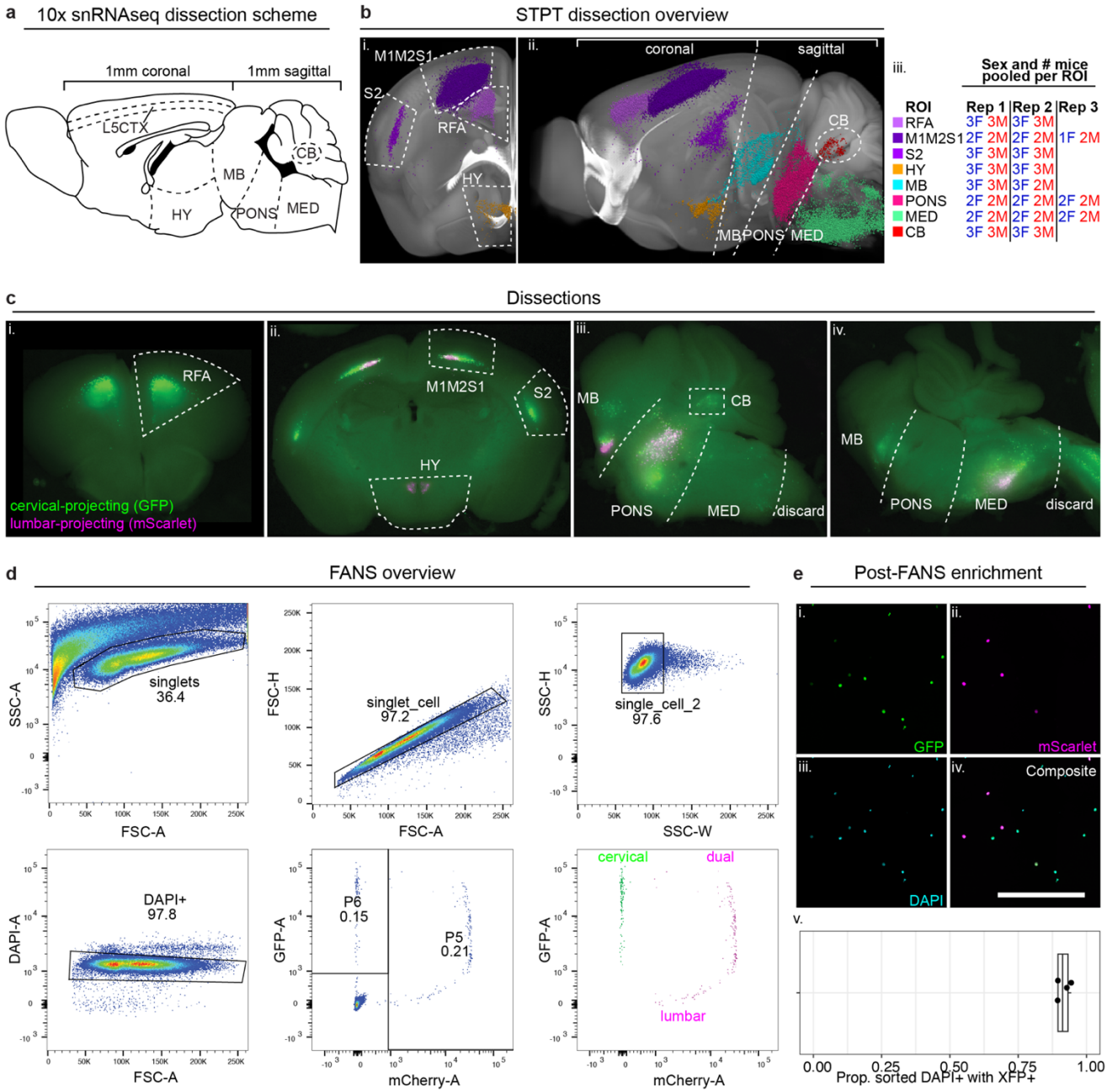


Figure 2-2: High-throughput isolation of retrogradely labeled spinal projecting neuron nuclei for snRNAseq. a, The 8 major ROIs containing retrogradely labeled SPNs were dissected from P56 mice. A 1 mm coronal-oriented acrylic brain matrix was used to section retrogradely labeled brains from the olfactory bulb to Lambda, and a sagittal-oriented matrix was used to section the remaining subcortical regions. **b,** This scheme was based on serial two-photon tomography imaging, which revealed the cleanest dissection planes to separate these major regions containing SPNs are coronal for forebrain (**i**) and sagittal for midbrain and hindbrain (same as panel Figure 2-1b) (**ii**). Equal numbers of male and female

mice were pooled per ROI to input sufficient nuclei for FANS (**iii**). **c,** Example fluorescent dissecting microscope images showing the dissection planes based on the scheme in **a** and **b**. **d,** Following microdissections of fluorescently labeled regions, nuclei were isolated from each ROI (maintaining each dissection ROI as a separate sample) and SPNs enriched using FANS. FANS plots here are representative plots from an M1M2S1 sample. **e,** Enrichment for GFP+ and/or mScarlet+ nuclei was confirmed post-FANS. Scale = 100 μm. Box and whisker plot depicts the proportion of sorted nuclei (labeled with DAPI) that had detectable GFP and/or mScarlet via widefield microscopy (N = 4 M1M2S1 samples). Rep = replicate, FANS = fluorescent activated nuclear sorting, L5CTX = cortical layer 5, RFA = rostral forelimb area, M1 = primary motor cortex, M2 = secondary motor cortex, S1 = primary somatosensory cortex, S2 = secondary somatosensory cortex, HY = hypothalamus, MB = midbrain, CB = cerebellum, MED = medulla.

we applied this methodology to the whole snRNAseq dataset to identify the first- and second-order cell types (**Figure 2-3e-g**) and removed these putative second-order nuclei for downstream analyses. Of note, there is one exception: type MB-EW-Cck-Ucn was below the 10% threshold but was not removed because of literature support of Ucn+ Edinger Westphal (EW) neurons projecting to the spinal cord (Bittencourt et al., 1999).

2.3.3 OVERVIEW OF THE SPINAL PROJECTING NEURON TRANSCRIPTOMIC TAXONOMY.

After applying standard quality control metrics and removing second-order labeled nuclei *in silico*, we obtained 65,002 high-quality snRNAseq profiles of SPNs (N = 61,484 10x; N = 3,518 SSv4) (**Figure 2-4a**). A multi-level iterative clustering approach was used to generate a transcriptomic taxonomy of SPNs (see 'Methods', **Figure 2-4b**, **Figure 2-1c**). In first level of the global dendrogram (**Figure 2-1c**), SPNs were classified into three divisions: (1) glutamatergic neurons in cortex, midbrain, and cerebellum ('CTX MB CB Glutamatergic', 34,565 neurons, 53% of all SPNs), (2) glutamatergic and GABA/Glycinergic neurons in the midbrain and hindbrain ('MB HB Glutamatergic or

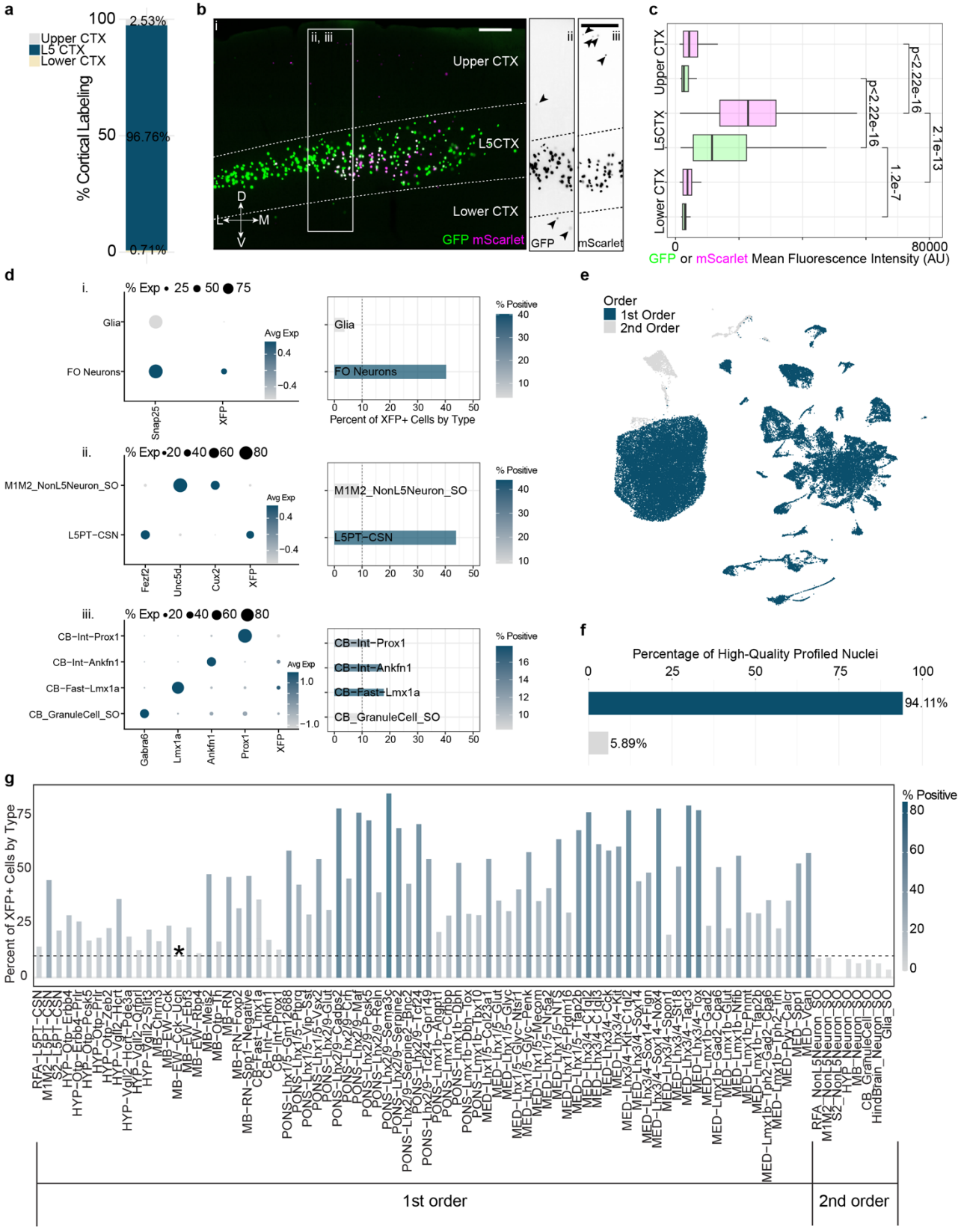

a
100
50
0
% Cortical Labeling
2.53%
96.76%
0.71%
Upper CTX
L5 CTX
Lower CTX
b
i
ii, iii
Upper CTX
L5CTX
Lower CTX
GFP mScarlet
D
L
M
V
ii
iii
GFP
mScarlet
c
Upper CTX
L5CTX
Lower CTX
p<2.22e-16
p<2.22e-16
2.1e-13
1.2e-7
0
80000
GFP or mScarlet Mean Fluorescence Intensity (AU)
d
i.
% Exp • 25 ● 50 ● 75
Glia
FO Neurons
Avg Exp
0.4
−0.4
Snap25
XFP
Glia
FO Neurons
0 10 20 30 40 50
Percent of XFP+ Cells by Type
% Positive
40
30
20
10
ii.
% Exp •20 ●40 ●60 ●80
M1M2_NonL5Neuron_SO
L5PT−CSN
Avg Exp
0.4
−0.4
Fezf2
Unc5d
Cux2
XFP
M1M2_NonL5Neuron_SO
L5PT−CSN
0 10 20 30 40 50
% Positive
40
30
20
10
iii.
% Exp •20 ●40 ●60 ●80
CB−Int−Prox1
CB−Int−Ankfn1
CB−Fast−Lmx1a
CB_GranuleCell_SO
Avg Exp
1.0
−1.0
Gabra6
Lmx1a
Ankfn1
Prox1
XFP
CB−Int−Prox1
CB−Int−Ankfn1
CB−Fast−Lmx1a
CB_GranuleCell_SO
0 10 20 30 40 50
% Positive
16
14
12
10
e
Order
1st Order
2nd Order
f
Percentage of High-Quality Profiled Nuclei
0
25
50
75
100
94.11%
5.89%
g
Percent of XFP+ Cells by Type
0
25
50
75
% Positive
80
60
40
20
0
*
1st order
2nd order

Figure 2-3: Identification of first- and second- order retrogradely labeled nuclei. a, The proportion of retrogradely labeled nuclei were quantified across L5 CTX, revealing 96.76% and 3.24% of nuclei were labeled within and outside of the corticospinal-containing layer 5, respectively (slide-scanner imaging, N = 5 mice, mean and standard deviation for number of nuclei in each ROI are as follows, L5 CTX: 33700.80 +/- 929.89, Upper CTX: 882.40+/-296.89, Lower CTX: 246.40+/-147.61). **b**, Qualitative assessment of labeled nuclei shows lower fluorescence intensity in non-layer 5 cortex compared to layer 5. Arrows indicate faintly labeled nuclei in upper and lower cortex. Scale bars = 200 μm. **c**, Box and whisker plot depicting mean fluorescence intensity of GFP- and mScarlet- labeled nuclei is significantly higher in layer 5 compared to upper (layers 1-4) and lower (layer 6) cortex. Numbers above boxplots indicate p-values (Wilcoxon test). **d**, GFP and mScarlet mRNA detection in 10x snRNAseq data in putative first- and second-order clusters across glial/neuronal (**i**), cortical (**ii**), and cerebellar (**iii**) nuclei. The three plots in the left column are dot plots of marker genes and XFP expression. The three plots on the right indicate the percent of XFP+ nuclei across types. **e,** UMAP visualization of putative first- and second-order clusters. First- and second-order clusters are defined as those with >10% and <10% of nuclei expressing XFP, respectively. **f,** Percentage of all nuclei that pass quality control thresholds (mitochondrial RNA counts < 5% and number of genes per nucleus > 2000) that are classified as first- and second-order. **g,** XFP mRNA detection in snRNAseq data across all 76 types within the final taxonomy and the putative second order clusters that do not pass the 10% XFP detection threshold, separated by dissection region and neurons vs. glia. Pons and medulla together were pooled together as 'Hindbrain' because they were clustered together (see 'Methods'). * indicates one SPN type that was below the 10% threshold that was designated as first-order because of literature support for its existence. XFP = GFP or mScarlet, CTX = cortex, L5 = layer 5, AU = arbitrary units, FO = first-order, SO = second-order.

GABAergic/Glycinergic', 23,174, 35.7%), and (3) subcortical modulatory neurons ('Modulatory', 7,263, 11.3%). The second round of clustering split these broad divisions into 13 subclasses, and a third round parcellated the subclasses into 76 types defined by differentially expressed (DE) marker genes (**Table 2-2**). Unsupervised clustering and visualization in uniform manifold approximation and projection (UMAP) space reveals nuclei from different ROI-enriching dissections are largely segregated yet have some overlapping types, likely reflecting anatomical continuity and/or transcriptomic similarities across multiple brain regions (**Figure 2-1d**). Divisions and subclasses span

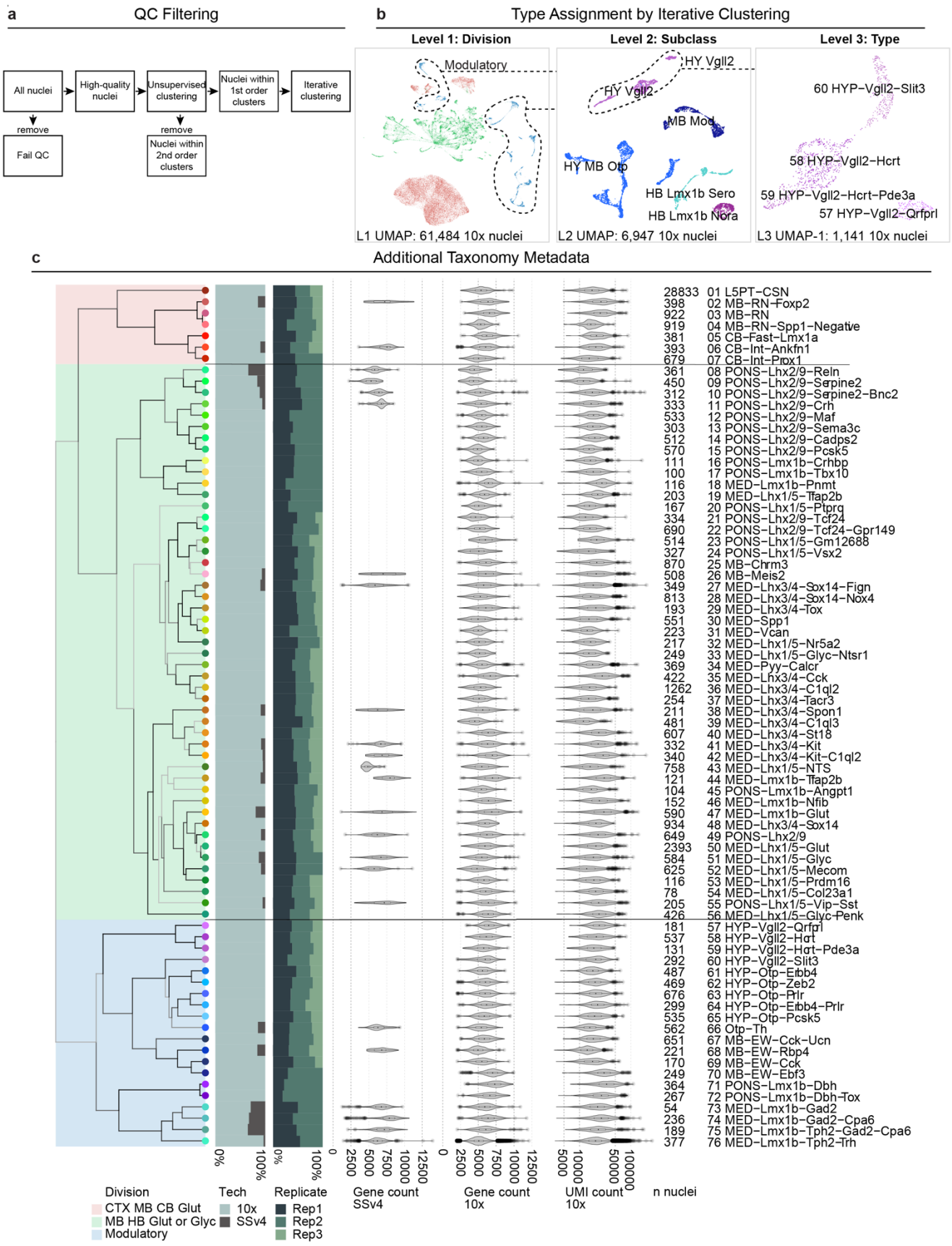

a
QC Filtering
All nuclei
High-quality nuclei
Unsupervised clustering
Nuclei within 1st order clusters
Iterative clustering
remove
Fail QC
remove
Nuclei within 2nd order clusters
b
Type Assignment by Iterative Clustering
Level 1: Division
Level 2: Subclass
Level 3: Type
Modulatory
HY Vgll2
HY Vgll2
MB Mod
HY MB Otp
HB Lmx1b Sero
HB Lmx1b Nora
60 HYP-Vgll2-Slit3
58 HYP-Vgll2-Hcrt
59 HYP-Vgll2-Hcrt-Pde3a
57 HYP-Vgll2-Qrfprl
L1 UMAP: 61,484 10x nuclei
L2 UMAP: 6,947 10x nuclei
L3 UMAP-1: 1,141 10x nuclei
c
Additional Taxonomy Metadata
28833 01 L5PT-CSN
398 02 MB-RN-Foxp2
922 03 MB-RN
919 04 MB-RN-Spp1-Negative
381 05 CB-Fast-Lmx1a
393 06 CB-Int-Ankfn1
679 07 CB-Int-Prox1
361 08 PONS-Lhx2/9-Reln
450 09 PONS-Lhx2/9-Serpine2
312 10 PONS-Lhx2/9-Serpine2-Bnc2
333 11 PONS-Lhx2/9-Crh
533 12 PONS-Lhx2/9-Maf
303 13 PONS-Lhx2/9-Sema3c
512 14 PONS-Lhx2/9-Cadps2
570 15 PONS-Lhx2/9-Pcsk5
111 16 PONS-Lmx1b-Crhbp
100 17 PONS-Lmx1b-Tbx10
116 18 MED-Lmx1b-Pnmt
203 19 MED-Lhx1/5-Tfap2b
167 20 PONS-Lhx1/5-Ptprq
334 21 PONS-Lhx2/9-Tcf24
690 22 PONS-Lhx2/9-Tcf24-Gpr149
514 23 PONS-Lhx1/5-Gm12688
327 24 PONS-Lhx1/5-Vsx2
870 25 MB-Chrm3
508 26 MB-Meis2
349 27 MED-Lhx3/4-Sox14-Fign
813 28 MED-Lhx3/4-Sox14-Nox4
193 29 MED-Lhx3/4-Tox
551 30 MED-Spp1
223 31 MED-Vcan
217 32 MED-Lhx1/5-Nr5a2
249 33 MED-Lhx1/5-Glyc-Ntsr1
369 34 MED-Pyy-Calcr
422 35 MED-Lhx3/4-Cck
1262 36 MED-Lhx3/4-C1ql2
254 37 MED-Lhx3/4-Tacr3
211 38 MED-Lhx3/4-Spon1
481 39 MED-Lhx3/4-C1ql3
607 40 MED-Lhx3/4-St18
332 41 MED-Lhx3/4-Kit
340 42 MED-Lhx3/4-Kit-C1ql2
758 43 MED-Lhx1/5-NTS
121 44 MED-Lmx1b-Tfap2b
104 45 PONS-Lmx1b-Angpt1
152 46 MED-Lmx1b-Nfib
590 47 MED-Lmx1b-Glut
934 48 MED-Lhx3/4-Sox14
649 49 PONS-Lhx2/9
2393 50 MED-Lhx1/5-Glut
584 51 MED-Lhx1/5-Glyc
625 52 MED-Lhx1/5-Mecom
116 53 MED-Lhx1/5-Prdm16
78 54 MED-Lhx1/5-Col23a1
205 55 PONS-Lhx1/5-Vip-Sst
426 56 MED-Lhx1/5-Glyc-Penk
181 57 HYP-Vgll2-Qrfprl
537 58 HYP-Vgll2-Hcrt
131 59 HYP-Vgll2-Hcrt-Pde3a
292 60 HYP-Vgll2-Slit3
487 61 HYP-Otp-Erbb4
469 62 HYP-Otp-Zeb2
676 63 HYP-Otp-Prlr
299 64 HYP-Otp-Erbb4-Prlr
535 65 HYP-Otp-Pcsk5
562 66 Otp-Th
651 67 MB-EW-Cck-Ucn
221 68 MB-EW-Rbp4
170 69 MB-EW-Cck
249 70 MB-EW-Ebf3
364 71 PONS-Lmx1b-Dbh
267 72 PONS-Lmx1b-Dbh-Tox
54 73 MED-Lmx1b-Gad2
236 74 MED-Lmx1b-Gad2-Cpa6
189 75 MED-Lmx1b-Tph2-Gad2-Cpa6
377 76 MED-Lmx1b-Tph2-Trh
0% 100%
0% 100%
0 2500 5000 7500 10000 12500
0 2500 5000 7500 10000 12500
5000 10000 50000 100000
Division
CTX MB CB Glut
MB HB Glut or Glyc
Modulatory
Tech
10x
SSv4
Replicate
Rep1
Rep2
Rep3
Gene count SSv4
Gene count 10x
UMI count 10x
n nuclei

Figure 2-4: Development of a spinal projecting neuron taxonomy. a, Workflow diagram of QC filtering of snRNAseq datasets. Nuclei that passed standard QC metrics were assessed for putative first- and second-order labeling. Putative second-order nuclei were removed, and first-order nuclei underwent multi-level iterative clustering. **b**, UMAPs at three levels of the taxonomy from iterative analysis. Example shown here shows iterative clustering of the Modulatory Division into 5 HY Vgll2 Subclasses to yield 4 final HY Vgll2 Types. **c**, Dendrogram of SPN taxonomy as in Figure 2-1, showing additional metadata. The color blocks shading the taxonomy tree indicate division. The nodes at the end of the dendrogram indicate 'type', with type number labels and names on the far right. From left to right, the bar plots represent fractions of nuclei profiled with 10x and SSv4 platforms and replicate contribution to each type. Violin plots show gene counts in SSv4 and 10x data, and UMI count in 10x data. The number of nuclei (n nuclei) profiled per type is labeled. QC = quality control, Tech = technology, Rep = replicate, UMI = Unique molecular identifier.

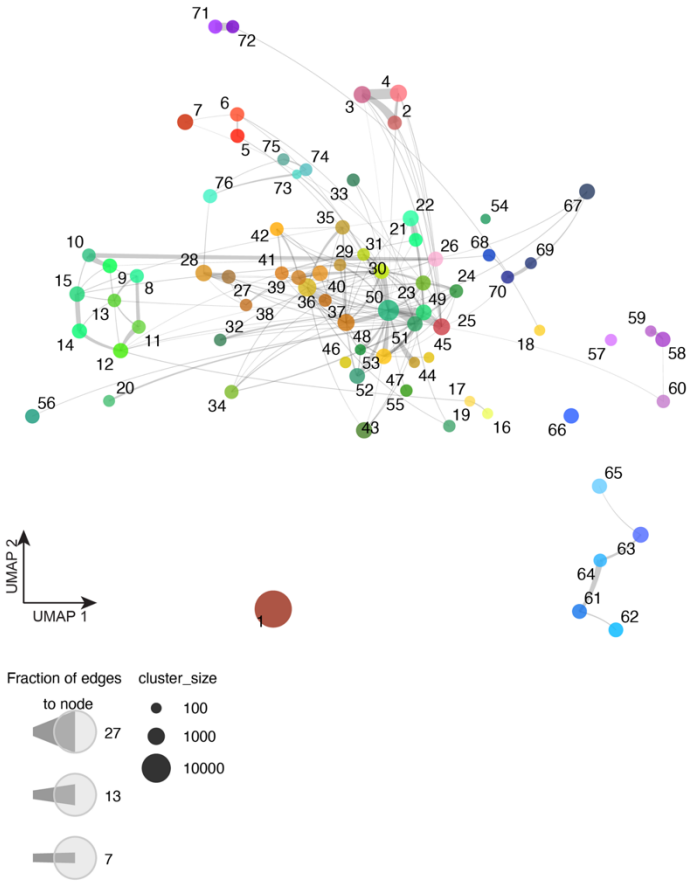


Figure 2-5: Global constellation plot of spinal projecting neurons. The constellation plot shows the global relatedness across all SPNs. Each transcriptomic type is represented by a node whose area represents the number of nuclei (log-scale).

Numbers labels and colors on nodes correspond to type number from Figure 2-1c. Nodes are positioned at the center of the corresponding type cluster in UMAP space in Figure 2-1d, e, f. Relationships between nodes are indicated by edges.

multiple brain regions, suggesting that segregation of cell type is a combination of regional and molecular identities (**Figure 2-1e, f**). The global relationships between types are represented by a constellation plot (**Figure 2-5**). Types are conserved across replicates and have a median transcript capture of 20,224 unique molecular identifiers (UMIs) per 10x profile (**Figure 2-4c**). This multi-level iterative clustering approach effectively assigns SPN types into traditionally defined spinal projecting populations, such as cortex-derived CSNs, cerebellum-derived cerebellospinal neurons (CbSNs), red nucleus-derived rubrospinal neurons (RuSNs), brainstem-derived reticulospinal neurons (ReSNs), and modulatory populations such as hypothalamospinal neurons (HySNs) and raphespinal neurons.

2.3.4 INTEGRATION OF SPINAL PROJECTING NEURON AND WHOLE BRAIN TAXONOMIES.

As a first step to validate the taxonomy, we leveraged whole brain scRNAseq and MERFISH datasets generated by the Allen Institute for Brain Science (AIBS) in a companion study (Yao et al., 2023). First, we mapped (**Tables 2-3 to 2-5**) and assessed the correspondence of (**Figure 2-6**) types defined in the SPN taxonomy to the AIBS whole brain (WB) scRNAseq taxonomy (see 'Methods'). While great cell type correspondence for the majority of SPN types in Divisions 1 and 3 is observed, SPNs from the red nucleus in Division 1 and many Division 2 SPN types from PONS and MED are mapped to a single AIBS WB cluster, 3734 MB/HB Lhx1 Glut_3. Neurons in these areas are highly heterogeneous, but distinctions between cell types are subtle. Additionally, these neurons are also heavily myelinated, making them very difficult to isolate for scRNAseq without substantial cell

damage. The results here show that the SPN taxonomy likely provides better distinction between SPN types in these areas than the WB taxonomy due to the more targeted sampling strategy.

To map SPNs to their anatomical locations, we integrated the SPN taxonomy with the AIBS WB MERFISH dataset (see 'Methods'). This mapping strategy successfully localized SPN types throughout each of the three divisions and is discussed in the sections below. With identified marker genes, we further verified the spatial distribution of different clusters of SPNs by performing retrograde labeling with AAVs expressing Cre-dependent H2B-GFP in 13 transgenic lines (Duan et al., 2014; Foster et al., 2015; Hippenmeyer et al., 2005; Matho et al., 2021; Rossi et al., 2011; Savitt et al., 2005; Scott et al., 2005, 2011; Shiota et al., 2017; Tasic et al., 2018; Tillage et al., 2020; Van Berlo et al., 2014) in which Cre was inserted to the locus of a specific marker gene (**Figure 2-7**). This Cre-dependent labeling allowed us to assess the anatomical distribution of SPNs expressing specific genes throughout the whole brain and is also discussed in the sections below.

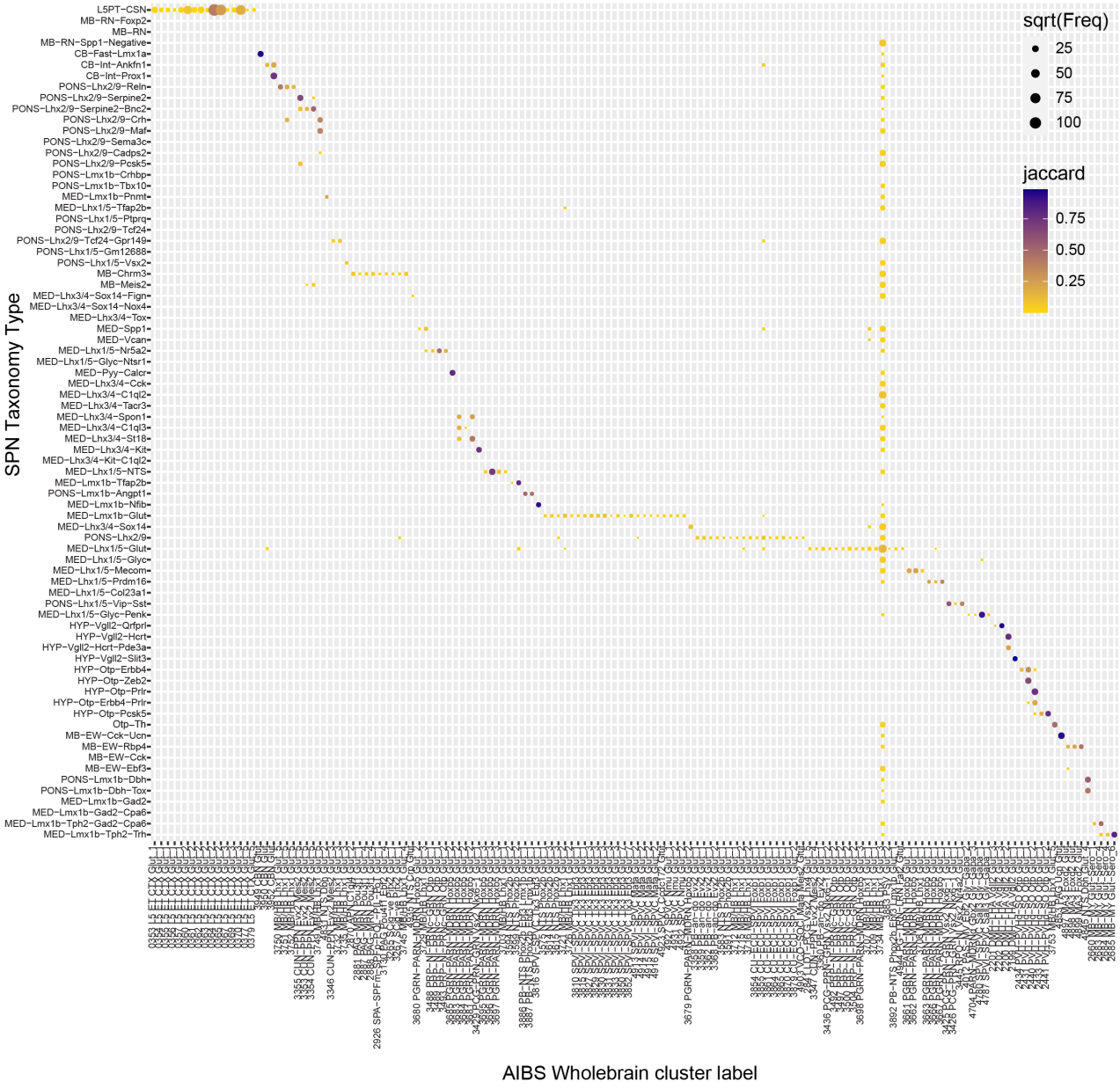


Figure 2-6: Correspondence between the spinal projecting neuron and AIBS whole brain taxonomies. A confusion matrix between the SPN snRNAseq taxonomy and AIBS whole brain scRNAseq taxonomy (cluster level) is shown. The size of each dot represents the number of overlapping cells/nuclei, and the color corresponds to the Jaccard similarity score between SPN 'type' and AIBS taxonomy 'cluster'. The matrix is filtered by Jaccard score > 0.1 or frequency (i.e., number of overlapping cells/nuclei) ≥ 5.

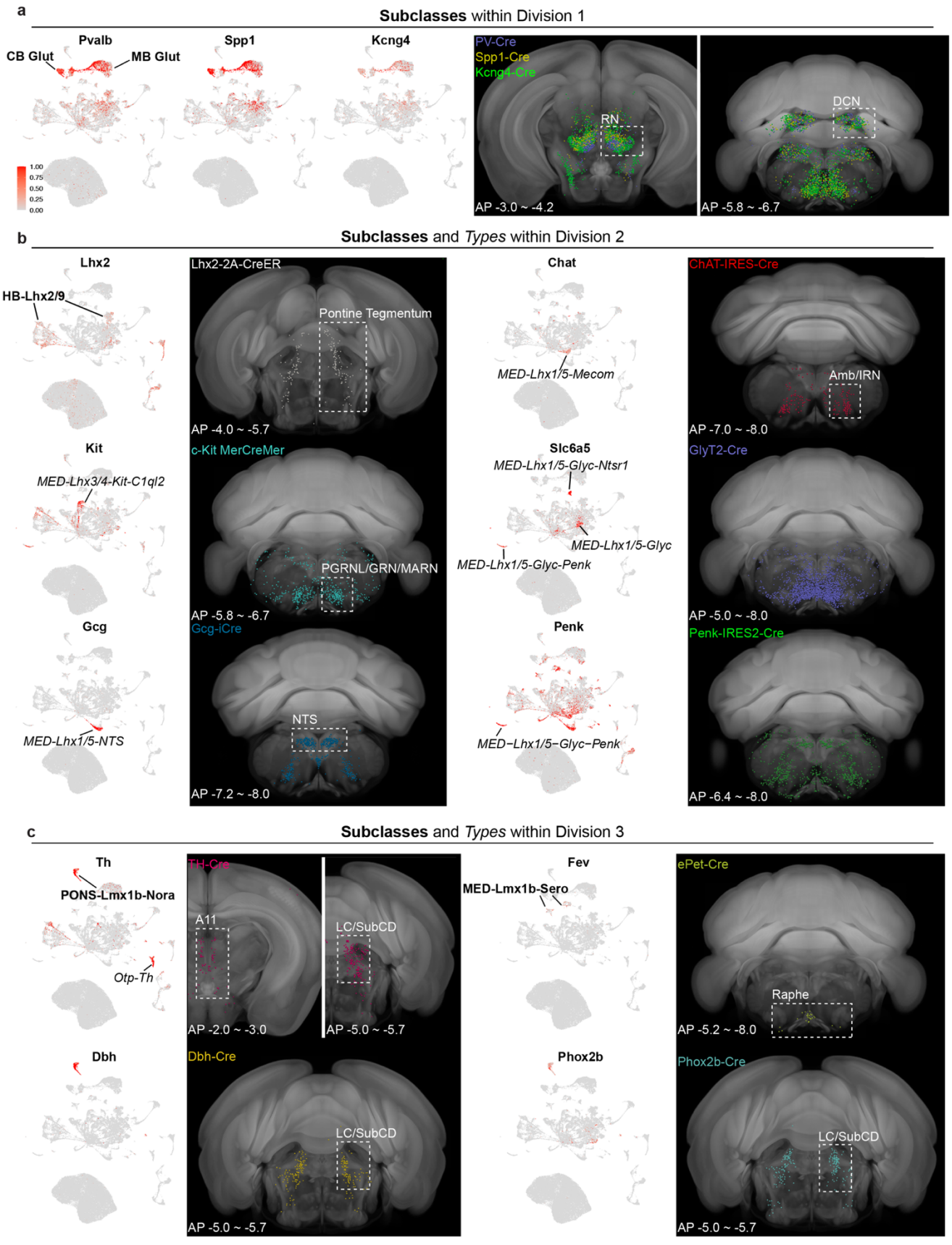

a
Subclasses within Division 1
Pvalb
CB Glut
MB Glut
Spp1
Kcng4
1.00
0.75
0.50
0.25
0.00
PV-Cre
Spp1-Cre
Kcng4-Cre
RN
AP -3.0 ~ -4.2
DCN
AP -5.8 ~ -6.7
b
Subclasses and Types within Division 2
Lhx2
HB-Lhx2/9
Lhx2-2A-CreER
Pontine Tegmentum
AP -4.0 ~ -5.7
Chat
MED-Lhx1/5-Mecom
ChAT-IRES-Cre
Amb/IRN
AP -7.0 ~ -8.0
Kit
MED-Lhx3/4-Kit-C1ql2
c-Kit MerCreMer
PGRNL/GRN/MARN
AP -5.8 ~ -6.7
Slc6a5
MED-Lhx1/5-Glyc-Ntsr1
MED-Lhx1/5-Glyc
MED-Lhx1/5-Glyc-Penk
GlyT2-Cre
AP -5.0 ~ -8.0
Gcg
MED-Lhx1/5-NTS
Gcg-iCre
NTS
AP -7.2 ~ -8.0
Penk
MED−Lhx1/5−Glyc−Penk
Penk-IRES2-Cre
AP -6.4 ~ -8.0
c
Subclasses and Types within Division 3
Th
PONS-Lmx1b-Nora
Otp-Th
TH-Cre
A11
AP -2.0 ~ -3.0
LC/SubCD
AP -5.0 ~ -5.7
Fev
MED-Lmx1b-Sero
ePet-Cre
Raphe
AP -5.2 ~ -8.0
Dbh
Dbh-Cre
LC/SubCD
AP -5.0 ~ -5.7
Phox2b
Phox2b-Cre
LC/SubCD
AP -5.0 ~ -5.7

Figure 2-7: Retrograde labeling with AAVs expressing Cre-dependent GFP in various transgenic mouse lines. UMAP plots show expression of marker genes in the SPN transcriptomic dataset, show alongside representative coronal reconstructions of Cre-dependent retrogradely labeled nuclei in 13 transgenic lines. Subclasses are annotated in **bold** and types are annotated in *italics*. Approximate AP position and anatomical regions are annotated. **a,** PV-Cre, Spp1-Cre, and Kcng4-Cre label RuSNs (MB Glut) and CbSNs (CB Glut) neurons in Division 1, as well as ReSNs in Division 2. **b,** Lhx2-2A-CreER, Chat-IRES-Cre, c-Kit MerCreMer, GlyT2-Cre, Gcg-iCre, and Penk-IRES2-Cre lines label ReSN populations throughout Division 2. **c,** TH-Cre, Dbh-Cre, Phox2b-Cre, ePet-Cre label modulatory populations in Division 3. AP = anterior-posterior position (relative to Bregma), RN = red nucleus, DCN = deep cerebellar nuclei, PGRNL = paragigantocellular reticular nucleus lateral part, GRN = gigantocellular reticular nucleus, MARN = magnocellular reticular nucleus, NTS = nucleus of the solitary tract, Amb = nucleus ambiguus, IRN = intermediate reticular nucleus, A11 = cell group A11, LC = locus coeruleus, SubCD = subcoeruleus nucleus dorsal part (Paxinos nomenclature).

2.3.5 TRANSCRIPTOMIC LANDSCAPE OF SPINAL PROJECTING NEURONS.

With both transcriptomic and spatial annotations, all SPNs could be classified into three major divisions (**Figure 2-1c**), representing three critical components of spinal projecting pathways.

CTX MB CB Glutamatergic Division (Division 1, types 1-7): The 'CTX MB CB Glutamatergic' division defined by the global dendrogram contains 3 subclasses and 7 types (**Figure 2-1c, Figure 2-8a**). This division is comprised of exclusively glutamatergic SPNs with concentrated anatomical locations (i.e., cortical layer 5, midbrain red nucleus, and deep cerebellar nuclei) and aggregated projections to the spinal cord (i.e., CST, RuST, and cerebellospinal tract). Perhaps reflecting their discrete anatomical origins, we find that types within this division are transcriptionally discrete (i.e., definable by high expression of one or two marker genes).

The 'CTX Glut' subclass corresponds to CSNs, which express Slc17a7+ (VGLUT1) and, as expected, other canonical layer 5 markers (e.g., Fezf2, Bcl11b, Crym) (Bareyre et al., 2005; Kamiyama et al., 2015; X. Wang et al., 2017) (**Figure 2-8b, c**). These CSNs arise in the rostral forelimb area (RFA,

here defined as the rostral cortical concentration of neurons), primary and secondary motor cortex / primary somatosensory cortex (M1M2S1, here defined as the caudal cortical concentration), and secondary somatosensory cortex (S2, here defined as the lateral cortical concentration) (**Figure 2-1b**). As expected, mapping CSN snRNAseq profiles onto AIBS WB MERFISH data localized profiles to cortical layer 5 (**Figure 2-8c**).

The 'MB Glut' subclass within this division includes 3 types corresponding to RuSNs. These types express Slc17a6+ (VGLUT2) and markers Rreb1 and Emx2os (**Figure 2-8b, d, e**). Mapping their snRNAseq profiles onto AIBS WB MERFISH data localizes these 3 types to the midbrain red nucleus (**Figure 2-8d**).

Finally, the 'CB Glut' subclass with 3 types, corresponds to CbSNs. Like RuSNs, they express Slc17a6+ (VGLUT2) and Rreb1 (**Figure 2-8b, e**). CbSNs are known to arise from the fastigial and interposed deep cerebellar nuclei (Sathyamurthy et al., 2020); accordingly, we find that the SPN types CB-Int-Prox1 and CB-Int-Ankfn1 map to the interposed nucleus and CB-Fast-Lmx1a maps to the fastigial nucleus (**Figure 2-8e**). Prox1 and Ankfn1 as markers of cerebellar nuclei from the interposed nucleus, and Lmx1a for those from the fastigial nucleus, are consistent with previous studies of deep cerebellar nuclei (Kebschull et al., 2020).

Another shared feature of Division 1 neurons is their somatotopic locations and spinal projections. Among all brain regions, only populations in Division 1 exhibit clear segregations of GFP and mScarlet cells (**Figure 2-8f**; see Chapter 1 **Figure 1-11, 1-12**). CSNs in the RFA and S2 are entirely cervical-projecting whereas those in M1, M2, and S1 display a distinctive somatotopic distribution with dual- and lumbar-projecting CSNs medial to cervical-projecting CSNs. Similarly, RuSNs also display a somatotopic distribution with cervical- and lumbar-projecting SPNs originating in the dorsomedial and ventrolateral RN, respectively. CbSNs from the anterior interposed nucleus also display somatotopic distribution of cervical- and lumbar- projecting populations (Sathyamurthy et al.,

2020). For the small number of dual-projecting CSNs, we cannot eliminate the possibility that these neurons only project to the lumbar cord and the AAVs injected to the cervical spinal cord label their passing axons. However, this is unlikely, because similarly injected AAVs to the cervical spinal cord did not label the lumbar projecting RuSNs and CbSNs, consistent with previous reports (Sathyamurthy et al., 2020; Steward et al., 2021; Z. Wang et al., 2018, 2022). Taken together, common anatomical features of all Division 1 subclasses are concentrated regions of origin with somatotopic distribution of cervical and lumbar projecting types. These features render these neurons well suited for transmitting point-to-point command signals.

MB HB Glutamatergic or GABAergic/Glycinergic Division (Division 2, types 8-56): The 'MB HB Glutamatergic or GABAergic/Glycinergic' division, defined by the global dendrogram with 6 subclasses and 49 types (**Figure 2-1c**), is the most transcriptionally complex division. Many types are highly related, as depicted by the global constellation plot (**Figure 2-5**) but can be defined by combinations of several marker genes. Most (46 of 49) types are glutamatergic (Slc17a6+), and a minority (3 of 49) of types are GABAergic/Glycinergic (Slc32a1+/Slc6a5+).

Integration with the AIBS WB scRNAseq and MERFISH datasets localized this widespread, transcriptionally complex division to the midbrain and pontomedullary reticular formation (**Figure 2-9**). Most types within this division were mapped throughout the pontomedullary reticular formation (**Figure 2-9b-f**, see 'LIM' section below). In addition, two types (i.e., MB-Meis2, MB-Chrm3) originated from MB-enriching dissections and localized to disperse areas in the midbrain reticular nucleus (MRN) (**Figure 2-9a**). The MRN is considered an origin of the ReST (Castiglioi et al., 1978; Perkins et al., 2009, 2013; Robinson et al., 1994; Warren et al., 2008); thus, this division corresponds to the excitatory and inhibitory ReSNs. As the most complex population of SPNs, sections below provide a more in-depth analysis of ReSNs.

Modulatory Division (Division 3, types 57-76): The 'Modulatory' division contains 5 subclasses and 20 types distributed across the hypothalamus, midbrain, and hindbrain, but not the brain regions harboring neurons of Division 1 (**Figure 2-10**). Different from SPNs in Divisions 1 and 2 which are largely defined by markers of fast-acting neurotransmission (i.e., glutamate, GABA, glycine), the 'Modulatory' branch is featured with unique neurotransmitter profiles, predominantly supporting neuropeptides and/or slow neurotransmitters (**Figure 2-11**). These modulatory inputs may amplify and/or extend the fast commands and have been considered as an "emotional motor pathway" (G. Holstege, 1998), acting in different physiological and pathological conditions (Arber & Costa, 2022; G. Holstege, 1998; Jordan et al., 2008; Lemon, 2008).

HySNs primarily originate from the paraventricular hypothalamus (PVH) and lateral hypothalamic area (LHA) and comprise the 'HY MB Otp' and 'HY Vgll2' subclasses, respectively (**Figure 2-10b, c**). All HySNs defined here are excitatory (Slc17a6+). However, they are unique for their high expression of various neuropeptides such as Arginine Vasopressin (Avp), Orexin (Hcrt), Growth hormone releasing hormone (Ghrh), and Oxytocin (Oxt) which influence whole body physiology (Cechetto & Saper, 1988; Faraco et al., 2006; Van Den Pol, 1999) (**Figure 2-11**). Additionally, type 'Otp-Th' within the 'HY MB Otp' subclass is defined by tyrosine hydroxylase (Th) (**Figure 2-10b**). This population is primarily present in the MB-enriching dissections but also a small proportion from HY-enriching dissections, indicating this population is present at the HY-MB border. This type is likely the A11 group of neurons (Skagerberg & Lindvall, 1985) based on spatial mapping via MERFISH (**Figure 2-10b**) and Cre-dependent retrograde labeling in a Th-Cre mouse line (**Figure 2-7c**). In addition to Slc17a6, this type expresses Th, Dopa Decarboxylase (Ddc), and vesicular monoamine transporter 2 (Slc18a2), suggesting monoaminergic activity; interestingly, however, the 'Otp-Th' type lacks expression of other monoamine transporters such as the dopamine transporter (Slc6a3). These results might be relevant to the notion that (with expression of Th, Ddc, and Slc18a2),

A11 neurons contain sufficient enzymatic machinery to generate dopamine despite not expressing Slc6a3 (Koblinger et al., 2014).

The remaining four MB types in this division comprise the 'MB Mod' subclass and originate in the Edinger Westphal (EW) nucleus (**Figure 2-10d**). In addition to sending parasympathetic projections to the oculomotor nerve, the EW contains non-cholinergic centrally-projecting neurons (Dos Santos Júnior et al., 2015). The 'MB-EW-Cck-Ucn' type is molecularly rather atypical: these neurons are depleted for markers of excitatory or inhibitory neurotransmission and are instead enriched for a set of genes encoding neuropeptides including Cck, Cartpt, and Ucn (**Figure 2-1c, Figure 2-10d**). In contrast, the MB-EW-Cck type expresses neuropeptides Cck and Cartpt, but not Ucn, and glutamatergic markers (Slc17a6). It is intriguing that the MB-EW-Cck-Ucn type expresses modulatory neuropeptides without detectable expression of fast-acting neurotransmitter machinery. However, the functional significance of these 'obligate neuropeptidergic' (Huang et al., 2019; Priest et al., 2021) neurons is unknown.

The pons and medulla also host modulatory SPNs. These types are in the 'HB Lmx1b Nora' and 'HB Lmx1b Sero' subclasses, corresponding to the monoaminergic locus coeruleus and medullary raphe nuclei, respectively (**Figure 2-10e**). Together, these subclasses comprise the modulatory component of the ReST. Notably, the 'HB Lmx1b Sero' subclass is comprised of heterogeneous neurotransmitter types, including Sero-Glut (Slc6a4+/Slc17a8+), Gaba (Slc32a1), and Glut-Gaba (Slc17a8+/Slc32a1+). Further, types in the 'HB Lmx1b Sero' subclass mapped to multiple spatial locations (**Figure 2-9b**), highlighting the transcriptomic and spatial heterogeneity of descending raphespinal systems. Previous studies emphasized different serotonin receptors in the spinal cord (Jordan et al., 2008); it is interesting to note such diversity of serotonergic inputs. The 'HB Lmx1b Sero' types have sparse expression of Slc17a8 (VGLUT3), a third vesicular glutamate transporter shown to be present in other serotonergic neuronal populations(Gras et al., 2002; Okaty et al., 2020;

Ren et al., 2019). Sparse Slc17a8 expression is also present in other subcortical types, such as SPNs from the nucleus of the solitary tract (NTS; MED-Lhx1/5-NTS) (**Figure 2-10f**). Though not within the 'Modulatory' division, MED-Lhx1/5-NTS highly expresses the neuropeptide glucagon (Gcg). As the NTS is a major parasympathetic sensory nucleus, its spinal projecting neuron components suggest direct supraspinal communication between visceral and spinal circuits.

It is worth noting that evidence of machinery for dual or partial neurotransmitter types is not unique to the 'Modulatory' division. For example, the GABA/Glyc populations in pons and medulla express GlyT2 (Slc6a5) and the common vesicular transporter for GABA and glycine, VGAT (Slc32a1). Additionally, there is evidence of partial neurotransmitter machinery among SPNs in the MED-Lhx1/5-NTS type, which are glutamatergic as they express Slc17a6: these neurons express Gad2 without Slc32a1, suggesting that they do not use GABA for synaptic transmission (**Figure 2-10f**). The function of Gad2 without Slc32a1 expression remains to be elucidated.

Together, these results suggest that SPNs carry distinct brain-derived information to the spinal cord. Different from SPNs in Divisions 1 and 2 that relay commands via fast neurotransmission, those in the modulatory Division 3 co-express modulatory neurotransmitters or neuropeptides, enabling complementary slow-acting modulation of distant spinal circuits. Furthermore, modulatory SPNs overlap spatially with diffuse-projecting Division 2 SPNs, but do not originate in the same brain regions as Division 1 SPNs. In other words, the cortex, red nucleus, and deep cerebellar nuclei elicit only fast-acting spinal commands, whereas the reticular formation elaborates both fast-acting and slow-acting signals to the spinal cord. This organization may account for the spatial and temporal control of spinal cord functions.

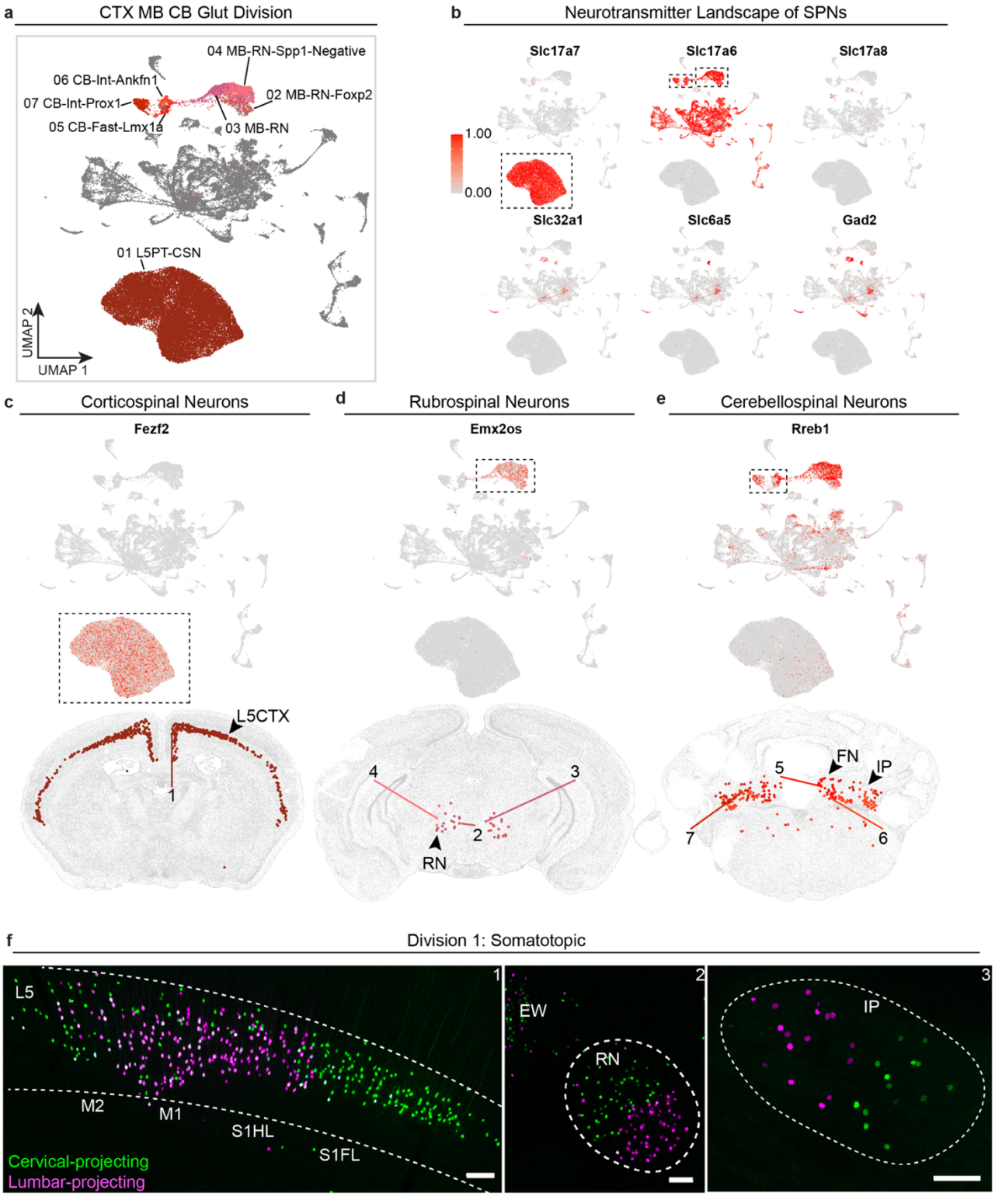

a
CTX MB CB Glut Division
04 MB-RN-Spp1-Negative
06 CB-Int-Ankfn1
07 CB-Int-Prox1
02 MB-RN-Foxp2
05 CB-Fast-Lmx1a
03 MB-RN
01 L5PT-CSN
UMAP 2
UMAP 1
b
Neurotransmitter Landscape of SPNs
Slc17a7
Slc17a6
Slc17a8
1.00
0.00
Slc32a1
Slc6a5
Gad2
c
Corticospinal Neurons
Fezf2
L5CTX
1
d
Rubrospinal Neurons
Emx2os
4
3
2
RN
e
Cerebellospinal Neurons
Rreb1
5
FN
IP
7
6
f
Division 1: Somatotopic
L5
M2
M1
S1HL
S1FL
Cervical-projecting
Lumbar-projecting
1
2
EW
RN
3
IP

Figure 2-8: Spinal projecting neurons from cortex, red nucleus, and cerebellum are transcriptionally and anatomically discrete. a, UMAP of all SPNs, colored by types within taxonomy Division 1. **b**, Expression of select genes for neurotransmission machinery. **c**-**e**, Expression of select marker genes (top) and representative MERFISH sections (bottom) of corticospinal neurons (**c**), rubrospinal neurons (**d**), and cerebellospinal neurons (**e**). Number labels depicted on the MERFISH panels correspond to SPN types in panel **a** and in the global dendrogram in Figure 2-1c. **f**, Confocal microscopy images of retrogradely labeled cervical- (green) and lumbar- (magenta) projecting corticospinal neurons (1), rubrospinal neurons (2), and cerebellospinal neurons (3). Expression scale in **b** applies to all expression plots. L5 = cortical layer 5, M2 = secondary motor cortex, M1 = primary motor cortex, S1HL = primary somatosensory cortex hindlimb region, S1FL = primary somatosensory cortex forelimb region, EW = Edinger Westphal Nucleus, RN = red nucleus, FN = fastigial nucleus, IP = interposed nucleus.

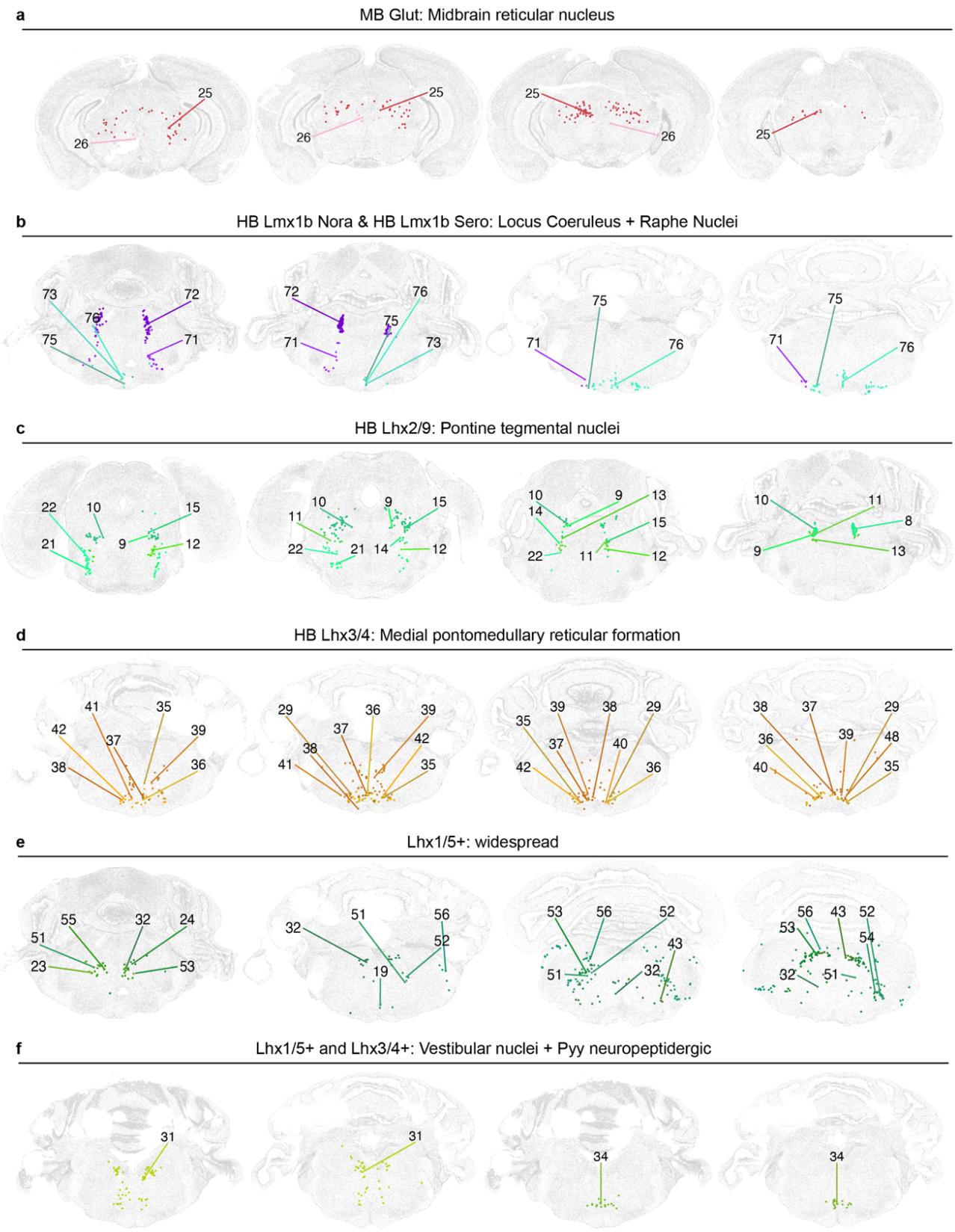


Figure 2-9: Spatial mapping of midbrain and pontomedullary reticulospinal neuron types. Representative MERFISH sections of ReSN types within the **a,** MB Glut subclass of Division 2, **b,** HB Lmx1b Nora and HB Lmx1b

Sero subclasses, **c,** HB Lhx2/9 subclass. **d,** HB Lhx3/4 subclass. **e,** HB Lhx1/5 subclass and **f,** HB Lhx1/5+Lhx3/4 subclass. Number labels and colors depicted on the MERFISH panels correspond to SPN types in the global dendrogram in Figure 2-1c. Panels depict 'type' information for 'subclass' panels shown in Figure 2-13c.

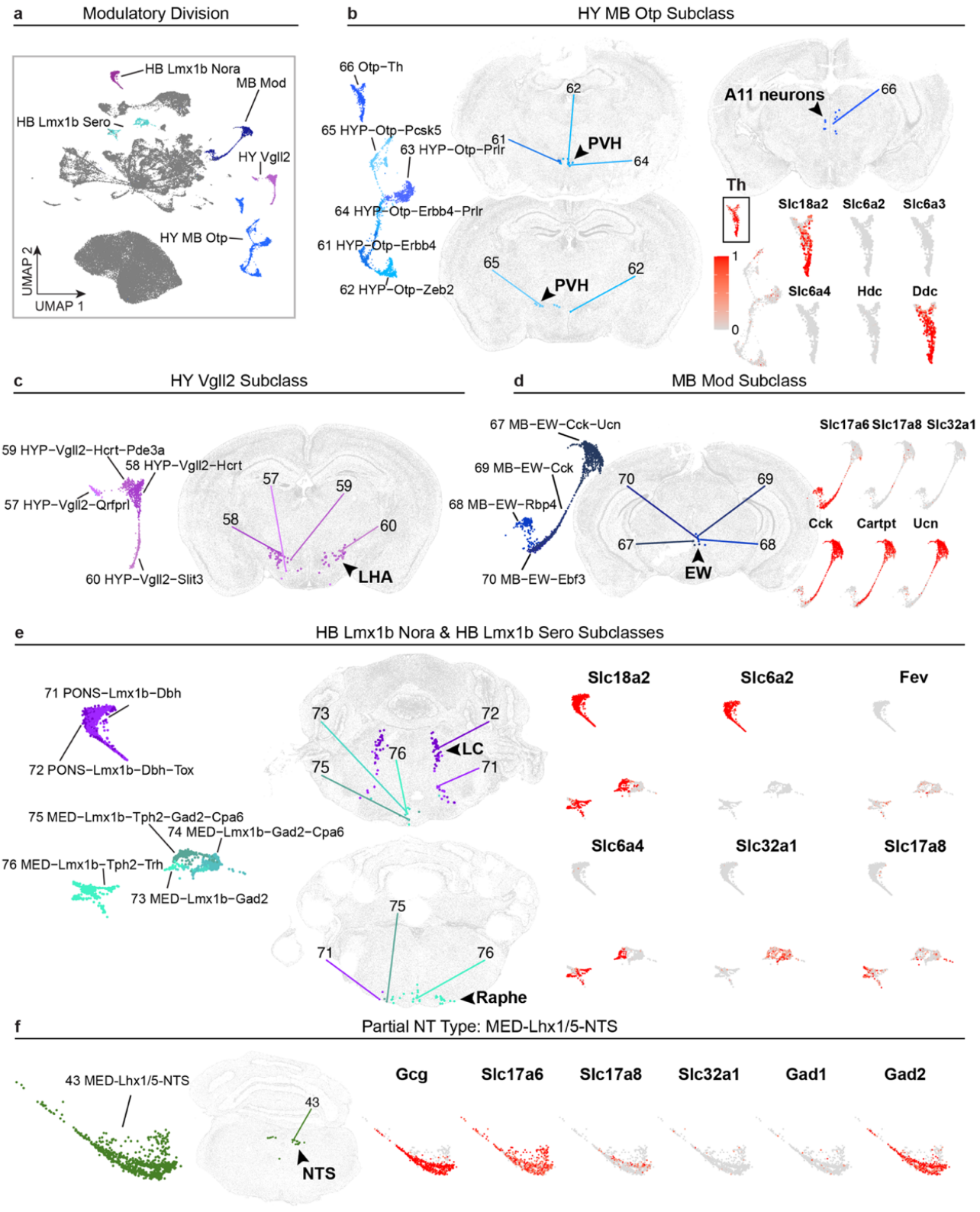


Figure 2-10: Diverse neurotransmitter identities of spinal projecting neurons. a, UMAP of all SPNs, colored by subclasses within taxonomy Division 3. **b,** Subset UMAP (left) and MERFISH representation (right) of types within HY MB Otp Subclass. Bottom right: Expression of Th and additional monoaminergic markers. **c,** Subset UMAP (left) and MERFISH representation (right) of types within HY Vgll2 Subclass. **d,** Subset UMAP (left) and MERFISH representation (middle) of types within the MB Mod subclass. Expression of select marker genes (right). **e, f,** Same as (**d**) but for types in HB Lmx1b Nora and Sero subclasses (**e**) and type MED-Lhx1/5-NTS (**f**). Expression scale in **b** applies to all expression plots. Types colored and assigned number labels as in Figure 2-1c.

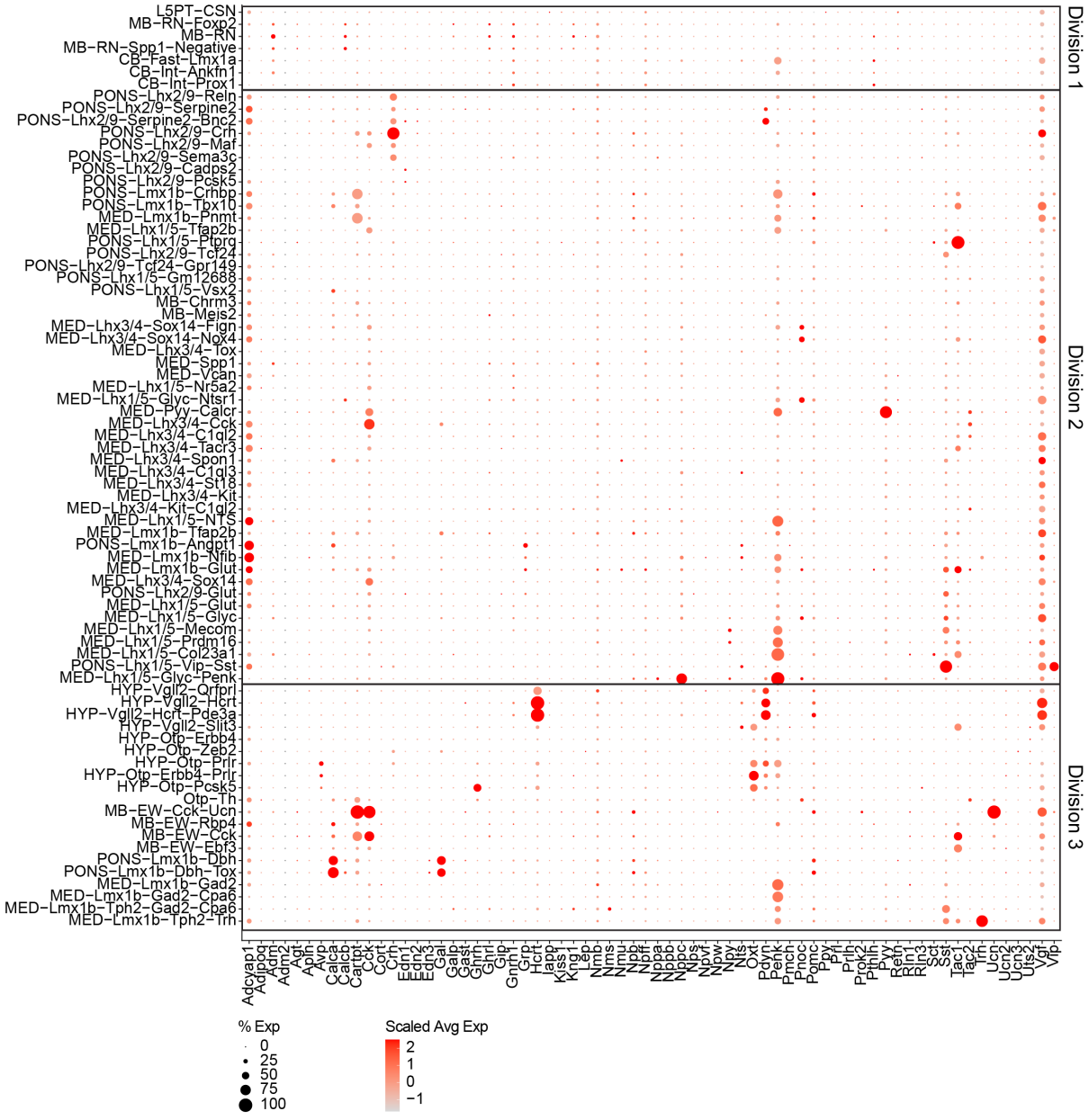


Figure 2-11: Neuropeptide expression across spinal projecting neuron types. Dot plot showing expression of neuropeptides across the 76 SPN types.

2.3.6 LIM HOMEODOMAIN TRANSCRIPTION FACTORS PARCELLATE ADULT PONTOMEDULLARY SPINAL PROJECTING NEURONS.

The most anatomically and transcriptionally complex group of SPNs are ReSNs originating from the pontomedullary reticular formation, which include the majority of SPNs in Division 2 and the noradrenergic and serotonergic SPNs from Division 3. Anatomically, the reticular formation is made up of a largely indiscrete, net-like structure of various brainstem nuclei (Brownstone & Chopek, 2018; Horn, 2006; Humphries et al., 2006). As the reticular formation's descending outputs toward the spinal cord, ReSNs are essential for regulating diverse functions such as movement, respiration, and autonomic function, yet their cellular diversity and organization remain poorly understood (Baker et al., 2015; Brownstone & Chopek, 2018; Capelli et al., 2017; Deliagina et al., 2002; Esposito et al., 2014; Ferreira-Pinto et al., 2018; Leiras et al., 2022). Studies to date have primarily relied on Chx10 (Vsx2) to characterize and target pontomedullary ReSNs (Bouvier et al., 2015; Chopek et al., 2021; Cregg et al., 2020; Kathe et al., 2022), but it is unknown if this marker covers some or all ReSNs. Further, while studies have shown that a combinatorial code of gene expression generates exquisite cellular diversity in defined anatomical zones in the developing hindbrain (Cepeda-Nieto et al., 2005; Diek et al., 2022; Gray, 2013; Krumlauf & Wilkinson, 2021), the resulting cellular composition of ReSNs and whether these organizational principles persist into adulthood are unknown.

To define the 53 pontomedullary reticular formation types in the final SPN taxonomy (**Figure 2-1c**), we subset, re-embedded, and analyzed nuclei from the pons- and medulla-enriching dissections together (see 'Methods') (**Figure 2-12a, b**). Here, we found a notable pattern of gene expression across ReSNs: LIM homeobox genes appear as DE genes in most clusters (**Table 2-6**). Specifically, we find

that Lmx1b and three paralogous pairs of LIM homeobox genes (Lhx2 and Lhx9, Lhx3 and Lhx4, and Lhx1 and Lhx5) are expressed in largely mutually exclusive clusters (**Figure 2-12c**). Taken together, we classified all pontomedullary ReSNs into one of five 'LIM Groups' (**Figure 2-13a**, **Figure 2-12d, e**) which each specifically express Lmx1b or one pair of paralogous LIM Homeobox genes (**Figure 2-13b, Figure 2-12f**). The Lmx1b group split into 3 subclasses based on major neurotransmitter (HB Lmx1b Nora, HB Lmx1b Sero, and HB Lmx1b Glut) in the final taxonomy (**Figure 2-1c**). Only three types (MED-Pyy, MED-Spp1, and MED-Vcan) are not exclusively defined by a single pair of LIM Homeobox genes and are classified into the Lhx1/5+Lhx3/4 Group. Notably, Chx10 (Vsx2), a commonly used marker for ReSNs (Bouvier et al., 2015; Chopek et al., 2021; Cregg et al., 2020; Kathe et al., 2022), exhibits nearly complete expression correspondence with the Lhx3/4 group (**Figure 2-12g**). Thus, a Chx10-Cre mouse likely labels only a subset of ReSNs. These results suggest the presence of a "LIM-code" for classifying adult ReSNs, perhaps reflecting the role of LIM genes in not only establishing but also maintaining neuronal identities (Cepeda-Nieto et al., 2005; Shirasaki & Pfaff, 2002). Single-cell regulatory network inference and clustering (Aibar et al., 2017; Van de Sande et al., 2020) (SCENIC) applied to pontomedullary ReSNs also identified these LIM genes among the top type-specific transcription factors (**Figure 2-14**).

We find ReSN types have varying levels of transcriptomic complexity. We demonstrate the relatedness of pontomedullary ReSN types with a constellation plot and find Lhx1/5+ types are most highly connected with other types, with type MED-Lhx1/5-Glut forming the central node (**Figure 2-15a**). A distinctive feature of ReSNs is the central portion of the UMAP which resembles a "splatter" of clusters. We find nuclei within this central region of the UMAP to be ill-defined by specific marker genes and contain the highest degree of heterogeneity at a single-nucleus level (**Figure 2-15b**). These features (i.e., highly heterogeneous nuclei with subtle distinctions between cell types) are similarly present in hindbrain neurons profiled in the AIBS scRNAseq companion study (Yao et al., 2023). The

LIM code identified here presents a valuable framework for deciphering the transcriptional logic of ReSNs and, possibly, the reticular formation as a whole.

We next sought to determine the anatomical distribution of these LIM-defined types in the adult hindbrain. Integrating the ReSN types with the AIBS WB MERFISH dataset identified a striking anatomical pattern of LIM-defined types (**Figure 2-13c, Figure 2-9**). Specifically, types within the HB-Lmx1b-Nora and HB-Lmx1b-Sero subclasses map to the locus coeruleus and medullary raphe nuclei, respectively. Types in the HB-Lhx2/9 subclass correspond to SPNs arising in the pontine tegmental nuclei such as the rostral pontine reticular nucleus (PRNr), Barrington's nucleus (B), pedunculopontine nucleus (PPN), and laterodorsal tegmental nucleus (LDT). Types in the HB-Lhx3/4 subclass correspond to nuclei in the medial reticular formation such as the caudal pontine reticular nucleus (PRNc) and gigantocellular reticular nucleus (GRN). These results were further confirmed by examining single-marker MERFISH data showing that Lhx9 expression is highest in the pontine tegmentum, Lhx1 expression is widespread throughout the hindbrain, and Vsx2 is expressed in the medial pontomedullary reticular formation (**Figure 2-12h**). The broad expression of Lhx1 and 5 suggest types in the HB-Lhx1/5 subclass may arise in widespread anatomical domains and therefore may or may not coincide with the anatomical domains of the other LIM-defined regions. For example, the widespread pontomedullary glycinergic types are within the HB Lhx1/5 subclass. Unifying these findings with the retrograde labeling studies assigns the LIM Groups to broad anatomical regions (**Figure 2-13d**).

Taken together, the LIM-defined types presented here comprehensively define the cellular composition of adult ReSNs and suggest a transcriptional logic underlying their heterogeneity and anatomical origin in the adult hindbrain.

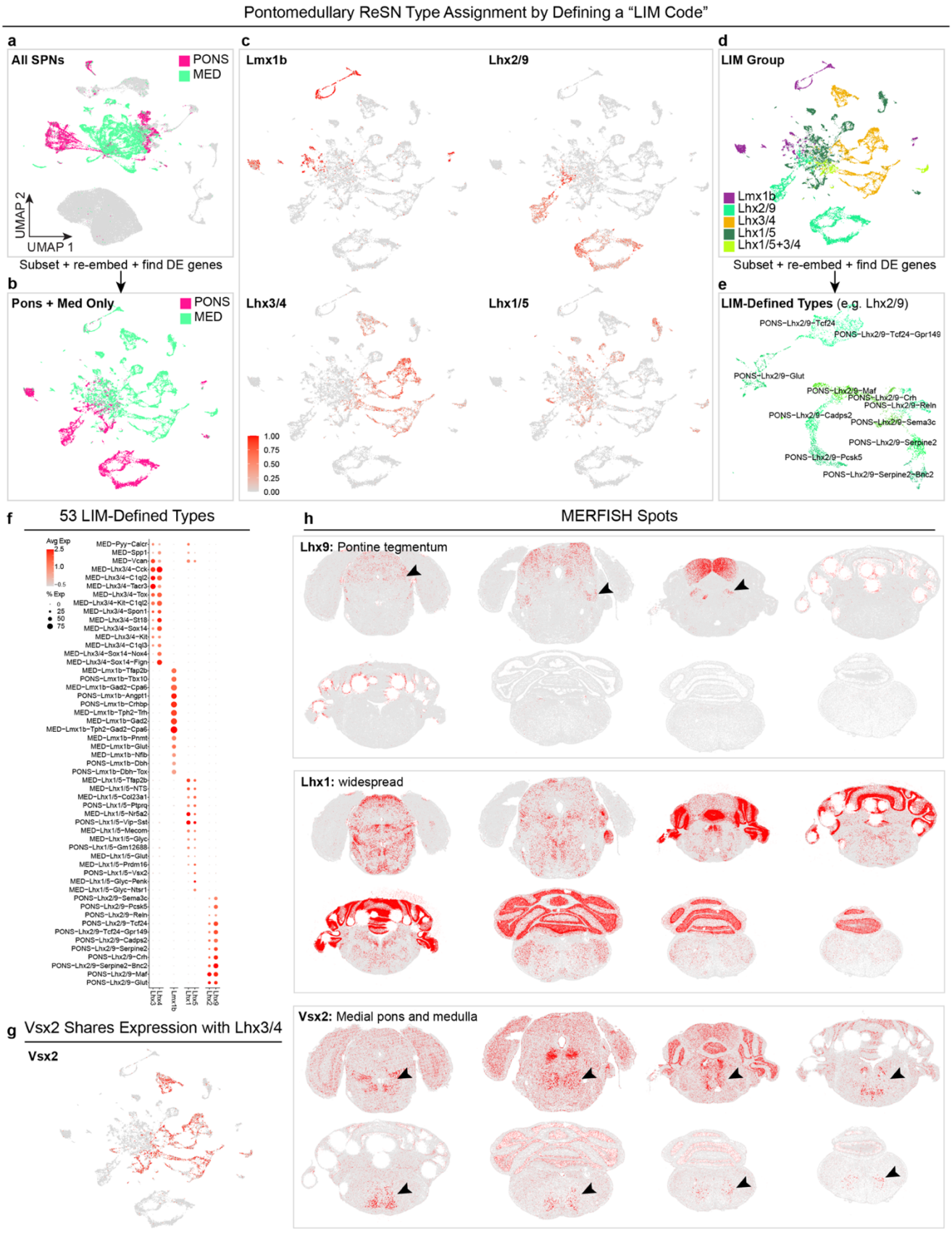

Pontomedullary ReSN Type Assignment by Defining a “LIM Code”
a
All SPNs
PONS
MED
UMAP 2
UMAP 1
Subset + re-embed + find DE genes
b
Pons + Med Only
PONS
MED
c
Lmx1b
Lhx2/9
Lhx3/4
Lhx1/5
1.00
0.75
0.50
0.25
0.00
d
LIM Group
Lmx1b
Lhx2/9
Lhx3/4
Lhx1/5
Lhx1/5+3/4
Subset + re-embed + find DE genes
e
LIM-Defined Types (e.g. Lhx2/9)
PONS−Lhx2/9−Tcf24
PONS−Lhx2/9−Tcf24−Gpr149
PONS−Lhx2/9−Glut
PONS−Lhx2/9−Maf
PONS−Lhx2/9−Crh
PONS−Lhx2/9−Reln
PONS−Lhx2/9−Cadps2
PONS−Lhx2/9−Sema3c
PONS−Lhx2/9−Serpine2
PONS−Lhx2/9−Pcsk5
PONS−Lhx2/9−Serpine2−Bnc2
f
53 LIM-Defined Types
Avg Exp
% Exp
Lhx4
Lhx3
Lmx1b
Lhx5
Lhx1
Lhx9
Lhx2
g
Vsx2 Shares Expression with Lhx3/4
Vsx2
h
MERFISH Spots
Lhx9: Pontine tegmentum
Lhx1: widespread
Vsx2: Medial pons and medulla

Figure 2-12: Multi-level clustering of pontomedullary reticulospinal neurons. a, UMAP of all SPNs with nuclei from pons- and medulla-enriching dissections colored as in Figure 2-1. **b,** Nuclei from pons- and medulla-enriching dissections were subset and re-embedded (10x data, N = 22,100 nuclei). **c,** Expression of Seurat ModuleScores of Lmx1b, Lhx2 and Lhx9, Lhx3 and Lhx4, Lhx1 and Lhx5 show these genes are expressed in mutually exclusive clusters. **d,** UMAP of nuclei from pons- and medulla-enriching dissections, colored by LIM groups (same as in Figure 2-13a). **e,** Each LIM group was subset and re-embedded to identify the final types in the taxonomy shown in Figure 2-1c. Shown here is the re-embedding of the Lhx2/9 LIM group. **f,** Dot plot showing expression of Lmx1b, Lhx2, Lhx9, Lhx3, Lhx4, Lhx1, and Lhx5 across the final 53 LIM-defined types. **g,** Expression of Vsx2 in nuclei from pons- and medulla-enriching dissections. **h,** MERFISH spot plots of expression of Lhx9, Lhx1, and Vsx2. Arrows to emphasize concentrated regions with expression.

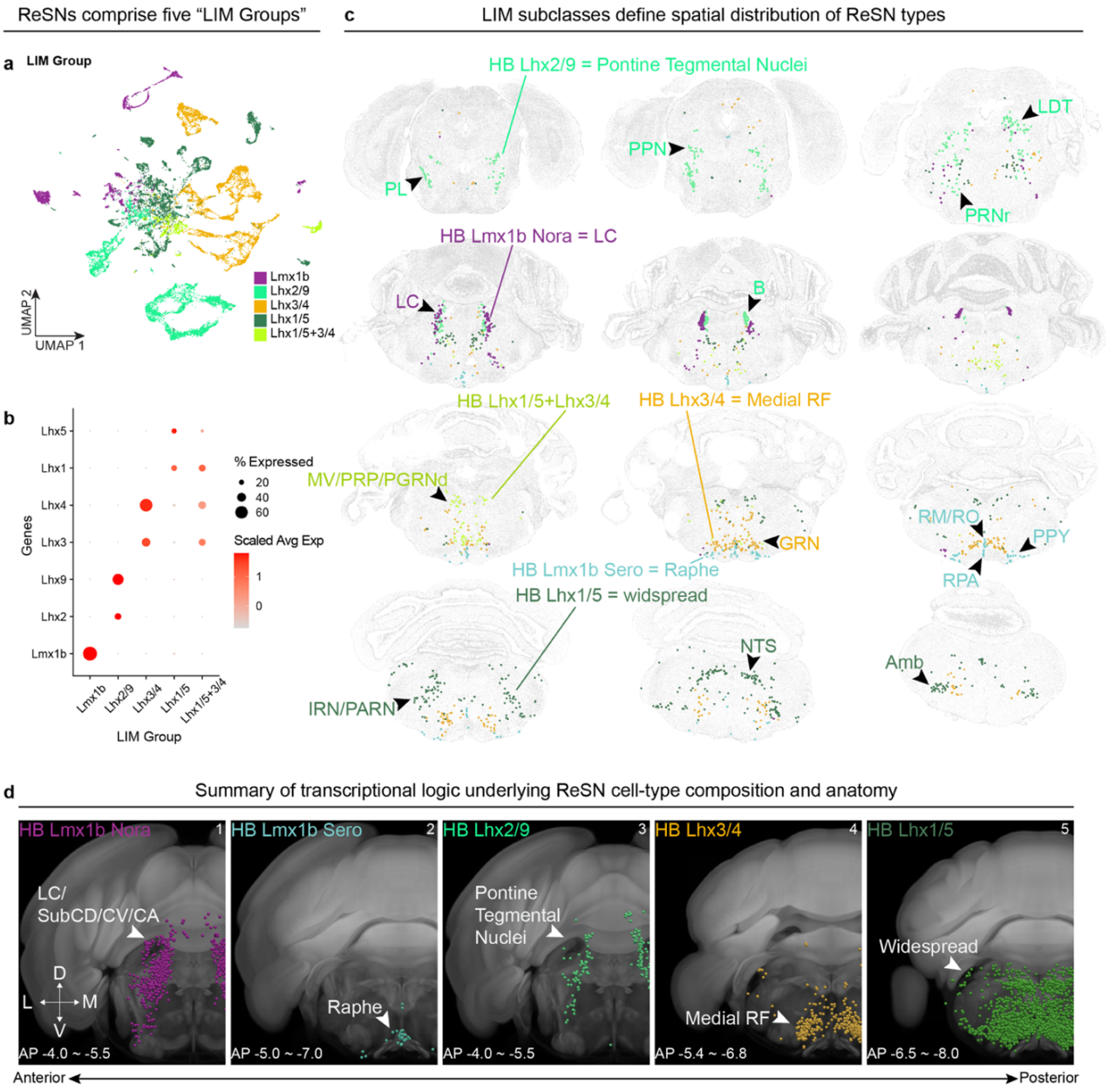


Figure 2-13: LIM Homeobox genes parcellate pontine and medullary spinal projecting neurons into spatially and transcriptionally distinct subsets. a, UMAP of nuclei from pons- and medulla-enriching dissections, colored by LIM groups (10x data, N = 22,100). **b,** Dot plot showing expression of Lmx1b, Lhx2, Lhx9, Lhx3, Lhx4, Lhx1, and Lhx5 grouped by the five "LIM Groups". **c,** Representative MERFISH sections of pontomedullary ReSN types, each colored by their respective LIM-defined subclass. **d,** The broad anatomical distributions of LIM-defined subclasses are summarized using representative coronal reconstructions of Cre-dependent retrogradely labeled nuclei in transgenic lines that are specific to LIM-defined subclasses (from Extended Data Fig. 7). Panel 1 shows labeling in the Dbh-Cre, TH-Cre, and Phox2b-Cre lines, colored by HB Lmxb1b Nora subclass color. Panel 2 shows labeling in the ePet-Cre line, colored by HB Lmx1b Sero subclass color. Panel 3 shows labeling in the Lhx2-2A-CreER line, colored by HB Lhx2/9 subclass color. Panel 4 shows labeling in the c-Kit MerCreMer line, colored by HB Lhx3/4 subclass color. Finally, Panel 5 shows labeling in the Chat-Cre, GlyT2-Cre, and Gcg-iCre lines, colored by HB Lhx1/5 subclass color. PL = paralemniscal nucleus (Paxinos nomenclature(Franklin & Paxinos, 2008)), PPN = pedunculopontine nucleus, PRNr = pontine reticular nucleus rostral part, LDT = laterodorsal tegmental nucleus, LC = locus coeruleus, SubCD = subcoeruelus nucleus dorsal part (Paxinos), SubCV = subcoeruelus nucleus ventral part (Paxinos), SubCA = subcoeruelus nucleus alpha part (Paxinos), B = Barrington's nucleus, MV = medial vestibular nucleus, PGRNd = paragigantocellular reticular nucleus dorsal part, PRP = nucleus prepositus, GRN = gigantocellular reticular nucleus, RM = nucleus raphe magnus, RO = nucleus raphe obscurus, PPY = parapyramidal nucleus, IRN = intermediate reticular nucleus, PARN = parvicellular reticular nucleus, NTS = nucleus of the solitary tract, Amb = nucleus ambiguus, AP = anterior-posterior position (relative to Bregma).

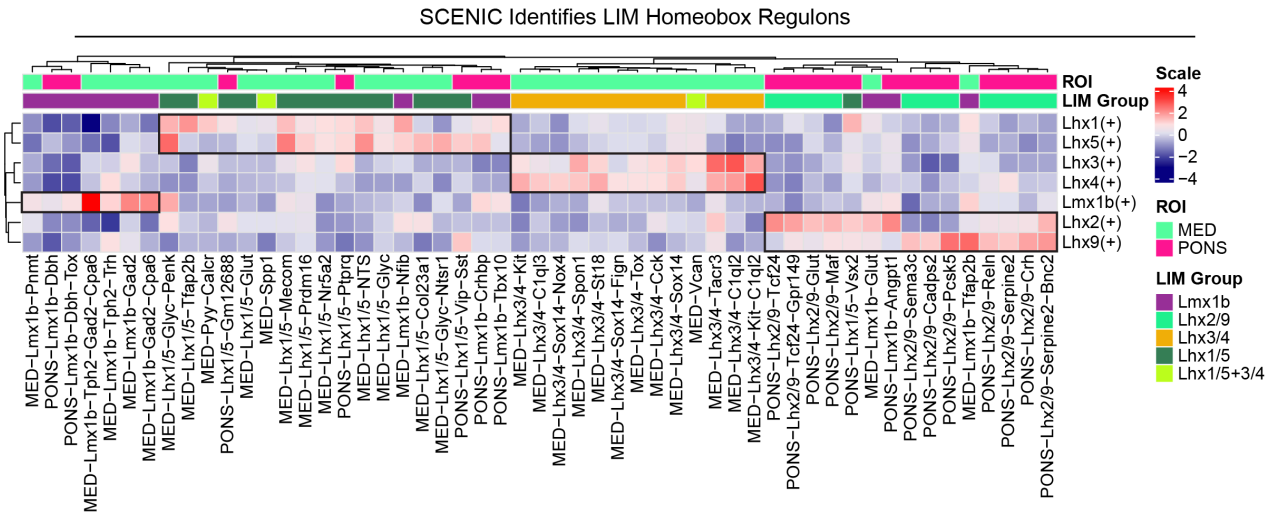


Figure 2-14: LIM Homeobox transcription factors make up regulatory modules determined by SCENIC. Heatmap of scaled regulon activity determined by single-cell regulatory network inference and clustering (SCENIC). Regulons are transcription factors and their putative downstream targets. Rows represent regulons, with transcription factor listed on the right. Columns are each one of the 53 pontomedullary ReSN types. Black outlines indicate LIM-defined modules.

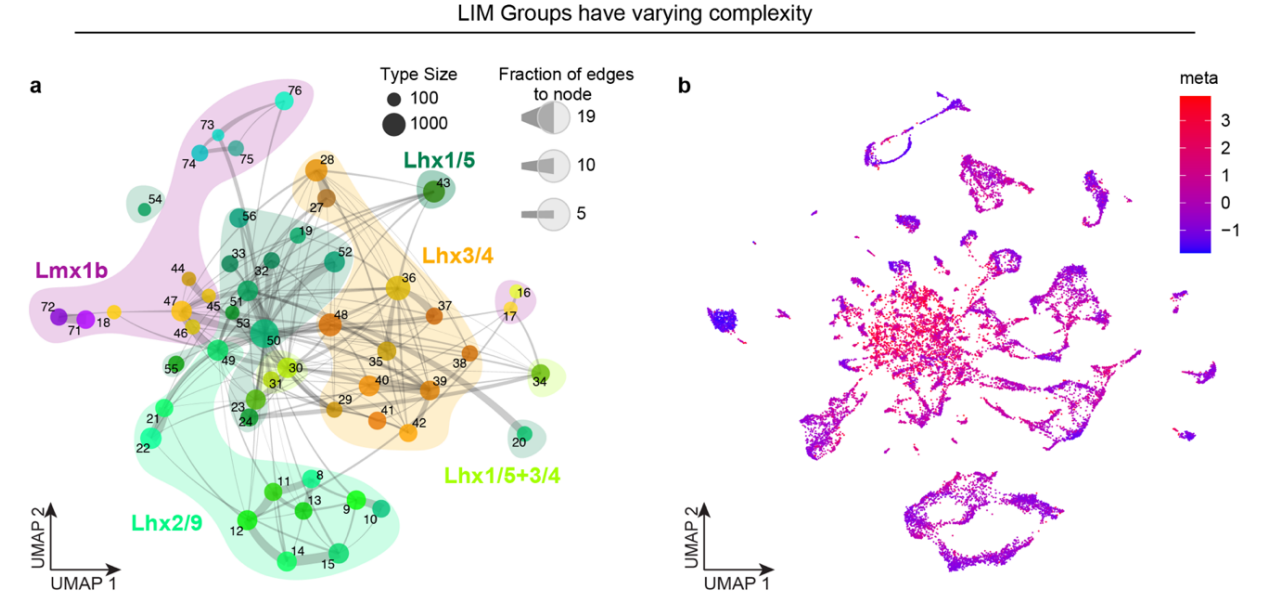


Figure 2-15: LIM-defined pontomedullary reticulospinal neurons have varying levels of complexity. a, Constellation plot showing global relatedness across all pontomedullary ReSNs. Each transcriptomic type is represented by a node whose area represents the number of nuclei (log-scale). Nodes are positioned at the center of the corresponding type in UMAP space in Figure 2-13a. Relationships between nodes are indicated by edges. Shading behind plot indicates

LIM group. Number labels and colors on nodes correspond to type number from Figure 2-1c. **b,** Average distance to the K nearest neighbors (KNN) for each nucleus. Nuclei in highly homogenous clusters have much shorter distance to their KNN compared to nuclei in highly heterogenous clusters. This metric can be used to measure for each nucleus, their local heterogeneity regardless of their cell type identities.

2.3.7 MOLECULAR SPECIFICATION OF SPINAL PROJECTION TARGETS.

SPNs differ in their projection patterns at different spinal levels according to their specific functions (see Chapter 1 **Section 1.3.3**). To inform the transcriptomic taxonomy with spinal cord projection properties, we analyzed differences among SPNs projecting to the cervical and/or lumbar spinal cord. First, we analyzed the projection-type composition of the 76 transcriptionally defined SPN types. The 10x dataset was generated from separately collected cervical-projecting (GFP+) versus dual- (GFP+/mScarlet+) and lumbar- (mScarlet+) projecting SPNs nuclei across the whole brain, and the SSv4 dataset used indexed plate-based sorting to separate cervical- (GFP+), lumbar- (mScarlet+), and dual- (GFP+/mScarlet+) projecting SPNs (**Figure 2-16a**). With this metadata, we assessed the distribution in UMAP space (**Figure 2-16b**) and determined the proportion of cervical- and dual-/lumbar- projecting neurons in each SPN type (**Figure 2-16c**). Most types are composed of SPNs with mixed projection targets (i.e., neurons have mixed cervical-, lumbar-, and dual-projecting types), but a few types project to only the cervical spinal cord (e.g. HB-Lhx1/5-Glyc-Penk). Types from the pontomedullary reticular formation contain high proportions of dual- and/or lumbar-projecting SPNs, as predicted by their highly branched axons (Brodal & Pompeiano, 1957; Peterson et al., 1979).

Second, we investigated the transcriptional signatures of SPNs with different spinal cord targets. We ran a differential gene expression analysis for cervical- vs. dual- and lumbar-projecting SPNs in each of the ROIs in the 10x dataset and assessed which DE genes were shared across these gene sets (**Table 2-7**). Notably, Epha4, Epha6, Epha7, and Efna5 are among the genes differentially expressed between cervical- and dual-/lumbar- projecting SPNs in all ROIs (**Figure 2-16d, g**). These

guidance molecules have been suggested to regulate topographic mapping of the CST (Canty et al., 2006; Iguchi et al., 2021; Vanderhaeghen et al., 2000), and their continued expression in adult SPNs may suggest a potential role in maintaining their respective spinal terminations.

To detect more subtle differences among cervical-, dual-, and lumbar- projecting SPNs, we analyzed the higher sequencing depth SSv4 data and focused our analyses on two regions that exhibit somatotopic segregation: CSNs and RuSNs (**Figure 2-8f**). While CSNs have a sizeable dual-projecting population, RuSNs have few, consistent with previous literature (Z. Wang et al., 2022) (**Figure 2-16e, f**; see Chapter 1 **Figure 1-11**). We find no significantly DE genes between dual- and lumbar-projecting CSNs; this may indicate these are lumbar projecting neurons with collaterals in the cervical cord. However, we identify a set of DE genes between cervical- and lumbar-/dual-projecting neurons in CSNs and RuSNs (**Figure 2-16g, Table 2-8 and 2-9**) and dual- vs. lumbar-projecting RuSNs (**Table 2-10**). Select DE genes were verified by single molecule FISH and the Allen ISH Atlas (**Figure 2-17a-e**). Gene Ontology enrichment analysis identified several relevant ontologies, including terms related to axon guidance, axon length, and neurotransmission (**Figure 2-16h**, **Figure 2-17f**). Thus, some of the molecular differences between cervical- and lumbar-projecting CSNs and RuSNs may be relevant to their functional tuning and structural maintenance.

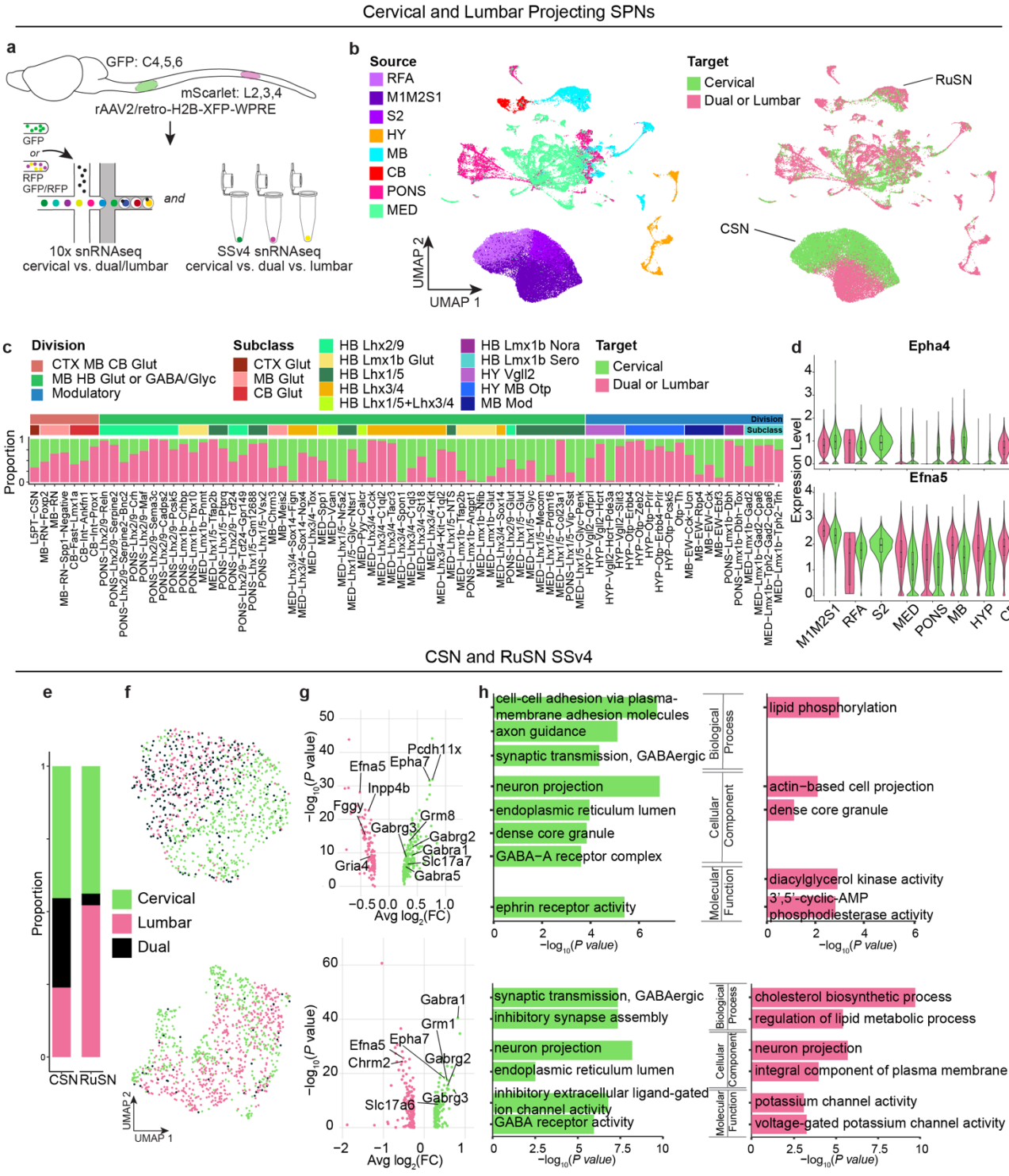


Figure 2-16: Transcriptomic differences among spinal projecting neurons terminating at different spinal targets.

a, The 10x data was generated from separately collecting cervical-projecting (GFP+) from dual- (GFP+/mScarlet+) and lumbar- (mScarlet+) projecting SPNs nuclei across the whole brain, and the SSv4 dataset used indexed plate-based sorting

to separate cervical- (GFP+), lumbar- (mScarlet+), and dual- (GFP+/mScarlet+) projecting SPNs. **b,** UMAP visualization of all SPNs colored by source (ROI, as in Figure 2-1d) and target (spinal cord level). **c,** Proportion of cervical (green) vs. dual or lumbar (pink) across SPN transcriptomic types. Bars above proportion plot indicate type subclass and division. Types ordered as in Figure 2-1c. **d,** Violin plot of differentially expressed genes, Epha4 and Efna5, across all SPNs, grouped by ROI. **e,** Proportion of cervical-, dual-, and lumbar-projecting neurons in the SSv4 CSN and RuSN datasets. **f,** SSv4 UMAPs of CSNs (top) and RuSNs (bottom). **g,** Volcano plots of differentially expressed genes for cervical- (green) vs. dual-/lumbar- (magenta) projecting CSNs (top) and RuSNs (bottom). Genes of interest are labeled. **h,** Select Gene Ontology terms of differentially expressed genes in (**g**) in CSNs (top) and RuSNs (bottom).

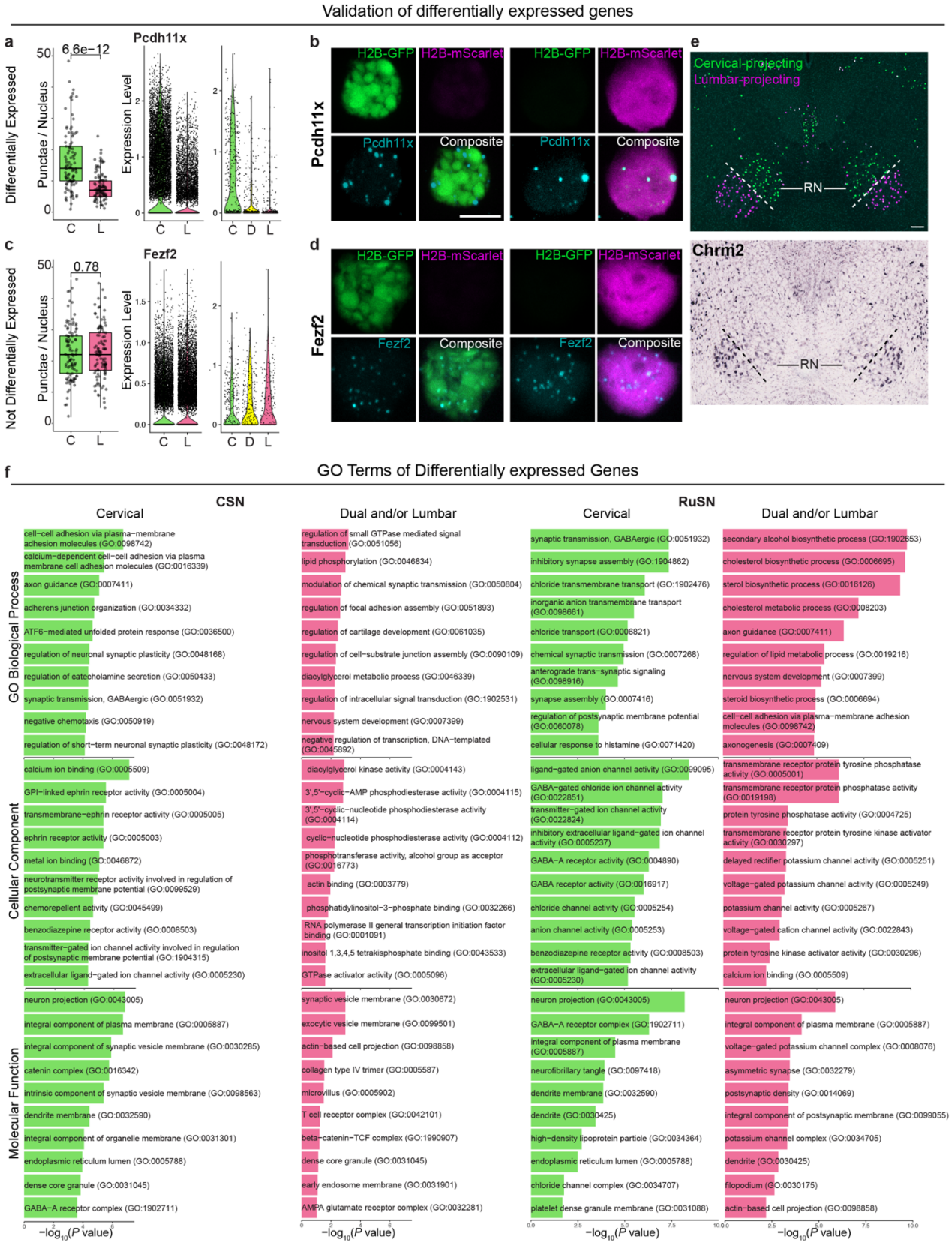

Validation of differentially expressed genes
a
Pcdh11x
6.6e−12
Differentially Expressed
Punctae / Nucleus
Expression Level
C L
C D L
b
H2B-GFP
H2B-mScarlet
Pcdh11x
Composite
e
Cervical-projecting
Lumbar-projecting
RN
c
Fezf2
0.78
Not Differentially Expressed
d
Chrm2
f
GO Terms of Differentially expressed Genes
CSN
RuSN
Cervical
Dual and/or Lumbar
GO Biological Process
Cellular Component
Molecular Function
cell−cell adhesion via plasma−membrane adhesion molecules (GO:0098742)
calcium−dependent cell−cell adhesion via plasma membrane cell adhesion molecules (GO:0016339)
axon guidance (GO:0007411)
adherens junction organization (GO:0034332)
ATF6−mediated unfolded protein response (GO:0036500)
regulation of neuronal synaptic plasticity (GO:0048168)
regulation of catecholamine secretion (GO:0050433)
synaptic transmission, GABAergic (GO:0051932)
negative chemotaxis (GO:0050919)
regulation of short−term neuronal synaptic plasticity (GO:0048172)
calcium ion binding (GO:0005509)
GPI−linked ephrin receptor activity (GO:0005004)
transmembrane−ephrin receptor activity (GO:0005005)
ephrin receptor activity (GO:0005003)
metal ion binding (GO:0046872)
neurotransmitter receptor activity involved in regulation of postsynaptic membrane potential (GO:0099529)
chemorepellent activity (GO:0045499)
benzodiazepine receptor activity (GO:0008503)
transmitter−gated ion channel activity involved in regulation of postsynaptic membrane potential (GO:1904315)
extracellular ligand−gated ion channel activity (GO:0005230)
neuron projection (GO:0043005)
integral component of plasma membrane (GO:0005887)
integral component of synaptic vesicle membrane (GO:0030285)
catenin complex (GO:0016342)
intrinsic component of synaptic vesicle membrane (GO:0098563)
dendrite membrane (GO:0032590)
integral component of organelle membrane (GO:0031301)
endoplasmic reticulum lumen (GO:0005788)
dense core granule (GO:0031045)
GABA−A receptor complex (GO:1902711)
−log10(P value)
regulation of small GTPase mediated signal transduction (GO:0051056)
lipid phosphorylation (GO:0046834)
modulation of chemical synaptic transmission (GO:0050804)
regulation of focal adhesion assembly (GO:0051893)
regulation of cartilage development (GO:0061035)
regulation of cell−substrate junction assembly (GO:0090109)
diacylglycerol metabolic process (GO:0046339)
regulation of intracellular signal transduction (GO:1902531)
nervous system development (GO:0007399)
negative regulation of transcription, DNA−templated (GO:0045892)
diacylglycerol kinase activity (GO:0004143)
3',5'−cyclic−AMP phosphodiesterase activity (GO:0004115)
3',5'−cyclic−nucleotide phosphodiesterase activity (GO:0004114)
cyclic−nucleotide phosphodiesterase activity (GO:0004112)
phosphotransferase activity, alcohol group as acceptor (GO:0016773)
actin binding (GO:0003779)
phosphatidylinositol−3−phosphate binding (GO:0032266)
RNA polymerase II general transcription initiation factor binding (GO:0001091)
inositol 1,3,4,5 tetrakisphosphate binding (GO:0043533)
GTPase activator activity (GO:0005096)
synaptic vesicle membrane (GO:0030672)
exocytic vesicle membrane (GO:0099501)
actin−based cell projection (GO:0098858)
collagen type IV trimer (GO:0005587)
microvillus (GO:0005902)
T cell receptor complex (GO:0042101)
beta−catenin−TCF complex (GO:1990907)
dense core granule (GO:0031045)
early endosome membrane (GO:0031901)
AMPA glutamate receptor complex (GO:0032281)
synaptic transmission, GABAergic (GO:0051932)
inhibitory synapse assembly (GO:1904862)
chloride transmembrane transport (GO:1902476)
inorganic anion transmembrane transport (GO:0098661)
chloride transport (GO:0006821)
chemical synaptic transmission (GO:0007268)
anterograde trans−synaptic signaling (GO:0098916)
synapse assembly (GO:0007416)
regulation of postsynaptic membrane potential (GO:0060078)
cellular response to histamine (GO:0071420)
ligand−gated anion channel activity (GO:0099095)
GABA−gated chloride ion channel activity (GO:0022851)
transmitter−gated ion channel activity (GO:0022824)
inhibitory extracellular ligand−gated ion channel activity (GO:0005237)
GABA−A receptor activity (GO:0004890)
GABA receptor activity (GO:0016917)
chloride channel activity (GO:0005254)
anion channel activity (GO:0005253)
benzodiazepine receptor activity (GO:0008503)
extracellular ligand−gated ion channel activity (GO:0005230)
neuron projection (GO:0043005)
GABA−A receptor complex (GO:1902711)
integral component of plasma membrane (GO:0005887)
neurofibrillary tangle (GO:0097418)
dendrite membrane (GO:0032590)
dendrite (GO:0030425)
high−density lipoprotein particle (GO:0034364)
endoplasmic reticulum lumen (GO:0005788)
chloride channel complex (GO:0034707)
platelet dense granule membrane (GO:0031088)
secondary alcohol biosynthetic process (GO:1902653)
cholesterol biosynthetic process (GO:0006695)
sterol biosynthetic process (GO:0016126)
cholesterol metabolic process (GO:0008203)
axon guidance (GO:0007411)
regulation of lipid metabolic process (GO:0019216)
nervous system development (GO:0007399)
steroid biosynthetic process (GO:0006694)
cell−cell adhesion via plasma−membrane adhesion molecules (GO:0098742)
axonogenesis (GO:0007409)
transmembrane receptor protein tyrosine phosphatase activity (GO:0005001)
transmembrane receptor protein phosphatase activity (GO:0019198)
protein tyrosine phosphatase activity (GO:0004725)
transmembrane receptor protein tyrosine kinase activator activity (GO:0030297)
delayed rectifier potassium channel activity (GO:0005251)
voltage−gated potassium channel activity (GO:0005249)
potassium channel activity (GO:0005267)
voltage−gated cation channel activity (GO:0022843)
protein tyrosine kinase activator activity (GO:0030296)
calcium ion binding (GO:0005509)
neuron projection (GO:0043005)
integral component of plasma membrane (GO:0005887)
voltage−gated potassium channel complex (GO:0008076)
asymmetric synapse (GO:0032279)
postsynaptic density (GO:0014069)
integral component of postsynaptic membrane (GO:0099055)
potassium channel complex (GO:0034705)
dendrite (GO:0030425)
filopodium (GO:0030175)
actin−based cell projection (GO:0098858)

Figure 2-17: Validation and functional significance of differentially expressed genes between cervical and lumbar projecting neurons. a-d, Select differentially expressed (i.e., Pcdh11x) and control (i.e., Fezf2) genes were validated with single molecule FISH on nuclei sorted from M1M2S1 dissections. The number of punctae per nucleus was quantified (**a, c,** left boxplot) shown with 10x (**a, c,** middle violin plot) and SSv4 (**a, c** right violin plot) snRNAseq expression data. Numbers above boxplots indicate p-values (Wilcoxon test). **b, d,** representative images of hybridized genes Pcdh11x (**b**) and Fezf2 (**c**) on sorted nuclei from M1M2S1-enriching dissections. Scale bar = 5 μm. **e,** Confocal image of retrogradely labeled rubrospinal neurons (top), and in situ validation of Chrm2 (a differentially expressed gene in lumbar-projecting RuSNs) using the Allen ISH database (bottom). Confocal image as shown in Figure 2-8f. **f,** Top 10 Gene Ontology (GO) terms for cervical- and lumbar-projecting CSNs and RuSNs.

2.4 DISCUSSION.

In this study, we created a comprehensive transcriptomic atlas of mouse SPNs by profiling 65,002 SPN nuclei defined by AAV-assisted retrograde labeling from different spinal cord levels. Multi-level iterative clustering, in combination with spatial characterization by MERFISH and other methods, classified SPNs into molecularly and functionally distinct groups (3 Divisions, 13 Subclasses, and 76 Types) with different spatial distributions. Thus, these results begin to reveal the organizational principles for the brain-spinal cord highways that turn "thoughts" into "actions".

2.4.1 TECHNICAL LIMITATIONS AND SOLUTIONS:

Although retro-AAV2 has been widely used to label long-projection neurons for both anatomical and functional purposes (Liu et al., 2020; Nassi et al., 2015), our studies reveal that intraspinal injection of this vector labels not only bona fide SPNs, but also small numbers of other non-specific cells (including neurons and non-neuronal cells). It remains to be determined if these secondary cells are from transsynaptic spread and/or the uptake of viral particles released from dying SPNs. To address this issue, we developed a computational method to remove such second-order cells. In addition to reducing the noise of this dataset, this method should be useful for other retro-AAV-based studies.

Another caveat of the retro-AAV2 is their low targeting efficiencies towards certain types of modulatory neurons (Ganley et al., 2021). For example, the data fail to identify adrenergic C1 neurons in the medulla, a relatively rare but well documented SPNs for regulating autonomic functions (Stornetta & Guyenet, 2018). Thus, caution is needed to interpret the proportion of different clusters of SPNs.

2.4.2 A THREE-COMPONENT ORGANIZATION OF SPN PROJECTIONS:

How brain commands are organized to control spinal cord function is a fundamental question. It has been assumed that the brain commands are organized by their functional modalities, such as motor, sensory or autonomic control. Here, our unbiased computational analyses suggest that the entire spinal projecting system consists of three distinct yet complementary components (or 'Divisions'). The first division includes the neurons in three discrete brain regions: cortex, red nucleus, and cerebellum. They are exclusively excitatory, relatively transcriptionally homogeneous, and have somatotopic spinal terminations, thus might be functionally important for transmitting specialized point-to-point command signals to the spinal cord. In contrast, SPNs in the second division include both excitatory and inhibitory neurons and are highly heterogeneous. These neurons are widely distributed in the midbrain and pontomedullary reticular formation, thus representing a major population of ReSNs. Together with their innervation throughout the spinal cord, these neurons are well suited for relaying commands related to different (sensory/motor/ autonomic and excitatory/inhibitory) activity levels and patterns of the entire spinal cord. Complementary to the fast-acting neurons in Divisions 1 and 2, Division 3 corresponds to modulatory SPNs which express slow-acting neurotransmitters and/or neuropeptides. These neurons are distributed in the hypothalamus, midbrain, and brainstem, but not in the cortex, red nucleus, and cerebellum where Division 1 SPNs arise. Their broad spinal terminations and neuromodulatory capacity render them as a potentially powerful level of "gain

control". Together, these results suggest a working model for the general organization of SPN populations: targeted or diffuse commands plus modulatory gain control. With different spinal innervation patterns (targeted and broad) and neuroeffectors (fast or slow neurotransmitter and neuropeptides), their complementary actions may allow both spatial and temporal control of spinal cord function for coordinated behaviors.

2.4.3 MOLECULAR INSIGHTS INTO RETICULAR FORMATION SPNS:

Previous efforts on SPNs have primarily focused on CSNs (Arlotta et al., 2005; Bareyre et al., 2005; Golan et al., 2021; Kamiyama et al., 2015; Sahni et al., 2021; Steward et al., 2021), leaving ReSNs and their hosting brainstem reticular formation poorly characterized. Even other studies from the BICCN have not yet provided detailed analysis on this complex yet important brain region (Yao et al., 2023). The reticular formation is well known for its anatomical and functional complexity (Horn, 2006; Humphries et al., 2006). Anatomically, it does not have distinct cytoarchitectural boundaries and is dispersed throughout the brainstem as a network of interconnected neurons with many projections rostrally to subcortical and cortical brain structures as well as caudally to the spinal cord. Functionally, it is considered a major center of integrating, coordinating, and influencing various regions of the central and peripheral nervous systems (Horn, 2006; Humphries et al., 2006). In this study, we found that all ReSNs could be defined by two complementary components: ReSNs in Division 2 are defined by fast-acting (excitatory or inhibitory) neurotransmitters and those in Division 3 are modulatory, suggesting that the reticular formation elaborates both fast and slow command signals to the spinal cord. Second, several LIM transcription factors assign most ReSNs into 5 groups with complementary spatial distribution: Lmx1b primarily for modulatory SPNs, Lhx2/9 for SPNs arising in the pontine tegmental nuclei, the other three groups (Lhx1/5 and/or Lhx3/4) for ReSNs arising in the caudal pons and medulla. Additionally, it appears that the Lhx3/4 and Lhx1/5 groups are associated with

two major forms of structures (concentrated nuclei vs. distributed network) of the reticular formation. Namely, Lhx3/4+ SPNs are mainly concentrated in several distinct nuclei in the medial pontomedullary RF, whereas Lhx1/5+ SPNs are sparsely and/or widely distributed throughout the brainstem. In addition to their complex 'reticular' anatomical distribution, the Lhx1/5+ SPNs also appear to be the most transcriptionally complex. Thus, our results not only verify the known Chx10+ ReSNs as equivalent to the Lhx3/4+ group, but we also define the molecular and anatomical properties of several new classes of ReSNs. Taken together, this atlas provides the first lens into how to start to probe into this transcriptionally complex population of ReSNs.

2.5 ACKNOWLEDGEMENTS.

We thank the Allen Institute Molecular Biology team and Imaging team for generating the SMART-seq (SSv4) and MERFISH datasets, respectively; Ronald Mathieu, Toska Berisha, and the BCH Flow Core; John Daley and the Dana Farber Cancer Institute Flow Core; Clifford Woolf for providing the Penk-Cre mouse line; Preston Ge for guidance on sorted nuclei cover slipping; and Yiming Wang and the BCH Viral Core for production of AAVs; and Preston Ge for guidance on sorted nuclei coverslipping.

2.6 TABLE LEGENDS.

Tables may be found at: https://tinyurl.com/WinterSupplement

Table 2-1: snRNAseq donor information. Mouse donors used in this study are listed alongside metadata, including the platform nuclei were profiled with, donor ID, strain, sex, and age. Multiple regions could be dissected per donor and are listed as ROI 1-8. GRN = gigantocellular reticular

nucleus, PRN = pontine reticular nucleus, DPT = dorsal pontine tegmentum, L5CTX = cortical layer 5, RN = red nucleus, RFA = rostral forelimb area, M1 = primary motor cortex, M2 = secondary motor cortex, S1 = primary somatosensory cortex, S2 = secondary somatosensory cortex, HY = hypothalamus, MB = midbrain, CB = cerebellum, MED = medulla.

Table 2-2: Marker genes of the 76 spinal projecting neuron types. Seurat's FindAllMarkers (MAST test) was used to find the marker genes of the 76 SPN types (10x and SSv4 data, N = 65,002). We tested only genes that were detected in a minimum of 25% of the nuclei (min.pct = 0.25) and that showed at least a 0.25-fold log-scale difference (logfc.threshold = 0.25) between the nuclei in the cluster and all other nuclei. Genes are annotated as 'significant' if adjusted p-value is less than 0.05.

Table 2-3: Results of mapping the SPN snRNAseq taxonomy to the AIBS whole brain scRNAseq taxonomy - Subclass. The SPN taxonomy was mapped to the AIBS whole brain scRNAseq taxonomy. Here is SPN 'type' mapping to AIBS 'Subclass' level. Freq = frequency of mapped nuclei, avg.cor2ref = average correlation score to reference AIBS WB scRNAseq taxonomy. Mappings with frequency of 1 were removed.

Table 2-4: **Results of mapping the SPN snRNAseq taxonomy to the AIBS whole brain scRNAseq taxonomy - Supertype.** The SPN taxonomy was mapped to the AIBS whole brain scRNAseq taxonomy. Here is SPN 'type' mapping to AIBS 'Supertype' level. Freq = frequency of mapped nuclei, avg.cor2ref = average correlation score to reference AIBS WB scRNAseq taxonomy. Mappings with frequency of 1 were removed.

Table 2-5: Results of mapping the SPN snRNAseq taxonomy to the AIBS whole brain scRNAseq taxonomy - Cluster. The SPN taxonomy was mapped to the AIBS whole brain scRNAseq taxonomy. Here is SPN 'type' mapping to AIBS 'Cluster' level. Freq = frequency of mapped nuclei, avg.cor2ref = average correlation score to reference AIBS WB scRNAseq taxonomy. Mappings with frequency of 1 were removed.

Table 2-6: Marker genes of the pontomedullary spinal projecting neuron types. Seurat's FindAllMarkers (MAST test) was used to find the marker genes of the 53 pontomedullary SPN types (10x dataset, N = 22,100). We tested only genes that were detected in a minimum of 10% of the nuclei (min.pct = 0.10) and that showed at least a 0.25-fold log-scale difference (logfc.threshold = 0.25) between the nuclei in the cluster and all other nuclei. Genes are annotated as 'significant' if adjusted p-value is less than 0.05.

Table 2-7: Genes that are differentially expressed between all cervical- vs. dual- and lumbar-spinal projecting neurons. Seurat's FindMarkers (MAST test) was used to find differentially expressed genes between cervical vs. dual and lumbar projecting SPNs in each ROI containing both projection types (i.e., M1M2S1, HY, MB, CB, PONS, MED). We tested only genes that were detected in a minimum of 10% of the nuclei (min.pct = 0.10) and that showed at least a 0.05-fold log-scale difference (logfc.threshold = 0.05) between the two groups. Loose $\log_2$(Fold Change) criteria was used to capture more differentially expressed genes across SPN ROI and to account for relatively low sequencing depth 10x data. We then removed any genes that were not significant (adjusted p-value greater than 0.05) and found the intersection across the 6 lists, to yield a final list of genes that are significantly differentially expressed in each ROI. Positive $\log_2$(Fold Change) indicates differentially expressed in cervical-projecting neurons.

Table 2-8: Differentially expressed genes between cervical- vs. dual- and lumbar- projecting corticospinal neurons. Seurat's FindMarkers (MAST test) was used to find differentially expressed genes between cervical vs. dual/lumbar projecting corticospinal neurons (SSv4 data, N = 1,009 nuclei). We tested only genes that were detected in a minimum of 10% of the nuclei (min.pct = 0.10) and that showed at least a 0.25-fold log-scale difference (logfc.threshold = 0.25) between the two groups. Genes are annotated as 'significant' if adjusted p-value is less than 0.05. Positive $\log_2$(Fold Change) indicates differentially expressed in cervical-projecting neurons.

Table 2-9: Differentially expressed genes between cervical- vs. dual- and lumbar- projecting rubrospinal neurons. Seurat's FindMarkers (MAST test) was used to find differentially expressed genes between cervical vs. dual/lumbar projecting rubrospinal neurons (SSv4 data, N = 1,031 nuclei). We tested only genes that were detected in a minimum of 10% of the nuclei (min.pct = 0.10) and that showed at least a 0.25-fold log-scale difference (logfc.threshold = 0.25) between the two groups. Genes are annotated as 'significant' if adjusted p-value is less than 0.05. Positive $\log_2$(Fold Change) indicates differentially expressed in cervical-projecting neurons.

Table 2-10: Differentially expressed genes between lumbar- and dual- projecting rubrospinal neurons. Seurat's FindMarkers (MAST test) was used to find differentially expressed genes between lumbar vs. dual projecting rubrospinal neurons (SSv4 data, N = 1,031 nuclei). We tested only genes that were detected in a minimum of 10% of the nuclei (min.pct = 0.10) and that showed at least a 0.25-fold log-scale difference (logfc.threshold = 0.25) between the two groups. Genes are annotated as 'significant' if adjusted p-value is less than 0.05. Positive $\log_2$(Fold Change) indicates differentially expressed in lumbar-projecting neurons.

Table 2-11: Mouse lines used for Cre-dependent retrograde labeling. Summary of mouse lines used for retrograde labeling with AAVs expressing Cre-dependent GFP. The Jackson Lab Strain and MGI number is provided for publicly available strains, and name of donating lab is listed for non-publicly available strains.

2.7 MATERIALS AND METHODS.

Animals

All experimental procedures were performed in compliance with animal protocols approved by the Institutional Animal Care and Use Committee at Boston Children's Hospital (Protocol #20-05-4165R). Mice were provided food and water *ad libitum*, housed on a 12-hour light-dark schedule (7am-7pm light period) with no more than 5 mice of the same sex per cage, and allowed to acclimate for 1 week after arrival. C57BL/6J wild-type mice (Jackson Labs, Strain #:000664) were used for all snRNAseq and electrophysiological experiments, and to generate the wild-type retrogradely labeled histological datasets. Transgenic driver lines (**Table 2-11**) were used for the histological Cre-dependent retrograde labeling datasets (i.e., those generated via retrograde labeling with AAVs expressing Cre-dependent GFP). Nuclei suspensions were generated from 15 adult mice (8 female and 7 male) for 10x and 15 mice (6 female and 9 male) for SSv4 (**Table 2-1**).

Virus production and retrograde labeling of adult spinal projecting neurons

To retrogradely label SPNs, AAV2/retro-Syn-H2B-GFP and AAV2/retro-Syn-H2B-mScarlet were injected (produced by Boston Children's Hospital Viral Core). Adult mice (P42) were anesthetized with intraperitoneal injection of ketamine-xylazine (KX, 100-120 mg/Kg ketamine, 10 mg/Kg xylazine) and placed on a stereotactic frame. For cervical level (C4-6) injection, a dorsal incision was

made along the vertebral column at cervical level. The overlying muscle was dissected to expose the cervical vertebral column and a laminectomy was performed at C4-6 to expose the spinal cord. 2.4 μL of AAV2/retro-Syn-H2B-GFP ($5x10^{12}$ genome copies per mL, gc/mL) were injected at 0.40 mm lateral to midline and 0.60 mm and 1.00 mm depth using a glass micropipette (tipped at 25 μm in diameter). The dorsal muscle layers were sutured, and skin closed with sterile wound clips. For lumbar level (L2-4) injections, this process was repeated with the AAV2/retro-Syn-H2B-mScarlet ($5x10^{12}$ gc/mL) virus at 0.35 mm lateral to midline and 0.60 mm and 1.00 mm depth.

Histology and slide scanner imaging of retrogradely labeled brains

At P56, retrogradely labeled mice were anesthetized with KX and sacrificed by transcardiac perfusion with phosphate buffered saline (PBS) followed by 4% paraformaldehyde (PFA) in PBS. The skull and spinal column were dissected and post-fixed in 4% PFA in PBS for 24 hours. The brain and spinal cord tissue were then microdissected and cryoprotected in 30% sucrose, embedded and frozen in optimal cutting temperature (OCT) medium and processed using a cryostat (50 μm coronal sections; olfactory bulb through caudal medulla; four series). Sections were washed with PBS and then treated with a blocking solution (5% normal donkey serum, 0.5% Triton-X) for 1 hour at room temperature (RT). Floating sections were incubated in primary antibodies (AVES Chicken anti-GFP, Rockland Rabbit-anti-RFP; 1:500 dilution in blocking solution) at 4ºC overnight, washed three times for 10 minutes with PBS, and subsequently incubated with secondary antibodies (Alexa Fluor 488 donkey-anti-chicken, Alexa Fluor 594 donkey-anti-rabbit; 1:500 dilution in PBS) for 2 hours at RT. Finally, sections were washed with PBS, mounted with DAPI Fluoromount-G mounting medium, sealed with clear nail polish, and stored at 4ºC until imaging. Whole sections were imaged on an Olympus VS120 Virtual Slide Microscope at 10x magnification. Higher magnification images were acquired as z-stacks with a 20x objective on a Zeiss LSM 900 Confocal Laser Scanning Microscope.

Quantification of spinal projecting neurons across major brain regions

SPNs were quantified across the eight major brain regions (i.e., RFA, M1M2S1, S2, HY, MB, PONS, MED) using QuPath. Briefly, VS120 slide scanner images of one (of four) IHC processed coronal series were loaded into QuPath as a project. The polygon tool was used to manually annotate ROIs. Classifiers were then created using 'Positive Cell Detection' (for GFP and mScarlet nuclei) and 'Composite Classifier' (for GFP+/mScarlet+ nuclei). 'Annotation results' were saved per ROI, and the number of nuclei quantified per ROI were multiplied by four (as only 1 of 4 coronal series was quantified) to get total brain counts. N = 5 retrogradely labeled brains were quantified to yield total SPN counts across each of the eight ROIs.

***In situ* fluorescent protein level measurement**

QuPath was used to measure the fluorescence intensity of GFP and mScarlet labeled nuclei in cortical layer 5 vs. non-layer 5 of retrogradely labeled tissue (without IHC to maintain unamplified fluorescence levels). As described above, the polygon tool was used to manually annotate cortical layer 5, upper cortex (Layers 1-4), and lower cortex (layer 6), and 'Positive Cell Detection' and 'Composite Classifiers' were run to detect GFP+, mScarlet+, and GFP+/mScarlet+ nuclei. 'Detection results' were saved per ROI, and fluorescence intensity was extracted from the 'Nucleus.GFP.mean' and 'Nucleus.mScarlet.mean' results. Statistical significance was assessed with the Wilcoxon test (ggpubr).

Serial two-photon tomography, registration, and nucleus segmentation

Image acquisition: Whole retrogradely labeled brains were imaged using the TissueCyte serial two-photon tomography platform. Briefly, at P56, retrogradely labeled mice were anesthetized with KX and

sacrificed by transcardiac perfusion with PBS and 4%PFA/PBS, the skull and spinal column were dissected and post-fixed in 4% PFA in PBS for 24 hours. The brain was then microdissected, rinsed with PBS, and embedded in covalent agarose. Briefly, a 4.5% agarose solution in 10mM NaIO4 was made by gently stirring agarose and NaIO4 with Phosphate Buffer (PB; 0.42g/L monobasic sodium phosphate, 0.92g/L Dibasic sodium phosphate) for 2-3 hours at RT in a hood protected from light and filtered with a 0.2 μm filter. A microwave was then used to bring agarose to a boil, then cooled down to 60-65ºC to embed the brain. The agarose-embedded brain was mounted in the TissueCyte using Quick Bond adhesive. The sample was immersed in PB during image acquisition. Images were captured at XY resolution of 1.38 μm/pixel with 10 μm stacks and 50 μm vibratome planes. Images were stitched with TissueVision's proprietary stitching algorithm 'Stitcher'.

Registration and segmentation: Labeled nuclei were segmented and reconstructed using NeuroInfo (MBF Bioscience). Briefly, stitched images were first stacked with MicroFile+. Stacked images were then registered to the Allen Mouse Common Coordinate Framework (Allen CFF) with the volume registration function in NeuroInfo. H2B signals in red (mScarlet) or green (GFP) channels were detected and labeled separately. The detected nuclei were manually annotated with different colors based on their mapped regions. Videos and horizontal, coronal, or sagittal projections of the three-dimension reconstructions were output via Neuroinfo's 3D visualization window.

Single nucleus RNA sequencing

Brain preparation: Brains were prepared by adapting a protocol from the AIBS available at protocols.io (dx.doi.org/10.17504/protocols.io.bq6wmzfe). At P56, retrogradely labeled mice were anesthetized with isoflurane and transcardially perfused with 25mL of ice cold oxygenated artificial cerebrospinal

fluid (aCSF-O2; 0.5mM Calcium Chloride dihydrate, 25mM D-Glucose 20mM HEPES, 10mM Magnesium Sulfate Heptahydrate, 1.25mM Sodium Phosphate monobasic monohydrate, 2.5mM Potassium Chloride, 3mM Sodium Pyruvate, 5mM Sodium L-Ascorbate, 25mM Sodium Bicarbonate, 2mM Thiourea, 96mM HCl, 96mM N-Methyl-D-glucamine, 3mM Myo-inositol, 12mM N-Acetyl-L-Cysteine, 0.01mM Taurine). The brain was then rapidly dissected and placed in an acrylic brain matrix in a bath of aCSF-O2. For 10x samples, brains were sliced with a 1 mm coronal matrix until -3 mm (relative to Bregma) to capture forebrain ROIs, then the brain was then transferred to a 1 mm sagittal matrix for mid and hindbrain to allow for comprehensive dissection of these ROIs. For SSv4, a 1 mm coronal matrix was used to section the entire brain to allow for finer dissections of ROIs. Slices were then transferred into a Sylgard-coated dissection dish containing ice cold aCSF-O2 with 0.0132M trehalose. Brightfield and fluorescent images were taken of the intact tissue to document ROIs with a Zeiss SteREO Discovery Dissecting Microscope and subsequently microdissected with a needle blade microknife. ROI dissection was guided by visualization of fluorescently labeled regions in the eyepiece. Brightfield and fluorescent images were acquired of the dissected ROI for verification. For 10x, target ROIs were RFA, M1M2S1, S2, HY (coronal slices), MB, CB, PONs, and MED (sagittal slices). Tissue was frozen between collection and nucleus isolation to allow pooling of ROIs from multiple animals to collect sufficient numbers of nuclei for the 10x platform. Briefly, ROIs were placed on a razor blade and Whatman filter paper was used to absorb excess aCSF. The razor blade was then held in liquid nitrogen vapor until the tissue froze. Frozen tissue was transferred into a microcentrifuge tube with a frozen moisture reservoir of OCT to prevent frost damage and stored at -80ºC until use. For SSv4, targeted dissections were made of cortical layer 5, RN, pontine reticular nucleus (PRN), and gigantocellular reticular nucleus (GRN). The dissected regions were not frozen and instead transferred into aCSF-trehalose in a microcentrifuge tube and stored on ice until nucleus isolation upon completion of dissections.

Nucleus isolation: Single nuclei were isolated by adapting a protocol from the AIBS available at protocols.io (dx.doi.org/10.17504/protocols.io.bq7emzje). Briefly, microdissected regions were transferred into homogenization buffer (HB; 10mM Tris pH 8.0, 250mM sucrose, 25mM KCl, 5mM MgCl2, 0.1% Triton-X 100, 0.5% RNAsin Plus, 1x protease inhibitor, and 0.1mM DTT) and placed into a 1 mL dounce homogenizer on ice. For 10x samples, frozen tissue from multiple animals was pooled per ROI for each replicate (**Figure 2-2b**). For SSv4 samples, each animal and ROI was maintained as a separate sample. Tissue was homogenized with 15-20 strokes of the loose pestle followed by 15-20 strokes of the tight pestle. Subcortical regions with more white matter tracts require a larger number of strokes to homogenize tissue, though unhomogenized pieces of white matter remain following douncing. An additional 1 mL of HB was added to the dounce and 1 mL of HB was used to wet a 30 μm cell strainer. Half of the nucleus suspension was passed through the cell strainer into a 15 mL conical tube to remove large debris. Another 1 mL of HB was added to the dounce and then all the nucleus suspension was passed through the cell strainer into a 15 mL conical tube. A final 2 mL of HB was added to the dounce to rinse any remaining nuclei into suspension and then passed through the strainer for a total of 6mL HB-nucleus suspension. The homogenate was spun at 900g for 10 minutes in a 4ºC swinging bucket centrifuge. After centrifugation, supernatant was removed without disturbing the visible pellet at the bottom of the conical tube and the pellet was resuspended in 0.5-1 mL of sort buffer (PBS with 0.8% BSA and 0.5% RNAsin Plus). Finally, 4'-6-diamidino-2-phenylindole (DAPI) was added to the nucleus suspensions at a final concentration of 0.1 μg/mL and incubated on ice until FANS.

Spinal projecting neuron enrichment via FANS: SPNs were enriched from the nucleus suspensions using FANS. For 10x, single SPN nuclei were sorted using a BD FACSARIA II with a 70 μm custom

pressure nozzle (50 psi). Briefly, single nuclei were captured by sorting on 'four-way-purity mode' and gating on DAPI-positive while excluding debris and aggregates, then gating on GFP and/or mScarlet signal (**Figure 2-2d**). Nuclei were sorted (to a maximum number of 16,000 nuclei) using two-way sorting (GFP-positive separate from mScarlet- and double-positive) into PCR tubes (pre-coated with 5% BSA overnight) containing 20uL of sort buffer. After sorting, PCR tubes were briefly centrifuged and then placed on ice until proceeding with the 10x platform. For SSv4, single nuclei were sorted using a Sony SH800 Cell Sorter or MA900 Multi-Application Cell Sorter using a 100 μm chip. Briefly, single nuclei were sorted on 'single-cell' mode and captured by gating on singlet DAPI-positive, then gating on GFP and/or mScarlet signal to specifically sort cervical and/or lumbar project SPNs, respectively. Indexed plate-based sorting was used to sort GFP-, mScarlet, and double-positive nuclei into strip tubes containing 11.5uL of SMART-Seq v4 lysis buffer. Lysed FANS-sorted nuclei were then briefly centrifuged, frozen on dry ice, and stored at -80ºC until proceeding with the SSv4 platform.

cDNA amplification and library construction: For 10x processing, we used the Chromium Next GEM Single Cell 3′ Kit v3.1 (1000268, 10x Genomics). To optimize yield, sorted nucleus suspensions were loaded directly into the 10x Chromium Controller without post-FANS spin down and re-suspension. Reverse transcription, cDNA amplification, and library construction were performed according to the manufacturer's protocol. Libraries were sequenced on an Illumina NovaSeq 6000, targeted at a sequencing depth of 120,000 reads per nucleus. Sequencing reads were aligned to the mouse reference transcriptome (mm10, version 2020-A) using CellRanger (version 6.1.2).

We performed SSv4 processing according to previously established procedures (Tasic et al., 2018) available at protocols.io (dx.doi.org/10.17504/protocols.io.8epv517xdl1b/v2). Briefly, poly(A) RNA

was reverse transcribed and full-length cDNA was amplified using the SMART-Seq v4 Ultra Low Input RNA Kit for Sequencing (634894, Takara). Samples were amplified for 16-21 cycles in eight-well strips. Nextera XT DNA Library Preparation (FC-131-1096, Illumina) with a custom index set (Integrated DNA Technologies) were used for library preparation following the manufacturer's instructions, with minor modifications to reduce the volumes of all reagents and cDNA input to 0.2x of the original protocol. Libraries were sequenced on either an Illumina NovaSeqSP-XP or an Illumina NextSeq2000, targeting 500,000 reads per nucleus. Samples were aligned to Mouse reference, mm10/genecode.vM23, using STAR (version 2.7.1a).

snRNA-seq pre-processing, quality control, and removal of second-order nuclei: Ambient RNA contamination was removed from each sample using CellBender (Fleming et al., 2022) (version 0.2.1, 'remove-background', default parameters). We then used Seurat version 4.3.0 for downstream analysis (Hao et al., 2021). First, each replicate from the same ROI-enriching dissection was merged using Seurat's 'merge' function (merge.data = TRUE) and then the percentage of counts originating from mitochondrial RNA per nucleus was calculated. Nuclei were filtered to retain only those with less than 5% mitochondrial counts and more than 2000 genes detected. Standard processing for each sample was performed, which consisted of normalization of feature expression (NormalizeData), identifying the most variable genes with FindVariableFeatures (selection.method = 'vst', nfeatures = 2000), and scaling expression values (ScaleData). We then performed principal component analysis (PCA; RunPCA) with 30 components (FindNeighbors) and clustered the nuclei using the Louvain algorithm with resolution set at 0.5, 1, 2, and 3 to obtain a spectrum of coarse to fine clusters (FindClusters). Finally, UMAP embedding was performed (RunUMAP).

Nuclei were then assessed for second-order labeling across each ROI. Briefly, GFP or mScarlet sequences were added to the mouse reference genome mm10-2020-A by mkref function from CellRanger (v5.0.1, on UCLA's server). The reference genomes with GFP or mScarlet sequence were uploaded to the 10x cloud analysis server, and the transcriptome counts including GFP or mScarlet were detected by CellRanger (v6.1.2). Since the GFP and mScarlet sequences are 93.60% similar, to increase the detection sensitivity and specificity, we used reference genome with GFP sequence to detect samples sorted on GFP signal and used reference genome with mScarlet sequence to detect samples sorted on mScarlet signal. The nuclei with at least one GFP or mScarlet count from the raw count matrix were considered as XFP+ nuclei, and the percentage of XFP+ nuclei were calculated within each cluster. In general, 10% cut off threshold was used to assess first- and second-order labeling.

Clustering and type assignment: SPN types were defined iteratively through multiple rounds of clustering of the 10x data. After clusters containing <10% of nuclei expressing XFP were removed, each Seurat object consisting of replicates from the same ROI-enriching dissection underwent the standard Seurat v4 workflow (normalization, variable feature identification, PCA, Louvain clustering, and UMAP embedding, as described above). Again, nuclei were clustered with resolution set at 0.5, 1, 2, and 3 to obtain a spectrum of coarse to fine clusters. Differential expression analysis was performed with model-based analysis of single-cell transcriptomes (MAST) (Finak et al., 2015) using Seurat's FindAllMarkers function (adjusted P <0.05) at the various resolutions. We reviewed the resulting markers and assigned type identity. In dissections from L5CTX, we merged several clusters based on shared expression of canonical marker genes (e.g., Fezf2, Bcl11b, Crym) and removed clusters with top DE genes that were mitochondrial and lncRNAs. We then merged Seurat objects from bordering regions (i.e., HY and MB; MB and PONS; PONS and MED) and re-ran the Seurat v4 workflow to

identify and merge duplicate types for those that are present across ROI-enriching dissections. At this point, clusters in RFA, M1M2S1, S2, HY, MB, and CB were well-resolved by marker genes but several clusters in PONS- and MED-enriching dissections were ill-defined. To define the final pons and medulla types in the SPN taxonomy (**Figure 2-1c**), we re-ran the Seurat v4 workflow on nuclei from PONS and MED together (**Figure 2-12**). Based on differential expression analysis of these clusters at the various resolutions, we identified a pattern of LIM Homeobox gene expression across nuclei from PONS and MED. We again subset and re-ran the Seurat v4 workflow on each of these five LIM-defined groups (i.e., Lmx1b, Lhx2/9, Lhx3/4, Lhx1/5, Lhx1/5+Lhx3/4 (**Figure 2-12d-f**).

This iterative annotation process identified 76 types across all SPNs. Seurat's FindAllMarkers (MAST test) was used to find the marker genes of the 76 SPN types. We tested only genes that were detected in a minimum of 25% of the nuclei (min.pct = 0.25) and that showed at least a 0.25-fold log-scale difference (logfc.threshold = 0.25) between the nuclei in type and all other nuclei. Genes are annotated as 'significant' if adjust p-value is less than 0.05 (**Table 2-2**).

Joint clustering 10x and SSv4 datasets: Types identified in the 10x dataset with the above iterative annotation process were then identified in the SSv4 data. Briefly, SSv4 data was processed with the Seurat v4 workflow and differential expression of clusters was performed. Clusters were assigned to one of the 76 SPN types based on top DE genes. Subsequently, all 10x and SSv4 were integrated together. To do this, all 10x Seurat objects from ROI-enriching dissections were merged using Seurat's 'merge' function (merge.data = TRUE) and the Seurat v4 workflow was run with SCTransform using 25 principal components. In parallel, all SSv4 Seurat objects from ROI-enriching dissections were similarly merged and the Seurat v4 workflow with SCTransform was run using 30 principal components. The 10x and SSv4 were then integrated using Seurat's integration pipeline. Briefly,

integration features were selected using Seurat's 'SelectIntegrationFeatures function (nfeatures = 3000). SCT-based integration was then run (PrepSCTIntegration, FindIntegrationAnchors, IntegrateData). Finally, the Seurat V4 workflow was run for a final time as above (RunPCA, FindNeighbors, FindClusters, RunUMAP) with 30 components and 0.5 resolution.

Constructing cell type taxonomy tree: To construct the SPN type taxonomy tree of all SPNs in the 10x and SSv4 datasets, we utilized the build_dend function in the scrattch.bigcat package, as described the companion study(Yao et al., 2023). Specifically, we calculated the average expression of 1,871 marker genes at the 'type' level and used this information to build the tree. To gain a comprehensive understanding of the cell type landscape and relationships between cell types, we considered the taxonomy tree, the UMAPs, and the constellation plot.

Assigning division, subclass, and type names: All SPNs were organized into a hierarchy with three levels (divisions, subclasses, and types) based on the cell type taxonomy tree (**Figure 2-1c**). Divisions were assigned based on the splits at the first level of the taxonomy tree (and fine-tuned based on neurotransmitter identity for the 'Modulatory' Division), resulting in three Divisions. Subclasses for Divisions 1 and 3 were determined based on splits at the subsequent taxonomy tree levels, resulting in 3 subclasses in Division 1 and 5 subclasses in Division 3. Two types within Division 2 were glutamatergic and arose from MB-enriching dissections, so were assigned to the 'MB Glut' subclass. As clustering the types within Division 2 was based on the abovementioned LIM Homeobox genes, subclasses for Division 2 were similarly defined by LIM Homeobox gene expression along with the major expressed neurotransmitter to yield 5 additional subclasses in Division 2. Subclasses and types were named using a combination of representative regions, major neurotransmitters, and, in some

cases, one or two marker genes. Type ID numbers were assigned sequentially based on the taxonomy tree order of types.

Constellation plot: To visualize the global relatedness between cell types, we employed a constellation plot. The plot was generated by representing each transcriptomic type as a node (circle) in log-scale, with the surface area of each node reflecting the number of nuclei within the type. The position of each node was determined by the centroid position of the corresponding type in UMAP coordinates. The relationships between nodes were represented by edges, which were calculated as follows. First, we identified the 15 nearest neighbors for each cell in reduced dimension space and summarized them by type. Next, we calculated the fraction of nearest neighbors that were assigned to other subclasses for each subclass. The edges were drawn between two nodes that had > 5% of nearest neighbors in the connecting node, and the width of the edge at the node was scaled to reflect the fraction of nearest neighbors that were assigned to the connecting node. We then set the maximum fraction of "outside" neighbors for all nodes in the plot as the edge width = 100% of the node width. To create the plot, we utilized the plot_constellation function (included in scrattch.bigcat).

Module scores for feature expression programs: Seurat's 'AddModuleScore' function was used to calculate the average expression levels of modules of multiple genes (i.e., paralogous LIM homeobox genes in **Figure 2-12**).

Differential expression and Gene Ontology analysis: Differential expression analysis for projection target differences and Spp1+ vs. Spp1- neurons was performed with MAST (Finak et al., 2015) using Seurat's FindAllMarkers or FindMarkers function (adjusted $P < 0.05$). To identify enriched biological processes or molecular functions in gene sets, we utilized enrichR (Xie et al., 2021) and the

GO_Biological_Process_2021, GO_Cellular_Component_2021, and GO_Molecular_Function_2021 libraries.

SCENIC: To evaluate the activity of transcription factor regulons in each cluster of SPNs (pons-, and medulla-enriching dissections), we employed SCENIC (Aibar et al., 2017; Van de Sande et al., 2020) on SPNs from pons- and medulla-enriching dissections. First, we extracted the raw count matrix of the merged Seurat object and used it as input to identify co-expression modules by "grn." Next, we performed cis-regulatory motif enrichment analysis using "ctx" with a nes_threshold of 2.5 and a min_genes of 10. We then used "aucell" to calculate the regulon activity in each individual cell. To visualize the regulon activity in each cluster, we averaged and scaled the regulon activity by cluster. Specifically, we visualized the regulon activity of Lhx1, Lhx2, Lhx3, Lhx4, Lhx5, Lhx9, and Lmx1b using "pheatmap" in R. We downloaded the list of transcription factors from mouse from https://github.com/aertslab/pySCENIC/tree/master/resources and the transcription factor annotation motifs v9 collection from mouse from https://resources.aertslab.org/cistarget/.

Assessing heterogeneity of nuclei: To produce a measure of heterogeneity within the snRNAseq dataset (**Figure 2-15b**), we computed for each nucleus the average distance to the K nearest neighbors (KNN, k=15) in the reduced principle dimensional space (dimension = 100) and normalized it as z-score by subtracting the means and divided by standard deviation. Nuclei in the highly homogenous clusters have much shorter distance to their KNN compared to nuclei in highly heterogenous clusters. This metric can be used to measure for each nucleus, their local heterogeneity regardless of their cell type identities.

Mapping to AIBS whole brain scRNAseq: To assess the correspondence between the SPN types identified in this study with those in the companion AIBS whole brain (WB) taxonomy (Yao et al., 2023), we mapped 10x v3 SPN nuclei data onto the mouse WB taxonomy using Hierarchical Approximate Nearest Neighbor (HANN) mapping available in scrattch-mapping package and calculated the confusion matrix at cluster, supertype, and subclass levels of WB taxonomy (cluster level correspondence is shown in **Figure 2-6**). The correspondence was summarized by each SPN cell type with its members' average correlation of available marker genes to the mapped WB taxonomy clusters (**Tables 2-3 to 2-5**), which showed that more fine-grained types were identified in the midbrain and hindbrain region in this study.

Spatial localization of SPN types

Integration with AIBS whole brain MERFISH: To map SPN types to their anatomical locations, we leveraged data available in the companion AIBS WB taxonomy (Yao et al., 2023). Briefly, we performed integrative clustering using WB 10x v3 cells, WB MERFISH cells, and the 10x v3 nuclei SPN dataset using i_harmonize function from the scrattch.bigcat package. While the integrated clustering show great cell type correspondence for majority of cell types, it remains ambiguous for cell types present in the ventral medial region of the midbrain and hindbrain. Neurons in these areas are highly heterogeneous, but distinctions between cell types are subtle. These neurons are also heavily myelinated, making them very difficult to isolate for scRNAseq without substantial cell damage. Some of these types are likely better represented in the SPN taxonomy due to the more targeted sampling strategy than in the WB taxonomy. To further elucidate the cell type correspondence, we identified a subset of integrative clusters that contained at least 5 nuclei from SPN taxonomy, mapped the WB MERFISH and WB 10x v3 cells from these clusters to the SPN taxonomy and mapped the 10x v3

nuclei from SPN taxonomy to the subset of WB taxonomy covered by these integrated clusters. Clusters in SPN taxonomy with fewer than 3 mapped cells in WB taxonomy and vice versa were removed from the correspondence comparison. We compared the identities of the nuclei from SPN taxonomy and their mapped clusters from the WB taxonomy, and generated the confusion matrix at cluster, supertype, and subclass level of WB taxonomy. MERFISH cells from the integrated clusters shared by SPN clusters were mapped to SPN taxonomy directly. All the mapping were performed by assigning cells/nuclei to the nearest cluster centroid for the corresponding taxonomy using the top DE genes between all pairs of clusters, except for MERFISH dataset, in which case, all the genes on the MERFISH gene panels were used.

MERFISH Spot Plotting: After decoding of raw MERFISH data we obtained a file containing the x, y, and z location of all detected mRNA molecules (detected_transcripts.csv) for each section. The data from each section was rotated to have the dorsal surface point upwards and ventral downwards using the rotate_2d function from the rearrr package. The locations of mRNA molecules were plotted as a scatterplot using the ggplot function from the ggplot2 package with the z-planes collapsed into one. Genes of interest were highlighted in red while the remaining molecules were colored in grey to provide anatomical context of the section. Files were exported as .png file with a resolution of 1200 dpi (**Figure 2-12h**).

Cre-dependent retrograde labeling: To validate anatomical locations of neurons expressing certain marker genes, retrograde labeling was performed in various recombinase driver lines (**Table 2-11**). Briefly, AAV2/retro-CAG-FLEX-H2B-GFP (produced by Boston Children's Hospital Viral core, $5x10^{12}$ gc/mL) was injected in the cervical and lumbar spinal cord as described above, animals were perfused 2 weeks post-injection, and tissue was processed as described above to locate GFP-expressing nuclei.

Mouse lines were selected based on clustering results. For lines requiring tamoxifen induction, tamoxifen was administered via oral gavage (100 μL per 25g body weight) consecutively for 7 days, starting from 7 days post spinal injection. Mice were sacrificed 7 days after completion of tamoxifen dosing. Tamoxifen (VWR IC15673883) was prepared by dissolving in corn oil (20 mg/ml) followed by overnight rotation. Tissue sections were cryosectioned (50 μm, coronal) and one fourth of the serial sections were IHC processed (AVES Chicken-anti-GFP primary 1:500 dilution, Donkey-anti-Chicken 488 secondary 1:1000 dilution) and imaged on a VS120 slide scanner as described above. Labeled nuclei were segmented and reconstructed using NeuroInfo. Briefly, images containing individual sections were aligned and registered to the Allen CFF with NeuroInfo. H2B-positive nuclei were then detected and mapped to the registered atlas. Cre-specific detections were merged into the same file for comparison and visualization purposes. Horizontal, coronal, or sagittal projections of the three-dimensional reconstructions were output via Neuroinfo's 3D visualization window.

Hybridization chain reaction on sorted nuclei

To validate select DE genes between cervical and lumbar projecting SPNs, digital hybridization chain reaction (dHCR; Molecular Instruments) and quantification was performed on sorted nuclei. GFP+ and/or mScarlet+ nuclei were FANS sorted as described above (BD FACSAria, 100 μm nozzle) into a PCR tube containing 100uL of sort buffer. The sorted nucleus suspension was transferred onto a poly-D-lysine coated glass coverslip, incubated for 30 minutes at 4ºC, fixed with 4% PFA for 15 minutes, and rinsed 3 times with PBS at RT. Subsequently, dHCR was performed by adapting manufacturer's protocols for mammalian cells on a slide. Briefly, coverslips were incubated in 70% ethanol overnight at -20ºC. Subsequently, ethanol was aspirated, samples allowed to air dry, washed three times with 2x SSC at RT, then pre-hybridized with probe hybridization buffer for 30 minutes at 37ºC. The probe hybridization buffer was then removed and a freshly prepared probe solution (16nM

probe in probe hybridization buffer) was added to the samples for overnight incubation at 37ºC. After 12-16 hours, the probe solution was removed and samples washed with probe wash buffer four times at 37ºC, followed by two washes with 5x SSCT (SSC + Tween-20) at RT. Samples were then pre-amplified in amplification buffer for 30 minutes at RT. Hairpins were freshly prepared by heating to 95ºC for 90 seconds, snap-cooling to RT for 30 minutes, then adding to the amplification buffer at a concentration of 0.06μM. The hairpin solution was added to the samples for 60 minutes to ensure single-molecule dots were diffraction limited. The hairpin solution was removed, and samples washed five times with 5x SSCT at RT. Nuclei were counterstained with DAPI at a final concentration of 1 μg/mL for 5 minutes and washed three times with PBS. Nuclei were mounted with ProLong Glass and sealed with clear nail polish. ProLong Glass was allowed to cure for 48-60 hours at RT and then stored at 4ºC until imaging. Forty probe sets were used for each probe, and probe names and associated accession numbers were as follows: Pcdh11x (NM_001271809.1), Fezf2 (NM_080433.3). Nuclei were imaged on a Zeiss LSM 900 confocal using a 63x oil immersion objective with 2x zoom, confocal resolution, and optimal z-stacks. For quantification, z-stacks were converted to maximal intensity orthogonal projections and the number of punctae were manually quantified per nucleus. Statistical significance was assessed with the Wilcoxon test (ggpubr).

2.8 REFERENCES.

Aibar, S., González-Blas, C. B., Moerman, T., Huynh-Thu, V. A., Imrichova, H., Hulselmans, G., Rambow, F., Marine, J. C., Geurts, P., Aerts, J., Van Den Oord, J., Atak, Z. K., Wouters, J., & Aerts, S. (2017). SCENIC: single-cell regulatory network inference and clustering. *Nature Methods 2017 14:11*, *14*(11), 1083–1086. https://doi.org/10.1038/nmeth.4463

Alkaslasi, M. R., Piccus, Z. E., Hareendran, S., Silberberg, H., Chen, L., Zhang, Y., Petros, T. J., & Le Pichon, C. E. (2021). Single nucleus RNA-sequencing defines unexpected diversity of cholinergic neuron types in the adult mouse spinal cord. *Nature Communications 2021 12:1*, *12*(1), 1–14. https://doi.org/10.1038/s41467-021-22691-2

Arber, S., & Costa, R. M. (2022). Networking brainstem and basal ganglia circuits for movement. *Nature Reviews. Neuroscience*, *23*(6), 342–360. https://doi.org/10.1038/S41583-022-00581-W

Arlotta, P., Molyneaux, B. J., Chen, J., Inoue, J., Kominami, R., & MacKlis, J. D. (2005). Neuronal subtype-specific genes that control corticospinal motor neuron development in vivo. *Neuron*, *45*(2), 207–221. https://doi.org/10.1016/J.NEURON.2004.12.036

Baker, S. N., Zaaimi, B., Fisher, K. M., Edgley, S. A., & Soteropoulos, D. S. (2015). Pathways mediating functional recovery. *Progress in Brain Research*, *218*, 389–412. https://doi.org/10.1016/BS.PBR.2014.12.010

Bareyre, F. M., Kerschensteiner, M., Misgeld, T., & Sanes, J. R. (2005). Transgenic labeling of the corticospinal tract for monitoring axonal responses to spinal cord injury. *Nature Medicine*, *11*(12), 1355–1360. https://doi.org/10.1038/NM1331

BICCN. (2021). A multimodal cell census and atlas of the mammalian primary motor cortex. *Nature 2021 598:7879*, *598*(7879), 86–102. https://doi.org/10.1038/s41586-021-03950-0

Bittencourt, J. C., Vaughan, J., Arias, C., Rissman, R. A., Vale, W. W., & Sawchenko, P. E. (1999). Rapid Publication Urocortin Expression in Rat Brain: Evidence Against a Pervasive Relationship of Urocortin-Containing Projections With Targets Bearing Type 2 CRF Receptors. *THE JOURNAL OF COMPARATIVE NEUROLOGY*, *415*, 285–312. https://doi.org/10.1002/(SICI)1096-9861(19991220)415:3

Blum, J. A., Klemm, S., Shadrach, J. L., Guttenplan, K. A., Nakayama, L., Kathiria, A., Hoang, P. T., Gautier, O., Kaltschmidt, J. A., Greenleaf, W. J., & Gitler, A. D. (2021). Single-cell transcriptomic analysis of the adult mouse spinal cord reveals molecular diversity of autonomic and skeletal motor neurons. *Nature Neuroscience 2021 24:4*, *24*(4), 572–583. https://doi.org/10.1038/s41593-020-00795-0

Bouvier, J., Caggiano, V., Leiras, R., Caldeira, V., Bellardita, C., Balueva, K., Fuchs, A., & Kiehn, O. (2015). Descending Command Neurons in the Brainstem that Halt Locomotion. *Cell*, *163*(5), 1191–1203. https://doi.org/10.1016/J.CELL.2015.10.074

Bretzner, F., & Brownstone, R. M. (2013). Lhx3-Chx10 Reticulospinal Neurons in Locomotor Circuits. *Journal of Neuroscience*, *33*(37), 14681–14692. https://doi.org/10.1523/JNEUROSCI.5231-12.2013

Brodal, A., & Pompeiano, O. (1957). The vestibular nuclei in the cat. *Journal of Anatomy*, *91*(Pt 4), 438. https://www.ncbi.nlm.nih.gov/pmc/articles/PMC1244900/

Brownstone, R. M., & Chopek, J. W. (2018). Reticulospinal systems for tuning motor commands. *Frontiers in Neural Circuits*, *12*, 1–10. https://doi.org/10.3389/FNCIR.2018.00030/BIBTEX

Canty, A. J., Greferath, U., Turnley, A. M., & Murphy, M. (2006). Eph tyrosine kinase receptor EphA4 is required for the topographic mapping of the corticospinal tract. *Proceedings of the National Academy of Sciences of the United States of America*, *103*(42), 15629. https://doi.org/10.1073/PNAS.0607350103

Capelli, P., Pivetta, C., Esposito, M. S., & Arber, S. (2017). Locomotor speed control circuits in the caudal brainstem. *Nature*, *551*(7680), 373–377. https://doi.org/10.1038/NATURE24064

Castiglioi, A. J., Gallaway, M. C., & Coulter, J. D. (1978). Spinal projections from the midbrain in monkey. *The Journal of Comparative Neurology*, *178*(2), 329–345. https://doi.org/10.1002/CNE.901780208

Cechetto, D. F., & Saper, C. B. (1988). Neurochemical organization of the hypothalamic projection to the spinal cord in the rat. *Journal of Comparative Neurology*, *272*(4), 579–604. https://doi.org/10.1002/CNE.902720410

Cepeda-Nieto, A. C., Pfaff, S. L., & Varela-Echavarría, A. (2005). Homeodomain transcription factors in the development of subsets of hindbrain reticulospinal neurons. *Molecular and Cellular Neuroscience*, *28*(1), 30–41. https://doi.org/10.1016/J.MCN.2004.06.016

Chopek, J. W., Zhang, Y., & Brownstone, R. M. (2021). Intrinsic brainstem circuits comprised of Chx10-expressing neurons contribute to reticulospinal output in mice. *Journal of Neurophysiology*, *126*(6), 1978–1990. https://doi.org/10.1152/JN.00322.2021

Courtine, G., & Sofroniew, M. V. (2019). Spinal cord repair: advances in biology and technology. *Nature Medicine*, *25*(6). https://doi.org/10.1038/S41591-019-0475-6

Cregg, J. M., Leiras, R., Montalant, A., Wanken, P., Wickersham, I. R., & Kiehn, O. (2020). Brainstem neurons that command mammalian locomotor asymmetries. *Nature Neuroscience 2020 23:6*, *23*(6), 730–740. https://doi.org/10.1038/s41593-020-0633-7

Deliagina, T. G., Zelenin, P. V., & Orlovsky, G. N. (2002). Encoding and decoding of reticulospinal commands. *Brain Research. Brain Research Reviews*, *40*(1–3), 166–177. https://doi.org/10.1016/S0165-0173(02)00199-6

Diek, D., Smidt, M. P., & Mesman, S. (2022). Molecular Organization and Patterning of the Medulla Oblongata in Health and Disease. *International Journal of Molecular Sciences*, *23*(16). https://doi.org/10.3390/IJMS23169260

Dos Santos Júnior, E. D., Da Silva, A. V., Da Silva, K. R. T., Haemmerle, C. A. S., Batagello, D. S., Da Silva, J. M., Lima, L. B., Da Silva, R. J., Diniz, G. B., Sita, L. V., Elias, C. F., & Bittencourt, J. C. (2015). The centrally projecting Edinger-Westphal nucleus--I: Efferents in the rat brain. *Journal of Chemical Neuroanatomy*, *68*, 22–38. https://doi.org/10.1016/J.JCHEMNEU.2015.07.002

Duan, X., Krishnaswamy, A., De La Huerta, I., & Sanes, J. R. (2014). Type II Cadherins Guide Assembly of a Direction-Selective Retinal Circuit. *Cell*, *158*(4), 793–807. https://doi.org/10.1016/J.CELL.2014.06.047

Ecker, J. R., Geschwind, D. H., Kriegstein, A. R., Ngai, J., Osten, P., Polioudakis, D., Regev, A., Sestan, N., Wickersham, I. R., & Zeng, H. (2017). The BRAIN Initiative Cell Census Consortium: Lessons Learned toward Generating a Comprehensive Brain Cell Atlas. *Neuron*, *96*(3), 542–557. https://doi.org/10.1016/J.NEURON.2017.10.007

Esposito, M. S., Capelli, P., & Arber, S. (2014). Brainstem nucleus MdV mediates skilled forelimb motor tasks. *Nature*, *508*(7496), 351–356. https://doi.org/10.1038/NATURE13023

Faraco, J. H., Appelbaum, L., Marin, W., Gaus, S. E., Mourrain, P., & Mignot, E. (2006). Regulation of hypocretin (orexin) expression in embryonic zebrafish. *The Journal of Biological Chemistry*, *281*(40), 29753–29761. https://doi.org/10.1074/JBC.M605811200

Ferreira-Pinto, M. J., Ruder, L., Capelli, P., & Arber, S. (2018). Connecting Circuits for Supraspinal Control of Locomotion. *Neuron*, *100*(2), 361–374. https://doi.org/10.1016/J.NEURON.2018.09.015

Finak, G., McDavid, A., Yajima, M., Deng, J., Gersuk, V., Shalek, A. K., Slichter, C. K., Miller, H. W., McElrath, M. J., Prlic, M., Linsley, P. S., & Gottardo, R. (2015). MAST: A flexible statistical framework for assessing transcriptional changes and characterizing heterogeneity in single-cell

RNA sequencing data. *Genome Biology*, *16*(1), 1–13. https://doi.org/10.1186/S13059-015-0844-5/FIGURES/6

Fleming, S. J., Chaffin, M. D., Arduini, A., Akkad, A.-D., Banks, E., Marioni, J. C., Philippakis, A. A., Ellinor, P. T., & Babadi, M. (2022). Unsupervised removal of systematic background noise from droplet-based single-cell experiments using CellBender. *BioRxiv*, 791699. https://doi.org/10.1101/791699

Foster, E., Wildner, H., Tudeau, L., Haueter, S., Ralvenius, W. T., Jegen, M., Johannssen, H., Hösli, L., Haenraets, K., Ghanem, A., Conzelmann, K. K., Bösl, M., & Zeilhofer, H. U. (2015). Targeted Ablation, Silencing, and Activation Establish Glycinergic Dorsal Horn Neurons as Key Components of a Spinal Gate for Pain and Itch. *Neuron*, *85*(6), 1289–1304. https://doi.org/10.1016/J.NEURON.2015.02.028

Franklin, K., & Paxinos, G. (2008). *The Mouse Brain in Stereotaxic Coordinates* (Third). Elsevier Academic Press. https://scholar.google.com/scholar_lookup?&title=The%20mouse%20brain%20in%20stereotaxic%20coordinates&publication_year=2008&author=Franklin%2CKBJ&author=Paxinos%2CG

Ganley, R. P., Werder, K., Wildner, H., & Zeilhofer, H. U. (2021). Spinally projecting noradrenergic neurons of the locus coeruleus display resistance to AAV2retro-mediated transduction. *Molecular Pain*, *17*. https://doi.org/10.1177/17448069211037887

Golan, N., Kauer, S., Ehrlich, D. B., Ravindra, N., Dijk, D. van, & Cafferty, W. B. (2021). Single-Cell Transcriptional Profiling of the Adult Corticospinal Tract Reveals Forelimb and Hindlimb Molecular Specialization. *BioRxiv*, 2021.06.02.446653. https://doi.org/10.1101/2021.06.02.446653

Gras, C., Herzog, E., Bellenchi, G. C., Bernard, V., Ravassard, P., Pohl, M., Gasnier, B., Giros, B., & El Mestikawy, S. (2002). A Third Vesicular Glutamate Transporter Expressed by Cholinergic and Serotoninergic Neurons. *Journal of Neuroscience*, *22*(13), 5442–5451. https://doi.org/10.1523/JNEUROSCI.22-13-05442.2002

Gray, P. A. (2013). Transcription factors define the neuroanatomical organization of the medullary reticular formation. *Frontiers in Neuroanatomy*, *7*(APR). https://doi.org/10.3389/FNANA.2013.00007

Griffin, J. M., & Bradke, F. (2020). Therapeutic repair for spinal cord injury: combinatory approaches to address a multifaceted problem. *EMBO Molecular Medicine*, *12*(3). https://doi.org/10.15252/EMMM.201911505

Grillner, S., & Wallén, P. (1985). Central pattern generators for locomotion, with special reference to vertebrates. *Annual Review of Neuroscience*, *8*(1), 233–261. https://doi.org/10.1146/ANNUREV.NE.08.030185.001313

Hao, Y., Hao, S., Andersen-Nissen, E., Mauck, W. M., Zheng, S., Butler, A., Lee, M. J., Wilk, A. J., Darby, C., Zager, M., Hoffman, P., Stoeckius, M., Papalexi, E., Mimitou, E. P., Jain, J., Srivastava, A., Stuart, T., Fleming, L. M., Yeung, B., … Satija, R. (2021). Integrated analysis of multimodal single-cell data. *Cell*, *184*(13), 3573-3587.e29. https://doi.org/10.1016/J.CELL.2021.04.048

Hardiman, O., Al-Chalabi, A., Chio, A., Corr, E. M., Logroscino, G., Robberecht, W., Shaw, P. J., Simmons, Z., & Van Den Berg, L. H. (2017). Amyotrophic lateral sclerosis. *Nature Reviews. Disease Primers*, *3*. https://doi.org/10.1038/NRDP.2017.71

Hippenmeyer, S., Vrieseling, E., Sigrist, M., Portmann, T., Laengle, C., Ladle, D. R., & Arber, S. (2005). A Developmental Switch in the Response of DRG Neurons to ETS Transcription Factor Signaling. *PLOS Biology*, *3*(5), e159. https://doi.org/10.1371/JOURNAL.PBIO.0030159

Holstege, G. (1998). The emotional motor system in relation to the supraspinal control of micturition and mating behavior. *Behavioural Brain Research*, *92*(2), 103–109. https://doi.org/10.1016/S0166-4328(97)00182-4

Holstege, J. C., & Kuypers, H. G. J. M. (1987). Brainstem projections to spinal motoneurons: An update. *Neuroscience*, *23*(3), 809–821. https://doi.org/10.1016/0306-4522(87)90160-6

Horn, A. K. E. (2006). The reticular formation. *Progress in Brain Research*, *151*, 127–155. https://doi.org/10.1016/S0079-6123(05)51005-7

Huang, K. W., Ochandarena, N. E., Philson, A. C., Hyun, M., Birnbaum, J. E., Cicconet, M., & Sabatini, B. L. (2019). Molecular and anatomical organization of the dorsal raphe nucleus. *ELife*, *8*. https://doi.org/10.7554/ELIFE.46464

Humphries, M. D., Gurney, K., & Prescott, T. J. (2006). The brainstem reticular formation is a small-world, not scale-free, network. *Proceedings. Biological Sciences*, *273*(1585), 503–511. https://doi.org/10.1098/RSPB.2005.3354

Iguchi, T., Oka, Y., Yasumura, M., Omi, M., Kuroda, K., Yagi, H., Xie, M. J., Taniguchi, M., Bastmeyer, M., & Sato, M. (2021). Mutually Repulsive EphA7–EfnA5 Organize Region-to-Region Corticopontine Projection by Inhibiting Collateral Extension. *Journal of Neuroscience*, *41*(22), 4795–4808. https://doi.org/10.1523/JNEUROSCI.0367-20.2021

Jordan, L. M., Liu, J., Hedlund, P. B., Akay, T., & Pearson, K. G. (2008). Descending command systems for the initiation of locomotion in mammals. *Brain Research Reviews*, *57*(1), 183–191. https://doi.org/10.1016/J.BRAINRESREV.2007.07.019

Kamiyama, T., Kameda, H., Murabe, N., Fukuda, S., Yoshioka, N., Mizukami, H., Ozawa, K., & Sakurai, M. (2015). Corticospinal tract development and spinal cord innervation differ between cervical and lumbar targets. *The Journal of Neuroscience : The Official Journal of the Society for Neuroscience*, *35*(3), 1181–1191. https://doi.org/10.1523/JNEUROSCI.2842-13.2015

Kathe, C., Skinnider, M. A., Hutson, T. H., Regazzi, N., Gautier, M., Demesmaeker, R., Komi, S., Ceto, S., James, N. D., Cho, N., Baud, L., Galan, K., Matson, K. J. E., Rowald, A., Kim, K., Wang, R., Minassian, K., Prior, J. O., Asboth, L., … Courtine, G. (2022). The neurons that restore walking after paralysis. *Nature*, *611*(7936), 540–547. https://doi.org/10.1038/S41586-022-05385-7

Kebschull, J. M., Richman, E. B., Ringach, N., Friedmann, D., Albarran, E., Kolluru, S. S., Jones, R. C., Allen, W. E., Wang, Y., Cho, S. W., Zhou, H., Ding, J. B., Chang, H. Y., Deisseroth, K., Quake, S. R., & Luo, L. (2020). Cerebellar nuclei evolved by repeatedly duplicating a conserved cell-type set. *Science*, *370*(6523). https://doi.org/10.1126/SCIENCE.ABD5059/SUPPL_FILE/ABD5059_TABLE_S5.XLS

Kiehn, O. (2011). Development and functional organization of spinal locomotor circuits. *Current Opinion in Neurobiology*, *21*(1), 100–109. https://doi.org/10.1016/J.CONB.2010.09.004

Kim, G., Gautier, O., Tassoni-Tsuchida, E., Ma, X. R., & Gitler, A. D. (2020). ALS Genetics: Gains, Losses, and Implications for Future Therapies. *Neuron*, *108*(5), 822–842. https://doi.org/10.1016/J.NEURON.2020.08.022

Koblinger, K., Füzesi, T., Ejdrygiewicz, J., Krajacic, A., Bains, J. S., & Whelan, P. J. (2014). Characterization of A11 Neurons Projecting to the Spinal Cord of Mice. *PLoS ONE*, *9*(10), 109636. https://doi.org/10.1371/JOURNAL.PONE.0109636

Krumlauf, R., & Wilkinson, D. G. (2021). Segmentation and patterning of the vertebrate hindbrain. *Development (Cambridge, England)*, *148*(15). https://doi.org/10.1242/DEV.186460

Kuypers, H. (1981). Anatomy of the descending pathways. In J. Brookhart & V. Mountcastle (Eds.), *Handbook of Physiology - The Nervous System* (Vol. 2, pp. 597–666). American Physiological Society.

https://www.scirp.org/(S(i43dyn45teexjx455qlt3d2q))/reference/ReferencesPapers.aspx?ReferenceID=895167

Leiras, R., Cregg, J. M., & Kiehn, O. (2022). Brainstem Circuits for Locomotion. *Annual Review of Neuroscience*, *45*, 63–85. https://doi.org/10.1146/ANNUREV-NEURO-082321-025137

Lemon, R. N. (2008). Descending pathways in motor control. *Annual Review of Neuroscience*, *31*, 195–218. https://doi.org/10.1146/ANNUREV.NEURO.31.060407.125547

Liang, H., Paxinos, G., & Watson, C. (2011). Projections from the brain to the spinal cord in the mouse. *Brain Structure and Function*, *215*(3), 159–186. https://doi.org/10.1007/S00429-010-0281-X

Liang, H., Paxinos, G., & Watson, C. (2012). The red nucleus and the rubrospinal projection in the mouse. *Brain Structure and Function*, *217*(2), 221–232. https://doi.org/10.1007/S00429-011-0348-3/FIGURES/7

Liu, Y., Hegarty, S., Winter, C., Wang, F., & He, Z. (2020). Viral vectors for neuronal cell type-specific visualization and manipulations. *Current Opinion in Neurobiology*, *63*, 67–76. https://doi.org/10.1016/J.CONB.2020.03.011

Marin, M. A., & Carmichael, S. T. (2018). Stroke in CNS white matter: Models and mechanisms. *Neuroscience Letters*, *684*, 193–199. https://doi.org/10.1016/J.NEULET.2018.07.039

Matho, K. S., Huilgol, D., Galbavy, W., He, M., Kim, G., An, X., Lu, J., Wu, P., Di Bella, D. J., Shetty, A. S., Palaniswamy, R., Hatfield, J., Raudales, R., Narasimhan, A., Gamache, E., Levine, J. M., Tucciarone, J., Szelenyi, E., Harris, J. A., … Huang, Z. J. (2021). Genetic dissection of the glutamatergic neuron system in cerebral cortex. *Nature 2021 598:7879*, *598*(7879), 182–187. https://doi.org/10.1038/S41586-021-03955-9

Molyneaux, B. J., Goff, L. A., Brettler, A. C., Chen, H. H., Brown, J. R., Hrvatin, S., Rinn, J. L., & Arlotta, P. (2015). DeCoN: Genome-wide Analysis of In Vivo Transcriptional Dynamics during Pyramidal Neuron Fate Selection in Neocortex. *Neuron*, *85*(2), 275–288. https://doi.org/10.1016/J.NEURON.2014.12.024

Nassi, J. J., Cepko, C. L., Born, R. T., & Beier, K. T. (2015). Neuroanatomy goes viral! *Frontiers in Neuroanatomy*, *9*(July), 80. https://doi.org/10.3389/FNANA.2015.00080/BIBTEX

Okaty, B. W., Sturrock, N., Lozoya, Y. E., Chang, Y., Senft, R. A., Lyon, K. A., Alekseyenko, O. V., & Dymecki, S. M. (2020). A single-cell transcriptomic and anatomic atlas of mouse dorsal raphe Pet1 neurons. *ELife*, *9*, 1–44. https://doi.org/10.7554/ELIFE.55523

Perkins, E., May, P. J., & Warren, S. (2013). Feed-forward and feedback projections of midbrain reticular formation neurons in the cat. *Frontiers in Neuroanatomy*, *7*(JAN). https://doi.org/10.3389/FNANA.2013.00055

Perkins, E., Warren, S., & May, P. J. (2009). The mesencephalic reticular formation as a conduit for primate collicular gaze control: tectal inputs to neurons targeting the spinal cord and medulla. *Anatomical Record (Hoboken, N.J. : 2007)*, *292*(8), 1162–1181. https://doi.org/10.1002/AR.20935

Peterson, B. W., Pitts, N. G., & Fukushima, K. (1979). Reticulospinal connections with limb and axial motoneurons. *Experimental Brain Research*, *36*(1), 1–20. https://doi.org/10.1007/BF00238464/METRICS

Pirondini, E., Carranza, E., Balaguer, J. M., Sorensen, E., Weber, D. J., Krakauer, J. W., & Capogrosso, M. (2022). Poststroke arm and hand paresis: should we target the cervical spinal cord? *Trends in Neurosciences*, *45*(8), 568–578. https://doi.org/10.1016/J.TINS.2022.05.002

Priest, M. F., Freda, S. N., Badong, D., Dumrongprechachan, V., & Kozorovitskiy, Y. (2021). Peptidergic modulation of fear responses by the Edinger-Westphal nucleus. *BioRxiv*, 2021.08.05.455317. https://doi.org/10.1101/2021.08.05.455317

Ren, J., Isakova, A., Friedmann, D., Zeng, J., Grutzner, S. M., Pun, A., Zhao, G. Q., Kolluru, S. S., Wang, R., Lin, R., Li, P., Li, A., Raymond, J. L., Luo, Q., Luo, M., Quake, S. R., & Luo, L. (2019). Single-cell transcriptomes and whole-brain projections of serotonin neurons in the mouse dorsal and median raphe nuclei. *ELife*, *8*. https://doi.org/10.7554/ELIFE.49424

Rheaume, B. A., Jereen, A., Bolisetty, M., Sajid, M. S., Yang, Y., Renna, K., Sun, L., Robson, P., & Trakhtenberg, E. F. (2018). Single cell transcriptome profiling of retinal ganglion cells identifies cellular subtypes. *Nature Communications 2018 9:1*, *9*(1), 1–17. https://doi.org/10.1038/s41467-018-05134-3

Robinson, F. R., Phillips, J. O., & Fuchs, A. F. (1994). Coordination of gaze shifts in primates: brainstem inputs to neck and extraocular motoneuron pools. *The Journal of Comparative Neurology*, *346*(1), 43–62. https://doi.org/10.1002/CNE.903460104

Rossi, J., Balthasar, N., Olson, D., Scott, M., Berglund, E., Lee, C. E., Choi, M. J., Lauzon, D., Lowell, B. B., & Elmquist, J. K. (2011). Melanocortin-4 Receptors Expressed by Cholinergic Neurons Regulate Energy Balance and Glucose Homeostasis. *Cell Metabolism*, *13*(2), 195–204. https://doi.org/10.1016/J.CMET.2011.01.010

Russ, D. E., Cross, R. B. P., Li, L., Koch, S. C., Matson, K. J. E., Yadav, A., Alkaslasi, M. R., Lee, D. I., Le Pichon, C. E., Menon, V., & Levine, A. J. (2021). A harmonized atlas of mouse spinal cord cell types and their spatial organization. *Nature Communications 2021 12:1*, *12*(1), 1–20. https://doi.org/10.1038/s41467-021-25125-1

Sahni, V., Shnider, S. J., Jabaudon, D., Song, J. H. T., Itoh, Y., Greig, L. C., & Macklis, J. D. (2021). Corticospinal neuron subpopulation-specific developmental genes prospectively indicate mature segmentally specific axon projection targeting. *Cell Reports*, *37*(3), 109843. https://doi.org/10.1016/J.CELREP.2021.109843

Sathyamurthy, A., Barik, A., Dobrott, C. I., Matson, K. J. E., Stoica, S., Pursley, R., Chesler, A. T., & Levine, A. J. (2020). Cerebellospinal Neurons Regulate Motor Performance and Motor Learning. *Cell Reports*, *31*(6), 107595. https://doi.org/10.1016/J.CELREP.2020.107595

Sathyamurthy, A., Johnson, K. R., Matson, K. J. E., Dobrott, C. I., Li, L., Ryba, A. R., Bergman, T. B., Kelly, M. C., Kelley, M. W., & Levine, A. J. (2018). Massively Parallel Single Nucleus Transcriptional Profiling Defines Spinal Cord Neurons and Their Activity during Behavior. *Cell Reports*, *22*(8), 2216–2225. https://doi.org/10.1016/J.CELREP.2018.02.003

Savitt, J. M., Jang, S. S., Mu, W., Dawson, V. L., & Dawson, T. M. (2005). Bcl-x Is Required for Proper Development of the Mouse Substantia Nigra. *Journal of Neuroscience*, *25*(29), 6721–6728. https://doi.org/10.1523/JNEUROSCI.0760-05.2005

Scott, M. M., Williams, K. W., Rossi, J., Lee, C. E., & Elmquist, J. K. (2011). Leptin receptor expression in hindbrain Glp-1 neurons regulates food intake and energy balance in mice. *The Journal of Clinical Investigation*, *121*(6), 2413–2421. https://doi.org/10.1172/JCI43703

Scott, M. M., Wylie, C. J., Lerch, J. K., Murphy, R. A., Lobur, K., Herlitze, S., Jiang, W., Conlon, R. A., Strowbridge, B. W., & Deneris, E. S. (2005). A genetic approach to access serotonin neurons for in vivo and in vitro studies. *Proceedings of the National Academy of Sciences of the United States of America*, *102*(45), 16472–16477. https://doi.org/10.1073/PNAS.0504510102/SUPPL_FILE/04510FIG7.JPG

Shiota, C., Prasadan, K., Guo, P., Fusco, J., Xiao, X., & Gittes, G. K. (2017). GcgCreERT2knockin mice as a tool for genetic manipulation in pancreatic alpha cells. *Diabetologia*, *60*(12), 2399–2408. https://doi.org/10.1007/S00125-017-4425-X/TABLES/3

Shirasaki, R., & Pfaff, S. L. (2002). Transcriptional codes and the control of neuronal identity. *Annual Review of Neuroscience*, *25*, 251–281. https://doi.org/10.1146/ANNUREV.NEURO.25.112701.142916

Skagerberg, G., & Lindvall, O. (1985). Organization of diencephalic dopamine neurones projecting to the spinal cord in the rat. *Brain Research*, *342*(2), 340–351. https://doi.org/10.1016/0006-8993(85)91134-5

Steward, O., Yee, K. M., Metcalfe, M., Willenberg, R., Luo, J., Azevedo, R., Martin-Thompson, J. H., & Gandhi, S. P. (2021). Rostro-Caudal Specificity of Corticospinal Tract Projections in Mice. *Cerebral Cortex (New York, N.Y.: 1991)*, *31*(5), 2322–2344. https://doi.org/10.1093/CERCOR/BHAA338

Stornetta, R. L., & Guyenet, P. G. (2018). C1 neurons: a nodal point for stress? *Experimental Physiology*, *103*(3), 332–336. https://doi.org/10.1113/EP086435

Tasic, B., Menon, V., Nguyen, T. N., Kim, T. K., Jarsky, T., Yao, Z., Levi, B., Gray, L. T., Sorensen, S. A., Dolbeare, T., Bertagnolli, D., Goldy, J., Shapovalova, N., Parry, S., Lee, C., Smith, K., Bernard, A., Madisen, L., Sunkin, S. M., … Zeng, H. (2016). Adult mouse cortical cell taxonomy revealed by single cell transcriptomics. *Nature Neuroscience 2016 19:2*, *19*(2), 335–346. https://doi.org/10.1038/nn.4216

Tasic, B., Yao, Z., Graybuck, L. T., Smith, K. A., Nguyen, T. N., Bertagnolli, D., Goldy, J., Garren, E., Economo, M. N., Viswanathan, S., Penn, O., Bakken, T., Menon, V., Miller, J., Fong, O., Hirokawa, K. E., Lathia, K., Rimorin, C., Tieu, M., … Zeng, H. (2018). Shared and distinct transcriptomic cell types across neocortical areas. *Nature 2018 563:7729*, *563*(7729), 72–78. https://doi.org/10.1038/S41586-018-0654-5

Tervo, D. G. R., Hwang, B. Y., Viswanathan, S., Gaj, T., Lavzin, M., Ritola, K. D., Lindo, S., Michael, S., Kuleshova, E., Ojala, D., Huang, C. C., Gerfen, C. R., Schiller, J., Dudman, J. T., Hantman, A. W., Looger, L. L., Schaffer, D. V., & Karpova, A. Y. (2016). A designer AAV variant permits efficient retrograde access to projection neurons. *Neuron*, *92*(2), 372. https://doi.org/10.1016/J.NEURON.2016.09.021

Tillage, R. P., Sciolino, N. R., Plummer, N. W., Lustberg, D., Liles, L. C., Hsiang, M., Powell, J. M., Smith, K. G., Jensen, P., & Weinshenker, D. (2020). Elimination of galanin synthesis in noradrenergic neurons reduces galanin in select brain areas and promotes active coping behaviors. *Brain Structure and Function*, *225*(2), 785–803. https://doi.org/10.1007/S00429-020-02035-4/FIGURES/9

Tran, N. M., Shekhar, K., Whitney, I. E., Jacobi, A., Benhar, I., Hong, G., Yan, W., Adiconis, X., Arnold, M. E., Lee, J. M., Levin, J. Z., Lin, D., Wang, C., Lieber, C. M., Regev, A., He, Z., & Sanes, J. R. (2019). Single-Cell Profiles of Retinal Ganglion Cells Differing in Resilience to Injury Reveal Neuroprotective Genes. *Neuron*, *104*(6), 1039-1055.e12. https://doi.org/10.1016/J.NEURON.2019.11.006

Tuszynski, M. H., & Steward, O. (2012). Concepts and methods for the study of axonal regeneration in the CNS. *Neuron*, *74*(5), 777–791. https://doi.org/10.1016/J.NEURON.2012.05.006

Van Berlo, J. H., Kanisicak, O., Maillet, M., Vagnozzi, R. J., Karch, J., Lin, S. C. J., Middleton, R. C., Marbán, E., & Molkentin, J. D. (2014). c-kit+ cells minimally contribute cardiomyocytes to the heart. *Nature 2014 509:7500*, *509*(7500), 337–341. https://doi.org/10.1038/NATURE13309

Van de Sande, B., Flerin, C., Davie, K., De Waegeneer, M., Hulselmans, G., Aibar, S., Seurinck, R., Saelens, W., Cannoodt, R., Rouchon, Q., Verbeiren, T., De Maeyer, D., Reumers, J., Saeys, Y., & Aerts, S. (2020). A scalable SCENIC workflow for single-cell gene regulatory network analysis. *Nature Protocols 2020 15:7*, *15*(7), 2247–2276. https://doi.org/10.1038/s41596-020-0336-2

Van Den Pol, A. N. (1999). Hypothalamic hypocretin (orexin): robust innervation of the spinal cord. *The Journal of Neuroscience : The Official Journal of the Society for Neuroscience*, *19*(8), 3171–3182. https://doi.org/10.1523/JNEUROSCI.19-08-03171.1999

Vanderhaeghen, P., Lu, Q., Prakash, N., Frisén, J., Walsh, C. A., Frostig, R. D., & Flanagan, J. G. (2000). A mapping label required for normal scale of body representation in the cortex. *Nature Neuroscience*, *3*(4), 358–365. https://doi.org/10.1038/73929

Wang, X., Liu, Y., Li, X., Zhang, Z., Yang, H., Zhang, Y., Williams, P. R., Alwahab, N. S. A., Kapur, K., Yu, B., Zhang, Y., Chen, M., Ding, H., Gerfen, C. R., Wang, K. H., & He, Z. (2017). Deconstruction of Corticospinal Circuits for Goal-Directed Motor Skills. *Cell*, *171*(2), 440-455.e14. https://doi.org/10.1016/J.CELL.2017.08.014

Wang, Z., Maunze, B., Wang, Y., Tsoulfas, P., & Blackmore, M. G. (2018). Global Connectivity and Function of Descending Spinal Input Revealed by 3D Microscopy and Retrograde Transduction. *Journal of Neuroscience*, *38*(49), 10566–10581. https://doi.org/10.1523/JNEUROSCI.1196-18.2018

Wang, Z., Romanski, A., Mehra, V., Wang, Y., Brannigan, M., Campbell, B. C., Petsko, G. A., Tsoulfas, P., & Blackmore, M. G. (2022). Brain-wide analysis of the supraspinal connectome reveals anatomical correlates to functional recovery after spinal injury. *ELife*, *11*. https://doi.org/10.7554/ELIFE.76254

Warren, S., Waitzman, D. M., & May, P. J. (2008). Anatomical evidence for interconnections between the central mesencephalic reticular formation and cervical spinal cord in the cat and macaque. *Anatomical Record (Hoboken, N.J. : 2007)*, *291*(2), 141–160. https://doi.org/10.1002/AR.20644

Xie, Z., Bailey, A., Kuleshov, M. V., Clarke, D. J. B., Evangelista, J. E., Jenkins, S. L., Lachmann, A., Wojciechowicz, M. L., Kropiwnicki, E., Jagodnik, K. M., Jeon, M., & Ma'ayan, A. (2021). Gene Set Knowledge Discovery with Enrichr. *Current Protocols*, *1*(3), e90. https://doi.org/10.1002/CPZ1.90

Yao, Z., Velthoven, C. T. J. van, Kunst, M., Zhang, M., McMillen, D., Lee, C., Jung, W., Goldy, J., Abdelhak, A., Baker, P., Barkan, E., Bertagnolli, D., Campos, J., Carey, D., Casper, T., Chakka, A. B., Chakrabarty, R., Chavan, S., Chen, M., … Zeng, H. (2023). A high-resolution transcriptomic and spatial atlas of cell types in the whole mouse brain. *BioRxiv*, 2023.03.06.531121. https://doi.org/10.1101/2023.03.06.531121

Zheng, B., & Tuszynski, M. H. (2023). Regulation of axonal regeneration after mammalian spinal cord injury. *Nature Reviews. Molecular Cell Biology*. https://doi.org/10.1038/S41580-022-00562-Y

Zingg, B., Chou, X. lin, Zhang, Z. gang, Mesik, L., Liang, F., Tao, H. W., & Zhang, L. I. (2017). AAV-Mediated Anterograde Transsynaptic Tagging: Mapping Corticocollicular Input-Defined Neural Pathways for Defense Behaviors. *Neuron*, *93*(1), 33–47. https://doi.org/10.1016/J.NEURON.2016.11.045

3

Transcriptional and morphological characteristics of fast-conducting spinal projecting neurons

Publication: This chapter was adapted from a manuscript under revision at *Nature*, revision submitted in September 2023.

A taxonomy of transcriptomic cell types reveals organizational and functional principles of brain-wide spinal projecting neurons

Carla C. Winter[1,2,3,4,12], Anne Jacobi[1,2,11,12,✉], Junfeng Su[1,2,12], Leeyup Chung[1,2], Cindy T. J. van Velthoven[5], Zizhen Yao[5], Changkyu Lee[5], Zicong Zhang[1,2], Shuguang Yu[1,2], Kun Gao[6,7], Geraldine Duque Salazar[1,2], Evgenii Kegeles[1,2,3], Riki Kawaguchi[6,7], Yu Zhang[1,2], Makenzie C. Tomihiro[1,2], Junjie Zhu[1,2], Jing Tang[1,2], Xuan Song[1,2], Ryan J. Donahue[1,2], Qing Wang[6,7], Delissa McMillen[5], Michael Kunst[5], Kimberly A. Smith[5], Alexandra Krol[8], Guoping Feng[8,9], Yuanyuan Liu[10], Daniel H. Geschwind[6,7], Bosiljka Tasic[5], Hongkui Zeng[5,✉], Zhigang He[1,2,✉]

1. F.M. Kirby Neurobiology Center, Boston Children's Hospital, Boston, MA, USA
2. Departments of Neurology and Ophthalmology, Harvard Medical School, Boston, MA, USA
3. PhD Program in Biological and Biomedical Sciences, Harvard Medical School, Boston, MA, USA
4. Harvard-MIT MD-PhD Program, Harvard Medical School, Boston, MA, USA
5. Allen Institute for Brain Science, Seattle, WA, USA
6. Program in Neurogenetics, Department of Neurology, David Geffen School of Medicine, University of California Los Angeles, Los Angeles, CA, USA
7. Semel Institute for Neuroscience and Human Behavior, David Geffen School of Medicine, University of California Los Angeles, Los Angeles, CA, USA
8. McGovern Institute for Brain Research and the Department of Brain and Cognitive Sciences, Massachusetts Institute of Technology, Cambridge, MA, USA
9. The Stanley Center for Psychiatric Research, Broad Institute of MIT and Harvard, Cambridge, MA, USA
10. Somatosensation and Pain Unit, National Institute of Dental and Craniofacial Research, National Center for Complementary and Integrative Health, National Institutes of Health, Bethesda, MD, USA
11. Present address: F. Hoffman-La Roche, pRED, Basel, Switzerland
12. These authors contributed equally.

✉Correspondence: Zhigang He (zhigang.he@childrens.harvard.edu), Hongkui Zeng (HongkuiZ@alleninstitute.org), and Anne Jacobi (Anne.Jacobi@roche.com)

Author contributions: Conceptualization: C.C.W., A.J., H.Z., Z.H. Manuscript writing: C.C.W. and Z.H. Figure generation: Led by C.C.W, with help from J.S, L.C., E.K. Manuscript review and editing: contributions from all authors. Data analysis lead and coordination: C.C.W. Retrograde Injections: Led by Z.Z., with help from J.Z. and J.T. Histology and analysis: Led by C.C.W., with help from G.D.S. and R.J.D. Electrophysiological experiments and data analysis: Led by L.C., with help from C.C.W. and E.K.

3.1 ABSTRACT.

Spinal projecting neurons (SPNs) play crucial roles in transmitting brain commands to spinal cord circuits, influencing a wide range of functions. Understanding the electrophysiological properties of these neurons is essential for deciphering their functional outputs. We leveraged the transcriptomic atlas generated in **Chapter 2** to gain insights into the electrophysiological properties of SPN types. Focusing on rubrospinal neuron (RuSN) transcriptomic types, we analyzed gene expression patterns and identified heterogeneous RuSN subtypes expressing Pvalb, Kcng4, and Spp1. Immunohistochemistry confirmed the presence of distinct Spp1-positive (Spp1+) and Spp1-negative (Spp1-) RuSN populations. Electrophysiological recordings of Spp1+ and Spp1- RuSNs revealed significant differences in soma sizes, action potential characteristics, firing rates, and excitability. These findings highlight functionally distinct SPN populations with diverse electrophysiological profiles, suggesting the existence of multiple "cable lines" for relaying brain-derived commands. Our study enhances the understanding of descending pathways and provides insights into the physiological implications of different SPN subtypes.

3.2 INTRODUCTION.

Spinal projecting neurons (SPNs) transmit commands via action potentials from the brain to downstream spinal cord circuits to instruct an exceptionally diverse set of functions. The functional output of these commands is, in part, determined by their electrophysiological properties. Corticospinal neurons (CSNs), which arise in cortical layer 5 and project directly to the spinal cord, are among the best characterized population of SPNs in terms of their electrophysiological properties. Decades of research have established CSNs as large neurons with fast-conducting axons across various species (Chen et al., 1996b, 1996a; Dykes et al., 1988; Evarts, 1965; Suter et al., 2013; Vigneswaran et al., 2011). However, more recent literature has reported on the diversity of corticospinal projections

in the primate brain, indicating that the corticospinal system is comprised of both small and large neurons with slow- and fast- conducting properties, respectively (Firmin et al., 2014; Innocenti et al., 2019; Kraskov et al., 2019). The 100-fold size difference between the smallest and largest CSN axon (Firmin et al., 2014), and their corresponding difference in conduction velocity (Hursh, 1939), likely reflects their diverse functional outputs ranging from fine motor control to descending sensory modulation (Liu et al., 2018; X. Wang et al., 2017).

The presence of these morphologically and electrophysiologically distinct corticospinal pathways is only just beginning to be appreciated but offers an intriguing framework for understanding brain control of bodily function: descending pathways comprised of axons conducting at different velocities may be flexibly engaged to generate specific functions (Innocenti et al., 2019; Miri et al., 2017). Beyond CSNs, however, the electrophysiological properties of subcortical SPN populations remains even more uncharted, likely due to the lack of molecular handles by which to study these heterogeneous populations, limiting the ability to target them for electrophysiological recordings or manipulate them for functional interrogation. Therefore, the existence of "fast" and "slow" conducting pathways as a general functional principle of descending pathways remains unknown. As a first step toward probing the electrophysiological principles underlying brain control of bodily function, here we sought to leverage the recently generated transcriptomic atlas of SPNs across the entire mouse brain (**Chapter 2**[*]) to link molecular signatures with electrophysiological properties.

[*] **Chapter 3** is an extension of the transcriptomic taxonomy generated in **Chapter 2**, seeking to layer functional information on top of the anatomical and transcriptomic studies characteristics of cell types in the SPN taxonomy. For more background information and context for the results presented here, please refer to **Chapter 2**.

3.3 RESULTS.

3.3.1 ANATOMICAL DISTRIBUTION OF RUBROSPINAL TRANSCRIPTOMIC TYPES.

Despite being composed of a majority glutamatergic output, it is unknown if these SPNs differ in their electrophysiological properties. By analyzing the expression of top marker and activity-related genes across SPN types, we noticed a notable pattern of gene expression: Pvalb and Kcng4 were expressed in most rubrospinal neurons (RuSNs) and cerebellospinal neurons (CbSNs) and subsets of reticulospinal neurons (ReSNs), and these neurons strongly co-express Spp1 (**Figure 3-1a, b**). Parvalbumin (Pvalb) is well known for its expression in fast-spiking inhibitory cortical neurons (Bartholome et al., 2020), and Pvalb, Kcng4, and Spp1 are all associated with fast-conducting projection neurons such as alpha retinal ganglion cells (Krieger et al., 2017) and fast motor neurons (Müller et al., 2014), suggesting a similar electrophysiological profile in Pvalb/Kcng4/Spp1 positive SPNs.

To test this, we focused further analysis on RuSNs because of anatomical and electrophysiological accessibility of the midbrain red nucleus (RN). Clustering of RuSNs revealed heterogeneity in Pvalb/Kcng4/Spp1 expression among RuSN types: MB-RN and MB-RN-Foxp2 types have high expression of these genes, whereas MB-RN-Spp1-Negative has low expression, which is further confirmed by the higher sequencing depth SSv4 dataset (**Figure 3-2**). As Spp1 has the most robust immunohistochemistry (IHC) signal compared to Pvalb and Kcng4 (data not shown), we used Spp1 as a molecular handle to investigate Pvalb/Kcng4/Spp1 positive and negative populations. As expected, differential gene expression analysis between Spp1 positive (Spp1+) and negative (Spp1-) RuSNs revealed top differentially expressed genes that support electrophysiological (e.g., Pvalb, Kcng4, Kcnip4, Hpca, Kcnn3, Kcnc4, Gabrb1) and cell size (e.g., Spp1, Nefh, Nefm, Nefl, S100b) differences (**Figure 3-2**, **Figure 3-1c**, **Table 3-1**). IHC for Spp1 in retrogradely labeled tissue revealed that Spp1- RuSNs are primarily present in the rostral-lateral red nucleus (likely corresponding to the

parvocellular red nucleus, RPC) and Spp1+ RuSNs are abundant in the medial red nucleus (likely magnocellular red nucleus, RMC) (Z. Wang et al., 2018) (**Figure 3-3**).

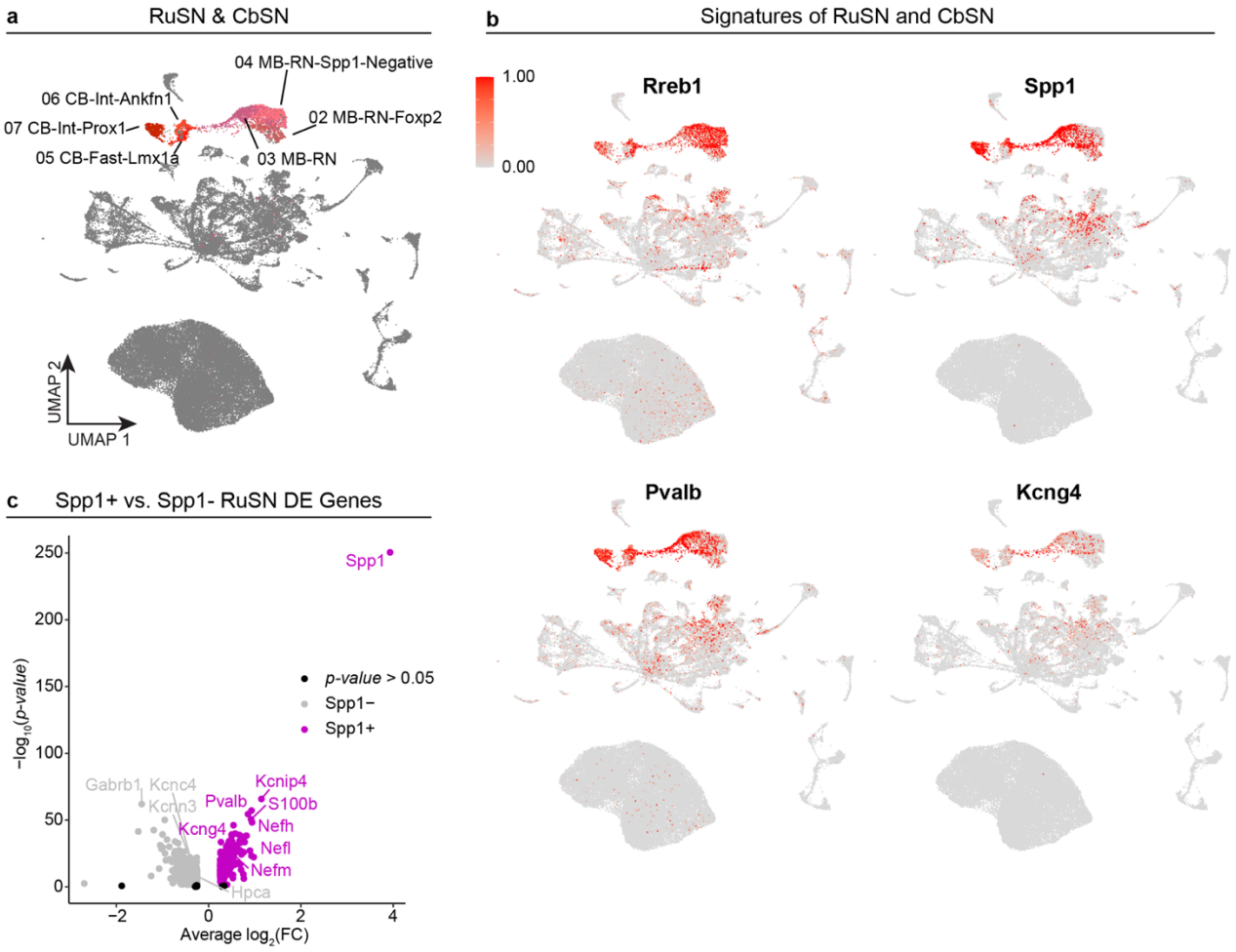


Figure 3-1: Activity- and size-related signatures of rubrospinal, cerebellospinal, and select reticulospinal neurons. a, UMAP representation of all SPNs with RuSNs and CbSNs highlighted. **b,** Expression of RuSN and CbSN marker genes (Rreb1, Spp1) and activity-related genes (Pvalb, Kcng4). **c,** Volcano plot of differentially expressed genes between Spp1+ and Spp1- RuSNs (SSv4 dataset, N = 1,031 nuclei). Select genes relevant for cell size (Spp1, Nefh, Nefm, Nefl, S100b) and activity (Pvalb, Kcng4, Kcnip4, Hpca, Kcnn3, Kcnc4, Gabrb1) are annotated.

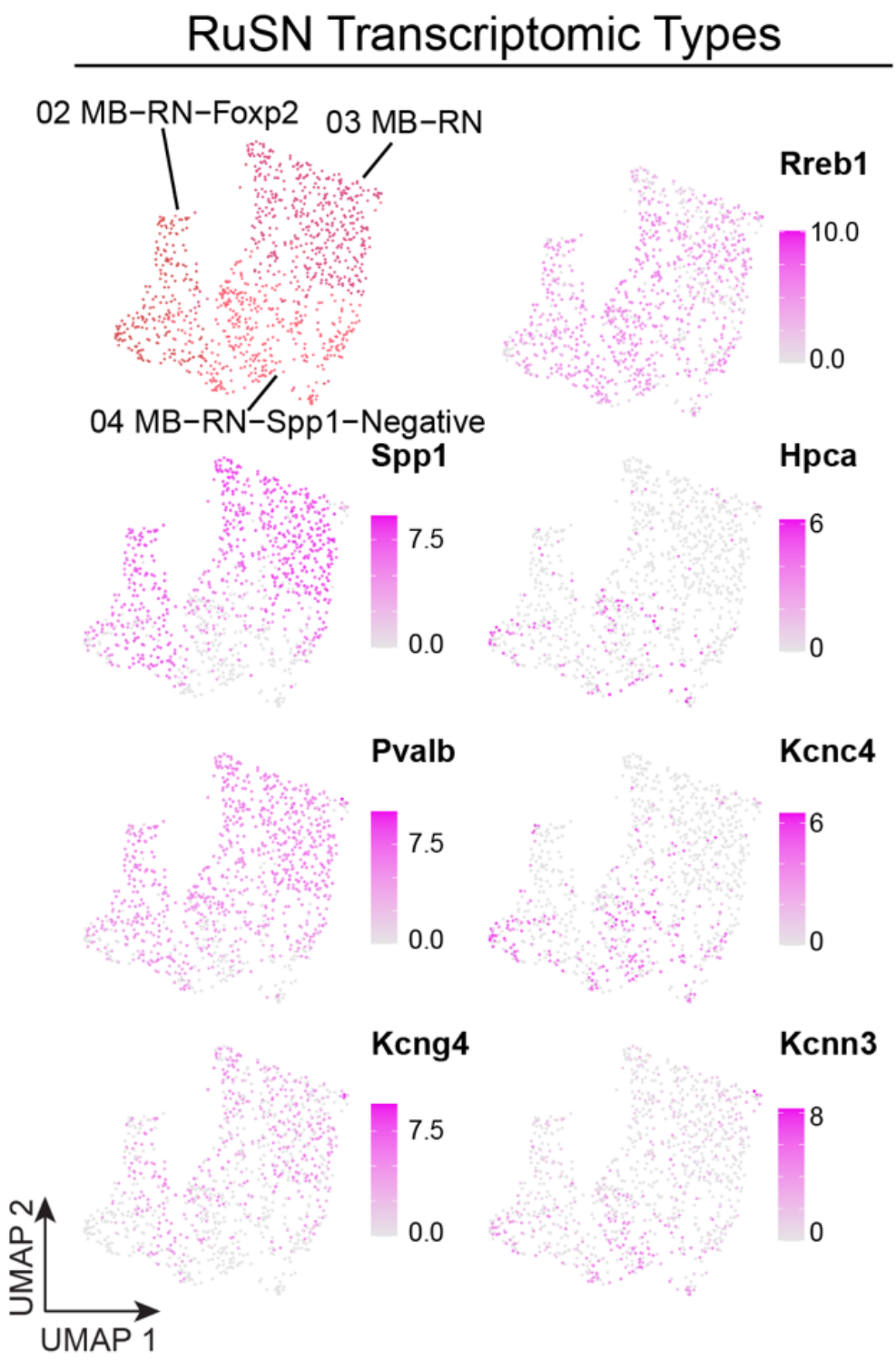


Figure 3-2: Rubrospinal transcriptomic types. UMAP visualization of RuSNs (SSv4, N = 1,031 nuclei) colored by transcriptomic types (top left) and expression of general RuSN marker gene (Rreb1, top right). Expression of differentially

expressed genes for Spp1+ (Spp1, Pvalb, Kcng4; left, bottom three) and Spp1- (Hpca, Kcnc4, Kcnn3; right, bottom three) RuSNs. RuSN = rubrospinal neuron.

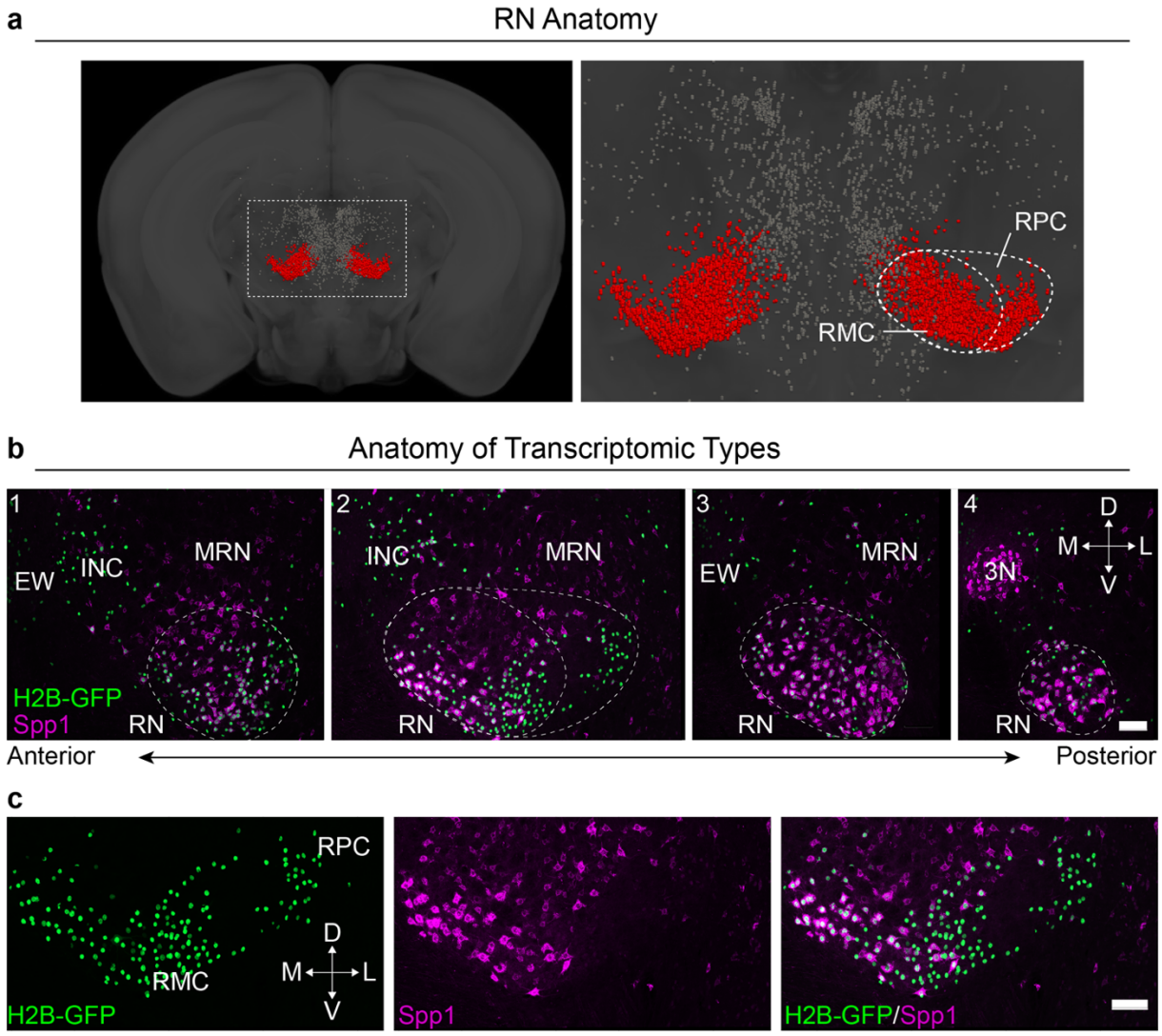


Figure 3-3: Anatomy of rubrospinal transcriptomic types. a, Coronal reconstruction of segmented and registered RuSN nuclei imaged with serial two-photon tomography across the medial RMC and lateral RPC. **b, c**, Immunohistochemistry for Spp1 (magenta) on retrogradely labeled RuSNs (green) (**c**, zoom in on panel 2 in **b**). Scale bars = 100 μm. RuSN = rubrospinal neuron, RMC = magnocellular red nucleus, RPC = parvocellular red nucleus, RN = red nucleus, EW = Edinger Westphal, INC = interstitial nucleus of Cajal, MRN = midbrain reticular nucleus, 3N = cranial nerve 3.

3.3.2 MORPHOLOGICAL AND ELECTROPHYSIOLOGICAL CHARACTERISTICS OF RUBROSPINAL TRANSCRIPTOMIC TYPES.

To assess electrophysiological features of these types, we performed loose cell-attached and whole-cell recordings of Spp1+ and Spp1- RuSNs in brain slices prepared from retrogradely labeled C57BL/6J mice. Spp1 positive or negative identities and morphologies were ascertained by post-recording IHC (**Figure 3-4a**). Consistent with the anatomical analysis above that suggests Spp1+ and Spp1- RuSNs correspond to the RMC and RPC, respectively, we find that soma of recorded RuSNs and number of genes per nucleus is larger in the Spp1+ population (**Figure 3-4b, c**). While Spp1- RuSNs are enriched in the lateral RN, we identified and recorded Spp1- RuSNs in both the medial and lateral RN. In cell-attached recordings, we found the negative phase of the action potential spike waveform was significantly shorter in Spp1+ RuSNs, suggesting they have a membrane physiology that supports fast action potentials (**Figure 3-4d**). In whole-cell recordings, we similarly found Spp1+ RuSNs had narrower action potentials (**Figure 3-4e**), and higher average spontaneous firing rate (**Figure 3-4f, g**). Additionally, Spp1+ RuSNs had smaller input resistance and were less excitable compared to Spp1- RuSNs (**Figure 3-4h, i**). We found no significant difference in action potential threshold, amplitude, peak, or fast afterhyperpolarization (**Figure 3-5**). Number of cells and statistical tests are summarized in **Table 3-2**. Thus, these results support the notion that fast-firing properties might be a shared feature of Spp1+ RuSNs and Spp1+ retinal ganglion cells or motor neurons. Given these larger cell sizes and fast conducting properties, these neurons may also have thicker axons for action potential conduction (Hursh, 1939; Perge et al., 2012).

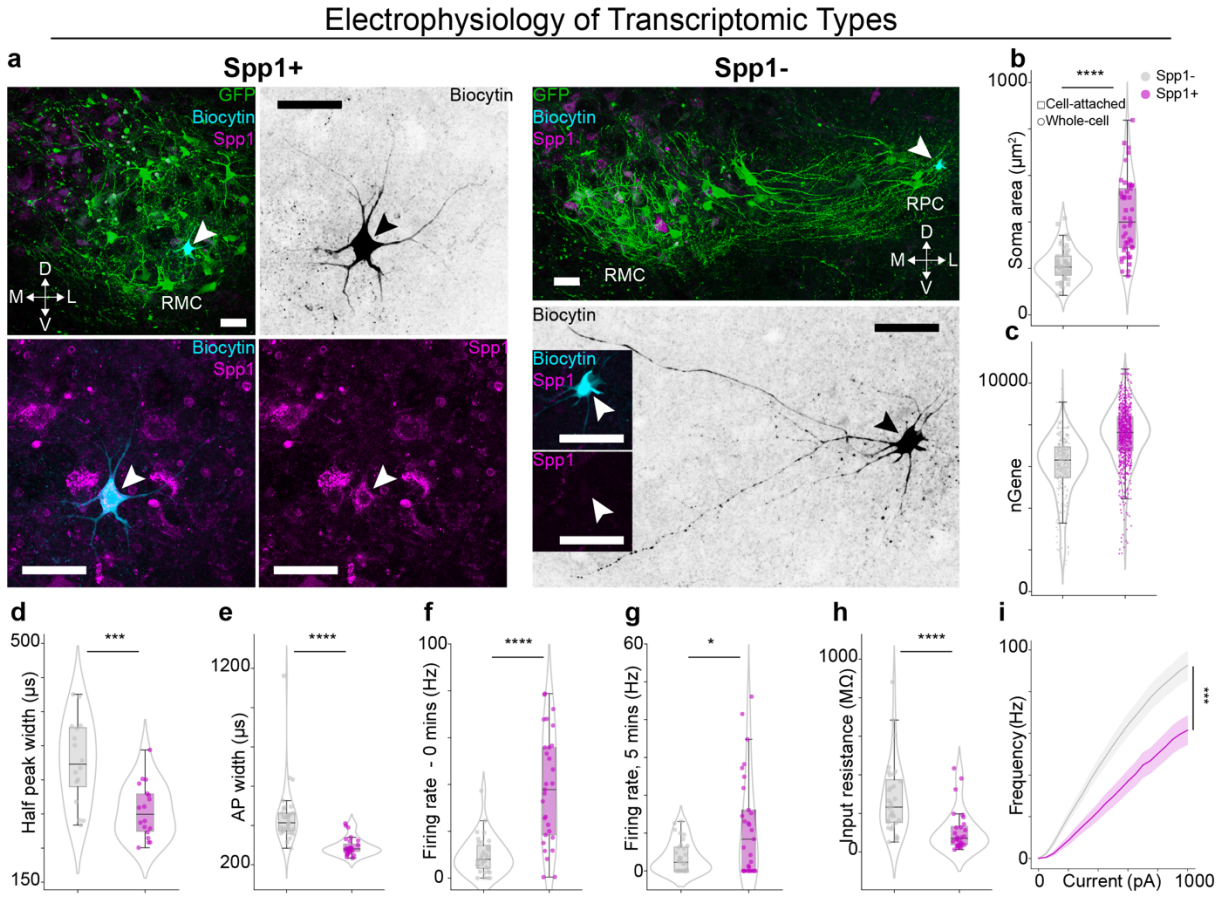


Figure 3-4: Rubrospinal transcriptomic types exhibit distinct morphological and electrophysiological signatures. **a,** Confocal images of representative Spp1+ and Spp1- RuSNs in slices from cell-attached recordings. Biocytin was injected into recorded cells upon completion of recording and labeled with fluorophore-conjugated Streptavidin. Scale bars = 50 µm. **b,** Quantification of soma size from cell-attached and whole-cell recordings. **c,** Number of genes detected in Spp1+ and Spp1- RuSNs (SSv4, N = 1,031 nuclei). **d,** Half peak width of spike waveforms obtained from cell-attached recordings. **e-i,** Whole-cell recordings show differences in action potential width (**e**), spontaneous firing rate at 0 minutes (**f**) and 5 minutes (**g**), input resistance (**h**), and frequency-current injection (**i**). RuSN = rubrospinal neuron, RMC = magnocellular red nucleus, RPC = parvocellular red nucleus. **** = $p < 0.0001$, *** = $p < 0.001$, ** = $p < 0.01$, * = $p < 0.05$, Mann-Whitney test (**b**, **d-h**); generalized linear mixed effect model (**i**). Error bars depict standard error of the mean. Number of cells and statistical tests are summarized in **Table 3-2**.

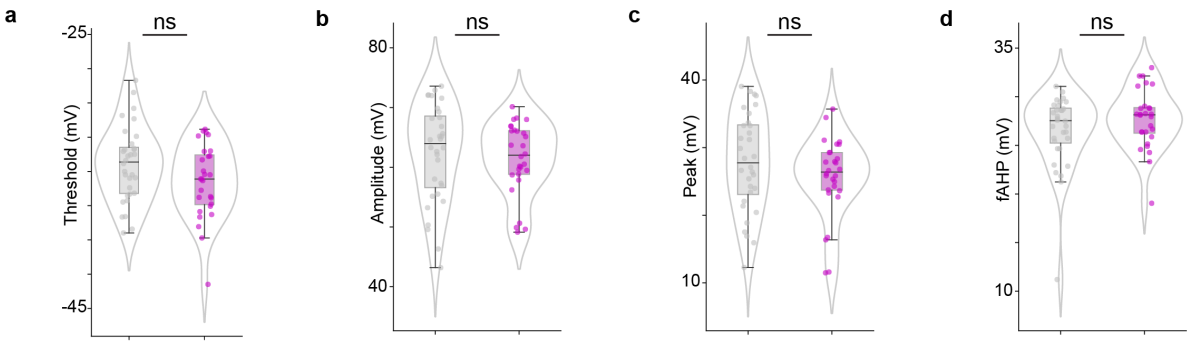


Figure 3-5: Additional electrical properties of Spp1 positive and negative rubrospinal neurons. Whole-cell recordings of Spp1+ and Spp1- RuSNs showed no significant difference in action potential **a,** threshold, **b,** amplitude, **c,** peak, or **d,** fast afterhyperpolarization (fAHP). ns = not significant (p value > 0.05, Mann-Whitney). Number of cells and statistical tests are summarized in Table 3-2.

3.3.3 SOMA SIZE AND SPP1 STATUS ACROSS SPINAL PROJECTING NEURON POPULATIONS.

Importantly, such expression and cell size correlation are not limited to RuSNs but extends to CbSNs and subsets of ReSNs (**Figure 3-6a-d**). Spp1+ ReSNs primarily correspond to 'MED-Vcan' and 'MED-Spp1' types, which are likely vestibulospinal neurons, as indicated by MERFISH mapping and the Allen ISH Atlas (see **Chapter 2 Figure 2-9f**; **Figure 3-6e**). Together, these results suggest transcriptional signatures of SPNs with large soma size which correlate with fast-firing electrophysiological properties, pointing to different physiological channels in relaying brain-derived commands.

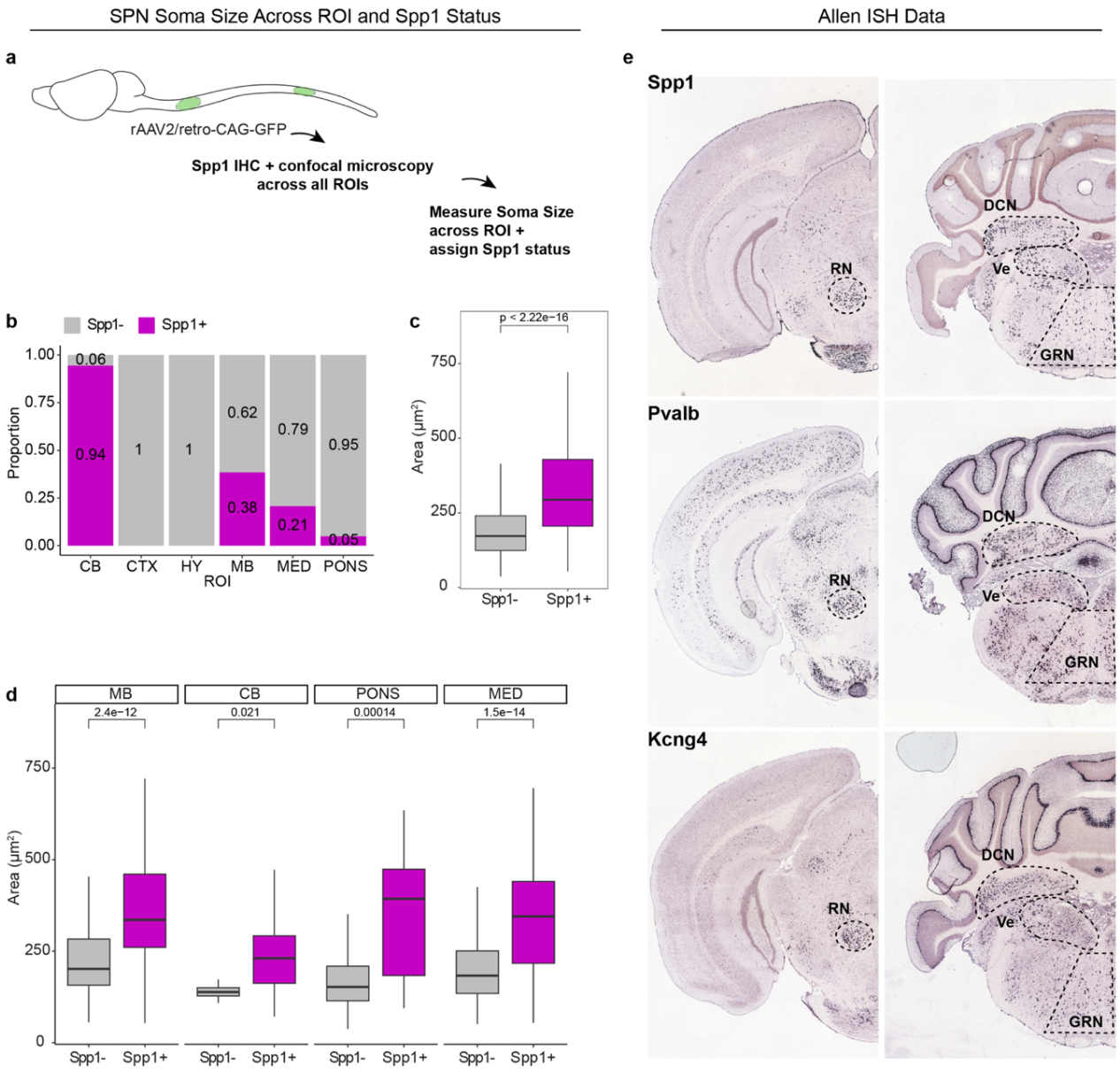


Figure 3-6: Soma size and Spp1 status across spinal projecting neuron populations. a, Soma of SPNs were labeled with a retrograde AAV expressing GFP under a CAG promoter. Subsequently, IHC for Spp1 was performed, confocal images of each ROI were taken, and soma size / Spp1 status across each major ROI was measured (see 'Methods'). **b,** Proportion of Spp1+ SPNs across each ROI, as determined by IHC. **c,** Soma area of Spp1+ and Spp1- SPNs in ROIs that contained Spp1+ SPNs (i.e., CB, MB, MED, PONS regions quantified together). **d,** Soma area of Spp1+ and Spp1- SPNs in ROIs that contained Spp1+ SPNs, separated by ROI. Numbers above boxplots indicate p-values (Wilcoxon test). **e,** Allen ISH data of Spp1, Pvalb, and Kcng4 in RN, DCN, Ve, and GRN. SPN = spinal projecting neuron, IHC =

immunohistochemistry, ISH = in situ hybridization, ROI = region of interest, CB = cerebellum, CTX = cortex, HY = hypothalamus, MB = midbrain, MED = medulla, PONS = pons, ISH = in situ hybridization, RN = red nucleus, DCN = deep cerebellar nuclei, Ve = vestibular nucleus, GRN = gigantocellular reticular nucleus.

3.4 DISCUSSION.

This study is an extension of the transcriptomic taxonomy generated in **Chapter 2**, seeking to layer electrophysiological characteristics on top of anatomical and transcriptomic features defined by the SPN cell type taxonomy. Here, molecular signature-guided electrophysiological studies identified functionally distinct SPN populations that differ in their firing properties, pointing to different functional "cable lines" for relaying brain-derived commands.

Among excitatory SPNs, we found most RuSNs and CbSNs and subsets of ReSNs express a set of genes, namely Pvalb, Kcng4, and Spp1, characteristic of fast-spiking and fast-conducting neurons in subsets of retinal ganglion cells (Krieger et al., 2017) and spinal motor neurons (Müller et al., 2014). Through electrophysiological recordings, we show that Spp1+ RuSNs indeed have fast firing properties and are larger than their Spp1- counterparts. These results are reminiscent of our emerging understanding of corticospinal pathways, which have recently been shown to be comprised of both small and large neurons with slow- and fast- conducting properties, respectively (Firmin et al., 2014; Innocenti et al., 2019; Kraskov et al., 2019). Additionally, we show that Spp1+ SPNs arising across subcortical regions (i.e., midbrain, pons, medulla, cerebellum) are, in general, larger than Spp1- cells in the same anatomical regions. Together, these results suggest the existence of "fast" and "slow" conducting pathways as a general functional principle of descending pathways. The functional implications of these different types of cable lines, however, remains to be elucidated.

3.5 ACKNOWLEDGEMENTS.

We thank Chinfei Chen for input on the electrophysiological study design; Mark Scimone and the Boston Children's Hospital (BCH) Cellular Imaging Core; and Yiming Wang and the BCH Viral Core for production of AAVs, funded by 1351 NIH grants HD018655 and P30EY012196.

3.6 TABLE LEGENDS.

Tables may be found at: https://tinyurl.com/WinterSupplement

Table 3-1: Differentially expressed genes between Spp1 positive and negative rubrospinal neurons. Seurat's FindAllMarkers (MAST test) was used to find differentially expressed genes between Spp1 positive and negative rubrospinal neurons (SSv4 data, N = 1,031 nuclei). We tested only genes that were detected in a minimum of 10% of the nuclei (min.pct = 0.10) and that showed at least a 0.25-fold log-scale difference (logfc.threshold = 0.25) between the two groups. Genes are annotated as 'significant' if adjusted p-value is less than 0.05.

Table 3-2: Summary of electrophysiological data. Summary of number of cells measured and statistical tests for data appearing in Figures 3-1 to 3-3 and Figure 3-5.

3.7 MATERIALS AND METHODS.

Electrophysiology experiments:

Retrograde labeling: To retrogradely label SPNs for cell-attached slice recording, AAV2/retro-CAG-GFP (produced by Boston Children's Hospital Viral Core) was injected into the lumbar (L2-4) spinal cord

of P42 mice as described above. To retrogradely label SPNs for whole-cell slice recording, AAV2/retro-CAG-tdTomato (produced by Boston Children's Hospital Viral Core) was injected at P4. In brief, P4 pups were anesthetized with ice and placed under the ultrasound probe (MS550, Ultrasonic Vevo 3100). A glass pipette was guided to the L3-4 enlargement and 0.8 μl of AAV2/retro-CAG-tdTomato was injected bilaterally at L3 and L4 segments. Pups were then placed on a heat pad to recover.

Brain slice preparation: Acute coronal slices were prepared at P60-70 for cell-attached recording or P20-30 for whole-cell recording. Briefly, after isoflurane anesthesia and transcardiac perfusion with ice-cold slicing solution, brains were rapidly extracted. Coronal brain slices (200 μm) were cut with a Leica VT 1200 vibratome in ice-cold slicing solution and subsequently incubated in aCSF solution for 40 minutes at 36°C. Slices were then kept at RT until transferring to the recording chamber. Slicing solution consisted of (in mM): sucrose 75, NaCl 80, KCl 2.5, NaH_2PO_4 1.25, $NaHCO_3$ 26, $CaCl_2$ 0.5, $MgCl_2$ 3.5, Na-ascorbate 1.3, Na-pyruvate 3. aCSF consisted of (in mM): NaCl 125, KCl 2.5, NaH_2PO_4 1.25, glucose 25, $NaHCO_3$ 26, $CaCl_2$ 2, $MgCl_2$ 1, Na-ascorbate 1.3, Na-pyruvate 3.

Cell-attached and whole-cell recordings: After localizing retrogradely labeled RuSNs using GFP or tdTomato fluorescence, loose-seal cell-attached recordings were made with pipette-solution filled pipettes of 20-60 MΩ resistance in voltage-clamp mode at 0mV holding potential. Whole-cell recordings were performed in current-clamp mode with 3-5 MΩ resistance. Pipette solution consisted of (in mM): K-Gluconate 130, KCl 5, HEPES 10, EGTA 0.5, MgATP 4, NaGTP 0.5, biocytin (~0.2 %, Tocris 3349) and Alexa 488 or Alexa 594 fluorescent dye (20 μM, ThermoFisher, A10436, A10438) (mOsm, 280-300; pH adjusted to 7.3-7.4 with KOH). At the end of cell-attached recording, membrane was ruptured to fill the recorded cell with biocytin and dye. Signals sampled at 20 KHz were passed through

DigiData 1440A and amplified via a Multiclamp 700B amplifier, and recorded with pClamp software (Version 11, Molecular Devices). All cell-attached and whole-cell recordings were done at RT (18-22ºC) and 30-32ºC, respectively, in aCSF.

For spike shape analysis in cell-attached recording, single spikes with negative peak (±5 ms around the peak) were detected for a 10 second period at 10 minutes from the recording start. Each negative peak was normalized to have 0 baseline level and -1 amplitude at the peak. Baseline was determined based on 3.75 ms period at the trace beginning. Individual normalized spikes were averaged for each cell and used to determine the half-peak width. Spike width was calculated as the time difference between the intersections of averaged waveform after linear interpolation and the horizontal line at the amplitude -0.5.

In whole-cell recording, spontaneous firing rate at 0 minutes was measured from the firing rate during the 10 seconds immediately after whole-cell configuration. At this time, MultiClamp was in "I=0" mode. Spontaneous firing rate at 5 minutes was calculated 5 minutes later for 10 seconds in "I=C" mode. To measure action potential (AP) related parameters, membrane potential was maintained between -65 to -60 mV with current injection at least 10 minutes after whole-cell configuration. Action potential evoking current was determined by 10 or 50 pA steps. Current injection at this value was repeated 3 times. The first AP waveform was used for AP related variable calculation. AP threshold (mV) was the first point right below the dV/dt threshold (12V/s or 0.6 mV/50μs). AP peak was the maximum membrane potential above the threshold. AP amplitude was the difference between the AP threshold and AP peak. AP half width (μs) was the time difference at half of AP amplitude membrane potential with linear interpolation between samples. fAHP was the membrane potential difference between AP threshold and negative peak within 4 ms past AP peak. Input resistance was estimated from the slope of linear regression fit (Clampfit 10) between membrane potential changes after current steps from 0 to -50 pA with -10 pA steps or from 0 to -250 pA with -

50 pA steps. For frequency-current relationship, action potential number was counted during current steps (50 pA, 1 second) increasing from 0 to 1000 pA.

Floating immunohistochemistry on acute slices: Acute slices containing Alexa 488 or Alexa 594 and biocytin filled patched cells were fixed overnight in 4% PFA at 4ºC. Slices were washed with PBS and then treated with a blocking solution (5% normal donkey serum, 0.5% Triton-X) for 2 hours at RT. Floating slices were incubated in primary antibodies (AVES Chicken anti-GFP or Rockland Rabbit-anti-RFP, R&D Systems Goat anti-Osteopontin, Millipore Mouse anti-NeuN clone A60; all 1:500 dilution in blocking solution) at 4ºC overnight. After 12-16 hours, slices were washed three times for 15 minutes with PBS at RT, and subsequently incubated with streptavidin (conjugated with Alexa Fluor 488 or 594; 1:500 dilution in PBS) and secondary antibodies (Alexa Fluor 488 donkey-anti-chicken or Alexa Fluor 594 donkey-anti-rabbit, Alexa Fluor 647 donkey-anti-goat, Alexa Fluor 405 donkey-anti-mouse; all 1:500 dilution in PBS) for 2 hours at RT. Finally, sections were washed with PBS three times for 15 minutes at RT, mounted with ProLong Glass mounting medium, and sealed with clear nail polish. ProLong Glass was allowed to cure for 48-60 hours at RT and then stored at 4ºC until imaging. Patched cells were imaged on a Leica TCS SP8 Laser Scanning Confocal with a 20x objective and optimal z-stack. Soma area was manually measured using the 'Freehand Selection' tool in Fiji. Spp1 status was determined by assessing Spp1 and Streptavidin co-localization; in cells determined to be Spp1-, NeuN signal was confirmed to ensure antigens were retained in cytoplasm despite cell membrane puncturing during electrophysiological recording.

Statistics: Statistical analysis was performed using the Mann-Whitney test or mixed-effects model as indicated in **Table 3-2**.

Immunohistochemistry for Spp1 on rubrospinal neurons: To retrogradely label RuSNs, AAV2/retro-Syn-H2B-GFP was injected into the cervical (C4-6) and lumbar (L2-4) spinal cord of P42 mice as described above. Tissue sections and immunocytochemistry were prepared as described above with AVES Chicken-anti-GFP and R&D Systems Goat anti-Osteopontin primary antibodies (1:500 dilution in blocking solution), and Donkey-anti-Chicken 488 and Donkey-anti-Goat 647 secondary antibodies (1:1000 dilution in PBS). Images were acquired as z-stacks with a 20x objective on a Zeiss LSM 900 Confocal Laser Scanning Microscope.

Soma size measurement and Spp1 status assignment for spinal projecting neurons: To measure soma size and Spp1 status of SPNs throughout the entire mouse brain, AAV2/retro-CAG-GFP was injected into the cervical (C4-6) and lumbar (L2-4) spinal cord of P42 mice as described above. At P56, mice were perfused and tissue sections and immunocytochemistry were prepared as described above with AVES Chicken-anti-GFP and R&D Systems Goat anti-Osteopontin primary antibodies (1:500 dilution in blocking solution), and Donkey-anti-Chicken 488 and Donkey-anti-Goat 647 secondary antibodies (1:1000 dilution in PBS). Images of all ROIs in one coronal series were acquired as z-stacks with a 20x objective on a Zeiss LSM 900 Confocal Laser Scanning Microscope. Automated segmentation of GFP+ cells was performed using a neural network model fine-tuned on manually annotated images using CellPose (Stringer et al., 2020). A customized quantification, measurement, and classification pipeline was implemented using Python. Cell size measurements were obtained from the segmentation masks. Identification of double positive GFP+/Spp1+ cells was done by pixel overlap intensity thresholding, counting Spp1+ cells as those with at least 65% of the pixels within the mask having high co-occurrent intensity in both channels, which accounts for the cytoplasmic but not nuclear staining pattern characteristic of Spp1. False colocalization positives were manually

corrected. Statistical significance was assessed with the Wilcoxon test (ggpubr).

3.8 REFERENCES.

Bartholome, O., de la Brassinne Bonardeaux, O., Neirinckx, V., & Rogister, B. (2020). A Composite Sketch of Fast-Spiking Parvalbumin-Positive Neurons. *Cerebral Cortex Communications*, *1*(1). https://doi.org/10.1093/TEXCOM/TGAA026

Chen, W., Zhang, J. J., Hu, G. Y., & Wu, C. P. (1996a). Different mechanisms underlying the repolarization of narrow and wide action potentials in pyramidal cells and interneurons of cat motor cortex. *Neuroscience*, *73*(1), 57–68. https://doi.org/10.1016/0306-4522(96)00010-3

Chen, W., Zhang, J. J., Hu, G. Y., & Wu, C. P. (1996b). Electrophysiological and morphological properties of pyramidal and nonpyramidal neurons in the cat motor cortex in vitro. *Neuroscience*, *73*(1), 39–55. https://doi.org/10.1016/0306-4522(96)00009-7

Dykes, R. W., Lamour, Y., Diadori, P., Landry, P., & Dutar, P. (1988). Somatosensory cortical neurons with an identifiable electrophysiological signature. *Brain Research*, *441*(1–2), 48–58. https://doi.org/10.1016/0006-8993(88)91382-0

Evarts, E. (1965). Relation of discharge frequency to conduction velocity in pyramidal tract neurons. *Journal of Neurophysiology*, *28*, 216–228. https://doi.org/10.1152/JN.1965.28.2.216

Firmin, L., Field, P., Maier, M. A., Kraskov, A., Kirkwood, P. A., Nakajima, K., Lemon, R. N., & Glickstein, M. (2014). Axon diameters and conduction velocities in the macaque pyramidal tract. *Journal of Neurophysiology*, *112*(6), 1229–1240. https://doi.org/10.1152/JN.00720.2013/ASSET/IMAGES/LARGE/Z9K0161425540005.JPEG

Hursh, J. B. (1939). Conduction velocity and diameter of nerve fibers. *American Journal of Physiology-Legacy Content*, *127*(1), 131–139. https://doi.org/10.1152/AJPLEGACY.1939.127.1.131

Innocenti, G. M., Caminiti, R., Rouiller, E. M., Knott, G., Dyrby, T. B., Descoteaux, M., & Thiran, J. P. (2019). Diversity of Cortico-descending Projections: Histological and Diffusion MRI Characterization in the Monkey. *Cerebral Cortex*, *29*(2), 788–801. https://doi.org/10.1093/CERCOR/BHX363

Kraskov, A., Baker, S., Soteropoulos, D., Kirkwood, P., & Lemon, R. (2019). The Corticospinal Discrepancy: Where are all the Slow Pyramidal Tract Neurons? *Cerebral Cortex (New York, NY)*, *29*(9), 3977. https://doi.org/10.1093/CERCOR/BHY278

Krieger, B., Qiao, M., Rousso, D. L., Sanes, J. R., & Meister, M. (2017). Four alpha ganglion cell types in mouse retina: Function, structure, and molecular signatures. *PLOS ONE*, *12*(7), e0180091. https://doi.org/10.1371/JOURNAL.PONE.0180091

Liu, Y., Latremoliere, A., Li, X., Zhang, Z., Chen, M., Wang, X., Fang, C., Zhu, J., Alexandre, C., Gao, Z., Chen, B., Ding, X., Zhou, J. Y., Zhang, Y., Chen, C., Wang, K. H., Woolf, C. J., & He, Z. (2018). Touch and tactile neuropathic pain sensitivity are set by corticospinal projections. *Nature 2018 561:7724*, *561*(7724), 547–550. https://doi.org/10.1038/s41586-018-0515-2

Miri, A., Warriner, C. L., Seely, J. S., Elsayed, G. F., Cunningham, J. P., Churchland, M. M., & Jessell, T. M. (2017). Behaviorally Selective Engagement of Short-Latency Effector Pathways by Motor Cortex. *Neuron*, *95*(3), 683-696.e11. https://doi.org/10.1016/J.NEURON.2017.06.042

Müller, D., Cherukuri, P., Henningfeld, K., Poh, C. H., Wittler, L., Grote, P., Schlüter, O., Schmidt, J., Laborda, J., Bauer, S. R., Brownstone, R. M., & Marquardt, T. (2014). Dlk1 promotes a fast motor neuron biophysical signature required for peak force execution. *Science (New York, N.Y.)*, *343*(6176), 1264–1266. https://doi.org/10.1126/SCIENCE.1246448

Perge, J. A., Niven, J. E., Mugnaini, E., Balasubramanian, V., & Sterling, P. (2012). Why Do Axons Differ in Caliber? *Journal of Neuroscience*, *32*(2), 626–638. https://doi.org/10.1523/JNEUROSCI.4254-11.2012

Stringer, C., Wang, T., Michaelos, M., & Pachitariu, M. (2020). Cellpose: a generalist algorithm for cellular segmentation. *Nature Methods 2020 18:1*, *18*(1), 100–106. https://doi.org/10.1038/s41592-020-01018-x

Suter, B. A., Migliore, M., & Shepherd, G. M. G. (2013). Intrinsic Electrophysiology of Mouse Corticospinal Neurons: a Class-Specific Triad of Spike-Related Properties. *Cerebral Cortex (New York, NY)*, *23*(8), 1965. https://doi.org/10.1093/CERCOR/BHS184

Vigneswaran, G., Kraskov, A., & Lemon, R. N. (2011). Large Identified Pyramidal Cells in Macaque Motor and Premotor Cortex Exhibit "Thin Spikes": Implications for Cell Type Classification. *Journal of Neuroscience*, *31*(40), 14235–14242. https://doi.org/10.1523/JNEUROSCI.3142-11.2011

Wang, X., Liu, Y., Li, X., Zhang, Z., Yang, H., Zhang, Y., Williams, P. R., Alwahab, N. S. A., Kapur, K., Yu, B., Zhang, Y., Chen, M., Ding, H., Gerfen, C. R., Wang, K. H., & He, Z. (2017). Deconstruction of Corticospinal Circuits for Goal-Directed Motor Skills. *Cell*, *171*(2), 440-455.e14. https://doi.org/10.1016/J.CELL.2017.08.014

Wang, Z., Maunze, B., Wang, Y., Tsoulfas, P., & Blackmore, M. G. (2018). Global Connectivity and Function of Descending Spinal Input Revealed by 3D Microscopy and Retrograde Transduction. *Journal of Neuroscience*, *38*(49), 10566–10581. https://doi.org/10.1523/JNEUROSCI.1196-18.2018

4

Concluding Remarks

Publication: This chapter was written for this thesis and was not adapted from a publication.

Author contributions: This chapter was written by Carla C. Winter.

4.1 SUMMARY OF THIS WORK.

This doctoral work is the first to systematically characterize brain-wide spinal projecting neurons (SPNs) at single-cell resolution. The three chapters of this research (i.e., anatomical characterization, molecular identification, and assessment of physiological properties of SPNs) have collectively provided a substantial step toward understanding and unifying their complex organization.

Chapter 1 developed a comprehensive anatomical atlas of cervical- and lumbar-projecting SPNs. The synergistic application of viral-mediated retrograde labeling and whole-brain imaging enabled a more precise investigation of the anatomical features of these neurons than prior efforts. In **Chapter 2**, transcriptional profiling and analysis of 65,002 SPNs created a comprehensive transcriptomic taxonomy, establishing a hierarchical classification based on their molecular identities. Notably, the three broad divisions of SPNs provided insights into the heterogeneity of these neurons, their communication modes, and the diversity of their functions. **Chapter 3** exploited the insights gleaned from the molecular atlas to investigate the physiological properties of SPNs. The analysis of electrophysiological features of a subset of SPNs, i.e., the fast-firing Spp1+ SPNs, added a new dimension to our understanding of the physiological properties of these neurons. These findings underscored the existence of distinct transmission paths within the brain-spinal cord communication network, introducing the concept of "fast and slow" cable lines that might be flexibly engaged to generate specific functions.

In conclusion, this research marks an important advance towards understanding the organizational principles of SPNs. It fills a crucial knowledge gap by creating a brain-wide atlas that integrates the anatomy, molecular identity, and physiology of these neurons. It is my hope that this work serves as a reliable roadmap for future researchers studying descending pathways in both health and disease.

4.2 THE CONTINUING EFFORT TO BUILD A "PARTS LIST" OF THE BRAIN.

So, what really is a cell type and where do we go from here? Classifying cell types, whether SPNs or otherwise, requires us to establish their precise molecular composition, connectivity, morphology, physiology, and function (Zeng, 2022). The atlas presented here delves into the first four components for SPNs, yet it is far from complete – each of these features contains an immense rabbit hole we could venture down. For example, "molecular composition" is explored in this dissertation in terms of the transcriptome, but the molecular machinery inside each cell is vast. Recent and emerging technologies have allowed us to investigate neurons beyond RNA expression, including whole-genome investigations (Miller et al., 2022), epigenomic analyses (Zhang et al., 2021), and even proteomics (Zhang et al., 2021), each at the single-cell level. It is also important to acknowledge these molecular techniques primarily focus on the neuronal soma (or nucleus, as presented in this dissertation), yet most of a neuron's volume is composed of its dendrites and axon (Misgeld & Schwarz, 2017). Further techniques must be developed or modified to peer into the immense non-soma territory in a cell type specific manner (Heiman et al., 2008; Ostroff et al., 2019). Even still more complex is the consideration of neurons beyond the snapshot in time in which they are observed: how does development, environment, aging, experience, and disease affect our interpretations of their molecular makeup? And we must not overlook our use of a model system, the mouse, who's brain seems infinitely complex in its own right but pales in comparison to the human. Now layer equally complex investigations of their morphology, connectivity, physiology, and function on top and the task seems to scale infinitely.

It is easy to feel daunted by the enormity of the task at hand, and even question its feasibility at times (as I frequently have done throughout my PhD), but we must start somewhere. For neuroscientists, that "somewhere" was over 100 years ago when Ramón y Cajal provided among the first morphological characterizations of neuronal subtypes (Ramón y Cajal, 1909). Since then, modern

technologies have revolutionized our understanding of what a cell type is and systematic, team-based efforts (BICCN, 2021) make the task appear more realistic. With the advent of new technologies and approaches for cell type classifications such as single cell RNA sequencing and subcellular-resolution whole-brain imaging, we will continue to layer more information onto our understanding of neuronal subtypes. Classify. Advance technology. Classify. Repeat – until we approach a full understanding of the brain. As Hongkui Zeng, a pioneer in cell type classification who I would liken to a modern-day Ramón y Cajal, poignantly writes, "with each iteration, the definition of cell types will become more mature and unified, and the repertoire of cell types defined will better align with the functional architecture of the organism" (Zeng, 2022).

4.3 HYPOTHESIS GENERATION VS. DATA GENERATION.

"Data should be a means to knowledge, not an end in themselves." (Nurse, 2021)

Coming from a bioengineering background, I was drawn to work in the Zhigang He Lab to develop a stronger foundation in neurobiology and hone skills in hypothesis-driven research during my PhD. I recognized that direct testing of predictions and refinement of scientific understanding is crucial to neuroscience research, in addition to the goal-directed process of engineering. The profound influence of hypothesis-driven research is illustrated in a paradigm-shifting example (and one that drew me to work in the He Lab) wherein authors hypothesized that cell growth control genes that are expressed in postmitotic mature neurons hinder regeneration potential (Liu et al., 2010; Park et al., 2008). In support of their hypothesis, the authors demonstrated that a single gene knockout of the PTEN tumor suppressor gene enabled robust axonal regrowth after injury, demonstrating that, despite decades of evidence to the contrary, mammalian central nervous system neurons did indeed have the potential for regeneration!

As illuminating as these focused studies are, however, the field has made relatively little progress towards developing clinically relevant treatments for SPN injuries (e.g., following spinal cord injury or amyotrophic lateral sclerosis). Dr. Lisa Goodrich, my PhD preliminary qualifying exam chair, underscored this lack of progress when she questioned me during my PQE: "Zhigang showed very similar slides during his job talks twenty years ago, what do you think is holding the field back?". I didn't have a great answer for her at the time, and I certainly still don't have a solution, but through my PhD I have developed a better understanding of what we must do to advance.

It sounds silly to state, but I believe the answer to Lisa's question lies in the inherent complexity of biological systems. While model organisms such as *C. elegans* or mouse can yield important insights about specific biological phenomena, the brain's complexity precludes single gene knockout experiments, such as the PTEN knockout discovery in mice, from providing panaceas to problems such as paralysis. Recognizing this, neuroscientists must embrace the inherent complexity of the brain. The modern scientific era's ability to generate large-scale datasets, like what is presented in this dissertation, will be pivotal to this effort for several reasons. Among others, this approach will give us unprecedented access to the true molecular and cellular diversity of the mammalian brain and allow unbiased identification of molecular phenomena that would otherwise be overlook with hypothesis-driven studies.

Nonetheless, as the above quote from Nobel laureate Paul Nurse implies, an avalanche of data is meaningful only when it informs understanding – the insights from data-generation should guide development of new hypotheses to be tested. Taken together, the future of neuroscience research should not be a choice between data generation and hypothesis-driven research, as is often debated by scientists sitting on the two ends of the spectrum. Instead, my PhD has taught me that the path towards developing translatable cures for neurological ailments lies in a synergistic approach between large-scale dataset generation and direct hypothesis testing.

4.4 TO MY FELLOW TRAINEES.

"One of the beautiful things about science is that it allows us to bumble along, getting it wrong time after time, and feel perfectly fine as long as we learn something each time." (Schwartz, 2008)

As I conclude this dissertation, I leave behind some parting thoughts for my fellow trainees and reminders to my future self.

Throughout my graduate studies, I've had my fair share of bumbling. I've cried. I've felt beaten down. At times I've even questioned if the constant challenges were "worth it". I often found myself unsure what question to ask next. And, when the question finally came to me, I often felt I lacked the tools necessary to address it. Reflecting on my graduate journey, I now recognize all this struggle and uncertainty is the point of being a trainee. This brings me to my first parting thought: graduate school is a period of growth, of learning new tools, and of collaborating with others to fill in the gaps of skills and knowledge. Remember to take a step back and savor this time dedicated solely to your growth and development as a scientist.

My second parting thought, spurred by Schwartz's insightful essay (quoted above) which Zhigang shared with me early on in my PhD: science does not promise easy answers. Science will continually challenge us. We will develop and test the wrong hypotheses time after time. These challenges that science presents to us are not indications of personal inadequacy, however, they are intrinsic to the process of scientific discovery. As trainees, the PhD is meant to teach us how to pick ourselves up after an experiment failed for the 100^{th} time as much as it to teach us how to do the experiment "the right way".

In conclusion, science is hard, but that's the beauty of it. The struggle, the failures, and the tenacious search for scientific truths despite it all reflect what it means to be a scientist. Embrace it – these challenges are what make this journey so profoundly fulfilling and worthwhile.

4.5 REFERENCES:

BICCN. (2021). A multimodal cell census and atlas of the mammalian primary motor cortex. *Nature 2021 598:7879*, *598*(7879), 86–102. https://doi.org/10.1038/s41586-021-03950-0

Heiman, M., Schaefer, A., Gong, S., Peterson, J. D., Day, M., Ramsey, K. E., Suárez-Fariñas, M., Schwarz, C., Stephan, D. A., Surmeier, D. J., Greengard, P., & Heintz, N. (2008). A Translational Profiling Approach for the Molecular Characterization of CNS Cell Types. *Cell*, *135*(4), 738–748. https://doi.org/10.1016/J.CELL.2008.10.028

Liu, K., Lu, Y., Lee, J. K., Samara, R., Willenberg, R., Sears-Kraxberger, I., Tedeschi, A., Park, K. K., Jin, D., Cai, B., Xu, B., Connolly, L., Steward, O., Zheng, B., & He, Z. (2010). PTEN deletion enhances the regenerative ability of adult corticospinal neurons. *Nature Neuroscience*, *13*(9), 1075–1081. https://doi.org/10.1038/nn.2603

Miller, M. B., Huang, A. Y., Kim, J., Zhou, Z., Kirkham, S. L., Maury, E. A., Ziegenfuss, J. S., Reed, H. C., Neil, J. E., Rento, L., Ryu, S. C., Ma, C. C., Luquette, L. J., Ames, H. M., Oakley, D. H., Frosch, M. P., Hyman, B. T., Lodato, M. A., Lee, E. A., & Walsh, C. A. (2022). Somatic genomic changes in single Alzheimer's disease neurons. *Nature 2022 604:7907*, *604*(7907), 714–722. https://doi.org/10.1038/s41586-022-04640-1

Misgeld, T., & Schwarz, T. L. (2017). Mitostasis in Neurons: Maintaining Mitochondria in an Extended Cellular Architecture. *Neuron*, *96*(3), 651–666. https://doi.org/10.1016/J.NEURON.2017.09.055

Nurse, P. (2021). Biology must generate ideas as well as data. *Nature*.

Ostroff, L. E., Santini, E., Sears, R., Deane, Z., Kanadia, R. N., Ledoux, J. E., Lhakhang, T., Tsirigos, A., Heguy, A., & Klann, E. (2019). Axon TRAP reveals learning-associated alterations in cortical axonal mRNAs in the lateral amgydala. *ELife*, *8*. https://doi.org/10.7554/ELIFE.51607

Park, K. K., Liu, K., Hu, Y., Smith, P. D., Wang, C., Cai, B., Xu, B., Connolly, L., Kramvis, I., Sahin, M., & He, Z. (2008). Promoting axon regeneration in the adult CNS by modulation of the PTEN/mTOR pathway. *Science*, *322*(5903), 963–966. https://doi.org/10.1126/science.1161566

Ramón y Cajal, S. (1909). Histologie du système nerveux de l'homme & des vertébrés. In *Histologie du système nerveux de l'homme & des vertébrés*. Maloine. https://doi.org/10.5962/bhl.title.48637

Schwartz, M. (2008). The importance of stupidity in scientific research. *Journal of Cell Science*. https://doi.org/10.1242/jcs.033340

Zeng, H. (2022). What is a cell type and how to define it? *Cell*, *185*, 2739–2755. https://doi.org/10.1016/j.cell.2022.06.031

Zhang, Z., Zhou, J., Tan, P., Pang, Y., Rivkin, A. C., Kirchgessner, M. A., Williams, E., Lee, C. T., Liu, H., Franklin, A. D., Miyazaki, P. A., Bartlett, A., Aldridge, A. I., Vu, M., Boggeman, L., Fitzpatrick, C., Nery, J. R., Castanon, R. G., Rashid, M., … Callaway, E. M. (2021). Epigenomic diversity of cortical projection neurons in the mouse brain. *Nature 2021 598:7879*, *598*(7879), 167–173. https://doi.org/10.1038/s41586-021-03223-w

A

Appendix

A.1 Review article:

Publication: This review article is published in Cold Spring Harbor Perspectives in Biology

Winter, C. C., He, Z., & Jacobi, A. (2022). Axon Regeneration: A Subcellular Extension in Multiple Dimensions. *Cold Spring Harbor Perspectives in Biology*, *14*(3), 1–20.
https://doi.org/10.1101/cshperspect.a040923

Author contributions: I planned this review article in collaboration with postdoctoral fellow Dr. Anne Jacobi. I wrote most of the text myself, with insight and proofreading from Drs. Anne Jacobi and Zhigang He. I prepared Figure 1, 3, and 4; Dr. Jacobi prepared Figure 2.

Axon regeneration: A subcellular extension in multiple dimensions

Carla C. Winter[1-3], Zhigang He[1,2], Anne Jacobi[1,2]

[1]F.M. Kirby Neurobiology Center, Boston Children's Hospital, Boston, MA, USA
[2]Department of Neurology and Ophthalmology, Harvard Medical School, Boston, MA, USA
[3]PhD Program in Biological and Biomedical Sciences, Harvard Medical School, Boston, MA, USA
Correspondence: Zhigang.He@childrens.harvard.edu

ABSTRACT

Axons are a unique cellular structure that allows for the communication between neurons. Axon damage compromises neuronal communications and often leads to functional deficits. Thus, developing strategies that promote effective axon regeneration for functional restoration is highly desirable. One fruitful approach is to dissect the regenerative mechanisms used by some types of neurons, in both mammalian and non-mammalian systems, that exhibit spontaneous regenerative capacity. Additionally, numerous efforts have been devoted to deciphering the barriers that prevent successful axon regeneration in the most regeneration-refractory system – the adult mammalian central nervous system. As a result, several regeneration-promoting strategies have been developed, but significant limitations remain. This review is aimed to summarize historic progression and current understanding of this exciting yet incomplete endeavor.

INTRODUCTION

Different from other cell types, the functional identity of a neuron in all organisms is largely defined by its synaptic connections (i.e., the inputs it receives on the cell body and dendrites and the outputs its axon innervates). Neuronal injury or disease can disrupt this critical neural circuitry via damage to both dendrites and axons and eventually cell death. Magnifying the problem, neurons are

postmitotic and thus lose the ability to proliferate. Fortunately, many injured neurons can survive and are sometimes able to regenerate their axons and dendrites, as seen in evolutionarily older organisms, the peripheral nervous system (PNS), and even the immature mammalian central nervous system (CNS). However, such regenerative events are largely inefficient in the adult mammalian CNS, often resulting in permanent functional deficits after injury and disease. Thus, there has been a long-term interest to develop strategies that promote neuronal regeneration and functional restoration.

At the cellular level, neuronal regeneration could occur at the axonal or dendritic compartments. Perhaps due to their importance for neuronal function and distinctive structure (i.e., impressive lengths) that contributes to high injury vulnerability, most efforts have been devoted to studying axon, rather than dendrite, regeneration. Depending on the regrowth initiation site (the axon shaft, branch, or terminals), the generic term "axon regeneration" is sometimes used for different morphological forms, including regenerative regrowth from injured sites or the distal uninjured segment, and compensatory sprouting from spared axons. Inefficient axonal regeneration in the mammalian adult CNS is attributed to a variety of cell intrinsic and extrinsic factors, as this chapter will discuss.

MILESTONES IN AXON REGENERATION

Understanding the processes and limitations of axon regeneration has been a key research topic for many decades. In the early 20th century, Santiago Ramón y Cajal made a keystone contribution to the field by identifying axons as the basic unit of neuronal connectivity. He noted structural changes within axons and the surrounding environment occurred following injury. Since then, science has made tremendous progress in understanding the different factors necessary for, or limiting, the induction of axon regeneration. The current section aims to review milestones in

mammalian axon regeneration research that have shaped the field and laid a critical foundation for future studies.

Pre-1985: Peripheral nerve grafts enable central nervous axon regeneration in mammals

Based on morphological observations, Ramón y Cajal concluded that the CNS does not have the capacity for regeneration following injury and disease (Ramon y Cajal 1928). This stands in stark contrast to the PNS which is intrinsically more regenerative than the CNS. An obvious question is what differences account for the dichotomy between the CNS and PNS. Ramón y Cajal hypothesized that CNS axons can regenerate if placed near the growth-permissive environment of the PNS. His pupil, Jorge Francisco Tello, tested this by anastomosing a sciatic nerve graft (i.e., PNS) to a cut optic nerve (i.e., CNS), and observed axons growing from the optic nerve into the sciatic nerve graft (Tello 1907). Tello suspected these axons were from regenerating retinal ganglion cells (RGCs) (Fig. 1A).

It wasn't until the early 1980s in which Ramón y Cajal and Tello's hypothesis was proven by Aguayo and his colleagues (David and Aguayo 1981). In a landmark study, the authors used autologous sciatic nerve grafts to serve as a bridge between the medulla and spinal cord. Later, the authors examined the extent of CNS axon ingrowth into the PNS grafts via horseradish peroxidase (HRP) mediated tracing. This provided definitive proof that the axons in the grafts were of CNS origin (Fig. 1B). Despite a small number of regenerating axons, Aguayo's work served to reinvigorate modern CNS research.

1985-1995: The injury environment dictates capacity for axon regeneration in mammals

Inspired by Aguayo's results, the field began to search for factors within the CNS injury environment responsible for inhibiting regeneration. The hypothesis was that if these inhibitory factors are identified and removed, then CNS axon regeneration would be possible. The advent of

neuronal culture techniques in the 1980s enabled the dissection of putative inhibitory molecules *in vitro* via reductionist approaches. In 1988, studies from Caroni and Schwab implicated CNS myelin-associated inhibitors (MAIs) as major contributors, in particular NogoA, to the inhibitory CNS environment (Caroni and Schwab 1988a, 1988b). Since these early studies, numerous additional inhibitory factors have been identified (Filbin 2003; Wang et al. 2002).

However, removing these MAIs by genetic or pharmacological means only modestly improved axon regrowth *in vivo* (Schwab and Strittmatter 2014; Zheng et al. 2003), suggesting the existence of other inhibitors independent of oligodendrocytes or myelin *in vivo*. Indeed, components of the fibrotic/glial scar, which forms at the lesion site, appear to be another major source of inhibitory activity. Like in other parts of the body, the immediate injury response in the CNS initially serves to isolate the injury and protect the surrounding spared tissue, but later evolves into a barrier for axon regrowth (O'Shea et al. 2017; Tran et al. 2018). Deciphering the molecular nature of the inhibitory activity associated with such scar structures has been a major focus of the field for the past decades. Silver observed that growing axons cease around the region enriched in chondroitin sulfate proteoglycans (CSPGs), and proposed those, and perhaps other extracellular matrix molecules, are key factors for limiting axon regeneration (McKeon et al. 1995). Supporting this idea, application of chondroitinase ABC, an enzyme that degrades CSPGs, is able to promote axon regrowth *in vivo* to a limited extent (Bradbury et al. 2002; Lang et al. 2015). Thus, these studies provide convincing evidence for environmental inhibition, but also point to the insufficiency of removing these in promoting robust axon regrowth.

1990s: Switching of neuronal state impacting axon regeneration in mammals

Parallel to studying environmental factors, several observations pointed to the importance of neuronal intrinsic mechanisms. For example, pioneering work by Marie Filbin suggested that different

cAMP levels in PNS and CNS neurons contribute to the dichotomous regenerative responses (Filbin 2003). From the perspective of neuronal development, axon growth stops upon the completion of development, even for PNS neurons. So the question became, how can they re-enter a growth-competent state following injury? Initial insights came from a series of studies on "conditioning lesion models" first described by Richardson and Issa (1984), and later extensively characterized by Neumann and Woolf (1999). Dorsal root ganglion (DRG) neurons have a unique morphology, with their soma residing within the DRG and a single stem axon bifurcating into a central and peripheral branch: the peripheral branch (i.e., PNS) innervates peripheral targets, and the central branch (i.e., CNS) relays somatosensory information to the brain. A lesion to the peripheral branch will repair itself but a lesion to the central branch will not. Remarkably, an initial injury to the peripheral branch allows the central branch to regenerate when it is injured days later (Neumann and Woolf 1999; Richardson and Issa 1984). This phenomenon is known as the "conditioning effect," as the peripheral injury "conditions" the initially dormant DRG neuron to re-enter a growth competent state by upregulating a genetic program for regeneration. This internal change in cell state is sufficient for the central branch to overcome the "inhibitory" CNS injury environment. Although a set of regeneration-associated genes that include transcription factors (TFs) (e.g., ATF3, Sox11, STAT3) and growth-associated proteins (e.g., GAP43, SPRR1a, and cytoskeletal proteins), have been described as molecular players, it remains unclear which are the drivers or passengers of the conditioning lesion effects.

2000s: Altering the intrinsic state of neurons can promote axon regeneration

Despite studies in PNS neurons, it was not clear if an intrinsic growth program plays a role in axon regeneration of adult CNS neurons. Drawing inspiration from evolutionarily conserved pathways that regulate cell growth, Park et al. hypothesized that mechanisms preventing overgrowth upon the completion of development are likely responsible for the reduced regenerative ability of adult CNS

axons (Park et al., 2008). In the early 2000s, the development of different transgenic mouse lines and the advance of AAV-based manipulation methods made it possible to seek for neuronal inhibitors of axon regeneration *in vivo*. Screening specific tumor suppressor genes in adult RGCs identified that the gene encoding phosphatase and tensin homolog (PTEN) prevents apoptosis and promotes exceptionally robust axon regeneration following optic nerve crush (ONC). PTEN is a known inhibitor of the cell growth promoting PI3K/mTOR pathway. Follow-up studies showed that PTEN deletion is also effective in promoting regeneration in more complex cell types such as corticospinal neurons (Liu et al. 2010), and is effective even one year after injury (Du et al. 2015). These studies raised the possibility of manipulating intrinsic programs as an effective means of promoting CNS axon regeneration.

Intriguingly, manipulating PTEN/mTOR leads to the regeneration of only subsets of injured axons (Duan et al. 2015). Further studies revealed that even in a seemingly homogenous population of neurons, such as RGCs, different subtypes differ in intrinsic regenerative ability and response to injury and manipulations (Duan et al. 2015; Norsworthy et al. 2017; Tran et al. 2019). Importantly, the characterization of molecular properties of these different types of neurons (e.g., via modern single-cell technologies), offers a new perspective to dissect the mechanisms of the selective axon regenerative ability.

MODEL SYSTEMS FOR AXON REGENERATION

Mechanistically, axon regeneration is a multi-faceted cell biological process, making it difficult to study. Experimental models to study the neuronal response to an injury *in vitro* or *in vivo*, can either focus only on one aspect to dissect the cellular and molecular events of axon growth or aim at more closely resembling the complex *in vivo* conditions. In the following section, we will introduce a limited number of these model systems and touch on their advantages to study axon regeneration.

Invertebrates and zebrafish:

Equipped with ample genetic and experimental tools (such as *in vivo* imaging and large-scale screening), invertebrates, in particular *C. elegans* and *Drosophila*, and zebrafish are the leading genetic model systems used to decipher axon regeneration (Fig. 2A) (Brace and DiAntonio 2017; Fang et al. 2012; He and Jin 2016; Rasmussen and Sagasti 2017). For example, *C. elegans* has a simple nervous system containing only 302 neurons and a transparent cuticle, facilitating the study of axon injury of individual neurons labeled with a fluorescent marker and monitoring their regenerative response *in vivo*. In 2004, Yanik et al. presented the first study using a femtosecond laser surgery to axotomize a single axon without perturbing nearby processes in the living worm (Yanik et al. 2004). Due to their spontaneous regenerative capacity and short reproductive cycle, the *C. elegans* model system is particularly powerful to identify molecules, such as dual leucine zipper kinase (DLK; discussed later), associated with axon regeneration. As vertebrates, zebrafish offer the advantage of sharing more similarities with mammals while providing an intrinsically pro-regenerative system to study axon regeneration (Becker and Becker 2014). For example, the growth-permissive bridge formed by astrocytes and other cell types following CNS injury in zebrafish offers a useful model to dissect the mechanisms of inhibitory scar formation in mammals versus the permissive cell bridge in zebrafish (Mokalled et al. 2016).

Mammals

In vitro injury models: Upon isolation, most PNS neurons from all developmental stages and early developing CNS neurons can survive in culture, permitting the dissection of cellular and molecular mechanisms of axon growth. These neurons can be cultured on different substrates (e.g., MAIs and CSPGs), thereby offering unique models to probe into cellular mechanisms of axon regeneration (Al-

Ali et al. 2017; Rodemer et al. 2020; Witte et al. 2008). Furthermore, with advanced technologies, these culture systems provide powerful systems to address questions about subcellular events of axon growth, such as structural organization of the cytoskeleton (Xu et al. 2013) and the source driving axon extension (Santos et al. 2020).

In vivo PNS injury models: In comparison to *in vitro* models, *in vivo* models have additional advantages to assess (1) complex interactions between injured axons and its surroundings, and (2) functional/behavioral outcomes. Here we summarize the most used surgical paradigms (Fig. 2B). For PNS, sciatic nerve crush (SNC) is a well characterized model to study axon regeneration (Bauder and Ferguson 2012). Typically, a crush lesion transects axons of the nerve and the distal stumps undergo Wallerian degeneration. However, usually the Schwann cell basal laminae and endoneurial tube are left intact, providing a growth permissive environment for axon regeneration from the proximal stump into the tube to allow re-innervation of target cells (Gordon 2020; Namgung 2014). In addition to analyzing neuronal mechanisms, this model has been a powerful system to probe the neuron-immune interaction and their impact on axon regeneration (Kalinski et al. 2020).

In vivo CNS injury models: As adult mammalian CNS neurons often do not survive in culture, *in vitro* systems have clear limitations. Despite being prone to variations and technical artifacts (Di Maio et al. 2011; Fischer et al. 2017; Tuszynski and Steward 2012), several *in vivo* models have been instrumental in studying axon regeneration.

Optic nerve crush (ONC): As a part of the CNS, the optic nerve consists of the axons of all retinal ganglion cells (RGCs), relaying visual information to the brain. The non-invasive surgical access to the optic nerve allows for the induction of a highly reproducible injury with the complete transection of

all RGC axons. Because of the unique anatomical structure this model represents a pure white matter injury model after which nearly no axons spontaneously regenerate. The RGCs are easily accessible to test different manipulations for their effects on neuronal survival and axon regeneration. For example, introduction of zymosan, an inflammation-inducing agent, was shown to trigger axon regeneration (Fischer et al. 2001; Leon et al. 2000). Furthermore, the intravitreal injection of AAV's to transduce and/or manipulate genes expressed by the RGCs has identified many factors as positive or negative regulators of axon regeneration (Norsworthy et al. 2017; Sun et al. 2011; Park et al. 2008), some of which have also shown their pro-regenerative effect in other CNS areas (Liu et al. 2010, 2017).

Spinal cord injury (SCI): Conserved injury responses and regenerative outcomes are shared after SCI in humans and other mammals. Thus, SCI models are used to (1) analyze axon regeneration, (2) the correlation and causality of an individual axon tract with behavioral performance, and (3) the clinical relevance of experimental treatments via assessing functional recovery. Different types of SCI models have been devised. As distinguishing regenerating axons from spared axons could be difficult, several consistent injury models with relatively clean background have been designed (Tuszynski and Steward 2012). For example, complete and lateral hemisection models involve precise transection of the entire or half spinal cord and are better for assessing the effects of specific manipulations on axon regeneration. On the other hand, as many human SCI involves incomplete contusive injury, several versions of contusion injury have been designed to inflict a transient and acute injury to the spinal cord (Gruner 1992; Stokes 1992). Despite having more variable lesions, these models are widely used as pre-clinical experimental models. In addition, all of these traumatic injuries trigger complex injury responses in the environment, thus being useful to study the evolving interactions among different cell types (O'Shea et al. 2017).

FROM INJURY TO REGENERATION: A FEW DECISION-MAKING PROCESSES

Upon an injury, neurons have a series of decisions to make, starting with if and how the axon will seal its injured terminal and communicate local injury information to the soma? Followed by, will the injured neuron survive, subsequently regenerate, and to what extent? Lastly, how, why, and at what point does regeneration stop? Importantly, such decision-making processes depend not only on axons, but also on their cell bodies and local environment. Using the various models described above, numerous observations have shed light onto these questions and this section will give an overview on the current understanding of different decision-making events in axons, cell bodies, and their environment following injury.

Axonal decisions

Axonal decision 1 - whether or not to form a growth cone or retraction bulb

Following injury and Ca^{2+} mediated membrane resealing (Fig. 3(1), the injured axons need to reorganize the membrane and cytoskeleton structure. During development, axon growth is guided by a growth cone at the axonal terminal (Lowery and Vactor 2009). The cytoskeleton associated with the growth cone and axon shaft provide the driving force for extension. A plausible hypothesis is that a growth cone-like structure forms in the tip of injured axons, which supports axonal stability and extension of regeneration-competent neurons (Blanquie and Bradke 2018). In contrast, regeneration-incompetent axons attempt to sprout following an injury but ultimately fail and form a "retraction bulb" with disorganized microtubule networks (Ertürk et al. 2007). Microtubule stabilizers/de-stabilizers have been shown to significantly alter regeneration phenotypes. For example, addition of pharmacological destabilizers to *in vitro* cultures of injured PNS neurons transforms their growth cones into growth-incompetent retraction bulbs (Derry et al. 1997; Khan and Ludueña 2003), whereas

pharmacologic stabilization of microtubules reduces degeneration in CNS neurons *in vitro* (Hellal et al. 2011; Ruschel et al. 2015).

Axonal decision 2 - how to inform the cell body

Early studies showed that some forms of axon regrowth can occur in the absence of cell bodies (Harris et al. 1987), indicating an axon-intrinsic injury response. However, for most types of sustained axon regrowth, the coordinated action between axonal compartments and their cell bodies is required. Thus, an important question is what and how injury signals are generated and transported to the soma.

Several pathways have been implicated, with the evolutionary conserved DLK/MAPK pathway having been studied most extensively (Fig. 3(2)). Increased activity of DLK-1 in response to axon injury was first discovered in *C. elegan*s (Hammarlund et al. 2009). Axon-localized DLK, and perhaps its homolog LZK (leucine zipper–bearing kinase), acts as an injury sensor activated by calcium elevation and cytoskeleton disruption (Ghosh-Roy et al. 2010; Hammarlund et al. 2009; Hao et al. 2016). Both DLK and LZK belong to the evolutionarily conserved family of mitogen activated protein kinase kinase kinases (MAPKKKs). Their activation leads to the activation of JNK and p38 MAP kinases, which are then retrogradely transported to the soma in a JIP3-dependent manner. As a result, the injury signals generated in injured axons are broadcasted in the entire neuron. A striking demonstration of the importance of the DLK mediated injury signaling is that the genetic deletion of DLK prevents the axon regeneration induced by PTEN inhibition (Watkins et al. 2013). However, DLK and LZK were also identified as pro-apoptotic molecules in RGCs (Welsbie et al. 2013), consistent with the notion that uncontrollable activation of this stress pathway may result in neuronal death.

In addition to calcium influx at the severed axon tip, elevated intra-axonal calcium may arise from L-type voltage gated calcium channels and the endoplasmic reticulum (ER), both engendering

changes in signaling and gene expression (Fig. 3(3)). For example, protein kinase Cμ (PKCμ) mediated export of HDAC5 induces epigenetic changes in DRG neurons that allow expression of immediate early genes (e.g., ATF3, Fig. 3(4–6)) (Cho et al. 2013). In addition, many other molecules have also been implicated as putative retrograde injury signals (Terenzio et al. 2017).

Cell body decisions

Cell body decision 1 - apoptosis or survival

Upon transmission of injury signals, the soma response results in one of three different outcomes: (1) neuronal death, (2) neuronal survival with or (3) without axon regeneration. Many injured descending projection neurons survive but fail to regenerate after SCI, in contrast to injured PNS neurons, which survive and regenerate. After an ONC close to the proximal axonal segment, the majority of injured RGCs undergo cell death (Hu et al. 2012; Tran et al. 2019). However, neuronal survival increases if the axotomy occurs in the distal axonal segments within the optic tract. There are at least two explanations for such length-dependent death: the distal injury may spare other axonal branches (thus preserving some target-derived trophic signals) and/or induce less injury signals compared to the proximal lesion. However, it is unknown why the activation of these injury signals fails to induce neuronal death in other types of neurons such as peripheral DRG neurons.

Cell body decision 2 - conversion to a growth-competent or -incompetent state

To support axon extension during development, different building blocks need to be synthesized and transported to axon terminals. Thus, proper coordination of signaling, metabolism, and gene expression is required. However, in later developmental stages, neurons need to switch to a "synapse-growth mode," devoting metabolic and growth resources to synapse development and function. In RGCs, this switch occurs in the early postnatal period (Goldberg et al. 2002). For adult

axon regeneration, it is necessary to re-activate the axon growth program in injured neurons. Understanding mechanisms that control axon growth programs has been an active frontier. Here we have listed a few examples.

Transcriptional regulation: Neuronal injury induces extensive changes in gene expression programs. Of these, studies suggest correlative regeneration-associated genes (RAGs) and TFs that are causal determinants in axon regeneration. For example, in comparing axon growth-competent and -incompetent RGCs, Goldberg and his colleagues identified several members of the Krüppel-like factor (KLF) TF family as crucial gene regulators (Moore et al. 2009). In particular, KLF4 and KLF9 deletion or KLF6 and KLF7 overexpression can promote regeneration following injury during adulthood (Apara et al. 2017; Blackmore et al. 2012; Moore et al. 2009).

Newly developed RNA sequencing technology permits unbiased genome-wide comparison of gene expression in neurons under different conditions to predict putative master regulators. For example, profiling injured DRG neurons led to the identification of several putative master regulators including ATF3, SOX1, and Jun (Chandran et al. 2016; Renthal et al. 2020). Interestingly, injury-induced ATF3 expression returns to its resting level after their regenerating axons are reconnected with their targets (Renthal et al. 2020). While ATF3 deletion prevents large-scale gene expression alterations in injured DRG neurons (Renthal et al. 2020), constitutive expression of ATF3 enhances regeneration in the peripheral branch of DRG neurons (Seijffers et al. 2007). STAT3 is another important pro-regenerative TF that is activated following peripheral, but not central, injury (Schwaiger et al. 2000). However, overexpression of STAT3 in DRG neurons *can* promote new growth and collateral sprouting of central axons (Bareyre et al. 2011). Importantly, as a key cytokine signaling pathway, the STAT3 pathway can also evoke regenerative responses of CNS neurons (Jin et al. 2015; Smith 2009; Sun et al. 2011).

In addition, Norsworthy et al. (2017), hypothesized that developmental axon growth programs might be encoded by certain TFs whose expression is diminished in the adult and showed SOX11 promotes axon regeneration after ONC. Independent studies showed that SOX11 expression also promotes the regrowth of corticospinal tract axons (Wang et al. 2015). Intriguingly, while SOX11 overexpression promotes regeneration of some RGC subtypes, it has been shown to cause cell death of other RGCs populations (Norsworthy et al. 2017). Thus, there might be a functional crosstalk between the programs for injury-induced neuronal death and axon regeneration.

Epigenetic regulation: TFs impact the transcription of their target genes by binding to specific DNA sequence motifs across the genome. However, the chromatin accessibility around these binding sites is tightly regulated under conditions such as injury (Finelli et al. 2013; Gaub et al. 2010; Palmisano et al. 2019; Puttagunta et al. 2014). By using the assay of transposase-accessible chromatin using sequencing (ATAC-seq) to quantify genome-wide accessible chromatin (Buenrostro et al. 2013, 2015; Corces et al. 2017), many gene expression changes in injured and regenerating DRG neurons could be attributed to epigenetic regulation (Palmisano et al. 2019). This suggests an "epigenetic barrier" in which TF binding sites may simply not be accessible in regeneration-incompetent neurons. Intriguingly, this "epigenetic barrier" to axon regeneration appears to preferentially silence many genes associated with axon growth in adulthood (Venkatesh et al. 2018).

DNA methylation alterations might be another avenue of epigenetic regulation (Fig. 3(4–6)). Age-related DNA methylation patterns can serve as a proxy for an epigenetic clock (Horvath 2013). Strikingly, this epigenetic clock can be reset by overexpressing Yamanaka TFs (OCT4, SOX2, KLF4, [OSK] and c-MYC) in somatic cells, which results in the loss of cellular identity and transforming them into pluripotent stem cells (Takahashi and Yamanaka 2006). Similarly, overexpression of c-MYC (Belin et al. 2015) or OSK (Lu et al. 2020) promote axon regeneration in injured RGCs. Understanding

why and how these epigenetic barriers form, and how to manipulate them, will be crucial to future efforts that seek to use pro-regenerative TFs with naturally inaccessible promoter or enhancer sites in mature CNS neurons.

Signaling cascades: Several signaling cascades are activated in response to injury. To define key regulators at least two approaches have been informative: (1) identifying the pathways required for axon growth in regeneration-competent neurons and (2) defining the manipulations that enable axon regeneration in regeneration-incompetent neurons. As mentioned above, the DLK/MAPK pathway only functions in regeneration-competent neurons. In contrast, two other pathways have been documented to regulate axon regeneration in both conditions.

Phosphoinositide 3-kinases (PI3Ks)/mammalian target of rapamycin (mTOR): The PI3K/mTOR pathway is a central regulator of metabolism and cell growth (Saxton and Sabatini 2017), and has been implicated as an evolutionarily conserved regulator of axon regeneration. PTEN is a negative regulator of this pathway (Fig. 4). As aforementioned, PTEN deletion or inhibition is sufficient to promote regeneration of regeneration-incompetent neurons. Inhibiting mTOR abolishes the regeneration induced by PTEN deletion, suggesting the requirement of mTOR in this regenerative outcome. However, activating mTOR only, by genetic deletion of TSC2, led to less axon regeneration (Park et al. 2008), indicating that additional effectors, such as GSK3, might mediate the regeneration induced by PTEN inhibition. Additionally, mTOR is endogenously activated in regeneration-competent peripheral axons to enhance axon outgrowth following peripheral nerve injury (Abe et al. 2010). Thus, leveraging PI3K/mTOR regulated metabolism to develop manipulations that elevate PI3K/mTOR activity could be a useful approach to promote axon regeneration.

In fact, PI3K/mTOR is a major signaling pathway that mediates the neurotrophic effects of growth factors such as brain derived neurotrophic factor (BDNF) or neurotrophin-3. However, despite the established roles of these growth factors in regulating neuronal survival and axon growth during development, direct administration of these factors has limited effects on promoting axon regeneration in adults (Giehl and Tetzlaff 1996; Hollis et al. 2009; Lu et al. 2001). This suggests that, in comparison to immature neurons, mature corticospinal neurons have reduced responsiveness to growth factors. Recent studies suggest that osteopontin, an integrin-binding protein, could sensitize neuronal responsiveness to insulin-like growth factor 1 (IGF1) and promote IGF1-induced axon regeneration, perhaps by facilitating IGF1-triggered IGF1 receptor clustering and activation (Bei et al. 2016; Duan et al. 2015; Liu et al. 2017). Thus, it would be interesting to develop other methods of sensitizing neuronal responses to neurotrophic factors for promoting axon regeneration.

Jak/Stat: The second pathway central to axon regeneration is JAK/STAT. Cytokines such as ciliary neurotrophic factor (CNTF) or interleukin 6 (IL6), released by non-neuronal cells in response to injury, bind to their specific receptors to initiate signal transduction to the intracellular compartment by their shared receptor component gp130. Together this results in the activation of JAK kinases and STAT TFs (Heinrich et al. 1998). Early studies documented activation of this pathway in injured DRG neurons (Cafferty et al. 2004). The causal relationship of this pathway to axon regeneration was supported by the observation that deletion of SOCS3, a negative regulator of the JAK/STAT pathway, following ONC promotes axon regeneration. This process is further enhanced by additional treatment with CNTF (Sun et al. 2011). Moreover, the JAK/STAT pathway is thought to mediate, at least partially, the effects of inflammation-triggered axon regeneration (Leibinger et al. 2013). Manipulating this pathway to promote axon regeneration has been an active area of neural repair research (Leibinger et al. 2021).

Metabolic switch: During early development, growing neurons require anabolic metabolism, using ATPs for synthesizing building blocks for neuronal growth. Upon completion of neural development, mature neurons convert to homeostatic metabolism. To support sustained axon regeneration, it is conceivable that injured neurons may need to re-establish anabolic metabolism. In fact, some regeneration-promoting molecules, such as mTOR and c-MYC, are known master regulators of anabolic metabolism (Saxton and Sabatini 2017; Stine et al. 2015). In light of active research of metabolic regulation in non-neuronal cells, it will be interesting to identify other novel avenues of manipulating cellular metabolism for axon regeneration.

The environmental decision: *Whether or not to form an inhibitory scar*

The initial traumatic injury immediately disrupts the axon, surrounding glial cells, and blood vessels (Fig. 3(7)). Depending on species, location, and developmental stage, subsequent injury responses lead to varied outcomes. In non-mammalian vertebrates, such as newt and zebrafish, a permissive bridge forms after SCI allowing regenerating axons to cross the lesion (Cigliola et al. 2020; Mokalled et al. 2016; Zukor et al. 2013). In mammals, a glial or fibrotic scar develops after a lesion to the CNS, but not the PNS. Understanding the mechanisms mediating such distinct responses has been intensely investigated for many years but many mysteries still remain (Sofroniew 2018; Tran et al. 2018).

In all types of injury, the initial insult leads to breakdown of the blood brain barrier (BBB) and the infiltration of blood-derived immune cells. Simultaneously, non-neuronal residential cells, in particular astrocytes and microglia, are activated and participate in the formation of glial and fibrotic scar in the adult CNS. Such fibrotic scars appear to be built from stromal cells, but the precise origin is still under debate. While some studies suggested that the fibrotic scar is mainly from pericytes

associated with blood vessels (Dias et al. 2018; Göritz et al. 2011), others support the predominant contribution of proliferative CNS fibroblasts (Dorrier et al. 2021).

Another major focus is whether inflammation is beneficial or detrimental. Depletion of macrophages has been shown to improve regenerative outcomes following SCI (Popovich et al. 1999), suggesting that macrophages contribute to the inhibitory environment of the CNS. Though inflammation following CNS injury certainly has deleterious effects, the immune response has also been reported to have beneficial effects on axon regeneration (Benowitz and Popovich 2011; Schwartz and Raposo 2014). A recent study shows the multifaceted ways in which microglia act in the process of scar-free wound healing after SCI in neonatal mice (Li et al. 2020). After neonatal and adult injury, microglia become activated; however, while their activation is sustained in adults, after neonatal injury microglia reestablish homeostasis within a few days. These transiently activated microglia express not only fibronectin and other extracellular matrix molecules to form bridges reconnecting the spinal cord but also proteinase inhibitors to facilitate inflammation resolution (Li et al. 2020). Importantly the downregulation of these molecules in re-established microglia prevents the formation of a fibrotic scar after neonatal injury. Similarly, transient induction of connective tissue growth factor a (CTGFa) is important for initial bridging events after SCI in zebrafish, but its persistent expression might contribute to the scar formation in the adult lesions (Mokalled et al. 2016). Thus, such tight temporal control of microglial responses might be crucial for efficient wound healing. Modulating microglia and perhaps other inflammatory cells represent a potential strategy to temper neuroinflammation and enhance wound healing and axon regeneration.

Astrocytes are resident cells unique to CNS. As an essential part of the BBB, one of their functions is the communication between the blood and the brain. Upon injury, astrocytes undergo rapid reactive gliosis with massive cellular and molecular changes. This drastic change allows astrocytes to isolate the injury from surrounding neural tissue and restore the BBB (Burda and Sofroniew 2014).

However, later these reactive astrocytes may become detrimental to regeneration. Early studies emphasized the inhibitory nature of these cells, largely due to their expression of CSPGs and other types of growth-inhibiting ECMs (Silver and Miller 2004). As a component of the glial scar, some reactive astrocytes are tightly interwoven with other non-neuronal cells (fibroblasts or pericytes) within the gradually accumulating and disorganized ECM. This alters the molecular and physical properties of local tissues and causes the formation of physical and biochemical barriers to axon growth (Hara et al. 2017). On the other hand, mounting evidence suggests that some reactive astrocytes may be supportive for axon regeneration via the secretion of growth factors (Anderson et al. 2016, 2018) and the formation of elongated cell processes that act as a physical scaffold for such axons (Wanner et al. 2013). It is interesting to note that most regenerating axons induced by PTEN deletion cross the lesion in association with astrocyte bridges (Zukor et al. 2013), reminiscent of the observations that immature astrocytes are permissive for axon growth (Filous et al. 2010; White and Jakeman 2008). Thus, like microglia, astrocytes might exhibit different functional states (i.e., naïve, reactive, and scar-forming), thereby dynamically impacting axon regeneration and tissue reconstitution after injury. Similar to wound-healing responses in non-neural tissues, reactive astrocytes may undergo epithelial-to-mesenchymal transitions (Vivinetto et al. 2020). Further understanding cellular and molecular mechanisms that control the switch between these different states might offer new insights into developing methods which encourage a more permissive environment within the lesion.

Final decision: to regenerate or not

After successful growth cone formation, there are at least two requirements for a regeneration-competent axon to sustain extension: (1) supply and transport of cellular building blocks and (2) their assembly into new axonal segments. Accordingly, proper cell body responses, axonal transport, and membrane insertion are required.

Building blocks and energy for regeneration: axonal transport and translation. Unlike developing neurons, which have relatively short axons in embryos, axotomy in the adult often occurs in the distant, distal axonal segments. The required building blocks and energy necessary for regeneration must therefore be supplied to newly forming growth cones via local recycling (e.g., of actin and microtubules), local protein synthesis, and axonal transport. Considering that the diffusion of proteins requires ~60 days to travel a length of 1mm (Futerman and Banker 1996), axons largely rely on active transport along microtubule "highways" to both receive retrograde signals and send building blocks to an axon tip. These "*cargoes*" move along axons, utilizing kinesins for anterograde transport and dyneins for retrograde transport.

Like proteins, diffusion of ATP from the soma to the regenerating tip does not happen at a rate sufficient to support the energy requirements of new outgrowth. Since most of a cell's energy is generated by mitochondria, it is essential that mitochondria are located near the areas of high energy demand. Microtubule-based transport of mitochondria to a growing axon occurs via a conserved motor/adaptor complex consisting of the mitochondrial RhoGTPases Miro1/2 and TRAK1/2 (Schwarz 2013). Increasing mitochondrial motility may promote axon regeneration (Cartoni et al. 2016; Zhou et al. 2016). While such molecular machinery and regulation have been extensively characterized (Hirokawa and Takemura 2005), it is unknown whether it is possible to speed up such systems for more efficient axon regeneration. Local protein synthesis via axonal translation appears to be an evolved solution (Sahoo et al. 2018), but it remains unknown if non-regenerative adult mammalian axons undergo axonal translation.

Membrane insertion: Once the building blocks are in axons, they need to be properly assembled for axon extension. It is hypothesized that materials are added to the tip of extending axons during development via plasmalemmal precursor vesicles. However, little is known about membrane

transport and insertion during stretch growth in postnatal development or post-injury axon regeneration (Pfenninger 2009). Economically speaking, adding new membranes to the proximal end of networked axons, followed by lateral diffusion, reduces the need for long-distance transport. On the other hand, membranes could be inserted at multiple sites along the entire length of an axon. The smooth ER (SER) is distributed throughout axons as a continuous tubular network, raising the possibility that phospholipids may be synthesized locally in the axonal SER (Renvoisé and Blackstone 2010). Intriguingly, over-expression of protrudin, an integral ER membrane protein, promotes axon regeneration through the mobilization of endosomes and ER into the distal part of injured axons (Petrova et al. 2020). Thus, it will be interesting to develop other manipulations that could increase the axonal supply of growth molecules and organelles to enhance axon regeneration.

PERSPECTIVE

Despite tremendous progress made in the past decades, there is still no effective treatment of promoting axon regeneration in clinical settings. This is due to a few issues. First, the adult mammalian CNS exhibits limited axonal regeneration, both in length and number, even when using the best combinations of treatments. It is still a mystery why some, but not other, types of neurons remain refractory to regenerate under these manipulations. The application of new technologies like single-cell 'omics is promising to tease out the underlying mechanisms (Belin et al. 2015; Bray et al. 2019; Poplawski et al. 2020; Tran et al. 2019). Additionally, we do not understand why mammalian axon regeneration is so slow. This might be due to certain molecular and cellular limitations of adult neurons. During development, axon growth has two stages: relatively short distance growth cone-guided extension in early embryogenesis, followed by "stretch growth" exerted by increased distance between the neuronal soma and tethered axon terminus during later development (Smith 2009). However, axon regeneration is completely growth cone-dependent. It is unclear whether the cellular

and molecular machinery of adult neurons can support the lengths and speed of axon extension needed for regeneration. Considering growth cone-free stretch growth, it would be interesting to explore the possibilities of speeding up axon regeneration with mechanistic-based manipulations (de Vincentiis et al. 2020; Franze 2020). Second, regenerating axons may not automatically translate into functional recovery. At least in injured optic nerves, most, if not all, regenerated axons are not myelinated, representing an additional hurdle for functional recovery (Bei et al. 2016; Wang et al. 2020). Further, regenerating axons may not be able to integrate into the functional circuits in injured spinal cord, because of injury-induced circuit-level alterations such as excitation-inhibition imbalance (Courtine et al. 2009; Edgerton et al. 2001; Rossignol and Frigon 2011). In this regard, different manipulations have been developed to adjust the functional states of injuried spinal cords by electrical stimulation (Gerasimenko et al. 2015; Gill et al. 2020; Harkema et al. 2011) and other forms of neuromodulation (Brommer et al. 2021; Chen et al. 2018). Thus, ultimately combining these complemenary strategies to deal with both hardware (anatomical connections) and software (neuromodulation) issues might be able to achieve effective functional restoration after injury and dieases.

ACKNOWLEDGEMENTS: We wish to thank Tracey A.C.S Suter and Rahul Gupta for critically reading the manuscript. Our work is funded by NIH (R01NS096294, R01EY021526, and R01EY030204), the Dr. Miriam and Sheldon G. Adelson Medical Research Foundation, and Wings for Life.

FIGURES:

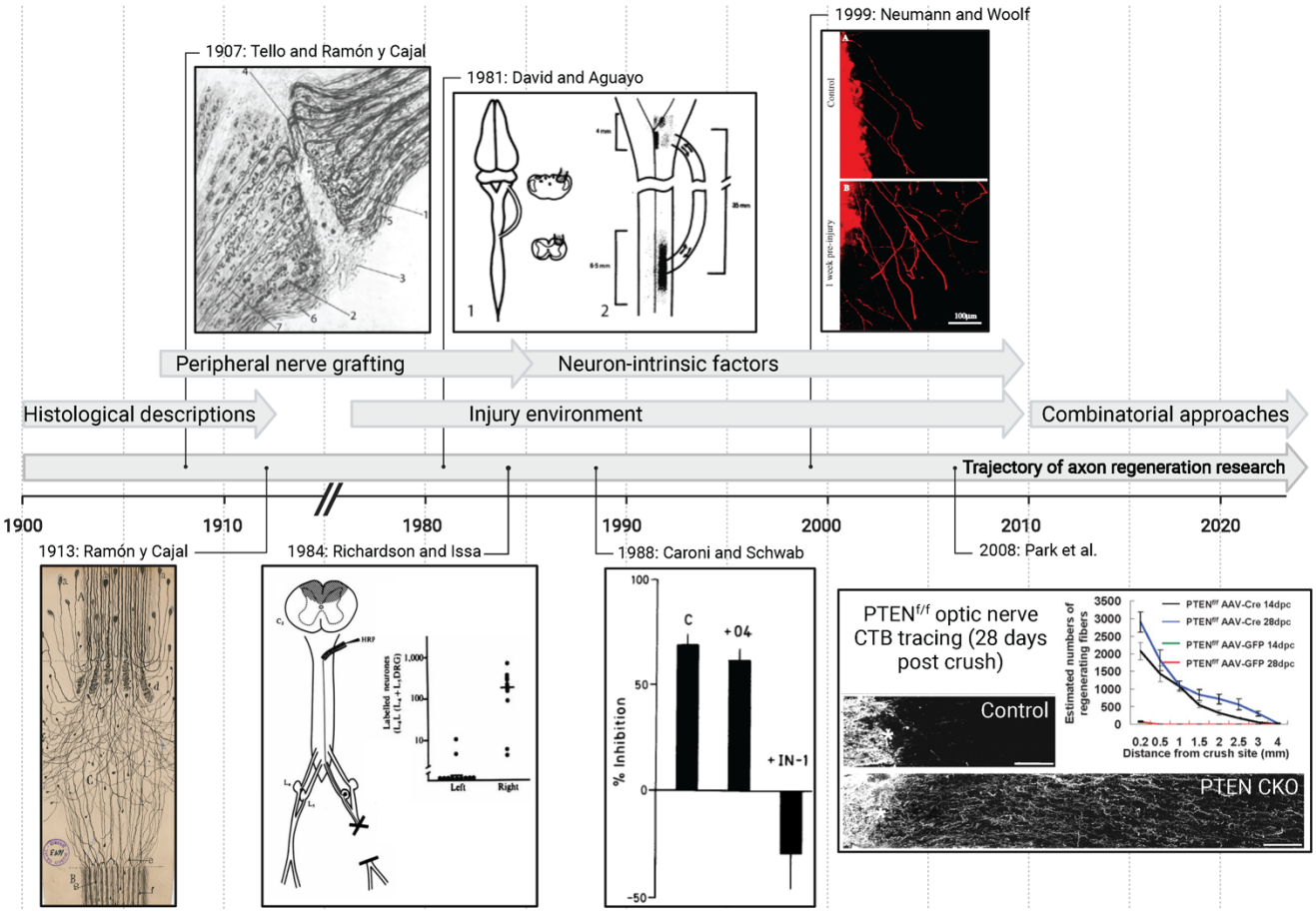


Figure 1: Major milestones of axon regeneration research. In **1907**, Tello (pupil of Ramón y Cajal) produced the first evidence that damaged CNS axons can regenerate if placed near the permissive PNS environment. Tello anastomosed an optic nerve stump (1) to a sciatic nerve graft (2) and observed a scar (3) as well as purported RGC axons crossing the site of anastomosis (4) regenerating into the sciatic nerve (7). (5) indicates a vein, (6) indicates neurilemma of the sciatic nerve (adapted from Tello, 1907). Tello's work was complemented by Ramón y Cajal's histological descriptions of the degeneration and regeneration of the CNS, published in **1913** and translated in 1928 (adapted from Ramón y Cajal, 1928). In **1981**, David and Aguayo confirmed Tello's findings that CNS neurons can regenerate in the permissive PNS. (1) Diagram of the dorsal aspect of a rat spinal cord, with a

peripheral nerve "bridge" between the medulla and thoracic spinal cord. Cross sections of the medulla and spinal cord illustrate where the bridge was directly attached. (2) The origin of axons innervating the graft were determined with horseradish peroxidase (HRP) retrograde labeling and found to originate in the brainstem and spinal cord (figure adapted from David and Aguayo, 1981). In **1984,** Richardson and Issa used peripheral nerve grafts to investigate the neuron *intrinsic* mechanisms of CNS injury and regeneration; long spinal axons of dorsal root ganglia (DRG) were 100 times more likely to regenerate into peripheral nerve grafts in the dorsal column (following bilateral dorsal column lesions) if their peripheral axons were also cut (adapted from Richardson and Issa, 1984). In **1999** Neumann and Woolf showed that altering intrinsic growth capacity of DRGs with a similar preconditioning lesion can promote regeneration of central axons in *CNS* tissue. Animals with a peripheral axotomy 1 to 2 weeks prior to (but not concomitant with) a dorsal column lesion show growth into and above the lesion, and that DRG explants show increased neurite outgrowth following preconditioning lesion (image shows explant results, adapted from Neumann and Woolf, 1999). Focusing on neuron extrinsic factors inhibiting regeneration, in **1988** Caroni and Schwab identified myelin-derived membrane proteins with nonpermissive substrate properties; a monoclonal antibody, IN-1, neutralizes the nonpermissive substrate properties (adapted from Caroni and Schwab, 1988a). A landmark study by Park et al. in **2008** highlighted the utility of altering the intrinsic state of neurons to promote axon regeneration – PTEN deletion (conditional knockout, CKO) was shown to promote exceptionally robust axon regeneration in an optic nerve crush model (scale bar: 100μm) (adapted from Park et al, 2008). Figure created with BioRender.com

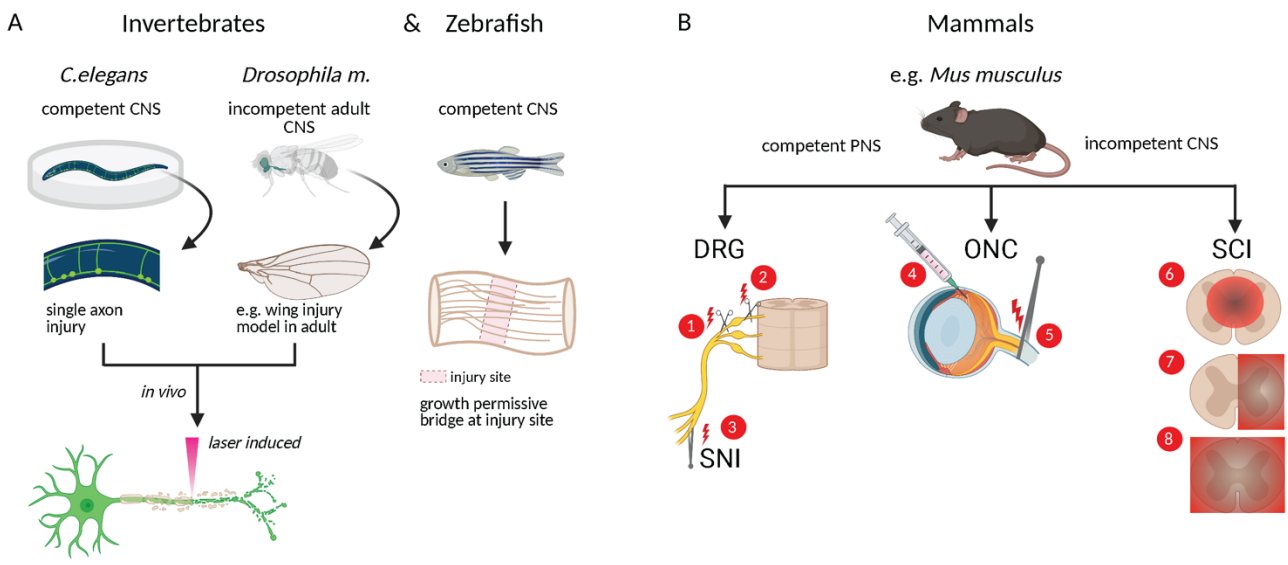


Figure 2: Models to study axon regeneration. (A) Invertebrates, e.g., *C. elegans* and *Drosophila melanogaster*, and zebrafish are well established models to study axon regeneration. They have short reproductive cycles to quickly screen gene function. The transparent cuticle and wings, of C. elegans and Drosophila can be used for laser induced axon regeneration studies *in vivo*. The growth permissive bridge at the injury site distinguishes the zebrafish as a CNS regeneration-competent vertebrate. **(B)** Other vertebrates or mammals like the mouse, *Mus musculus*, have a regeneration competent PNS, but incompetent CNS. In the mammalian system, (1) the DRG injury is used to model regeneration competent PNS injury or (2) to study the "preconditioning" effect for central branch injury. (3) SNI is another PNS injury model that keeps the neural tube intact to facilitate regeneration. In the ONC, viral vectors are used to manipulate RGC gene expression and/or anterograde axon labeling (4) to assess axon regeneration. Generally, this is measured from the injury site (5) and divided into short (> 2mm) and long (< 2mm) distance regeneration. SCI models used are (6) the contusion model to mimic clinical relevance, or more consistent models like (7) lateral or (8) full transection to study specific aspects of axon regeneration and the environmental contribution. Key: DRG, dorsal root ganglion; ONC, optic nerve crush; RGC, retinal ganglion cell; SCI, spinal cord injury; SNI, sciatic nerve injury. Figure created with BioRender.com

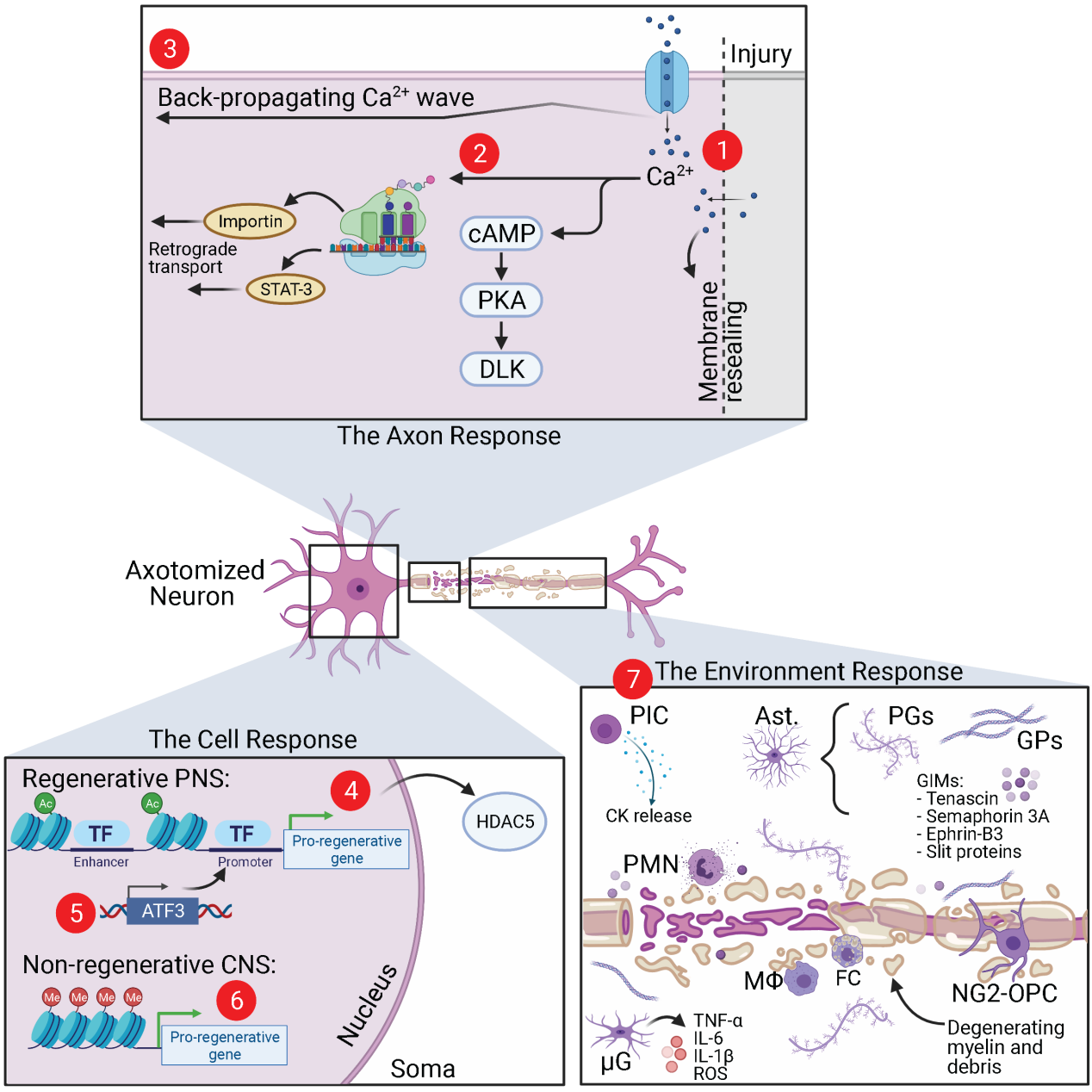


Figure 3: Soma, axonal, and environmental events following axon injury. (1). The initial response to injury of any axon is an immediate influx of calcium into the tip of the severed axon, which triggers activation of calpains and subsequent Ca^{2+}-dependent membrane fusion to re-seal the ruptured end of the axon. (2) Calcium also leads to activation of local protein synthesis (e.g., of STAT3 and importin-β which are retrogradely transported to initiate regenerative programs at the soma) and protein activity such as DLK-1. (3) Additionally, an injury-induced back-propagating calcium wave

induces changes in gene expression, such as the (4) epigenetic changes seen in regenerative PNS neurons (e.g., DRG) via activation of PKCμ resulting nuclear export of HDAC5 (histone deacetylase 5). HDAC5's absence in the nucleus enables a transition from repressive DNA histone methylation to permissive acetylation within the nucleus, which (5) allows transcription factors such as ATF3 to bind to accessible sites. (6) In contrast, non-regenerative axons of the adult CNS do not induce similar epigenetic changes so that DNA remains in a methylated, repressive state. (7) The post-injury microenvironment plays a critical role in dictating regeneration-competence. Activated microglia clear apoptotic cells and debris from the damaged extracellular matrix, while releasing inflammatory mediators to recruit leukocytes from the periphery. Neutrophils secrete damaging proteolytic enzymes. Recruited macrophages to the injury site become indistinguishable from activated microglia, performing phagocytosis and pro-inflammatory roles. NG2-expressing OPCs also contribute to inhibition of axon regeneration. Finally, astrocytes contribute to the formation of the glial scar in the CNS but not PNS to form a chemical and physical barrier to axon regeneration. Key: PIC, peripheral immune cell; CK, cytokine; Ast., astrocyte; PGs, proteoglycans; GPs, glycoproteins; GIMs, growth inhibitory molecules; FC, foam cell; MΦ, macrophage; μG, microglia; ROS, reactive oxygen species; OPC, oligodendrocyte precursor cell; PMN, polymorphonuclear cell (neutrophil). Figure created with BioRender.com

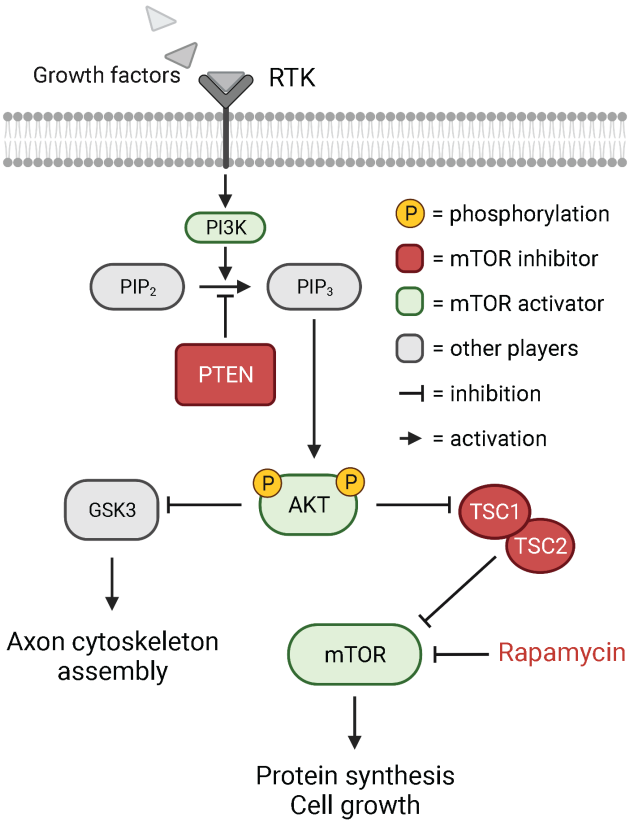


Figure 4: The PI3K/AKT/mTOR pathway. The PI3K/AKT/mTOR pathway is activated through the binding of growth factors to the receptor tyrosine kinase (RTK) complex, which in turn activates PI3K. The activated form of PI3K converts PIP2 to PIP3 which then mediates the phosphorylation of AKT. AKT acts on a wide range of substrates involved in the regulation of important cellular function. This includes blocking negative regulators of mTOR, such as TSC1 or TSC2. Active mTOR is associated with high protein synthesis, cell proliferation, and cell growth. PTEN acts as a tumor suppressor that negatively regulates this pathway by removing the 3-phosphate from PIP3. Loss of PTEN leads to over-activation of the mTOR pathway and has been shown to promote exceptionally robust axon regeneration following CNS injury (Park et al, 2008, Liu et al., 2010). This effect can be abolished with the application of rapamycin, a known inhibitor of mTOR, indicating that the pro-regenerative effects of this treatment are mTOR-dependent (Park et al, 2008). mTOR-independent signaling mechanisms, however, appear to also be important for axon

regeneration. This is underscored by the finding that genetic deletion of other negative regulators of mTOR, such as TSC2, only partially mimic the effects of PTEN deletion in the CNS (Park et al, 2008); therefore, PTEN deletion likely works via additional effectors (such as GSK3) to promote axon regeneration. Key: RTK, receptor tyrosine kinase; PI3K, phosphoinositide 3-kinase; PIP_2, phosphatidylinositol 4,5-bisphosphate; PIP_3, phosphatidylinositol 3,4,5-triphosphate; PTEN, phosphatase and tensin homolog; GSK3, glycogen synthase kinase 3; TSC, tuberous sclerosis complex; mTOR, mammalian target of rapamycin. Figure created with BioRender.com.

REFERENCES:

Abe N, Borson SH, Gambello MJ, Wang F, Cavalli V. 2010. Mammalian Target of Rapamycin (mTOR) activation increases axonal growth capacity of injured peripheral nerves. *J Biol Chem* **285**: 28034–28043.

Al-Ali H, Beckerman SR, Bixby JL, Lemmon VP. 2017. In vitro models of axon regeneration. *Exp Neurol* **287**: 423–434.

Anderson MA, Burda JE, Ren Y, Ao Y, O'Shea TM, Kawaguchi R, Coppola G, Khakh BS, Deming TJ, Sofroniew M V. 2016. Astrocyte scar formation AIDS central nervous system axon regeneration. *Nature* **532**: 195–200.

Anderson MA, O'Shea TM, Burda JE, Ao Y, Barlatey SL, Bernstein AM, Kim JH, James ND, Rogers A, Kato B, et al. 2018. Required growth facilitators propel axon regeneration across complete spinal cord injury. *Nature* **561**: 396–400.

Apara A, Galvao J, Wang Y, Blackmore M, Trillo A, Iwao K, Brown DP, Fernandes KA, Huang A, Nguyen T, et al. 2017. KLF9 and JNK3 interact to suppress axon regeneration in the adult CNS. *J Neurosci* **37**: 9632–9644.

Bareyre FM, Garzorz N, Lang C, Misgeld T, Büning H, Kerschensteiner M. 2011. In vivo imaging reveals a phase-Specific role of stat3 during central and peripheral nervous system axon regeneration. *Proc Natl Acad Sci U S A* **108**: 6282–6287.

Bauder AR, Ferguson TA. 2012. Reproducible mouse sciatic nerve crush and subsequent assessment of regeneration by whole mount muscle analysis. *J Vis Exp*.

Becker T, Becker CG. 2014. Axonal regeneration in zebrafish. *Curr Opin Neurobiol* **27**: 186–191.

Bei F, Lee HHC, Liu X, Gunner G, Jin H, Ma L, Wang C, Hou L, Hensch TK, Frank E, et al. 2016. Restoration of Visual Function by Enhancing Conduction in Regenerated Axons. *Cell* **164**: 219–232.

Belin S, Nawabi H, Wang C, Tang S, Latremoliere A, Warren P, Schorle H, Uncu C, Woolf CJ, He Z, et al. 2015. Injury-Induced Decline of Intrinsic Regenerative Ability Revealed by Quantitative Proteomics. *Neuron* **86**: 1000–1014.

Benowitz LI, Popovich PG. 2011. Inflammation and axon regeneration. *Curr Opin Neurol* **24**: 577–583.

Blackmore MG, Wang Z, Lerch JK, Motti D, Zhang YP, Shields CB, Lee JK, Goldberg JL, Lemmon VP, Bixby JL. 2012. Krüppel-like Factor 7 engineered for transcriptional activation promotes axon regeneration in the adult corticospinal tract. *Proc Natl Acad Sci U S A* **109**: 7517–7522.

Blanquie O, Bradke F. 2018. Cytoskeleton dynamics in axon regeneration. *Curr Opin Neurobiol* **51**: 60–69.

Brace EJ, DiAntonio A. 2017. Models of axon regeneration in Drosophila. *Exp Neurol* **287**: 310–317.

Bradbury EJ, Moon LDF, Popat RJ, King VR, Bennett GS, Patel PN, Fawcett JW, McMahon SB. 2002. Chondroitinase ABC promotes functional recovery after spinal cord injury. *Nature* **416**: 636–640.

Bray ER, Yungher BJ, Levay K, Ribeiro M, Dvoryanchikov G, Ayupe AC, Thakor K, Marks V, Randolph M, Danzi MC, et al. 2019. Thrombospondin-1 Mediates Axon Regeneration in Retinal Ganglion Cells. *Neuron* **103**: 642-657.e7.

Brommer B, He M, Zhang Z, Yang Z, Page JC, Su J, Zhang Y, Zhu J, Gouy E, Tang J, et al. 2021. Improving hindlimb locomotor function by Non-invasive AAV-mediated manipulations of propriospinal neurons in mice with complete spinal cord injury. *Nat Commun* **12**: 1–14.

Buenrostro JD, Giresi PG, Zaba LC, Chang HY, Greenleaf WJ. 2013. Transposition of native

chromatin for fast and sensitive epigenomic profiling of open chromatin, DNA-binding proteins and nucleosome position. *Nat Methods* **10**: 1213–1218.
Buenrostro JD, Wu B, Chang HY, Greenleaf WJ. 2015. ATAC-seq: A method for assaying chromatin accessibility genome-wide. *Curr Protoc Mol Biol* **2015**: 21.29.1-21.29.9.
Burda JE, Sofroniew M V. 2014. Reactive gliosis and the multicellular response to CNS damage and disease. *Neuron* **81**: 229–248.
Cafferty WBJ, Gardiner NJ, Das P, Qiu J, McMahon SB, Thompson SWN. 2004. Conditioning Injury-Induced Spinal Axon Regeneration Fails in Interleukin-6 Knock-Out Mice. *J Neurosci* **24**: 4432–4443.
Caroni P, Schwab ME. 1988a. *Antibody against Myelin-Associated Inhibitor of Neurite Growth Neutralizes Nonpermissive Substrate Properties of CNS White Matter*.
Caroni P, Schwab ME. 1988b. Two membrane protein fractions from rat central myelin with inhibitory properties for neurite growth and fibroblast spreading. *J Cell Biol* **106**: 1281–1288.
Cartoni R, Norsworthy MW, Bei F, Wang C, Li S, Zhang Y, Gabel C V., Schwarz TL, He Z. 2016. The Mammalian-Specific Protein Armcx1 Regulates Mitochondrial Transport during Axon Regeneration. *Neuron* **92**: 1294–1307.
Chandran V, Coppola G, Nawabi H, Omura T, Versano R, Huebner EA, Zhang A, Costigan M, Yekkirala A, Barrett L, et al. 2016. A Systems-Level Analysis of the Peripheral Nerve Intrinsic Axonal Growth Program. *Neuron* **89**: 956–970.
Chen B, Li Y, Yu B, Zhang Z, Brommer B, Williams PR, Liu Y, Hegarty SV, Zhou S, Zhu J, et al. 2018. Reactivation of Dormant Relay Pathways in Injured Spinal Cord by KCC2 Manipulations. *Cell* **174**: 1599.
Cho Y, Sloutsky R, Naegle KM, Cavalli V. 2013. XInjury-Induced HDAC5 nuclear export is essential for axon regeneration. *Cell* **155**: 894.
Cigliola V, Becker CJ, Poss KD. 2020. Building bridges, not walls: Spinal cord regeneration in zebrafish. *DMM Dis Model Mech* **13**.
Corces MR, Trevino AE, Hamilton EG, Greenside PG, Sinnott-Armstrong NA, Vesuna S, Satpathy AT, Rubin AJ, Montine KS, Wu B, et al. 2017. An improved ATAC-seq protocol reduces background and enables interrogation of frozen tissues. *Nat Methods* **14**: 959–962.
Courtine G, Gerasimenko Y, Van Den Brand R, Yew A, Musienko P, Zhong H, Song B, Ao Y, Ichiyama RM, Lavrov I, et al. 2009. Transformation of nonfunctional spinal circuits into functional states after the loss of brain input. *Nat Neurosci* **12**: 1333–1342.
David S, Aguayo AJ. 1981. Axonal elongation into peripheral nervous system "bridges" after central nervous system injury in adult rats. *Science (80-)* **214**: 931–933.
de Vincentiis S, Falconieri A, Mainardi M, Cappello V, Scribano V, Bizzarri R, Storti B, Dente L, Costa M, Raffa V. 2020. Extremely Low Forces Induce Extreme Axon Growth. *J Neurosci* **40**: 4997–5007.
Derry WB, Wilson L, Khan IA, Ludueña RF, Jordan MA. 1997. Taxol differentially modulates the dynamics of microtubules assembled from unfractionated and purified β-tubulin isotypes. *Biochemistry* **36**: 3554–3562.
Di Maio A, Skuba A, Himes BT, Bhagat SL, Hyun JK, Tessler A, Bishop D, Son YJ. 2011. In vivo imaging of dorsal root regeneration: Rapid immobilization and presynaptic differentiation at the CNS/PNS border. *J Neurosci* **31**: 4569–4582.
Dias DO, Kim H, Holl D, Werne Solnestam B, Lundeberg J, Carlén M, Göritz C, Frisén J. 2018. Reducing Pericyte-Derived Scarring Promotes Recovery after Spinal Cord Injury. *Cell* **173**: 153-165.e22.
Dorrier CE, Aran D, Haenelt EA, Sheehy RN, Hoi KK, Pintarić L, Chen Y, Lizama CO, Cautivo KM, Weiner GA, et al. 2021. CNS fibroblasts form a fibrotic scar in response to immune cell

infiltration. *Nat Neurosci* **24**: 234–244.
Du K, Zheng S, Zhang Q, Li S, Gao X, Wang J, Jiang L, Liu K. 2015. Pten deletion promotes regrowth of corticospinal tract axons 1 year after spinal cord injury. *J Neurosci* **35**: 9754–9763.
Duan X, Qiao M, Bei F, Kim IJ, He Z, Sanes JR. 2015. Subtype-Specific regeneration of retinal ganglion cells following axotomy: Effects of osteopontin and mtor signaling. *Neuron* **85**: 1244–1256.
Edgerton VR, Leon RD, Harkema SJ, Hodgson JA, London N, Reinkensmeyer DJ, Roy RR, Talmadge RJ, Tillakaratne NJ, Timoszyk W, et al. 2001. Retraining the injured spinal cord. *J Physiol* **533**: 15–22.
Ertürk A, Hellal F, Enes J, Bradke F. 2007. Disorganized microtubules underlie the formation of retraction bulbs and the failure of axonal regeneration. *J Neurosci* **27**: 9169–9180.
Fang Y, Soares L, Teng X, Geary M, Bonini NM. 2012. A novel drosophila model of nerve injury reveals an essential role of Nmnat in maintaining axonal integrity. *Curr Biol* **22**: 590–595.
Filbin MT. 2003. Myelin-associated inhibitors of axonal regeneration in the adult mammalian CNS. *Nat Rev Neurosci* **4**: 703–713.
Filous AR, Miller JH, Coulson-Thomas YM, Horn KP, Alilain WJ, Silver J. 2010. Immature astrocytes promote CNS axonal regeneration when combined with chondroitinase ABC. *Dev Neurobiol* **70**: 826–841.
Finelli MJ, Wong JK, Zou H. 2013. Epigenetic regulation of sensory axon regeneration after spinal cord injury. *J Neurosci* **33**: 19664–19676.
Fischer D, Harvey AR, Pernet V, Lemmon VP, Park KK. 2017. Optic nerve regeneration in mammals: Regenerated or spared axons? *Exp Neurol* **296**: 83–88.
Fischer D, Heiduschka P, Thanos S. 2001. Lens-injury-stimulated axonal regeneration throughout the optic pathway of adult rats. *Exp Neurol* **172**: 257–272.
Franze K. 2020. Integrating Chemistry and Mechanics: The Forces Driving Axon Growth. *Annu Rev Cell Dev Biol* **36**: 61–83.
Futerman AH, Banker GA. 1996. *The economics of neurite outgrowth-the addition of new membrane to growing axons*.
Gaub P, Tedeschi A, Puttagunta R, Nguyen T, Schmandke A, Di Giovanni S. 2010. HDAC inhibition promotes neuronal outgrowth and counteracts growth cone collapse through CBP/p300 and P/CAF-dependent p53 acetylation. *Cell Death Differ* **17**: 1392–1408.
Gerasimenko Y, Gorodnichev R, Moshonkina T, Sayenko D, Gad P, Reggie Edgerton V. 2015. Transcutaneous electrical spinal-cord stimulation in humans. *Ann Phys Rehabil Med* **58**: 225–231.
Ghosh-Roy A, Wu Z, Goncharov A, Jin Y, Chisholm AD. 2010. Calcium and cyclic AMP promote axonal regeneration in Caenorhabditis elegans and require DLK-1 kinase. *J Neurosci* **30**: 3175–3183.
Giehl KM, Tetzlaff W. 1996. BDNF and NT-3, but not NGF, Prevent Axotomy-induced Death of Rat Corticospinal Neurons *In Vivo*. *Eur J Neurosci* **8**: 1167–1175.
Gill M, Linde M, Fautsch K, Hale R, Lopez C, Veith D, Calvert J, Beck L, Garlanger K, Edgerton R, et al. 2020. Epidural Electrical Stimulation of the Lumbosacral Spinal Cord Improves Trunk Stability During Seated Reaching in Two Humans With Severe Thoracic Spinal Cord Injury. *Front Syst Neurosci* **14**.
Goldberg JL, Klassen MP, Hua Y, Barres BA. 2002. Amacrine-signaled loss of intrinsic axon growth ability by retinal ganglion cells. *Science (80-)* **296**: 1860–1864.
Gordon T. 2020. Peripheral nerve regeneration and muscle reinnervation. *Int J Mol Sci* **21**: 1–24.
Göritz C, Dias DO, Tomilin N, Barbacid M, Shupliakov O, Frisén J. 2011. A pericyte origin of spinal cord scar tissue. *Science (80-)* **333**: 238–242.
Gruner JA. 1992. A Monitored Contusion Model of Spinal Cord Injury in the Rat. *J Neurotrauma* **9**:

123–128.
Hammarlund M, Nix P, Hauth L, Jorgensen EM, Bastiani M. 2009. Axon regeneration requires a conserved MAP kinase pathway. *Science (80-)* **323**: 802–806.
Hao Y, Frey E, Yoon C, Wong H, Nestorovski D, Holzman LB, Giger RJ, DiAntonio A, Collins C. 2016. An evolutionarily conserved mechanism for cAMP elicited axonal regeneration involves direct activation of the dual leucine zipper kinase DLK. *Elife* **5**.
Hara M, Kobayakawa K, Ohkawa Y, Kumamaru H, Yokota K, Saito T, Kijima K, Yoshizaki S, Harimaya K, Nakashima Y, et al. 2017. Interaction of reactive astrocytes with type i collagen induces astrocytic scar formation through the integrin-N-cadherin pathway after spinal cord injury. *Nat Med* **23**: 818–828.
Harkema S, Gerasimenko Y, Hodes J, Burdick J, Angeli C, Chen Y, Ferreira C, Willhite A, Rejc E, Grossman RG, et al. 2011. Effect of epidural stimulation of the lumbosacral spinal cord on voluntary movement, standing, and assisted stepping after motor complete paraplegia: A case study. *Lancet* **377**: 1938–1947.
Harris WA, Holt CE, Bonhoeffer F. 1987. *Retinal axons with and without their somata, growing to and arborizing in the tectum of Xenopus embryos: a time-lapse video study of single fibres in vivo*.
He Z, Jin Y. 2016. Intrinsic Control of Axon Regeneration. *Neuron* **90**: 437–451.
Heinrich PC, Behrmann I, Müller-Newen G, Schaper F, Graeve L. 1998. Interleukin-6-type cytokine signalling through the gp130/Jak/STAT pathway. *Biochem J* **334**: 297–314.
Hellal F, Hurtado A, Ruschel J, Flynn KC, Laskowski CJ, Umlauf M, Kapitein LC, Strikis D, Lemmon V, Bixby J, et al. 2011. Microtubule stabilization reduces scarring and causes axon regeneration after spinal cord injury. *Science (80-)* **331**: 928–931.
Hirokawa N, Takemura R. 2005. Molecular motors and mechanisms of directional transport in neurons. *Nat Rev Neurosci* **6**: 201–214.
Hollis ER, Lu P, Blesch A, Tuszynski MH. 2009. IGF-I gene delivery promotes corticospinal neuronal survival but not regeneration after adult CNS injury. *Exp Neurol* **215**: 53–59.
Horvath S. 2013. DNA methylation age of human tissues and cell types. *Genome Biol* **14**: R115.
Hu Y, Park KK, Yang L, Wei X, Yang Q, Cho KS, Thielen P, Lee AH, Cartoni R, Glimcher LH, et al. 2012. Differential effects of unfolded protein response pathways on axon injury-induced death of retinal ganglion cells. *Neuron* **73**: 445–452.
Jin G, Zhao J, Yang Y, Liu K, Jiang Y, Zhang X, Zhang Y, Huang Y, Lu J, Dong Z. 2015. JAK/STAT3 signaling pathway mediates endothelial-like differentiation of immature dendritic cells. *Oncol Lett* **10**: 3471–3477.
Kalinski AL, Yoon C, Huffman LD, Duncker PC, Kohen R, Passino R, Hafner H, Johnson C, Kawaguchi R, Carbajal KS, et al. 2020. Analysis of the immune response to sciatic nerve injury identifies efferocytosis as a key mechanism of nerve debridement. *Elife* **9**: 1–41.
Khan IA, Ludueña RF. 2003. Different effects of vinblastine on the polymerization of isotypically purified tubulins from bovine brain. *Invest New Drugs* **21**: 3–13.
Lang BT, Cregg JM, Depaul MA, Tran AP, Xu K, Dyck SM, Madalena KM, Brown BP, Weng YL, Li S, et al. 2015. Modulation of the proteoglycan receptor PTPσ promotes recovery after spinal cord injury. *Nature* **518**: 404–408.
Leibinger M, Andreadaki A, Diekmann H, Fischer D. 2013. Neuronal STAT3 activation is essential for CNTF- and inflammatory stimulation-induced CNS axon regeneration. *Cell Death Dis* **4**: 805.
Leibinger M, Zeitler C, Gobrecht P, Andreadaki A, Gisselmann G, Fischer D. 2021. Transneuronal delivery of hyper-interleukin-6 enables functional recovery after severe spinal cord injury in mice. *Nat Commun* **12**: 1–14.
Leon S, Yin Y, Nguyen J, Irwin N, Benowitz LI. 2000. Lens injury stimulates axon regeneration in

the mature rat optic nerve. *J Neurosci* **20**: 4615–4626.
Li Y, He X, Kawaguchi R, Zhang Y, Wang Q, Monavarfeshani A, Yang Z, Chen B, Shi Z, Meng H, et al. 2020. Microglia-organized scar-free spinal cord repair in neonatal mice. *Nature* 1–6.
Liu K, Lu Y, Lee JK, Samara R, Willenberg R, Sears-Kraxberger I, Tedeschi A, Park KK, Jin D, Cai B, et al. 2010. PTEN deletion enhances the regenerative ability of adult corticospinal neurons. *Nat Neurosci* **13**: 1075–1081.
Liu Y, Wang X, Li W, Zhang Q, Li Y, Zhang Z, Zhu J, Chen B, Williams PR, Zhang Y, et al. 2017. A Sensitized IGF1 Treatment Restores Corticospinal Axon-Dependent Functions. *Neuron* **95**: 817-833.e4.
Lowery LA, Vactor D Van. 2009. The trip of the tip: Understanding the growth cone machinery. *Nat Rev Mol Cell Biol* **10**: 332–343.
Lu P, Blesch A, Tuszynski MH. 2001. Neurotrophism without neurotropism: BDNF promotes survival but not growth of lesioned corticospinal neurons. *J Comp Neurol* **436**: 456–470.
Lu Y, Brommer B, Tian X, Krishnan A, Meer M, Wang C, Vera DL, Zeng Q, Yu D, Bonkowski MS, et al. 2020. Reprogramming to recover youthful epigenetic information and restore vision. *Nature* **588**.
McKeon RJ, Höke A, Silver J. 1995. Injury-induced proteoglycans inhibit the potential for laminin-mediated axon growth on astrocytic scars. *Exp Neurol* **136**: 32–43.
Mokalled MH, Patra C, Dickson AL, Endo T, Stainier DYR, Poss KD. 2016. Injury-induced ctgfa directs glial bridging and spinal cord regeneration in zebrafish. *Science (80-)* **354**: 630–634.
Moore DL, Blackmore MG, Hu Y, Kaestner KH, Bixby JL, Lemmon VP, Goldberg JL. 2009. KLF family members regulate intrinsic axon regeneration ability. *Science (80-)* **326**: 298–301.
Namgung U. 2014. The role of schwann cell-axon interaction in peripheral nerve regeneration. *Cells Tissues Organs* **200**: 6–12.
Neumann S, Woolf CJ. 1999. Regeneration of dorsal column fibers into and beyond the lesion site following adult spinal cord injury. *Neuron* **23**: 83–91.
Norsworthy MW, Bei F, Kawaguchi R, Wang Q, Tran NM, Li Y, Brommer B, Zhang Y, Wang C, Sanes JR, et al. 2017. Sox11 Expression Promotes Regeneration of Some Retinal Ganglion Cell Types but Kills Others. *Neuron* **94**: 1112-1120.e4.
O'Shea TM, Burda JE, Sofroniew M V. 2017. Cell biology of spinal cord injury and repair. *J Clin Invest* **127**: 3259–3270.
Palmisano I, Danzi MC, Hutson TH, Zhou L, McLachlan E, Serger E, Shkura K, Srivastava PK, Hervera A, Neill NO, et al. 2019. Epigenomic signatures underpin the axonal regenerative ability of dorsal root ganglia sensory neurons. *Nat Neurosci* **22**: 1913–1924.
Park KK, Liu K, Hu Y, Smith PD, Wang C, Cai B, Xu B, Connolly L, Kramvis I, Sahin M, et al. 2008. Promoting axon regeneration in the adult CNS by modulation of the PTEN/mTOR pathway. *Science (80-)* **322**: 963–966.
Petrova V, Pearson CS, Ching J, Tribble JR, Solano AG, Yang Y, Love FM, Watt RJ, Osborne A, Reid E, et al. 2020. Protrudin functions from the endoplasmic reticulum to support axon regeneration in the adult CNS. *Nat Commun* **11**: 1–15.
Pfenninger KH. 2009. Plasma membrane expansion: A neuron's Herculean task. *Nat Rev Neurosci* **10**: 251–261.
Poplawski GHD, Kawaguchi R, Van Niekerk E, Lu P, Mehta N, Canete P, Lie R, Dragatsis I, Meves JM, Zheng B, et al. 2020. Injured adult neurons regress to an embryonic transcriptional growth state. *Nature* **581**: 77–82.
Popovich PG, Guan Z, Wei P, Huitinga I, Van Rooijen N, Stokes BT. 1999. Depletion of hematogenous macrophages promotes partial hindlimb recovery and neuroanatomical repair after experimental spinal cord injury. *Exp Neurol* **158**: 351–365.

Puttagunta R, Tedeschi A, Sória MG, Hervera A, Lindner R, Rathore KI, Gaub P, Joshi Y, Nguyen T, Schmandke A, et al. 2014. PCAF-dependent epigenetic changes promote axonal regeneration in the central nervous system. *Nat Commun* **5**: 1–13.
Ramon y Cajal S. 1928. Degeneration and regeneration of the nervous system.
Rasmussen JP, Sagasti A. 2017. Learning to swim, again: Axon regeneration in fish. *Exp Neurol* **287**: 318–330.
Renthal W, Tochitsky I, Yang L, Cheng YC, Li E, Kawaguchi R, Geschwind DH, Woolf CJ. 2020. Transcriptional Reprogramming of Distinct Peripheral Sensory Neuron Subtypes after Axonal Injury. *Neuron* **108**: 128-144.e9.
Renvoisé B, Blackstone C. 2010. Emerging themes of ER organization in the development and maintenance of axons. *Curr Opin Neurobiol* **20**: 531–537.
Richardson PM, Issa VMK. 1984. Peripheral injury enhances central regeneration of primary sensory neurones. *Nature* **309**: 791–793.
Rodemer W, Gallo G, Selzer ME. 2020. Mechanisms of Axon Elongation Following CNS Injury: What Is Happening at the Axon Tip? *Front Cell Neurosci* **14**: 177.
Rossignol S, Frigon A. 2011. Recovery of locomotion after spinal cord injury: Some facts and mechanisms. *Annu Rev Neurosci* **34**: 413–440.
Ruschel J, Hellal F, Flynn KC, Dupraz S, Elliott DA, Tedeschi A, Bates M, Sliwinski C, Brook G, Dobrindt K, et al. 2015. Systemic administration of epothilone B promotes axon regeneration after spinal cord injury. *Science (80-)* **348**: 347–352.
Sahoo PK, Smith DS, Perrone-Bizzozero N, Twiss JL. 2018. Axonal mRNA transport and translation at a glance. *J Cell Sci* **131**.
Santos TE, Schaffran B, Broguiè N, Meyn L, Zenobi-Wong M, Correspondence FB, Bradke F. 2020. Axon Growth of CNS Neurons in Three Dimensions Is Amoeboid and Independent of Adhesions.
Saxton RA, Sabatini DM. 2017. mTOR Signaling in Growth, Metabolism, and Disease. *Cell* **168**: 960–976.
Schwab ME, Strittmatter SM. 2014. Nogo limits neural plasticity and recovery from injury. *Curr Opin Neurobiol* **27**: 53–60.
Schwaiger F-W, Schmitt GH andreas B, Horvat A, Hager G, Streif R, Spitzer C, Gamal S, Breuer S, Brook GA, Nacimiento W, et al. 2000. Peripheral but not central axotomy induces changes in Janus kinases (JAK) and signal transducers and activators of transcription (STAT). *Eur J Neurosci* **12**: 1165–1176.
Schwartz M, Raposo C. 2014. Protective autoimmunity: A unifying model for the immune network involved in CNS repair. *Neuroscientist* **20**: 343–358.
Schwarz TL. 2013. Mitochondrial trafficking in neurons. *Cold Spring Harb Perspect Biol* **5**: a011304.
Seijffers R, Mills CD, Woolf CJ. 2007. ATF3 increases the intrinsic growth state of DRG neurons to enhance peripheral nerve regeneration. *J Neurosci* **27**: 7911–7920.
Silver J, Miller JH. 2004. Regeneration beyond the glial scar. *Nat Rev Neurosci* **5**: 146–156.
Smith DH. 2009. Stretch growth of integrated axon tracts: Extremes and exploitations. *Prog Neurobiol* **89**: 231–239.
Sofroniew M V. 2018. Dissecting spinal cord regeneration perspective. *Nature* **557**: 343–350.
Stine ZE, Walton ZE, Altman BJ, Hsieh AL, Dang C V. 2015. MYC, metabolism, and cancer. *Cancer Discov* **5**: 1024–1039.
Stokes BT. 1992. Experimental Spinal Cord Injury: A Dynamic and Verifiable Injury Device. *J Neurotrauma* **9**: 129–134.
Sun F, Park KK, Belin S, Wang D, Lu T, Chen G, Zhang K, Yeung C, Feng G, Yankner BA, et al. 2011. Sustained axon regeneration induced by co-deletion of PTEN and SOCS3. *Nature* **480**:

372–375.
Takahashi K, Yamanaka S. 2006. Induction of Pluripotent Stem Cells from Mouse Embryonic and Adult Fibroblast Cultures by Defined Factors. *Cell* **126**: 663–676.
Tello JF. 1907. La regeneration dans les voies optiques. *Trab Lab Invest Biol Univ Madrid* **5**: 237–248.
Terenzio M, Schiavo G, Fainzilber M. 2017. Compartmentalized Signaling in Neurons: From Cell Biology to Neuroscience. *Neuron* **96**: 667–679.
Tran AP, Warren PM, Silver J. 2018. The biology of regeneration failure and success after spinal cord injury. *Physiol Rev* **98**: 881–917.
Tran NM, Shekhar K, Whitney IE, Jacobi A, Benhar I, Hong G, Yan W, Adiconis X, Arnold ME, Lee JM, et al. 2019. Single-Cell Profiles of Retinal Ganglion Cells Differing in Resilience to Injury Reveal Neuroprotective Genes. *Neuron* **104**: 1039-1055.e12.
Tuszynski MH, Steward O. 2012. Concepts and Methods for the Study of Axonal Regeneration in the CNS. *Neuron* **74**: 777–791.
Venkatesh I, Mehra V, Wang Z, Califf B, Blackmore MG. 2018. Developmental Chromatin Restriction of Pro-Growth Gene Networks Acts as an Epigenetic Barrier to Axon Regeneration in Cortical Neurons. *Dev Neurobiol* **78**: 960–977.
Vivinetto AL, Kim I-D, Goldberg DC, Hill CE, Cho S, Cave JW, Fones L, Brown E, Tarabykin VS. 2020. Zeb2 Is a Regulator of Astrogliosis and Functional Recovery after CNS Injury Correspondence Zeb2 Is a Regulator of Astrogliosis and Functional Recovery after CNS Injury. *CellReports* **31**: 107834.
Wang J, He X, Meng H, Li Y, Dmitriev P, Tian F, Page JC, Lu QR, He Z. 2020. Robust Myelination of Regenerated Axons Induced by Combined Manipulations of GPR17 and Microglia. *Neuron* **108**: 876-886.e4.
Wang X, Chun SJ, Treloar H, Vartanian T, Greer CA, Strittmatter SM. 2002. Localization of Nogo-A and Nogo-66 receptor proteins at sites of axon-myelin and synaptic contact. *J Neurosci* **22**: 5505–5515.
Wang Z, Reynolds A, Kirry A, Nienhaus C, Blackmore MG. 2015. Overexpression of Sox11 promotes corticospinal tract regeneration after spinal injury while interfering with functional recovery. *J Neurosci* **35**: 3139–3145.
Wanner IB, Anderson MA, Song B, Levine J, Fernandez A, Gray-Thompson Z, Ao Y, Sofroniew M V. 2013. Glial scar borders are formed by newly proliferated, elongated astrocytes that interact to corral inflammatory and fibrotic cells via STAT3-dependent mechanisms after spinal cord injury. *J Neurosci* **33**: 12870–12886.
Watkins TA, Wang B, Huntwork-Rodriguez S, Yang J, Jiang Z, Eastham-Anderson J, Modrusan Z, Kaminker JS, Tessier-Lavigne M, Lewcock JW. 2013. DLK initiates a transcriptional program that couples apoptotic and regenerative responses to axonal injury. *Proc Natl Acad Sci U S A* **110**: 4039–4044.
Welsbie DS, Yang Z, Ge Y, Mitchell KL, Zhou X, Martin SE, Berlinicke CA, Hackler L, Fuller J, Fu J, et al. 2013. Functional genomic screening identifies dual leucine zipper kinase as a key mediator of retinal ganglion cell death. *Proc Natl Acad Sci U S A* **110**: 4045–4050.
White RE, Jakeman LB. 2008. Don't fence me in: Harnessing the beneficial roles of astrocytes for spinal cord repair. *Restor Neurol Neurosci* **26**: 197–214.
Witte H, Neukirchen D, Bradke F. 2008. Microtubule stabilization specifies initial neuronal polarization. *J Cell Biol* **180**: 619–632.
Xu K, Zhong G, Zhuang X. 2013. Actin, spectrin, and associated proteins form a periodic cytoskeletal structure in axons. *Science (80-)* **339**: 452–456.
Yanik MF, Cinar H, Cinar HN, Chisholm AD, Jin Y, Ben-Yakar A. 2004. Functional regeneration after laser axotomy. *Nature* **432**: 822.

Yiu G, He Z. 2006. Glial inhibition of CNS axon regeneration. *Nat Rev Neurosci* **7**: 617–627.
Zheng B, Ho C, Li S, Keirstead H, Steward O, Tessier-Lavigne M. 2003. Lack of enhanced spinal regeneration in Nogo-deficient mice. *Neuron* **38**: 213–224.
Zhou B, Yu P, Lin MY, Sun T, Chen Y, Sheng ZH. 2016. Facilitation of axon regeneration by enhancing mitochondrial transport and rescuing energy deficits. *J Cell Biol* **214**: 103–119.
Zukor K, Belin S, Wang C, Keelan N, Wang X, He Z. 2013. Short hairpin RNA against PTEN enhances regenerative growth of corticospinal tract axons after spinal cord injury. *J Neurosci* **33**: 15350–15361.

A.2 Review article:

Publication: This review article is published in Current Opinion in Neurobiology:

Liu, Y., Hegarty, S., Winter, C., Wang, F., & He, Z. (2020). Viral vectors for neuronal cell type-specific visualization and manipulations. *Current Opinion in Neurobiology*, *2020*, 67–76. https://doi.org/10.1016/j.conb.2020.03.011

Author contributions: The review was planned by Drs. Yuanyuan Liu, Shane Hegarty, Feng Wang, and Zhigang He, and written by Dr. Liu. The manuscript was critically reviewed and edited by all authors. I prepared Figure 1; Dr. Liu prepared Table 1 and Figure 2.

Viral vectors for neuronal cell type-specific visualization and manipulations

Yuanyuan Liu[1,2] Shane Hegarty[1,2], Carla Winter[1,3], Fan Wang[4], Zhigang He[1,2]

1. F. M. Kirby Neurobiology Center and Department of Neurology, Boston Children's Hospital, Boston, MA, USA
2. Department of Neurology, Harvard Medical School, Boston, MA, USA
3. PhD Program in Biological and Biomedical Sciences, Harvard Medical School, Boston, MA, USA
4. Department of Neurobiology, Duke University Medical Center, Durham, NC 27710, USA

Abstract

Characterizing neuronal cell types demands efficient strategies for specific labeling and manipulation of individual subtypes to dissect their connectivity and functions. Recombinant viral technology offers a powerful toolbox for targeted transgene expression in specific neuronal populations. In order to achieve cell type-specific targeting, exciting progress has been made to: alter viral tropisms, design rational delivery strategies, and drive selective expression patterns with engineered DNA sequences in viral genome. For the latter case, emerging single-cell genomic analyses provide rich databases. In this review, we will summarize the current status, and point out the challenges, of using viral vectors for neuronal cell type-specific visualization and manipulations. With concerted efforts, it is possible to develop viral vectors for all neuronal types in the mammalian brain.

Introduction

The ability to examine and manipulate the function of specific brain nuclei and neuronal types is critical for understanding how brain circuitry works. This is evident from the widespread applications of transgenic mouse driver lines, which enable specific transgene expression in a few selected cell types or brain regions [1]. In light of the complex nature of the nervous system, more versatile tools of this kind would be extremely desirable. This is an even more pressing issue with current advances in single cell analysis methods, such as single-cell RNA sequencing (scRNA-seq), that are characterizing ever-

growing numbers of neuronal cell types in an increasing number of mammalian species (including mice and humans). In principle, if a neuronal type is uniquely defined by the combinatorial expression of a set of genes, one could target such neurons specifically using sophisticated genetics. For example, multiple transgenic animals can be generated in which each marker gene is used to drive either a different DNA recombinase (e.g. Cre, Flp, Dre), or a reporter line, so that a desired transgene (e.g. XFP, opsins, activity indicators) is only expressed when *all* recombinases and the reporter are expressed in the same neuronal cells. While the advancement of CRISPR technology has made it possible to generate gene-targeted animals efficiently, crossing these different lines to achieve cell-type specific expression is still a lengthy and expensive process.

On the other hand, recombinant viral vectors with cross-species targeting and minimal cytotoxic effects offer unprecedented delivery systems to selectively express different desired transgenes in specific neuronal populations. In addition to the natural tropisms of individual viral types [2,3], their transduction specificity can, in principle, be refined by altering their capsid or envelope proteins (to dictate which cells to bind and enter) and/or the promoter/enhancer in the viral genome (to determine whether or when to express the target gene). Combining these techniques to alter viral tropism with various delivery methods would allow recombinant viral vectors to serve as a collection of region-selective, neuron type-specific, and activity-dependent tools that can be readily used in multiple species. Here we review four main strategies for, and recent progresses toward, designing and optimizing viral vectors for neuronal type-specific expression, namely: (1) axonal projection-dependent; (2) viral serotype/tropism-based; (3) gene regulatory element (promoter/enhancer/microRNA)-driven; and (4) delivery-controlled strategies for targeting of distinct neuronal cell types (**Figure 1**).

Viral vectors for axonal projection-dependent targeting of specific neurons

Neurons residing within one brain region expressing similar genetic markers can have distinct projection targets and can thereby be classified based on their efferent axonal innervation patterns [4-6]. Thus, one can use recombinant viruses capable of infecting neurons from their axon terminals to target a more specific cell type within a larger neuronal population through retrograde viral infection (**Figure 1A**). Many types of viral vectors have axonal tropism (**Table 1**), and four different types of retrograde viral vectors have been developed to this end.

Recombinant rabies viruses: It has long been known that rabies viruses infect mammalian neurons from axon terminals [7]. However, the use of rabies viruses for manipulating or labeling specific neuronal populations is limited because they are neurotoxic and uncontrollably propagate between hierarchically-connected neurons. Within the five genes of rabies viral genome, only *G* encodes the glycoprotein to mediate retrogradely trans-synaptic viral transmission. Thus, when the rabies envelope glycoprotein (RG) was replaced by fluorescent proteins (e.g. GFP), the recombinant rabies virus is used for non-transsynaptic retrograde neuronal labeling [8]. To further reduce its neurotoxicity, Wickersham's group developed double deletion (L and G proteins) recombinant rabies virus [9]. This new version enables long-term anatomical or physiological study of retrogradely-targeted projection neurons.

Retrograde lentiviruses: Considering the aforementioned limitations of the rabies viruses, a promising alternative candidate is the notably less toxic lentivirus genus. Lentiviruses are single stranded RNA viruses that stably integrate into the host genome of both pre- and post-mitotic cells [2]. Based on the discovery that the RG mediates axonal retrograde transport, Kobayashi's group decided to pseudotype lentiviruses using fusion proteins incorporating RG domains. They discovered that packaging lentiviruses with a fusion envelope composed of the extracellular domain of RG and the

transmembrane and intracellular domain of the vesicular stomatitis virus (VSV) glycoprotein resulted in retrograde lentiviral vectors (called HiRet-LV, also called RG-LV) that were highly effective in infecting axon terminals of long-distance projection neurons in both rodent and nonhuman primate in the brain and spinal cord [10-12]. Retrograde lentiviruses have since been successfully used by multiple labs for axonal projection-dependent labeling and manipulation of neuronal cell types [13-16].

CAV-2: Canine adenovirus type 2 (CAV-2) displays potent retrograde axonal transport ability, through its selective interaction with the coxsackievirus and adenovirus receptor (CAR) at axon terminals [17]. CAV-2 can drive stable long-term transgene expression with minimal cytotoxicity and has been effectively used as a retrograde vector to study many circuits [18,19]. However, CAV-2 has limited tropism since many neurons do not express the CAR receptor. This can be overcome by overexpression of CAR in candidate projection neurons [20].

rAAV2-retro: Using *in vivo* screening for adeno-associated virus (AAV) capsids that would enable the packaged AAVs to be efficiently taken up by axonal terminals, recombinant AAV2-retro (rAAV2-retro) capsid was discovered to exhibit high efficiency in retrograde labeling of long-projecting neurons such as corticospinal neurons [21]. rAAV2-retro vector has broad but *not* pan-neuronal tropism for retrograde infection and can drive high-level gene expression like other AAVs. Thus, it is a very versatile retrograde vector, but which needs its tropism for desired neurons tested before use.

Applications of retrograde vectors: The development of retrograde viral tools enables virus-based intersectional approaches to precisely manipulate target projection neurons that are embedded in a mixture of different neuronal populations. To achieve this, the retrograde viral vectors encoding

recombinases (e.g. Cre or Flp) are often injected at specific sites where the axons of the target projection neurons innervate. These viral particles are selectively absorbed by axon terminals and then undergo retrograde gene transfer. Next, AAVs encoding Cre- or Flp-dependent genes (e.g. XFP, DTR, ChR2 or GCamp6) are injected into areas where the somas of the targeted projection neurons are located (**Figure 2**). Such a multi-step, axonal projection-dependent intersectional approach has been successfully applied in sophisticated neuronal circuit mapping and functional characterization in both rodent and non-human primate (NHP) models [4,15,16,22-24]. More recently, combining this approach with brain clearing and 3D-imaging reconstruction, the Janelia MouseLight project has reconstructed the entire cell bodies and neurites of >1000 cortical projection neurons in the mouse brain, revealing previously unknown subtypes of cortical projection neurons [25] (MouseLight Neuron Browser: http://ml-neuronbrowser.janelia.org).

AAV serotype/capsids-based cell type-specific neuronal targeting

AAVs are comprised of a single-stranded DNA genome with a capsid outer shell and are unable to integrate into host genomes. Because of minimal cytotoxic effects and different tropisms associated with individual serotypes, AAV vectors have been increasingly used for mapping brain connectivity and for monitoring and manipulating neuronal functions in many vertebrate species, including mouse, rat, songbird, and NHPs. In addition, AAV vectors are also used clinically for gene therapy [26]. In most cases, the serotypes of recombinant AAV (rAAVs) are determined by variations in their capsid proteins [27], with AAV1-9 being the most commonly used. Most of these serotypes are capable of infecting many neuronal cells, although with various efficacies in targeting different neuronal and glial cell types [28-30]. For example, intravitreally-injected AAV2 is highly effective to generally target retinal ganglion cells [31,32].

The existence of many serotypes raises the possibility of altering/screening capsid proteins to achieve cell type-specific infection, and has inspired many such efforts. In fact, the above mentioned rAAV-retro capsid was developed based on similar ideas. Briefly, directed evolution, which involves mutagenesis of the Cap gene followed by iterative rounds of phenotypic screening, has been widely used to identify a desired viral capsid. For example, most natural AAVs have limited ability to cross the blood brain barrier (BBB). By using a Cre-dependent selection system, Gradinaru's group discovered novel capsids named PHP.B that can cross the BBB to infect the entire nervous system [33]. In a follow-up study, they further developed engineered capsids named PHP.eB and PHP.S that preferentially target CNS or PNS through systematic administration [34]. Using similar approaches, an AAV2 variant named 7m8 and an AAV6 variant named ShH10 have been identified for enhanced selectivity for photoreceptors and Muller glia in the murine retina, respectively [35,36] (**Figure 1B**). Another strategy adopts a reverse principle to identify ancestral nodes or putative parents of currently available Cap proteins. Using this "back to future" approach, Anc80L65 was discovered and has showed strong potency for gene therapy of the inner ear [37,38]. We envision more variants of capsid proteins for targeting distinct neuronal cell types will be developed and optimized in the near future.

Identifying promoters/enhancers and other regulatory elements that can drive cell type-specific expression

Since neuronal cell types (or non-neuronal cell types in the nervous system) are determined by expression of marker gene(s), an approach to specifically label or manipulate distinct populations is to identify unique gene regulatory elements (promoters/enhancers) that fit into the packaging capacity of AAVs (4.7kb) to drive cell type-specific gene expression. Previous studies have identified a number of promoters useful for this purpose, such as human synapsin 1 (hSyn1) promoter for (pan-)neuronal specific expression [39], GFAP promoter for astrocytes [40], MBP for oligodendrocytes [41], tyrosine

hydroxylase for catecholaminergic cells [34], L7/PCP2 for Purkinje cells [42], and FEV for serotonergic cells [43] (**Figure 1C**). In addition, since activity-dependent genetic methods are fruitful in tagging and manipulating functionally-activated ensembles of neurons [44-47], several studies have attempted to develop viral vectors using enhancers or promoters of immediate early genes, such as Fos or Arc [48] [49] [50] [51]. For example, an AAV vector in which the Fos promoter drives the expression of tTA was used to label different amygdala neurons activated by either aversive or appetitive stimuli [48], while AAVs containing the Arc promoter driving CreERT2 were used to label activated prefrontal cortex neurons [49]. The main caveat for AAVs using activity-dependent promoter/enhancers is a background basal expression which is independent of neuronal activity, and could therefore result in random labeling of non-functionally relevant neurons. To address this, Sorenson et al. developed AAVs with a Robust Activity Marking (RAM) system that consists of a synthetic neuronal activity-dependent promoter, which has very low expression in basal conditions and strong induction by neural activity and is under the temporal control of a modified Tet-Off system [52].

Suffice it to say, with the ever-increasing numbers of neuronal cell types being identified in the mammalian brain through the expansion of the single-cell RNAseq (scRNA-seq) technology, more enhancers/promoters that can drive specific expression using AAVs are urgently needed. Owing to recent advancement in scRNA-seq, Assay for Transposase-Accessible Chromatin using sequencing (ATAC-Seq) and other "omic" methods, important progress has been made toward this end. Below we briefly review these methods. One method to identify enhancers is to search for evolutionarily conserved DNA regulatory elements. By comparative genomic analysis, Visel and Pennacchino identified several hundreds of ultra-conserved non-coding elements in human genome [53,54]. When tested in early embryos using transient transgenesis, many elements drove gene expression

reproducibly in restricted regions of the embryonic brain [55]. Follow-up studies suggested many of these regulatory elements could act as enhancers for specific brain regions [56], and restrict expression to particular neuronal subtypes such as using the Dlx5/6 enhancer for GABAergic neurons [57]. However, many of the ultra-conserved enhancers are developmental enhancers, and fail to act in the adult brain (P. Williams and Z. He, unpublished data).

Second, mapping the open chromatin regions with advanced technologies has led to the identification of cell type-restricted gene regulatory elements (GREs) or enhancers. For example, Mich et al. used ATAC-seq to discover specific enhancer elements for diverse neural types within human cortex, which were then cloned into AAV vectors and tested in the mouse brain. Several enhancers were shown to enable labeling and perturbation of specific cortical neuronal subtypes [58] Furthermore, using the principles of massively parallel reporter assays (MPRA) with scRNA-seq, Hrvatin et al. designed a Paralleled Enhancer Single Cell Assay (PESCA) to identify and functionally assess the specificity of hundreds of GREs across the full complement of cell types present in the brain [59]. They identified GREs that confine AAV expression to somatostatin (SST)-expressing interneurons, which can be used to selectively modulate their neuronal activity [59]. We envision ATAC-seq and PESCA related approaches will generate a large database of neuronal subtype-specific enhancers.

Combining these different GREs may further optimize neuron-type specific AAV vectors. With this in mind, Jüttner et al created a library of 230 AAVs, each with a different synthetic promoter designed based on identified "transcriptional code" for adult retinal cell types [60], and found that a number of these AAVs specifically target expression to neuronal and glial cell types in mouse and NHP retina *in vivo* and in the human retina *in vitro* [61]. Using logical combinations of different AAVs containing different synthetic promoters in an intersectional manner, they further achieved specific targeting of retinal cell types for manipulation and recording of neuronal function [61]. Thus,

combinations of AAVs containing different GREs used in an intersectional manner will further improve the specificity of viral vectors for targeting desired neuronal types.

Third, promoters and enhancers may have sequences with the length beyond the packaging capacity of AAVs, but the recognition sites of microRNA (miRNA) are small (about 22 nucleotides) and can be easily packaged into viral vectors. Using the ability of miRNAs in restricting gene expression in certain neuronal types, AAVs with tandem copies of short miRNA-target sequences (miRNA-TSs) in their 3' untranslated region of the genome have been characterized [62]. Recently, Keaveney et al. developed a miRNA-guided neuron tag ("mAGNET") to restrict transgene expression to inhibitory ($GABA^+$) neurons in the mouse neocortex (GABA mAGNET) [63]. In light of highly enriched expression of miRNAs in the mammalian brain, microRNA-based methods have huge potential. Mining the single-cell miRNA-seq database should facilitate the identification of new cell type-specific miRNAs.

Delivery-method controlled cell type-restricted targeting

In the nervous system, neuronal cells are highly compartmentalized, and thus the methods of delivering viral vectors is another important consideration. The three most common virus delivery methods to target neurons are stereotaxic, intrathecal, and tail vein injection (**Figure 1D**), each with their own advantages and limitations, and which should be considered in parallel with the tropism of the particular viral vector of choice. For example, tail vein injection offers an accessible delivery method, but most viruses cannot cross the BBB. As discussed above, the newly developed AAV-PHP.B vectors are able to cross BBB in rodents, and are thus suitable for systematic injection to target CNS neurons [33]. Stereotaxic injection is most commonly used for targeting cells in different parts of the brain or spinal cord, however, is a more invasive route of administration. In contrast, intrathecal injection is less invasive, but preferentially targets the dorsal root ganglia (DRGs) and spinal dorsal

horn, with a decreasing expression gradient from lumbar to cervical spinal cord segments. Such physical limitations to viral vector spread or entry can be addressed through, for example, adjusting body positioning post viral delivery [64]. More recently, bilateral intravenous injection of relatively large volumes of AAV9 into the transverse sinuses of early postnatal animals has been employed as a simpler way to achieve widespread and robust infection of the mouse brain [65].

In addition to this, different viruses display distinct infection profiles even when the same delivery method is chosen. For example, AAV2 has a more restricted, localized expression profile than AAV9 when stereotaxically-injected into the CNS. It is important to note that structural constraints can create boundaries for viral diffusion. This is nicely illustrated by distinct efficacies of different injection protocols in targeting different populations of retinal cells [66]. For example, intravitreal injection of AAVs is optimal for targeting inner retinal neurons/Müller glia, while subretinal AAV delivery is optimal for targeting the RPE/photoreceptors [3]. Another example takes advantage of a transiently-compromised BBB after spinal cord injury. In this case, tail vein injection of AAV9 results in peri-lesion neuronal targeting [67]. Thus, the characteristic features and limitations of different delivery methods can be exploited to restrict infection of specific viral vectors to particular neuronal cell types and CNS regions of interest.

Other notes on using viral vectors to target specific cell types

While most efforts have aimed to achieve restricted and high-level gene expression with rAAV vectors, little attention has been paid to the toxicity associated with these AAV vectors, a crucial issue for their applications in human gene therapy [66,68]. Non-selective targeting of cell types represents a key issue. Based on the studies showing that AAV9 is able to transduce spinal motor neurons when administered intravenously at high doses [69,70], this approach was approved for expressing non-mutated survival of motor neuron (SMN) protein and treating infants with spinal muscular atrophy (SMA) [71].

However, recent studies have shown that high doses of AAV9 administration trigger sensory side-effects, with mononuclear cell inflammation in the dorsal root ganglion and cell death [72]. Based on such concerns, some of SMA clinical studies were halted (https://www.statnews.com/2019/10/30/novartis-zolgensma-gene-therapy-study-halted-by-fda-on-animal-safety-concerns/). Moreover, a recent clinical trial of an AAV9-mediated gene therapy for Duchenne muscular dystrophy was halted due to kidney injury and drops in red blood cell count in patients after intravenous viral infusion (https://www.the-scientist.com/news-opinion/trial-of-gene-therapy-for-duchenne-muscular-dystrophy-put-on-hold-66711). Similarly, by testing multiple AAV genome structures and capsid types using subretinal injection in mice, Xiong et al. found a strong correlation between *cis*-regulatory sequences and toxicity [73] . Interestingly, AAVs with any one of three broadly active promoters, or an RPE-specific promoter, were toxic, while AAVs with four different photoreceptor-specific promoters were not toxic at the highest doses tested. With increased efforts in using AAVs to express specific proteins to manipulate neuronal functions, distinguishing the true effects versus the noise/toxicity associated with viral vectors should be considered with greater caution. Thus, refining these viral vectors will facilitate the development of new gene therapy protocols.

Finally, the optimizations of viruses for neuronal targeting discussed herein have limitations in their transability due to diversity in cross-species tropism of viruses. Indeed, the retinal cell types targeted by specific synthetic promoter AAVs varied widely between mouse and NHP/human retinas [61]. Moreover, the PHP.B virus discussed above, which crosses BBB and remarkably transduces CNS following intravenous infusion in mice [33], was not found to do the same in NHPs [74]. Therefore, in these cases, optimizing cell-type targeting in mice yields vectors that are unlikely to optimally target the same cell type in NHPs/humans. On the other hand, the ability of an AAV to target a neural cell

group in NHPs is a good predictor for targeting the same cell group in humans [61], suggesting that phylogenetically closer species have more correlated responses to virus infection.

Concluding remarks

Developments in the past decade have shown that recombinant viral tools have started to transform our ability to map, observe and manipulate neuronal circuits in experimental models, and to design gene therapy strategies in humans. While this review has been mainly focused on targeting specific neuronal types, recombinant viral vectors have also been used for monosynaptic tracing of neuronal connections [1,75]. In brief, the vectors for retrograde trans-synaptic tracing include the SADB19-base vectors [76], and a less toxic CVS-N2c strain [77]. Recent studies also led to the development of anterograde trans-synaptic tracing vectors, such as the recombinant HSV-129 (**Table 1**) [78,79], AAV1 or AAV9-Cre [80], and VSV [81]. Furthermore, several studies have combined cell type-specific viral vectors with such "trans-synaptic" or "trans-neuronal vectors" to dissect input-output circuits [23].

In conclusion, it is an exciting time in neuroscience since we are on the brink of identifying all cell types. Using the methods (projection-based, serotype-restricted, GRE-dependent, and delivery method-controlled) described here, their combinations, and other yet to be discovered methods to generate viral vectors, in the not too distant future it will be possible to comprehensively target identified neuronal subtypes. This will allow us to determine the connectivity and functions of all types of neurons in the mammalian brain, and use such knowledge to guide therapies to treat brain disorders.

Acknowledgment

This work is supported by NIH grants U01MH109107, R01NS109947, and P30EY012196.

FIGURES:

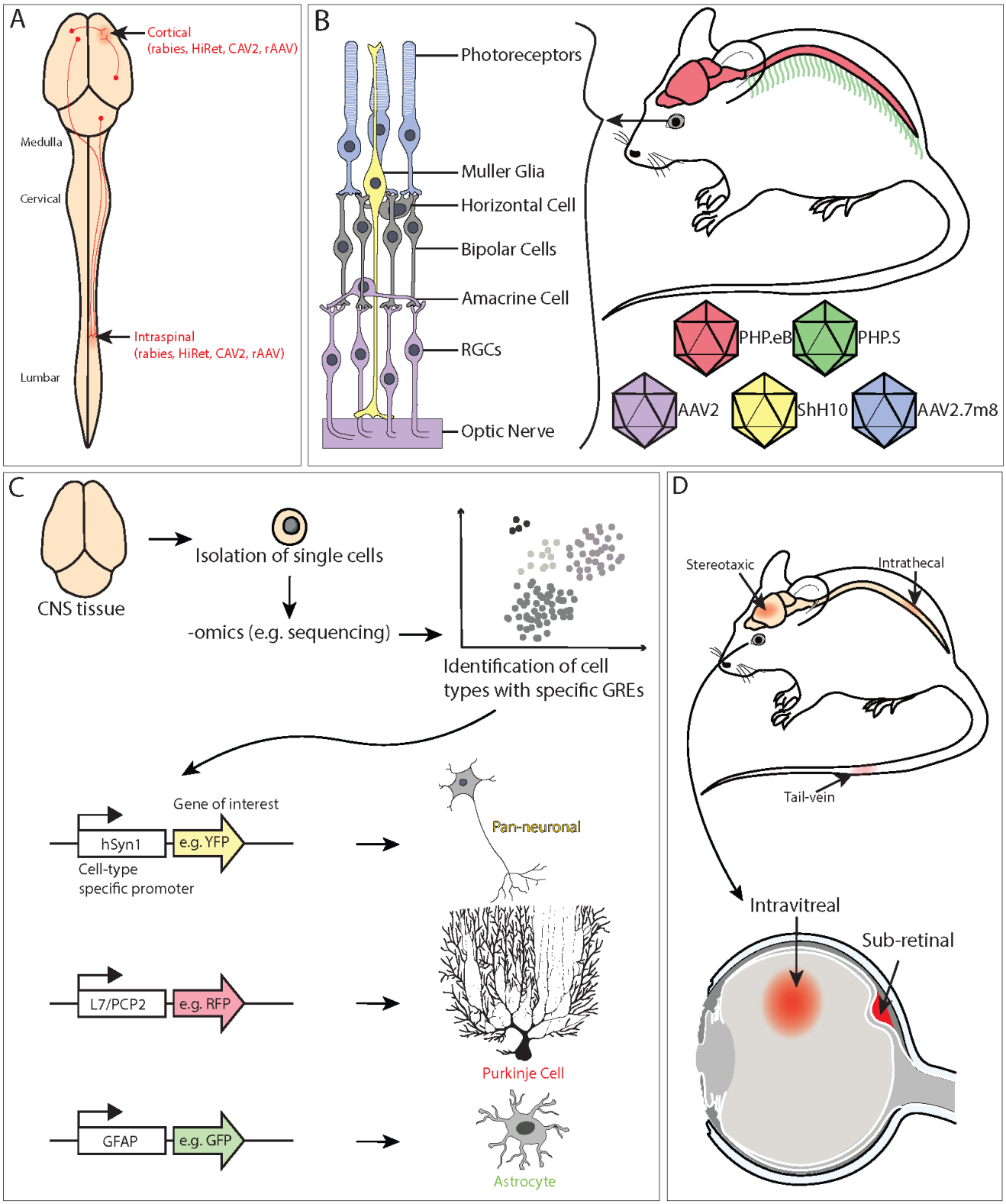


Fig. 1

Figure 1: Strategies for neuronal cell type-specific targeting with viral vectors. A) Axonal projection-dependent retrograde labeling: viruses with axonal tropism (rabies, HiRet lentivirus, CAV2, and retroAAV) mediate retrograde targeting for neurons of interest in both the brain and spinal cord. **B)** Viral serotype/capsid determines tissue, and in some cases cell-type specific, tropism. Here, AAV color indicates various capsids that correlate with the specific tissue or cell-type that the AAV is able to infect. Specifically: PHP.eB (red) is preferentially expressed in the CNS, PHP.S (green) in the PNS, AAV2 (purple) in RGCs and amacrine cells, ShH10 (yellow) in muller glia, and AAV2.7m8 (blue) in photoreceptors. Grey indicates cells that are not targeted. **C)** Sequencing and -omics approaches can be harnessed to identify novel gene regulatory elements (e.g. promoters, enhancers, microRNA) to label specific neuronal and non-neuronal subtypes. **D)** Finally, targeting of distinct neuronal cell types can be aided by unique delivering methods (stereotaxic, intrathecal, tail-vein, intravitreal, and sub-retinal). [Portions of this figure used and/or altered artwork from https://smart.servier.com/; Purkinje neuron from Ramón y Cajal].

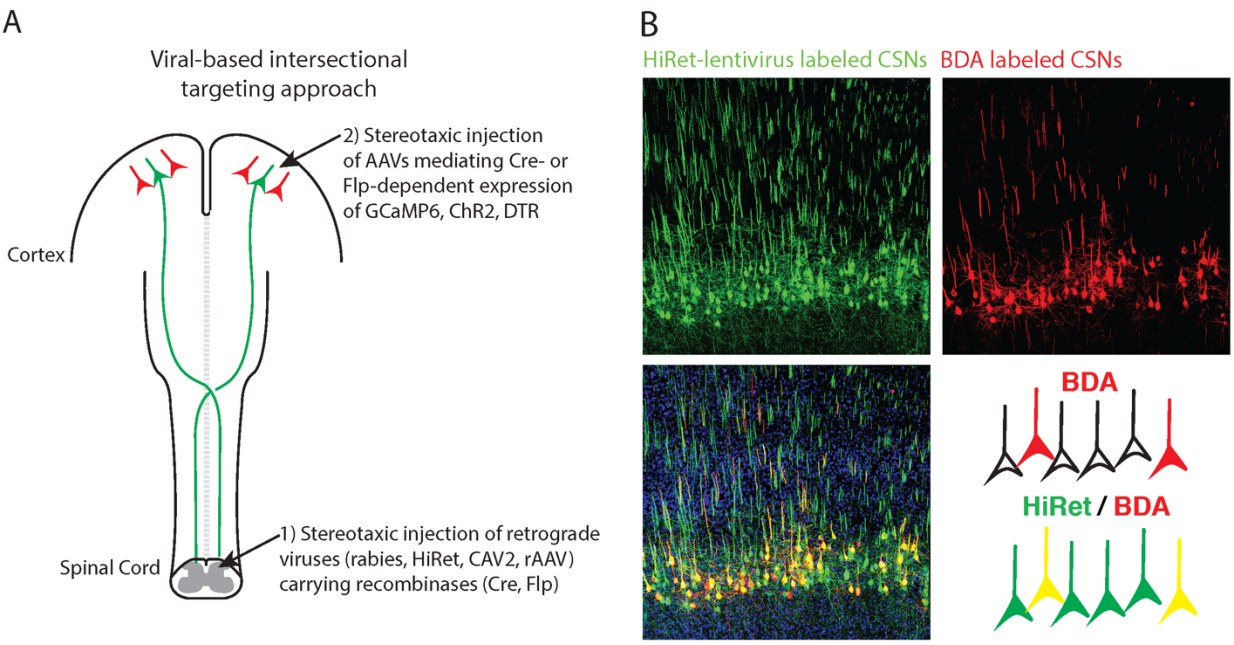


Fig. 2

Figure 2: Viral-based intersectional targeting approach. A) Schematic drawing of viral-based intersectional targeting approach. **B)** Images of a coronal brain section showing corticospinal neurons targeted by an engineered lenti-viral vector (HiRet-GFP, green), a traditional neuronal tracer (BDA, red) and their merge. The cartoon drawing demonstrated that almost all corticospinal neurons randomly labeled by BDA are co-labeled with HiRet-GFP and thus indicated the high efficiency of viral mediated retrograde labeling. In addition, compared to BDA, viral based retrograde labeling allows further functional observation and manipulations of targeted neurons.

Table 1 Summary of features of viruses commonly used in neuroscience

Family	Genome	Neurotropism	Neuronal transport		Features	Limitations
			Direction	Cross-synapse		
Adeno-associated virus (AAV)	Single strand DNA	Engineered capsid: e.g. PhP.eB (CNS), PhP.S (PNS) Enhancer/promoter specific	Anterograde; Engineered for retrograde: rAAV2-retro	No Exception: AAV1or 9-Cre, Anterograde	Do not integrate; High and stable expression; Selective neurotropism; Capable of recombinase-based modification	Low packaging capacity
Lentivirus	Single strand (+) RNA	No pseudotyping: immune cells Pseudotyping (VSV-G): neuron and glia	Anterograde; Engineered for retrograde: FuG-B, C & E	No	Viral genome integrates into host genome; Selective targeting by pseudotyping (EnV-TVA); Capable of recombinase-based modification	Expression level low
Rabies virus	Single strand (-) RNA	Neurotrophic	Retrograde	Retro- Exception: Sensory neurons, Anterograde	Engineered for non-crossing retrograde (RV-dG) or mono-synaptic (RV-dG with G) transmission; Selective targeting by pseudotyping (EnV-TVA)	Highly cyto-toxic; Incompatible with Cre/Flp
α-herpes viruses: Pseudorabies virus (PRV) and HSV1	Double strand DNA	Neurotrophic	Bi-directional	Strain dependent: PRV: Retrograde HSV1: Retro-/Anterograde	Poly-synaptic, bi-directional transmission; Engineered for mono-synaptic transmission (HSV: H129-dTK)	Difficult for genome engineering; Highly cyto-toxic

REFERENCES:

* of special interest:

** of outstanding interest:

1. Luo L, Callaway EM, Svoboda K: **Genetic Dissection of Neural Circuits: A Decade of Progress**. *Neuron* 2018, **98**:256-281.
2. Nassi JJ, Cepko CL, Born RT, Beier KT: **Neuroanatomy goes viral!** *Front Neuroanat* 2015, **9**:80.
3. Schon C, Biel M, Michalakis S: **Retinal gene delivery by adeno-associated virus (AAV) vectors: Strategies and applications**. *Eur J Pharm Biopharm* 2015, **95**:343-352.
4. Beier KT, Gao XJ, Xie S, DeLoach KE, Malenka RC, Luo L: **Topological Organization of Ventral Tegmental Area Connectivity Revealed by Viral-Genetic Dissection of Input-Output Relations**. *Cell Rep* 2019, **26**:159-167.e156.
5. Ren J, Friedmann D, Xiong J, Liu CD, Ferguson BR, Weerakkody T, DeLoach KE, Ran C, Pun A, Sun Y, et al.: **Anatomically Defined and Functionally Distinct Dorsal Raphe Serotonin Sub-systems**. *Cell* 2018, **175**:472-487.e420.
6. Stachniak TJ, Ghosh A, Sternson SM: **Chemogenetic synaptic silencing of neural circuits localizes a hypothalamus-->midbrain pathway for feeding behavior**. *Neuron* 2014, **82**:797-808.
7. Kelly RM, Strick PL: **Rabies as a transneuronal tracer of circuits in the central nervous system**. *J Neurosci Methods* 2000, **103**:63-71.
8. Wickersham IR, Finke S, Conzelmann KK, Callaway EM: **Retrograde neuronal tracing with a deletion-mutant rabies virus**. *Nat Methods* 2007, **4**:47-49.
9. * Chatterjee S, Sullivan HA, MacLennan BJ, Xu R, Hou Y, Lavin TK, Lea NE, Michalski JE, Babcock KR, Dietrich S, et al.: **Nontoxic, double-deletion-mutant rabies viral vectors for retrograde targeting of projection neurons**. *Nat Neurosci* 2018, **21**:638-646. This group deleted the viral polymerase gene (P) in "first-generation" rabies viral vectors, and found that this abolished cytotoxicity and reduced transgene expression to trace levels. Such "second-generation" rabies viral vectors were still able to retrogradely infect projection neurons and express recombinases, which allowed downstream expression of transgene products, such as fluorophores and calcium indicators.
10. Kato S, Kobayashi K, Inoue K, Kuramochi M, Okada T, Yaginuma H, Morimoto K, Shimada T, Takada M, Kobayashi K: **A lentiviral strategy for highly efficient retrograde gene transfer by pseudotyping with fusion envelope glycoprotein**. *Hum Gene Ther* 2011, **22**:197-206.
11. Kobayashi K, Inoue KI, Tanabe S, Kato S, Takada M, Kobayashi K: **Pseudotyped Lentiviral Vectors for Retrograde Gene Delivery into Target Brain Regions**. *Front Neuroanat* 2017, **11**:65.
12. Kato S, Sugawara M, Kobayashi K, Kimura K, Inoue KI, Takada M, Kobayashi K: **Enhancement of the transduction efficiency of a lentiviral vector for neuron-specific retrograde gene delivery through the point mutation of fusion glycoprotein type E**. *J Neurosci Methods* 2019, **311**:147-155.
13. Nelson A, Schneider DM, Takatoh J, Sakurai K, Wang F, Mooney R: **A circuit for motor cortical modulation of auditory cortical activity**. *J Neurosci* 2013, **33**:14342-14353.
14. Stanek Et, Rodriguez E, Zhao S, Han BX, Wang F: **Supratrigeminal Bilaterally Projecting Neurons Maintain Basal Tone and Enable Bilateral Phasic Activation of Jaw-Closing Muscles**. *J Neurosci* 2016, **36**:7663-7675.

15. Wang X, Liu Y, Li X, Zhang Z, Yang H, Zhang Y, Williams PR, Alwahab NSA, Kapur K, Yu B, et al.: **Deconstruction of Corticospinal Circuits for Goal-Directed Motor Skills**. *Cell* 2017, **171**:440-455.e414.
16. * Liu Y, Latremoliere A, Li X, Zhang Z, Chen M, Wang X, Fang C, Zhu J, Alexandre C, Gao Z, et al.: **Touch and tactile neuropathic pain sensitivity are set by corticospinal projections**. *Nature* 2018, **561**:547-550. This study provides a comprehensive example of how a multi-step, viral-based intersectional approach has been successfully applied in sophisticated neuronal circuit mapping and functional characterization.
17. Salinas S, Schiavo G, Kremer EJ: **A hitchhiker's guide to the nervous system: the complex journey of viruses and toxins**. *Nat Rev Microbiol* 2010, **8**:645-655.
18. Junyent F, Kremer EJ: **CAV-2--why a canine virus is a neurobiologist's best friend**. *Curr Opin Pharmacol* 2015, **24**:86-93.
19. Del Rio D, Beucher B, Lavigne M, Wehbi A, Gonzalez Dopeso-Reyes I, Saggio I, Kremer EJ: **CAV-2 Vector Development and Gene Transfer in the Central and Peripheral Nervous Systems**. *Front Mol Neurosci* 2019, **12**:71.
20. Li SJ, Vaughan A, Sturgill JF, Kepecs A: **A Viral Receptor Complementation Strategy to Overcome CAV-2 Tropism for Efficient Retrograde Targeting of Neurons**. *Neuron* 2018, **98**:905-917.e905.
21. Tervo DG, Hwang BY, Viswanathan S, Gaj T, Lavzin M, Ritola KD, Lindo S, Michael S, Kuleshova E, Ojala D, et al.: **A Designer AAV Variant Permits Efficient Retrograde Access to Projection Neurons**. *Neuron* 2016, **92**:372-382.
22. Beier KT, Steinberg EE, DeLoach KE, Xie S, Miyamichi K, Schwarz L, Gao XJ, Kremer EJ, Malenka RC, Luo L: **Circuit Architecture of VTA Dopamine Neurons Revealed by Systematic Input-Output Mapping**. *Cell* 2015, **162**:622-634.
23. Schwarz LA, Miyamichi K, Gao XJ, Beier KT, Weissbourd B, DeLoach KE, Ren J, Ibanes S, Malenka RC, Kremer EJ, et al.: **Viral-genetic tracing of the input-output organization of a central noradrenaline circuit**. *Nature* 2015, **524**:88-92.
24. Kinoshita M, Matsui R, Kato S, Hasegawa T, Kasahara H, Isa K, Watakabe A, Yamamori T, Nishimura Y, Alstermark B, et al.: **Genetic dissection of the circuit for hand dexterity in primates**. *Nature* 2012, **487**:235-238.
25. * Winnubst J, Bas E, Ferreira TA, Wu Z, Economo MN, Edson P, Arthur BJ, Bruns C, Rokicki K, Schauder D, et al.: **Reconstruction of 1,000 Projection Neurons Reveals New Cell Types and Organization of Long-Range Connectivity in the Mouse Brain**. *Cell* 2019, **179**:268-281.e213. The authors employed an axonal projection-dependent intersectional approach, in combination with brain clearing and 3D-imaging, to reconstruct the entire cell bodies and processes of more than 1000 cortical projection neurons. This approach identified previously unknown subtypes of cortical projection neurons, and characterized the organisation of long-range connections within the mouse brain.
26. High KA, Roncarolo MG: **Gene Therapy**. *N Engl J Med* 2019, **381**:455-464.
27. Chen SH, Haam J, Walker M, Scappini E, Naughton J, Martin NP: **Recombinant Viral Vectors as Neuroscience Tools**. *Curr Protoc Neurosci* 2019, **87**:e67.
28. Taymans JM, Vandenberghe LH, Haute CV, Thiry I, Deroose CM, Mortelmans L, Wilson JM, Debyser Z, Baekelandt V: **Comparative analysis of adeno-associated viral vector serotypes 1, 2, 5, 7, and 8 in mouse brain**. *Hum Gene Ther* 2007, **18**:195-206.
29. Howard DB, Powers K, Wang Y, Harvey BK: **Tropism and toxicity of adeno-associated viral vector serotypes 1, 2, 5, 6, 7, 8, and 9 in rat neurons and glia in vitro**. *Virology* 2008, **372**:24-34.

30. Srivastava A: **In vivo tissue-tropism of adeno-associated viral vectors**. *Curr Opin Virol* 2016, **21**:75-80.
31. Park KK, Liu K, Hu Y, Smith PD, Wang C, Cai B, Xu B, Connolly L, Kramvis I, Sahin M, et al.: **Promoting axon regeneration in the adult CNS by modulation of the PTEN/mTOR pathway**. *Science* 2008, **322**:963-966.
32. Petrs-Silva H, Dinculescu A, Li Q, Deng WT, Pang JJ, Min SH, Chiodo V, Neeley AW, Govindasamy L, Bennett A, et al.: **Novel properties of tyrosine-mutant AAV2 vectors in the mouse retina**. *Mol Ther* 2011, **19**:293-301.
33. Deverman BE, Pravdo PL, Simpson BP, Kumar SR, Chan KY, Banerjee A, Wu WL, Yang B, Huber N, Pasca SP, et al.: **Cre-dependent selection yields AAV variants for widespread gene transfer to the adult brain**. *Nat Biotechnol* 2016, **34**:204-209.
34. ** Chan KY, Jang MJ, Yoo BB, Greenbaum A, Ravi N, Wu WL, Sanchez-Guardado L, Lois C, Mazmanian SK, Deverman BE, et al.: **Engineered AAVs for efficient noninvasive gene delivery to the central and peripheral nervous systems**. *Nat Neurosci* 2017, **20**:1172-1179. In this paper, the authors used their *in vivo* capsid selection method CREATE to further evolve AAV-PHP.B into an enhanced varient, AAV-PHP.eB, which lowers the viral load required to transduce the majority of CNS neurons. They also report the characterization of a second capsid variant, AAV-PHP.S, that displays improved tropism toward PNS neurons.
35. Dalkara D, Byrne LC, Klimczak RR, Visel M, Yin L, Merigan WH, Flannery JG, Schaffer DV: **In vivo-directed evolution of a new adeno-associated virus for therapeutic outer retinal gene delivery from the vitreous**. *Sci Transl Med* 2013, **5**:189ra176.
36. Koerber JT, Klimczak R, Jang JH, Dalkara D, Flannery JG, Schaffer DV: **Molecular evolution of adeno-associated virus for enhanced glial gene delivery**. *Mol Ther* 2009, **17**:2088-2095.
37. Zinn E, Pacouret S, Khaychuk V, Turunen HT, Carvalho LS, Andres-Mateos E, Shah S, Shelke R, Maurer AC, Plovie E, et al.: **In Silico Reconstruction of the Viral Evolutionary Lineage Yields a Potent Gene Therapy Vector**. *Cell Rep* 2015, **12**:1056-1068.
38. Landegger LD, Pan B, Askew C, Wassmer SJ, Gluck SD, Galvin A, Taylor R, Forge A, Stankovic KM, Holt JR, et al.: **A synthetic AAV vector enables safe and efficient gene transfer to the mammalian inner ear**. *Nat Biotechnol* 2017, **35**:280-284.
39. Kugler S, Kilic E, Bahr M: **Human synapsin 1 gene promoter confers highly neuron-specific long-term transgene expression from an adenoviral vector in the adult rat brain depending on the transduced area**. *Gene Ther* 2003, **10**:337-347.
40. Lee Y, Messing A, Su M, Brenner M: **GFAP promoter elements required for region-specific and astrocyte-specific expression**. *Glia* 2008, **56**:481-493.
41. von Jonquieres G, Frohlich D, Klugmann CB, Wen X, Harasta AE, Ramkumar R, Spencer ZH, Housley GD, Klugmann M: **Recombinant Human Myelin-Associated Glycoprotein Promoter Drives Selective AAV-Mediated Transgene Expression in Oligodendrocytes**. *Front Mol Neurosci* 2016, **9**:13.
42. El-Shamayleh Y, Kojima Y, Soetedjo R, Horwitz GD: **Selective Optogenetic Control of Purkinje Cells in Monkey Cerebellum**. *Neuron* 2017, **95**:51-62.e54.
43. de Leeuw CN, Korecki AJ, Berry GE, Hickmott JW, Lam SL, Lengyell TC, Bonaguro RJ, Borretta LJ, Chopra V, Chou AY, et al.: **rAAV-compatible MiniPromoters for restricted expression in the brain and eye**. *Mol Brain* 2016, **9**:52.
44. Barth AL, Gerkin RC, Dean KL: **Alteration of neuronal firing properties after in vivo experience in a FosGFP transgenic mouse**. *J Neurosci* 2004, **24**:6466-6475.
45. Liu X, Ramirez S, Pang PT, Puryear CB, Govindarajan A, Deisseroth K, Tonegawa S: **Optogenetic stimulation of a hippocampal engram activates fear memory recall**. *Nature* 2012, **484**:381-385.

46. Allen WE, DeNardo LA, Chen MZ, Liu CD, Loh KM, Fenno LE, Ramakrishnan C, Deisseroth K, Luo L: **Thirst-associated preoptic neurons encode an aversive motivational drive**. *Science* 2017, **357**:1149-1155.
47. * Sakurai K, Zhao S, Takatoh J, Rodriguez E, Lu J, Leavitt AD, Fu M, Han BX, Wang F: **Capturing and Manipulating Activated Neuronal Ensembles with CANE Delineates a Hypothalamic Social-Fear Circuit**. *Neuron* 2016, **92**:739-753. The authors developed "CANE" Technology: a knock-in mouse (Fos-2AdsTVA) in which activity-induced Fos expression triggers co-expression of a destabilized TVA receptor, which then permits infection by pseudotyped lentiviruses (EnvA-LV) or rabies viruses (EnvA-RV) to selectively express desired transgenes to label and manipulate transiently Fos^+ neurons.

48. Kim J, Pignatelli M, Xu S, Itohara S, Tonegawa S: **Antagonistic negative and positive neurons of the basolateral amygdala**. *Nat Neurosci* 2016, **19**:1636-1646.
49. Ye L, Allen WE, Thompson KR, Tian Q, Hsueh B, Ramakrishnan C, Wang AC, Jennings JH, Adhikari A, Halpern CH, et al.: **Wiring and Molecular Features of Prefrontal Ensembles Representing Distinct Experiences**. *Cell* 2016, **165**:1776-1788.
50. Kawashima T, Okuno H, Nonaka M, Adachi-Morishima A, Kyo N, Okamura M, Takemoto-Kimura S, Worley PF, Bito H: **Synaptic activity-responsive element in the Arc/Arg3.1 promoter essential for synapse-to-nucleus signaling in activated neurons**. *Proc Natl Acad Sci U S A* 2009, **106**:316-321.
51. Kawashima T, Kitamura K, Suzuki K, Nonaka M, Kamijo S, Takemoto-Kimura S, Kano M, Okuno H, Ohki K, Bito H: **Functional labeling of neurons and their projections using the synthetic activity-dependent promoter E-SARE**. *Nat Methods* 2013, **10**:889-895.
52. Sorensen AT, Cooper YA, Baratta MV, Weng FJ, Zhang Y, Ramamoorthi K, Fropf R, LaVerriere E, Xue J, Young A, et al.: **A robust activity marking system for exploring active neuronal ensembles**. *Elife* 2016, **5**.
53. Pennacchio LA, Ahituv N, Moses AM, Prabhakar S, Nobrega MA, Shoukry M, Minovitsky S, Dubchak I, Holt A, Lewis KD, et al.: **In vivo enhancer analysis of human conserved non-coding sequences**. *Nature* 2006, **444**:499-502.
54. Visel A, Prabhakar S, Akiyama JA, Shoukry M, Lewis KD, Holt A, Plajzer-Frick I, Afzal V, Rubin EM, Pennacchio LA: **Ultraconservation identifies a small subset of extremely constrained developmental enhancers**. *Nat Genet* 2008, **40**:158-160.
55. Pattabiraman K, Golonzhka O, Lindtner S, Nord AS, Taher L, Hoch R, Silberberg SN, Zhang D, Chen B, Zeng H, et al.: **Transcriptional regulation of enhancers active in protodomains of the developing cerebral cortex**. *Neuron* 2014, **82**:989-1003.
56. Dickel DE, Ypsilanti AR, Pla R, Zhu Y, Barozzi I, Mannion BJ, Khin YS, Fukuda-Yuzawa Y, Plajzer-Frick I, Pickle CS, et al.: **Ultraconserved Enhancers Are Required for Normal Development**. *Cell* 2018, **172**:491-499.e415.
57. Dimidschstein J, Chen Q, Tremblay R, Rogers SL, Saldi GA, Guo L, Xu Q, Liu R, Lu C, Chu J, et al.: **A viral strategy for targeting and manipulating interneurons across vertebrate species**. *Nat Neurosci* 2016, **19**:1743-1749.
58. Mich JK, Hess EE, Graybuck LT, Somasundaram S, Miller JA, Ding Y, Shapovalova NV, Fong O, Yao S, Mortrud M, et al.: **Epigenetic landscape and AAV targeting of human neocortical cell classes**. *bioRxiv* 2019:555318.
59. Hrvatin S, Tzeng CP, Nagy MA, Stroud H, Koutsioumpa C, Wilcox OF, Assad EG, Green J, Harvey CD, Griffith EC, et al.: **A scalable platform for the development of cell-type-specific viral drivers**. *Elife* 2019, **8**.

60. Siegert S, Cabuy E, Scherf BG, Kohler H, Panda S, Le YZ, Fehling HJ, Gaidatzis D, Stadler MB, Roska B: **Transcriptional code and disease map for adult retinal cell types**. *Nat Neurosci* 2012, **15**:487-495, s481-482.
61. ** Juttner J, Szabo A, Gross-Scherf B, Morikawa RK, Rompani SB, Hantz P, Szikra T, Esposti F, Cowan CS, Bharioke A, et al.: **Targeting neuronal and glial cell types with synthetic promoter AAVs in mice, non-human primates and humans**. *Nat Neurosci* 2019, **22**:1345-1356. This study created a library of 230 AAVs, each with a different synthetic promoter designed based on: (1) sequences upstream of start codon of retinal cell type-specific genes; (2) phylogenetically-conserved DNA sequences preceding transcription initiation sites of ≤2 cell-specific genes; (3) repeated binding sites of cell type-specific transcription factors; and (4) low-methylated cis-regulatory elements transcriptionally active in different retinal cell types. The authors then screened logical combinations of these AAVs for their ability to target retinal cell subtypes in mice, NHPs and humans.
62. Sayeg MK, Weinberg BH, Cha SS, Goodloe M, Wong WW, Han X: **Rationally Designed MicroRNA-Based Genetic Classifiers Target Specific Neurons in the Brain**. *ACS Synth Biol* 2015, **4**:788-795.
63. Keaveney MK, Tseng HA, Ta TL, Gritton HJ, Man HY, Han X: **A MicroRNA-Based Gene-Targeting Tool for Virally Labeling Interneurons in the Rodent Cortex**. *Cell Rep* 2018, **24**:294-303.
64. Castle MJ, Cheng Y, Asokan A, Tuszynski MH: **Physical positioning markedly enhances brain transduction after intrathecal AAV9 infusion**. *Sci Adv* 2018, **4**:eaau9859.
65. Barson D, Hamodi AS, Shen X, Lur G, Constable RT, Cardin JA, Crair MC, Higley MJ: **Simultaneous mesoscopic and two-photon imaging of neuronal activity in cortical circuits**. *Nat Methods* 2019.
66. Roska B, Sahel JA: **Restoring vision**. *Nature* 2018, **557**:359-367.
67. Chen B, Li Y, Yu B, Zhang Z, Brommer B, Williams PR, Liu Y, Hegarty SV, Zhou S, Zhu J, et al.: **Reactivation of Dormant Relay Pathways in Injured Spinal Cord by KCC2 Manipulations**. *Cell* 2018, **174**:1599.
68. Trapani I, Auricchio A: **Seeing the Light after 25 Years of Retinal Gene Therapy**. *Trends Mol Med* 2018, **24**:669-681.
69. Foust KD, Wang X, McGovern VL, Braun L, Bevan AK, Haidet AM, Le TT, Morales PR, Rich MM, Burghes AH, et al.: **Rescue of the spinal muscular atrophy phenotype in a mouse model by early postnatal delivery of SMN**. *Nat Biotechnol* 2010, **28**:271-274.
70. Valori CF, Ning K, Wyles M, Mead RJ, Grierson AJ, Shaw PJ, Azzouz M: **Systemic delivery of scAAV9 expressing SMN prolongs survival in a model of spinal muscular atrophy**. *Sci Transl Med* 2010, **2**:35ra42.
71. Mendell JR, Al-Zaidy S, Shell R, Arnold WD, Rodino-Klapac LR, Prior TW, Lowes L, Alfano L, Berry K, Church K, et al.: **Single-Dose Gene-Replacement Therapy for Spinal Muscular Atrophy**. *N Engl J Med* 2017, **377**:1713-1722.
72. Hinderer C, Katz N, Buza EL, Dyer C, Goode T, Bell P, Richman LK, Wilson JM: **Severe Toxicity in Nonhuman Primates and Piglets Following High-Dose Intravenous Administration of an Adeno-Associated Virus Vector Expressing Human SMN**. *Hum Gene Ther* 2018, **29**:285-298.
73. Xiong W, Wu DM, Xue Y, Wang SK, Chung MJ, Ji X, Rana P, Zhao SR, Mai S, Cepko CL: **AAV cis-regulatory sequences are correlated with ocular toxicity**. *Proc Natl Acad Sci U S A* 2019, **116**:5785-5794.
74. Hordeaux J, Wang Q, Katz N, Buza EL, Bell P, Wilson JM: **The Neurotropic Properties of AAV-PHP.B Are Limited to C57BL/6J Mice**. *Mol Ther* 2018, **26**:664-668.

75. Callaway EM, Luo L: **Monosynaptic Circuit Tracing with Glycoprotein-Deleted Rabies Viruses**. *J Neurosci* 2015, **35**:8979-8985.
76. Wickersham IR, Lyon DC, Barnard RJ, Mori T, Finke S, Conzelmann KK, Young JA, Callaway EM: **Monosynaptic restriction of transsynaptic tracing from single, genetically targeted neurons**. *Neuron* 2007, **53**:639-647.
77. Reardon TR, Murray AJ, Turi GF, Wirblich C, Croce KR, Schnell MJ, Jessell TM, Losonczy A: **Rabies Virus CVS-N2c(DeltaG) Strain Enhances Retrograde Synaptic Transfer and Neuronal Viability**. *Neuron* 2016, **89**:711-724.
78. Zeng WB, Jiang HF, Gang YD, Song YG, Shen ZZ, Yang H, Dong X, Tian YL, Ni RJ, Liu Y, et al.: **Anterograde monosynaptic transneuronal tracers derived from herpes simplex virus 1 strain H129**. *Mol Neurodegener* 2017, **12**:38.
79. Wojaczynski GJ, Engel EA, Steren KE, Enquist LW, Patrick Card J: **The neuroinvasive profiles of H129 (herpes simplex virus type 1) recombinants with putative anterograde-only transneuronal spread properties**. *Brain Struct Funct* 2015, **220**:1395-1420.
80. Zingg B, Chou XL, Zhang ZG, Mesik L, Liang F, Tao HW, Zhang LI: **AAV-Mediated Anterograde Transsynaptic Tagging: Mapping Corticocollicular Input-Defined Neural Pathways for Defense Behaviors**. *Neuron* 2017, **93**:33-47.
81. Mundell NA, Beier KT, Pan YA, Lapan SW, Goz Ayturk D, Berezovskii VK, Wark AR, Drokhlyansky E, Bielecki J, Born RT, et al.: **Vesicular stomatitis virus enables gene transfer and transsynaptic tracing in a wide range of organisms**. *J Comp Neurol* 2015, **523**:1639-1663.